1. Award Information

Award Number: DE-FC36-04GO13156

Project Title: Microchannel Reactor System for Catalytic Hydrogenation

Project Period: 09/30/03 – 09/29/10 ***(No-cost Extension till 09/29/10)***

Recipient:
Stevens Institute of Technology
Castle Point on Hudson
Hoboken, NJ 07030
13th Congressional District

Partners:
Bristol-Myers Squibb (~$70,000/yr.)
Pharmaceutical Research Institute
One Squibb Drive, P.O. Box 191
New Brunswick, NJ 08903-0191
Donald C. Kientzler
(732) 227-6936
6th Congressional District

New Jersey Nanotechnology Consortium, $18,000/yr. (3 years, in-kind)
Lucent Technologies, Bell Laboratories,
600-700, Mountain Avenue, Murray Hill, NJ 07974
Stanley Pau
(908) 582-3994
7th Congressional District

ChemProcess Technologies, LLC, ~$40,000/yr. (in-kind)
1891 Adler Road,
Bensalem, PA 19020
Luke Achenie
(215) 850-1883
8th Congressional District

Information By Design, ~$3,333/yr. (in-kind)
720 Monroe Street, E-503
Hoboken, NJ 07030
Maddy Urken
(201) 420-4410
13th Congressional District

Mr. Frank Shinneman, ~$13,000/yr. (3 years, in-kind)
515 E. 85th St., #11B
New York, NY 10028
(908) 305-4986

14th Congressional District

Technical Contact: Adeniyi Lawal (PI, Stevens), (201) 216-8241, alawal@stevens.edu
Woo Lee (Co-PI, Stevens), (201) 216-8307, wlee@stevens.edu
Ron Besser (Co-PI, Stevens), (201) 216-5257,
rbesser@stevens.edu
Donald Kientzler (Co-PI, BMS), (732) 519-3963,
donald.kientzler@bms.com
Luke Achenie (Co-PI, CPT), (860) 486-2756,
achenie@engr.uconn.edu

2. No distribution limitations

3. Executive Summary

We successfully demonstrated a novel process intensification concept enabled by the development of microchannel reactors, for energy efficient catalytic hydrogenation reactions at moderate temperature, and pressure, and low solvent levels. We designed, fabricated, evaluated, and optimized a laboratory-scale microchannel reactor system for hydrogenation of o-nitroanisole and a proprietary BMS molecule. In the second phase of the program, as a prelude to full-scale commercialization, we designed and developed a fully-automated skid-mounted multichannel microreactor pilot plant system for multiphase reactions. The system is capable of processing 1 – 10 kg/h of liquid substrate, and an industrially relevant immiscible liquid-liquid was successfully demonstrated on the system. Our microreactor-based pilot plant is one-of-a-kind. We anticipate that this process intensification concept, if successfully demonstrated, will provide a paradigm-changing basis for replacing existing energy inefficient, cost ineffective, environmentally detrimental slurry semi-batch reactor-based manufacturing practiced in the pharmaceutical and fine chemicals industries.

4. Project Accomplishments

The following are the major accomplishments of the project:

- The design and evaluation of a laboratory microreactor system for controlled and safe hydrogenation of a model pharmaceutical substrate, nitro-anisole as well as a BMS molecule.
- Achievement of ~100% conversion, and selectivity at moderate operating conditions, and a residence time of a few seconds (~2 – 3 sec.)
- Development and formulation of in-house catalyst, and rapid screening of different catalysts, both commercial and in-house to identify the right combination of catalyst/support for the hydrogenation reaction.
- Development of closed-channel flow coating, open-channel surface-selective and dip coating methods to deposit sol-gel-based thin-film catalysts into microchannels, and cellular structures
- Determination of the kinetic rate expressions for hydrogenation of o-nitroanisole in both microreactor and semi-batch reactor
- Determination of the kinetic rate expressions for hydrogenation of BMS proprietary molecule in the microreactor

- Determination of the gas-liquid mass transfer parameter in both the microreactor and semi-batch reactor for hydrogenation reaction
- Comparison of the performance of the microreactor to that of a semi-batch reactor
- Development of a flexible integrated multiphase microreactor platform consisting of the "catalyst trap microreactor" as a test-bed for multiphase microchemical reactions, computer-interfaced instrumentation for flow, temperature, and pressure control, and digital acquisition of high quality microscope images in real time.
- Demonstration of methods for effectively loading catalyst particles into the catalyst trap microreactor.
- Developed approaches for characterizing flow regimes based on optical image analysis.
- Gained understanding of the key factors driving the various multiphase flow regimes in the catalyst trap microreactor and which are favorable for highest conversion.
- Demonstration of a unique microfabricated reactor which relieves the mass transport resistances of the multiphase catalytic hydrogenation reaction.
- Detailed design of the major pieces of equipment for the production of 10 kg/hr of cyclohexane
- Completion of the fixed capital cost and production cost analysis for the production of 10 kg/hr of cyclohexane
- Published twelve articles in refereed journals, one invited book chapter, two edited proceedings papers, and gave twenty-four presentations to disseminate the results of this task.
- Development of an optimized ASPEN model for the production of 1 – 10kg/h of liquid product in multiphase reactions in pharmaceutical industry
- Design and fabrication of the multichannel, multilayer reactor system for the pilot plant
- Development of a fully-automated skid-mounted multichannel micro-reactor pilot plant system for multiphase reactions
- Demonstration of immiscible liquid-liquid reaction in the pilot plant

5. Project Activities

TASK 1: Experimental Laboratory Reactor System Design, Fabrication & Initial Evaluation

I. Summary

A laboratory microreactor system was designed, evaluated and optimized for the catalytic hydrogenation of two nitro-aromatic compounds of importance to the pharmaceutical industry, o-nitroanisole and a proprietary nitro-aromatic ketone compound provided by the principal industrial partner, BMS. These highly exothermic reactions were safely conducted in the microreactor under a wide range of operating conditions. Both commercially available and proprietary catalysts were screened for their performance. The effects of different operating conditions on the microreactor performance were studied to identify the conditions under which the reactions are controlled by intrinsic kinetics. Then, the kinetic study of the two reactions was undertaken in the microreactor, and rate equations were developed that could be useful for the design of a multi-channel microreactor. The kinetics of hydrogenation of nitro aromatics is complicated as it involves a number of intermediates. This study has reduced the complexity involved in studying the intrinsic kinetics of this reaction by isolating the individual reactions of the overall reaction, and developing rate equations for each reaction separately.

Further, the feasibility of conducting kinetics of the two reactions in the semi-batch reactor was evaluated. It was shown that the semi-batch reactor can be used for studying intrinsic kinetics of hydrogenation of o-nitroanisole. However, it was difficult to study intrinsic kinetics of the hydrogenation of aromatic nitro ketone in the semi-batch reactor due to external mass transfer limitations. The two reactors, semi-batch reactor and microreactor, were modeled and the modeling results along with the experimental results were used to determine the mass transfer parameters in the two reactor systems for a wide range of operating conditions. The mass transfer parameters in the microreactor were found to be two to four orders of magnitude higher than in the semi-batch reactor. This order of magnitude difference in the mass transfer parameters enables the microreactor to be more suited than the semi-batch reactor for studying the intrinsic kinetics of fast hydrogenation reactions with half lives in the order of magnitude between 10^0 and 10^2 seconds (e.g. hydrogenation of nitro-aromatic ketone) whereas both batch and micro reactors can be used for studying the intrinsic kinetics of slow hydrogenation reactions with half lives in the order of magnitude of 10^2 s and above (e.g. hydrogenation of o-nitroanisole). Rapid catalyst deactivation was observed at low conversions of substrate. Possible explanations for catalyst deactivation along with procedures for regeneration of catalyst are also discussed.

II. Performance and Optimization Studies

II.1. Experimental Methods

II.1.1. Microreactor System

Figure 1.0a shows the experimental setup of microreactor used for conducting the reactions. Two gas lines, one for hydrogen reactant (H_2) and the other for nitrogen (N_2) are shown in the system. The purpose of the nitrogen line is to flush the reactor system at the end of each experiment and also to dilute the hydrogen gas to obtain different compositions of hydrogen for kinetic experiments. The compressed gas flows through a pneumatically actuated valve (BVC) and then through the Mass Flow Controller (MFC). The MFCs are from Porter, model 201 rated for 0-20sccm for the hydrogen line and 0-50sccm for nitrogen lines. From the MFC, the gas then flows through the check valve (CHV) and then through the flame arrester. The purpose of the check valve is to prevent fluid backflow, and thus liquid from entering into the MFC. In case of any ignition downstream during the experimental run, the flame arrester prevents the flame from traveling upstream to the gas line. From the check valve, the gas is then mixed with the liquid stream using a T-mixer. The liquid reactant and solvent are pumped using the HPLC pumps, from Lab Alliance.

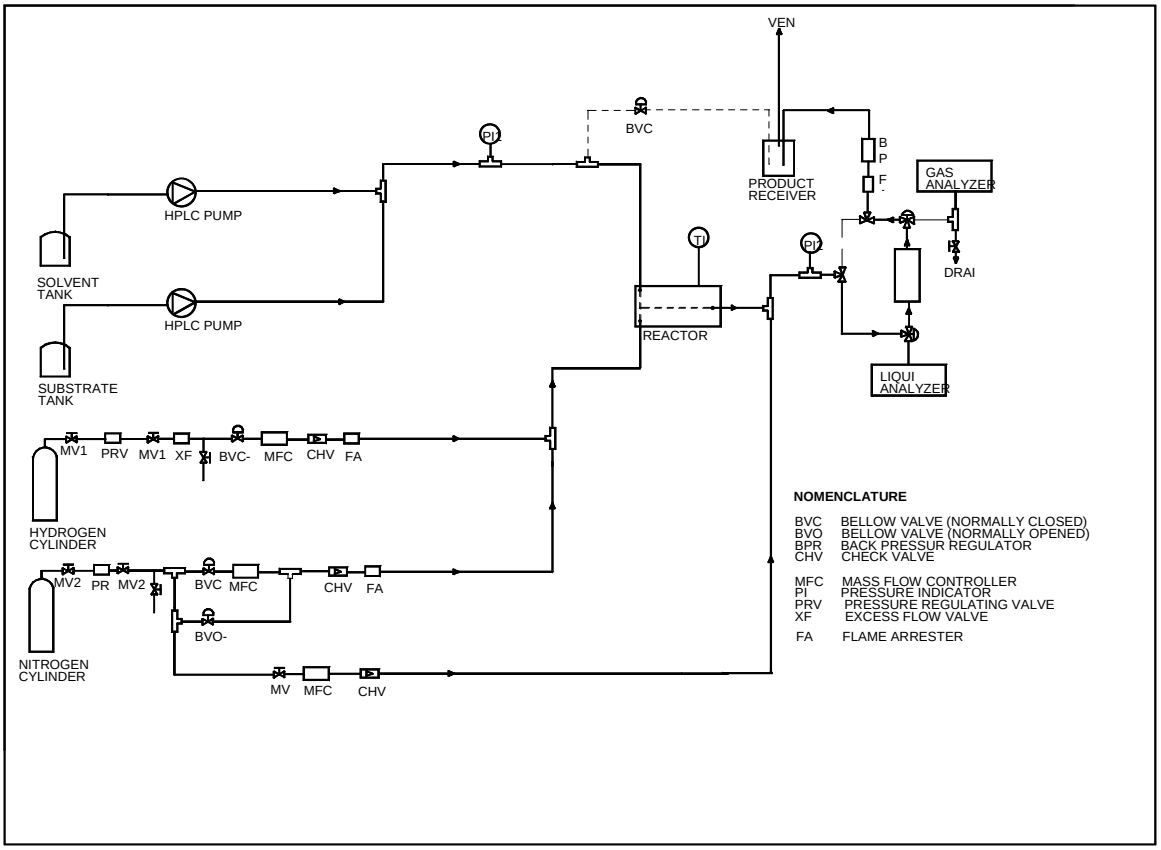

Fig. 1.0a Microreactor Experimental Set-up

The combined gas-liquid mixture then enters the reactor. The reactor is made of SS316L with an outer diameter of 1.5875mm and inner diameter of 0.775mm. The total length of the packed reactor varied from 6 to 8 cm of which the catalyst was packed within 1 to 6 cm of the reactor (depending upon the catalyst loading required for the experiment) and the remaining length of the reactor was filled with inert glass beads of the same size range as the catalyst particles. The glass beads were used to prevent any fine catalyst particles from clogging the frits placed at the entrance and exit of the reactor. As a result, the pressure drop in the reactor under all experimental conditions was always less than 10% of the reactor entrance pressure. The frits, made of polypropylene, act as retainers to prevent the catalyst from moving out of the reactor. The connectors for connecting the reactor end with the streams are PEEK unions and ferrules.

The reactor is immersed in a constant temperature water bath (HAAKE B3 Model) so as to maintain isothermal conditions. The pressure values at the entrance and the exit are measured using OMEGA DP-24E process meter and PX 541 series pressure transducers. From the reactor, the reaction mixture passes through a sampling loop where the product is collected for analysis. During sampling, the original stream is by-passed to another line so as to avoid the disturbances caused to the system by sampling. From the sampling loop, the reaction mixture passes through another flame arrester and then the back pressure regulator (CIRCLE VALVE BP66 series). The back pressure regulator is used to build up the desired pressure during an experimental run. From

the back pressure regulator, the mixture is passed to a product receiver where the liquid is collected in a glass vessel and the gas phase is vented to the atmosphere

Before starting any experimental run, the impurities from the previous run are purged from the system by replacing the reactor with an empty tube, and then passing nitrogen gas, followed by the pure solvent. The reactor is then placed into the system. A reaction run is made by first pumping the liquid through the system at a flow rate of approximately 2.0 – 2.5 ml/min. A few minutes after the liquid emerges at the receiver, the back pressure regulator is partially closed until the desired pressure is attained. The liquid flow rate is then adjusted to the desired value and the back pressure regulator adjusted to maintain the desired pressure in the system. The hydrogen gas is then passed through the system by opening the air actuated bellow valve (BVC). The flow rate of hydrogen is controlled to the desired value using the mass flow controller. The reactor temperature is maintained at the desired value using the water bath. After the system attains steady state, the product is collected from the sampling loop by by-passing the stream. These samples are diluted with methanol (HPLC grade) or de-ionized water for analysis.

II.1.2. Semi-batch Reactor

Figure 1.0b is a schematic of the experimental semi-batch reactor (25 ml PARR 5500 Series Compact Reactor) used for conducting the reactions. The compressed H_2 gas passed through the inlet pressure regulating valve into the reactor which was filled with the liquid reactant and the catalyst. The reactor was equipped with compact magnetic impeller designed to stir at speeds up to 1000 rpm. Heating was provided electrically using a heating coil. A continuous stream of cooling water was circulated around the reactor to control the temperature of the reactor. A thermocouple (T1) was incorporated into the reactor to read the reaction temperature at any given time. The pressure in the reactor was controlled using an electronic pressure controller attached to the gas cylinder. The gas consumption during the experiments was measured from the pressure transducer (P1) attached to the cylinder. The reactor pressure (P2) was maintained at a constant value throughout the experimental run. The reactor was equipped with a pressure relief valve to relieve the pressure at the end of the experiment, and a sampling valve to collect the liquid sample at regular intervals of time.

Before starting any experimental run, the reactor was filled with the liquid reactant and the catalyst, after which it was connected to the experimental system. Then the reactor was purged with hydrogen to replace any air remaining in the reactor. After the reactor temperature and pressure reached the desired values, the agitator was started and this time was recorded as the starting time of the reaction. The starting time is accurate with an error of less than 10 seconds. Even this error is attributed to the time for the stirrer to reach the desired stirrer speed. The product was collected from the sampling port at regular intervals of time. These samples were diluted with methanol (HPLC grade) or de-ionized water for analysis.

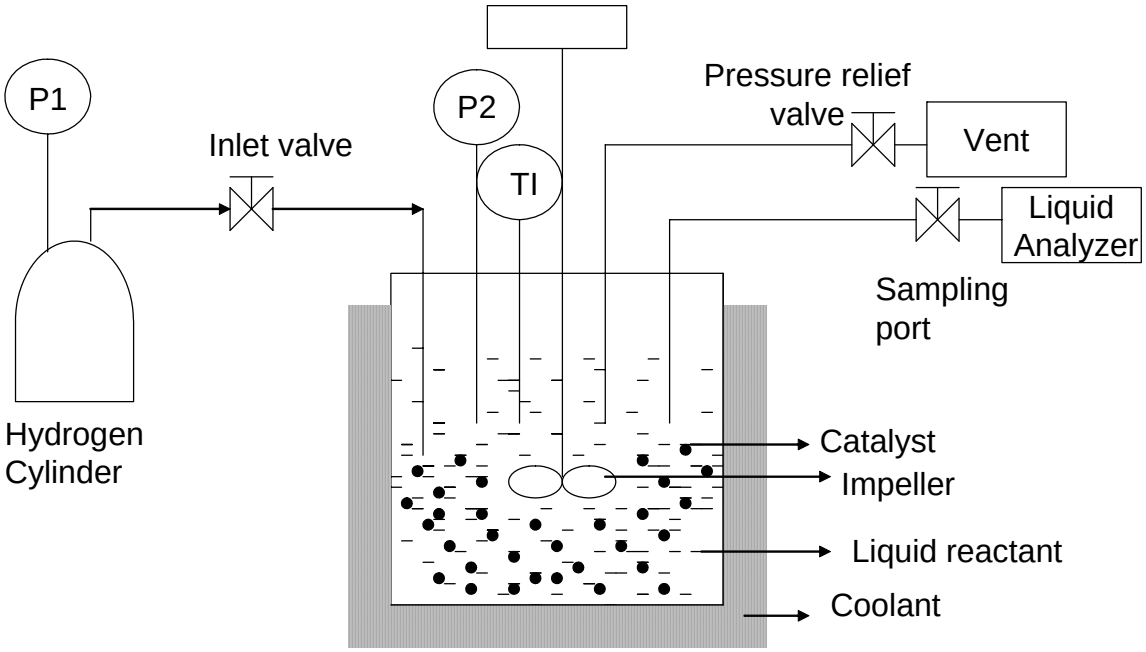

Fig. 1.0b Schematic of the Semi-batch Reactor Experimental Set-up

III. Kinetics of Hydrogenation of o-nitroanisole

III.1. Introduction

The catalytic hydrogenation of o-nitroanisole using transition metal catalysts is one of the most common reactions in the fine chemicals and pharmaceutical industries. There is limited literature available on the fundamental aspects such as reaction kinetics of this reaction (Chaudhari et al. 1983). Being a multiphase catalytic reaction, a systematic study on the effect of reaction parameters on the rate behavior and selectivity is most essential to optimize the process performance and generate information useful in the design of pilot-plant or production scale reactors.

Metal catalysts such as palladium, platinum, nickel and iron etc. have been reported in the prior literature for the hydrogenation of nitro aromatics. Among these, palladium catalyst has been shown to exhibit considerably higher activity/ selectivity and stability compared to others (Figueras and Coq 2001). Among the commercially available supported palladium catalysts, the catalyst that gives the highest selectivity and yield of the product has to be identified. Also, this reaction being a three-phase reaction involving gas (hydrogen), liquid (o-nitroanisole) and solid (catalyst), the overall performance may depend on various engineering factors such as gas to liquid mass transfer, liquid to solid mass transfer and intra-particle diffusion. To analyze such a multiphase catalytic reaction from the reaction engineering point of view, it is also important to understand the rate behavior and intrinsic kinetics of this reaction.

Hence, the first objective of this study was to identify the best catalyst among the commercially available palladium catalysts and to investigate the effect of various reaction conditions on the selectivity/ yield of o-anisidine using the best catalyst. The second objective was to investigate the kinetics of this reaction and develop rate equations which can be useful for the design of the multi-channel or large scale reactors.

Finally, the third objective is to compare the performance of the microreactor with the semi-batch reactor by comparing their reaction rates and mass transfer efficiencies.

III.2. Experimental

In this section, a list of the chemicals used for the experiments, and the description of the analytical method are provided. The description of the microreactor and semi-batch reactor experimental set-up as well as experimental procedure was described in section II. The raw materials o-nitroanisole and o-anisidine were purchased from Sigma Aldrich, and used without any purification. The solvent methanol (CH_3OH) was obtained from Pharmco Products Inc. The hydrogen and nitrogen were purchased from Praxair. The mobile phase used for the HPLC analysis comprised De-ionized water and Acetonitrile (HPLC grade), with the latter purchased from Pharmco Products Inc. The catalysts used for this study were 5% (w/w) Pd supported on Carbon and 0.5% (w/w) Pd supported on Carbon (from Degussa) and 2% (w/w) Pd supported on zeolite (Aluminum Sodium Silicate, proprietary catalyst). All the catalysts were sieved to obtain a particle size distribution of 45-75microns and 75-150 microns which were the particle size ranges used for the experiments.

All the liquid product samples collected at the end of each experimental run were diluted in methanol for analysis. The samples were analyzed using High Performance Liquid Chromatography (HPLC) from Shimadzu. A Diode Array detector is used for scanning so that the samples could be scanned at multiple wavelengths at the same time. A method was established in the HPLC using water and acetonitrile as the mobile phase in conjunction with an RP C^{18} column from Waters Corporation. Calibration was done for both the reactant and the product using standard solutions. The concentrations of the unknown product samples were determined from the calibration data.

III.3. Results and Discussion

III.3.1. Reaction

The catalytic hydrogenation of o-nitroanisole to o-anisidine involves a three-step reduction series reaction. First, the reduction of o-nitroanisole to 2-methoxynitrosobenzene, next to N-(2-methoxyphenyl) hydroxylamine, and, finally to o-anisidine. During the experiments only one intermediate was observed in the product stream along with the product, and reactant at all operating conditions. The HPLC Chromatograph of a sample product stream is shown in fig. 1.1. This intermediate was found to be 2-methoxynitrosobenzene by the Mass Spectrum Analysis shown in fig. 1.2. The presence of hydroxylamine derivative was not detected during analysis, indicating that it had only transient lifetime probably because of its instantaneous reaction with hydrogen to form o-anisidine, the rate of which far exceeds its formation from 2-methoxynitrosobenzene. Thus the hydrogenation of o-nitroanisole to o-anisidine was considered as a process consisting of two consecutive reactions, one leading to the formation of 2-methoxynitrosobenzene, and the other leading to the formation of o-anisidine.

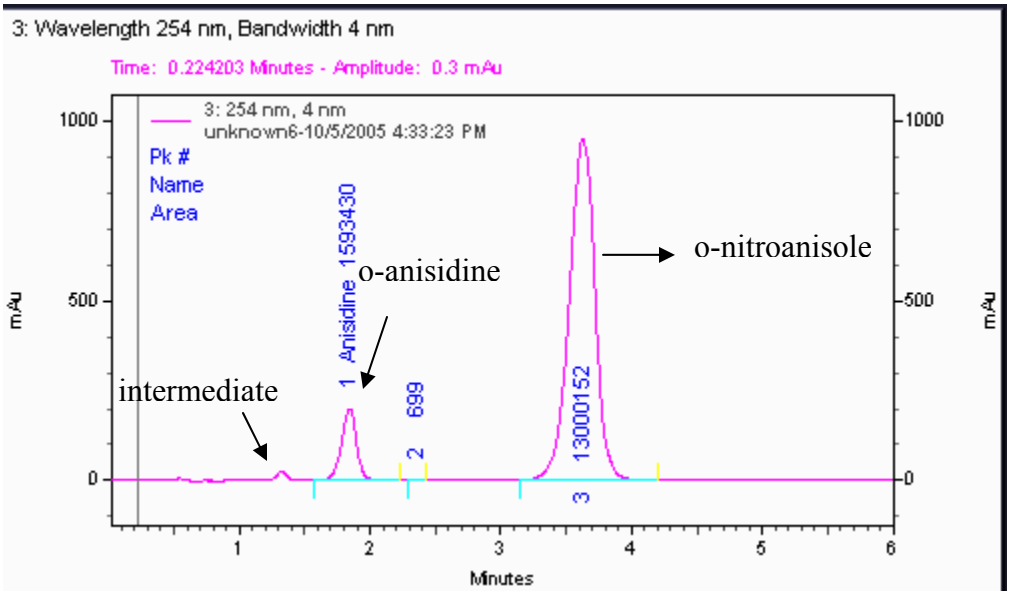

Fig. 1.1 Typical HPLC Chromatograph of the reaction mixture.

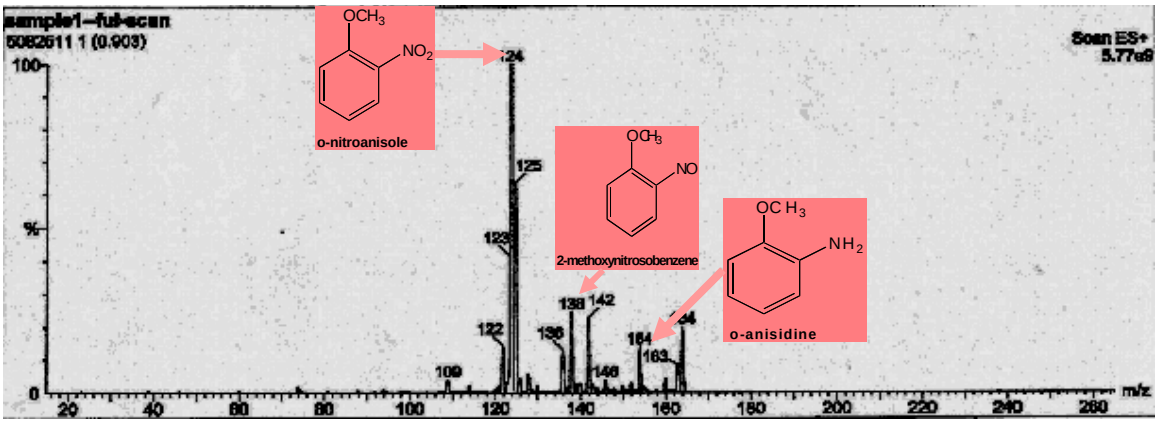

Fig. 1.2 Mass Spectrum Analysis of the reaction mixture.

III.3.2. Fluid flow characterization in microreactor

The fluid dynamics of reactors involving multi-phase flow has significant effect on the reactor performance. It is critical to understand the hydrodynamics in the microreactor before attempting to study the effect of operating conditions and the kinetics of the reaction in the microreactor. Various flow regimes ranging from bubbly flow to annular flow exist in small channel diameters (between 0.5 to 5mm) at different gas and liquid flow velocities (Kreutzer et al. 2001; Nijhuis et al. 2001; Kreutzer et al. 2005). We conducted flow visualization experiments using a transparent glass tube with the same dimensions as the microreactor. The liquid flowrates used in these experiments varied from 0.03 to 0.2 ml/min and gas flowrates from 2 to 10sccm. During these experiments, *Taylor flow* with alternating gas and liquid slugs was observed in the empty microreactor under all operating conditions. Numerical simulation using CFD and Fluent also proved that Taylor flow exists under these flow conditions (Qian and Lawal 2006).

Similar flow visualization experiments were conducted in a glass microreactor with a square cross-section measuring 500µm by 500µm packed with glass beads of the same size range as the catalyst particles used in all experiments. These experiments showed that slug flow exists in a packed bed microreactor as well, except that slug boundaries are broken-up by the particles. This type of flow is known as transitional slug flow. During gas-liquid reactions in micro channels, Taylor or slug flow has been shown to enhance mass transfer significantly (Kreutzer et al. 2001). Therefore, for all the experiments reported here, the reactor was operated in slug flow regime.

III.3.3. Catalyst screening in microreactor

Three different Pd catalysts were investigated to see the influence of different supports on the catalytic activity and selectivity for o-anisidine. These catalysts were:

2% Pd on Zeolite (Company A)
5.0% Pd supported on Carbon (Degussa Corporation)
0.5% Pd supported on Carbon (Degussa Corporation)

Experiments using these catalysts were carried out at a pressure of 200psig, substrate concentration of 8% (w/w) in methanol, and a temperature of 30°C. The liquid and gas flow rates were 0.1ml/min and 5sccm respectively.

For the hydrogenation of nitro compounds, Pd supported on carbon catalysts is usually preferred because of the chemically inert nature of carbon, its large specific surface area and ability to easily recover the precious metals. Since the reaction produces water, the hydrophobic character of carbon would also be of great advantage (Figueras and Coq 2001). Experimental runs were made using carbon supported Pd catalysts of different loading levels. As seen from fig. 1.3, 5%Pd/C gave almost 100% conversion and 100% selectivity using 9mg of catalyst, however, the carbon supported catalyst was found to deactivate rapidly. Therefore, experiments were conducted using Pd catalyst with different support: 2% Pd supported on sodium aluminum silicate (Zeolite, $NaAl(SiO_3)_2$). It was found that this catalyst has an activity similar to (or even higher than) the Pd supported on carbon. The deactivation rate of this catalyst was observed to be slower than that of Pd supported on carbon. Also, for the Pd/C catalysts the average pressure could not be maintained at a fixed value for exact comparison to other catalysts due to the gradual increase in pressure drop with time arising from catalyst attrition. Therefore, all further experiments were conducted using 2%Pd supported on Zeolite. The dispersion of palladium on this support was measured using TEM (FEG-TEM, Model CM20, Philips, Eindhoven, Netherlands) and was calculated to be 36%. The surface area and pore size of the catalyst were 170 - 220 m^2/g and 10-12 nm respectively measured by BET (multi-point BET technique, using Quantochrome Instruments Autosorb-1).

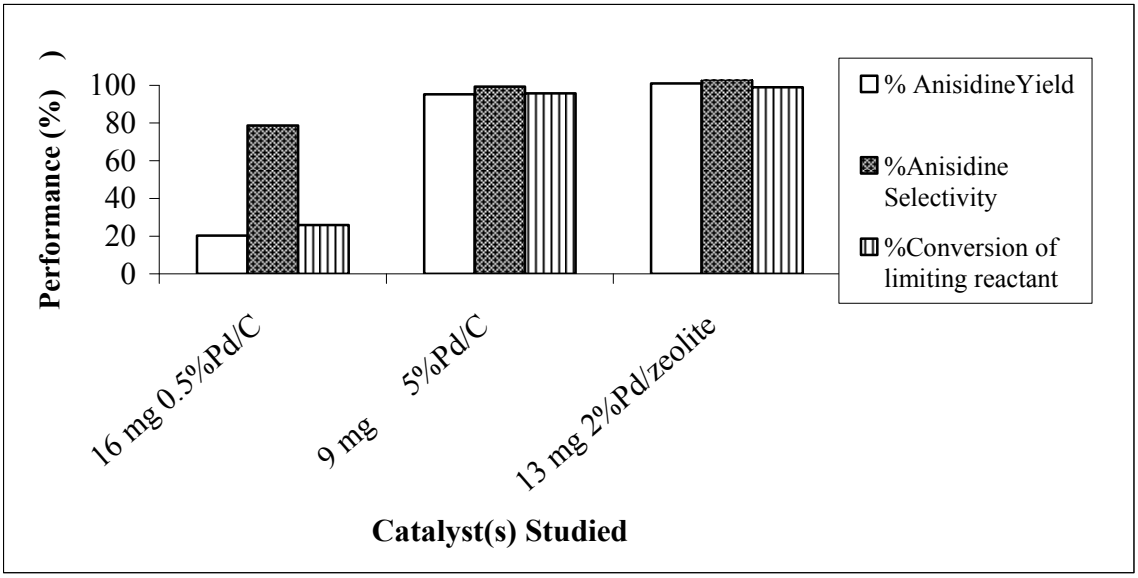

Fig. 1.3 Comparison of catalytic activity

(All runs were made at 45^{o}C, liquid (8% (w/w) o-nitroanisole in methanol) flow rate = 0.1 ml/min, pressure 100psig, H_2 flow rate = 5 sccm).

III.3.4. Effect of Operating Conditions on micro-reactor performance

The effect of operating conditions on micro-reactor performance was studied by comparing the conversion of o-nitroanisole, *selectivity* and S*pace-Time Yield* of o-anisidine under different reaction conditions. *Selectivity* is defined as the ratio of the number of moles of the desired product formed to the moles of the product that would have been formed if there were no side reactions. Yield is defined as the ratio of the number of moles of the desired product formed to the moles of the product that would have formed if there were no side reactions and the limiting reactant had reacted completely. Therefore, by industrial definition

Yield = Selectivity * Conversion *100.

Space-Time Yield (STY) is the rate of formation of the desired product per unit mass of the active metal (Pd) in the catalyst.

III.3.4.1. Effect of Pressure

To study the effect of pressure on conversion of o-nitroanisole, selectivity and STY of o-anisidine, experiments were carried out in the pressure range of 50-250 psig at a substrate concentration of 1.299 mol/L in methanol, temperature 30°C and a catalyst loading of 6.9mg of 2%Pd/Zeolite. The liquid and hydrogen flow rates were 0.05ml/min and 5sccm respectively.

As shown in fig. 1.4, the selectivity is close to 100% at all the pressure levels considered while both the conversion and STY increase with increase in pressure. Although fig.1.4 shows that the conversion increases with pressure, the reactor contact times are not the same in these runs. The reason is that gas flow rates are measured under standard conditions (the value was 5 sccm). Hence the actual gas flow rates are different in different runs shown in this figure. Therefore, the increase in conversion with increase in pressure may be due to the increase in residence time. In order to eliminate the effect of residence time, experiments were carried out at different pressure values but same residence time. Figure 1.5 shows a plot of the conversion vs.

pressure based on constant residence time of 1.1seconds (inlet conditions). Figure 1.5 indicates that the conversion remains almost constant with increase in pressure, but the STY or rate increases with increase in pressure in the range of pressures studied. This increase in STY is attributed to the increase in the concentration of dissolved hydrogen at the entrance of the reactor resulting in a higher reaction rate. However, pressure has no effect on the conversion at constant residence time because the increase in the reaction rate at higher pressure is countered by the decrease in the catalyst loading.

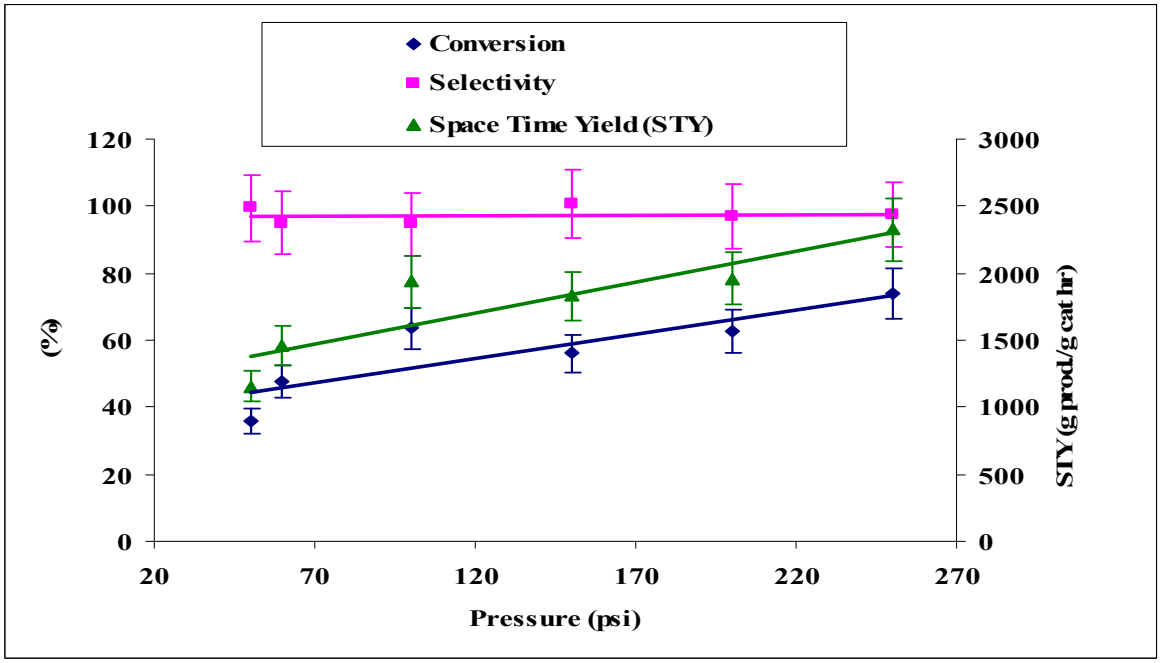

Fig. 1.4 Effect of pressure on reactor performance

(All the runs were made at 30°C, 1.299 mol/L o-nitroanisole in methanol, liquid flow rate = 0.05 ml/min, H_2 flow rate = 5 sccm, 6.9 mg of 2% Pd/Zeolite catalyst).

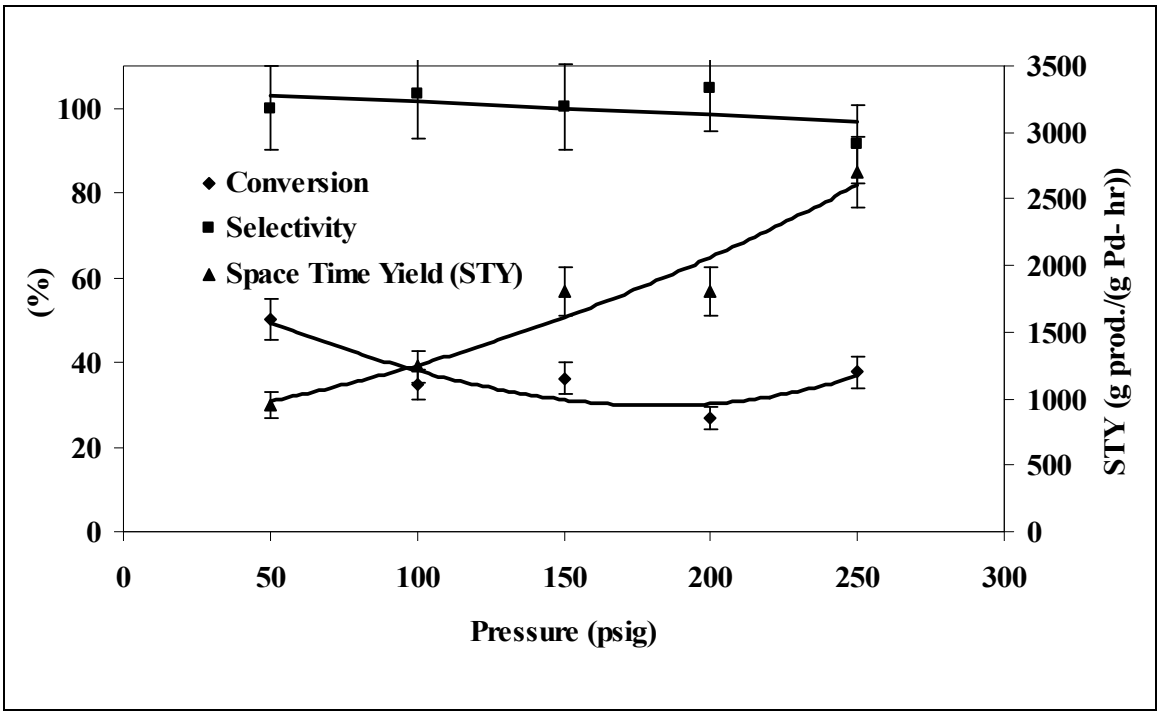

Fig. 1.5 Effect of pressure on reactor performance based on constant residence time (1.1sec) (All the runs were made at 30°C, 1.299 mol/L o-nitroanisole in methanol, liquid flow rate = 0.05 ml/min, H_2 flow rate = 5 sccm, 2% Pd/Zeolite catalyst).

III.3.4.2. Effect of Temperature

To study the effect of temperature on conversion of o-nitroanisole, selectivity and STY of o-anisidine, experiments were carried out in the temperature range of 25-55°C at a substrate concentration of 1.299 mol/L in methanol, pressure of 50psig and a catalyst (2%Pd/Zeolite) loading of 6.9mg. The liquid and hydrogen gas flow rates were 0.05ml/min and 5sccm respectively. Figure 1.6 shows that with increase in temperature, both the conversion and STY increase while the selectivity remains close to 100% at all the temperature levels. The trend in STY indicates that the reaction may be controlled by intrinsic kinetics, because the average reaction rate almost doubles for every 10 degrees increase in temperature. If the reaction were controlled by mass transfer there will be very slight increase in reaction rate with increase in temperature. However, this conclusion cannot be confirmed until the absence of mass transfer resistances both external and internal, has been established. The role played by mass transfer resistances in the kinetics of the reaction will be discussed in the kinetics section.

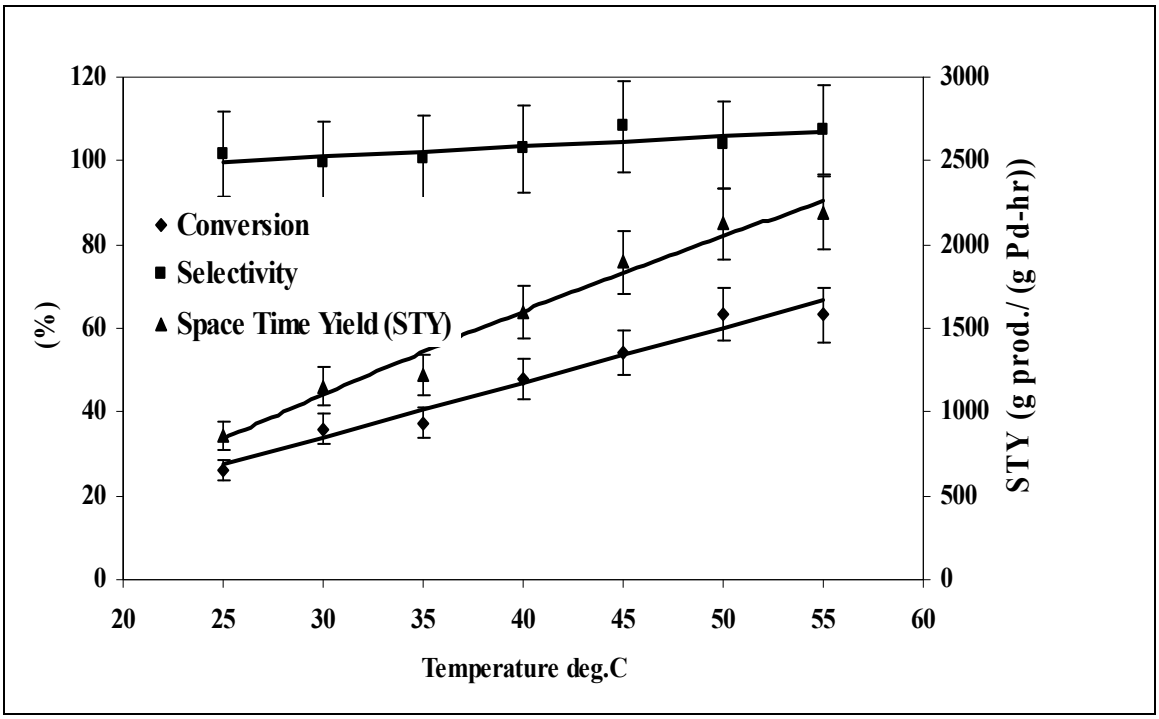

Fig. 1.6 Effect of temperature on reactor performance

(All the runs were made at a pressure of 50 psig, liquid composition of 1.299 mol/L o-nitroanisole in methanol, liquid flow rate of 0.05 ml/min, H_2 flow rate of 5 sccm and with 6.9 mg of 2% Pd/Zeolite catalyst.

III.3.4.3. Effect of Residence Time

In the current experimental reactor system, since the microreactor is in the form of a packed bed, it is important to define the residence time before we actually study the effect of varied residence time. Residence time in the packed bed reactor can be defined as the total volume of void space inside the reactor divided by the total superficial volumetric flow rate of the liquid and gas. Experiments for varying the residence time were done both by changing the liquid and gas flow rates, and also by changing the amount of catalyst in the reactor.

Experiments for varying the liquid flow rate were conducted to study its effect on the conversion, selectivity and STY of o-anisidine. All the experiments were carried out at a temperature of 45°C, substrate concentration of 1.2 mol/L in methanol, pressure of 100psig and a catalyst (2%Pd/Zeolite) loading of 13mg. The flow rate of the liquid was varied and the H_2 flow rate was kept constant at 5sccm. In these experiments, the actual gas flow rate is approximately 10 times the liquid flow rate. Therefore, a change in liquid flow rate does not change the residence time significantly. Figure 1.7 shows the effect of liquid flow rate on the conversion, selectivity and STY. The data shows that the conversion decreases with increase in liquid flow rate while the selectivity remains almost constant. However, STY or the overall reaction rate first increases with increase in liquid flow rate up to a liquid flow rate of 0.1ml/min and then decreases with further increase in liquid flow rate.

In the experiments that we conducted to see the effect of the liquid flow rate at constant gas flow rate, it was observed that the liquid slug length increases with increase in the liquid flow rate, whereas the gas slug length remains constant. As the liquid slug length increases, the rate of

convective mass transfer from gas to liquid decreases (Kreutzer et al. 2001). Small liquid slugs enhance the mass transfer from gas to the liquid. Therefore, STY increases with decrease in liquid flow rate (or decrease in liquid slug length). However, a decrease in STY at a liquid flow rate of 0.1ml/min may be attributed to the high conversion of o-nitroanisole under these conditions that results in decrease of average reaction rate or STY.

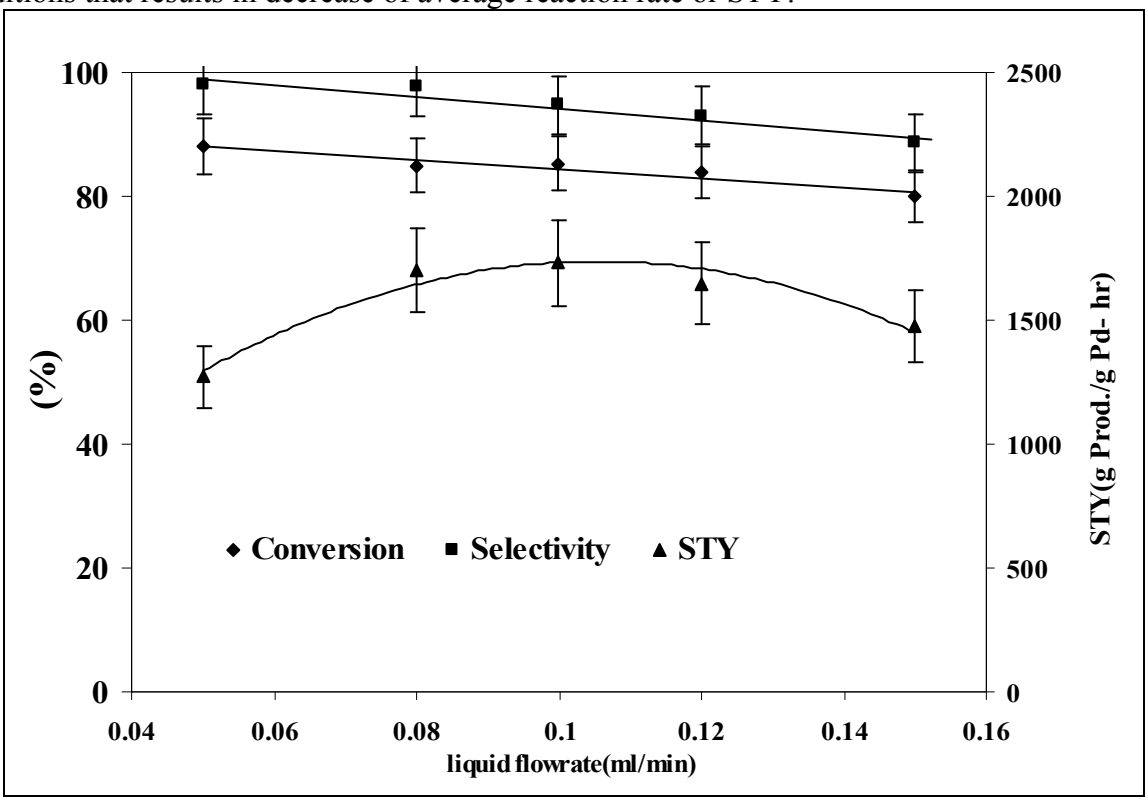

Fig. 1.7 Effect of liquid flow rate on reactor performance

(All runs were made at 45^{o}C, 100 psig reactor pressure, with a H_2 flowrate of 5 sccm, with a liquid feed containing 1.2 mol/L nitroanisole in methanol and 13 mg of 2% Pd /Zeolite catalyst)

Another method of changing the residence time is to change the gas flow rate. Experiments for varying the gas flow rate were conducted to study its effect on the conversion, selectivity and STY of o-anisidine. All the experiments were carried out at a temperature of 45°C, substrate concentration of 1.2 mol/L in methanol, pressure of 100psig, liquid flow rate 0.05ml/min, and a catalyst (2%Pd/Zeolite) loading of 13mg.

The effect of gas flow rate on conversion, STY and selectivity is shown in fig. 1.8. With increase in gas velocity, the conversion decreases while the selectivity remains at almost a constant value of 100%. The STY remains constant, and the change is almost negligible in the range of gas flow rates considered. With increase in gas flow rates, the residence time of the reactants in the reactor decreases thereby decreasing the conversion. Therefore, higher residence time is needed for high conversion of o-nitroanisole. However, the STY remains the same even at high conversions because the increase in the conversion or yield at higher residence time is balanced by the increase in residence time.

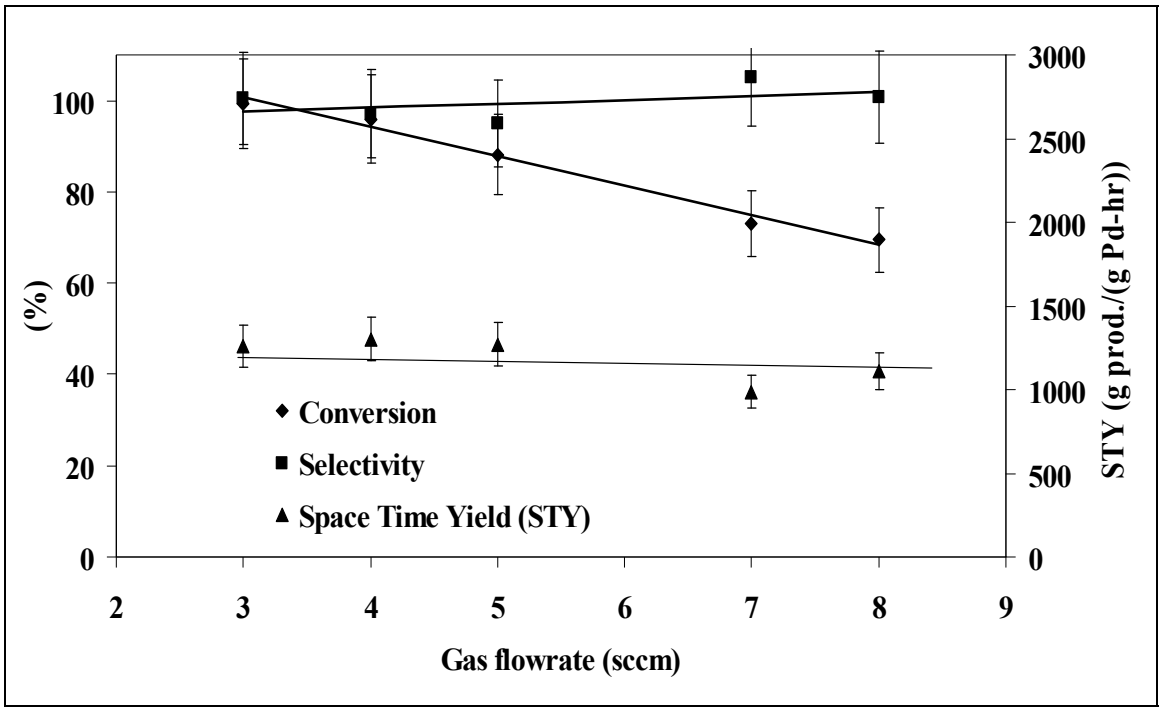

Fig. 1.8 Effect of gas flow rate on reactor performance (All the runs were made at 45^{o}C, 100 psig reactor pressure, with 1.2 mol/L o-nitroanisole in methanol, liquid flowrate of 0.05 ml/min and 13 mg of 2% Pd supported on zeolite catalyst)

The effect of residence time on the conversion, selectivity and STY was also studied by varying the catalyst loading, and keeping all the other operating conditions constant. All the experiments were carried out at a temperature of 30°C, substrate concentration of 1.299 mol/L in methanol, pressure of 50psig, liquid flow rate of 0.05ml/min, and H_2 flow rate of 5sccm. The reactor was packed with different amounts of catalyst to study the effect of the catalyst loading on reactor performance. Figure 1.9 shows the results obtained. Selectivity is close to 100% in all the runs. As expected the conversion increases with increase in catalyst loading. The value of STY decreases with increase in catalyst amount because the average reactant concentration decreases.

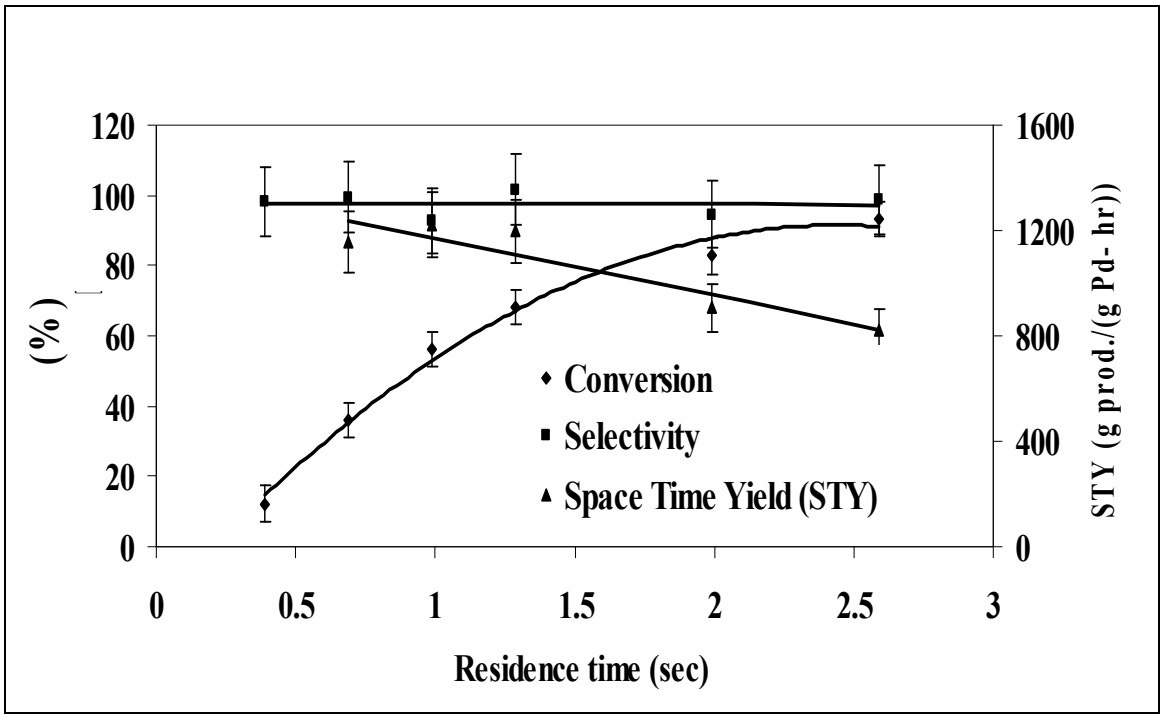

Fig. 1.9 Effect of residence time on reactor performance (based on catalyst loading)

(All the runs were made at 30^{o}C, 50 psig pressure, 1.299 mol/L o-nitroanisole in methanol, liquid flow rate of 0.05 ml/min, H_2 flow rate of 5 .0 sccm and 2% Pd/Zeolite catalyst).

Any of the three methods presented here can be used to change the residence time. However, when the residence time is varied by changing the flow velocity, then an additional variable may be introduced, namely the dependence of gas-liquid mass transfer coefficient on velocity. The effect of velocity was seen by measuring STY at the same residence time, but with different flow velocities. The residence time was kept constant by increasing the amount of catalyst in proportion to the increase in flow velocity. Figure 1.10 shows the results obtained from these experiments. The data clearly show that the reaction rate is independent of the flow velocity. Therefore, within the range of conditions considered in this study, the residence time can be varied either by changing the catalyst loading or the liquid and gas flow rates.

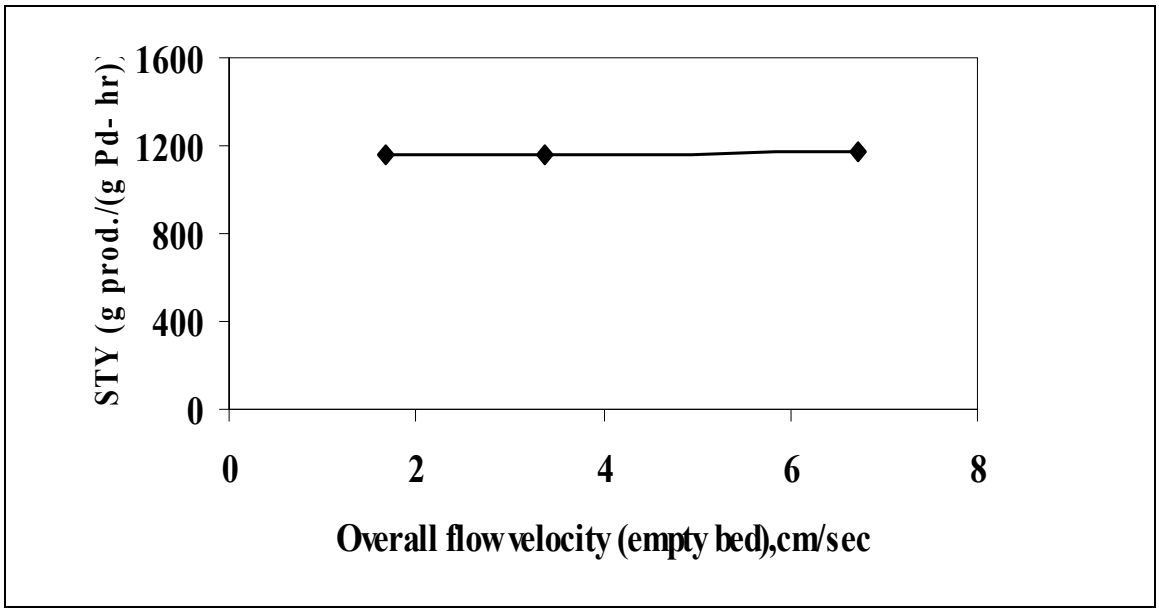

Fig. 1.10 Effect of overall flow velocity on overall reaction rate for the same residence time (All runs were made at 30°C, reactor pressure of 100 psig and 1.299 mol/L o-nitroanisole in methanol)

III.3.4.4. Effect of substrate concentration

To study the effect of substrate concentration on reactor performance, experiments were carried out in the concentration range of 0.4-6 mol/L o-nitroanisole in methanol, temperature of 45°C, 50psig reactor pressure, and a catalyst loading of 13mg of 2% Pd/Zeolite. The liquid and hydrogen gas flow rates were 0.05ml/min and 5sccm respectively. Figure 1.11 shows that decrease in o-nitroanisole concentration increases the conversion. The selectivity is lower at higher o-nitroanisole concentration indicating that the rate of intermediate formation may have a stronger dependency on the o-nitroanisole concentration. The STY increases up to nitroanisole concentration of 2.21 mol/L, and then starts to decrease thereafter. Mahajani et al. (2004) observed a similar trend at high concentrations of o-nitroanisole while conducting experiments in a batch reactor. They observed that the rate of o-anisidine formation at high concentrations of o-nitroanisole is low because of substrate inhibition effect present at such high concentrations. Another reason could be that at such high concentrations, external mass transfer resistance may become significant because of the low solubility of hydrogen at high concentrations of the reactant (Brahme et al. 1982). Therefore low concentrations (0.4-2 mol/L) of o-nitroanisole were used for the kinetics studies.

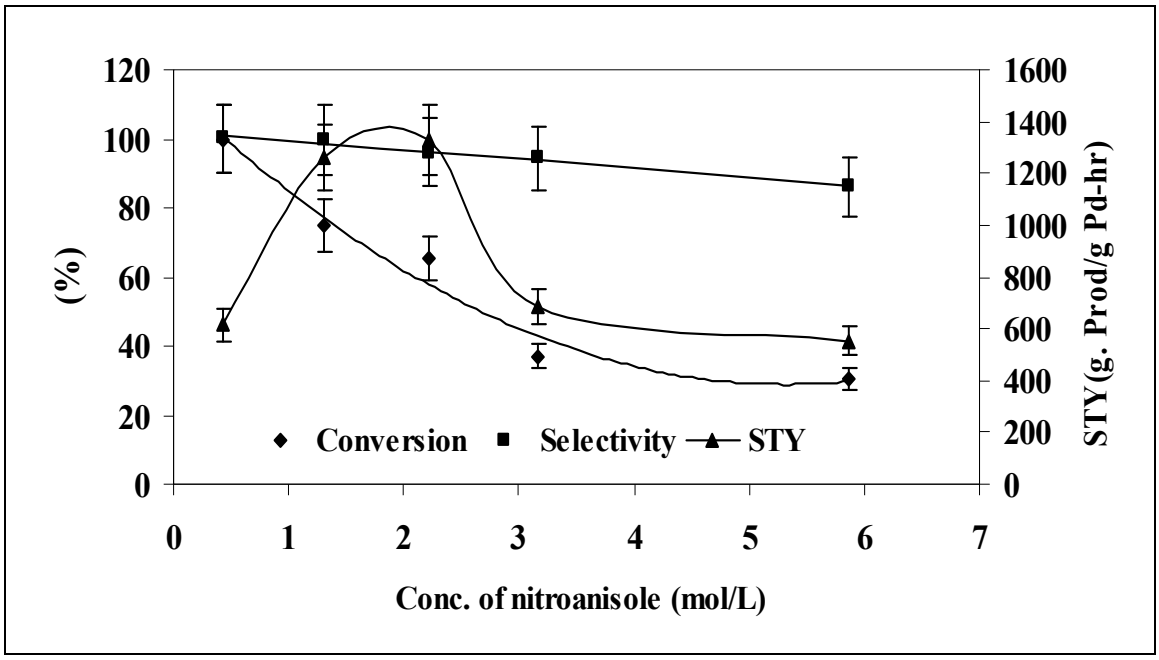

Fig. 1.11 Effect of nitroanisole concentration on reactor performance

(All runs were made at 45^{o}C, 50 psig reactor pressure, with a liquid flow rate of 0.05 ml/min, and gas flow rate of 5 sccm, and 13 mg of 2% Pd/Zeolite catalyst).

III.3.5. Kinetic Studies in microreactor

Three phase catalytic reactions involve a series of mass transfer and reaction steps that contribute to the overall observed reaction rate as shown in fig. 1.12. The step that has the greatest influence on the overall reaction rate is considered as the rate controlling or limiting step. From the bulk gas to the catalyst surface, the overall mass transfer resistance is determined by external mass transfer resistance and internal mass transfer resistance. External mass transfer resistance includes resistance to gas absorption at the gas-liquid interface and resistance to transport of the reactants to the catalyst surface. Internal mass transfer resistance refers to the resistance to diffusion of the reactants in the pores of the catalyst. The reaction is said to be controlled by external mass transfer if the external mass transfer resistance has a greater influence on the overall reaction rate than the internal mass transfer resistance and the intrinsic reaction. Similarly, the reaction is said to be controlled by internal mass transfer if the internal mass transfer resistance has a greater influence than the external mass transfer resistance and the intrinsic reaction on the overall reaction rate. The reaction is said to kinetically controlled if the both the external and internal mass transfer resistances are negligible.

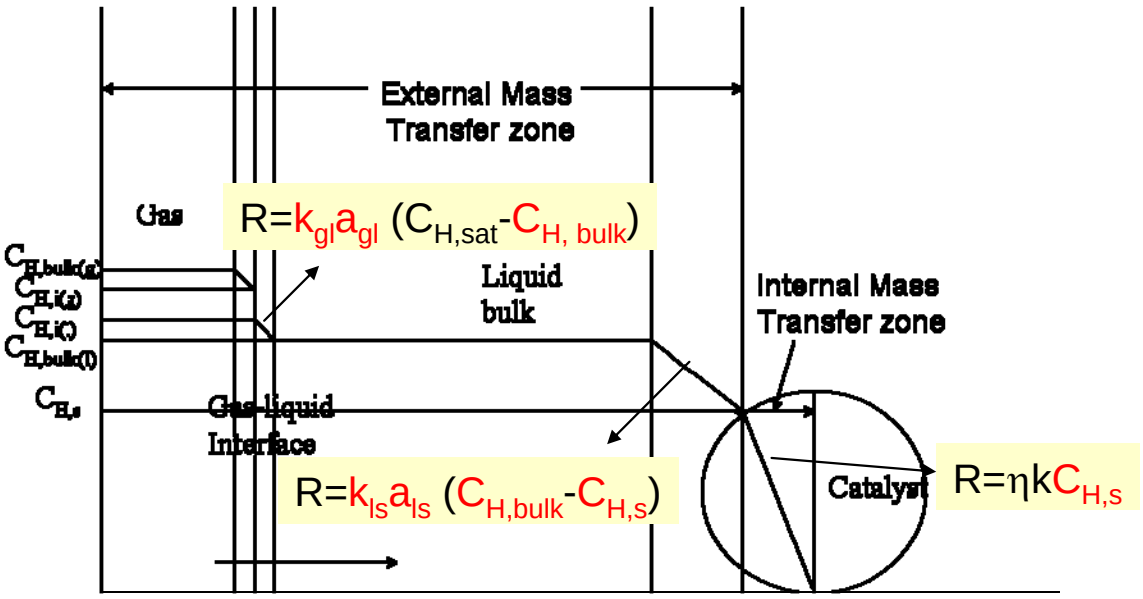

$$R_{obs}=k_{gl}a_{gl}\ (C_{H,sat}-C_{H,\ bulk})=k_{ls}a_{ls}\ (C_{H,bulk}-C_{H,s})=\eta k C_{H,s}$$

$$R_{obs}=\frac{C_{H,\ sat}-C_{H,\ s}}{\frac{1}{k_{gl}a_{gl}}+\frac{1}{k_{ls}a_{ls}}+\frac{1}{\eta k}}$$

Fig. 1.12 Concentration Profile of H_2 in gas-liquid solid reactions. ($C_{H,\ bulk(g)}$: Concentration of hydrogen in the gas phase, $C_{Hi(g)}$: Concentration of hydrogen at the gas-liquid interface (gas side), $C_{Hi(l)}$: Concentration of hydrogen at the gas-liquid interface(liquid side), $C_{H,bulk(l)}$: Concentration of hydrogen in the liquid bulk, $C_{H,s}$: Concentration of hydrogen at the catalyst surface, $R=R_{obs}$=Observed Reaction rate, $k_{gl}a_{gl}$=gas-liquid mass transfer coefficient, $k_{ls}a_{ls}$=liquid-solid mass transfer coefficient, η=effectiveness factor, k= intrinsic rate constant)(Hajek and Murzin 2004)

Optimization of any process requires that the contributing rate steps are understood individually, and that their impact on the total process rate is quantifiable. The influence of external mass transfer is especially significant in the case of multiphase or three phase reaction systems, which are often mass-transfer limited when operated under industrial conditions. In transitional slug flow observed in the packed microreactor, mass transfer of hydrogen to the catalyst surface can take place either directly in the gas slug or indirectly in the liquid slug region. The schematic representation of these mass transfer steps is depicted in fig. 1.13. *Direct* mass transfer refers to transfer of hydrogen from the gas slug through the thin liquid film surrounding the catalyst surface while '*Indirect'* mass transfer refers to transfer of hydrogen across the gas/liquid interface, then through the liquid slugs to the catalyst surface. Both direct and indirect mass transfers contribute to the overall external mass transfer.

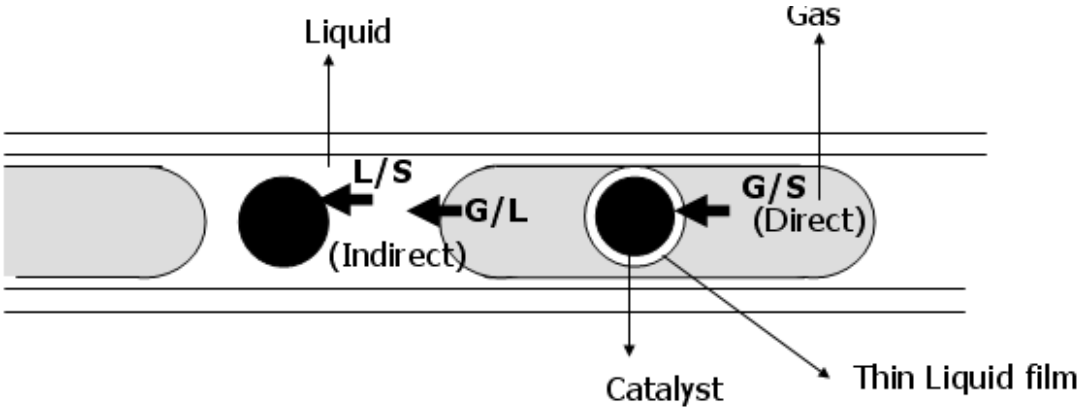

Fig. 1.13 Schematic representation of mass transfer steps in a packed bed microreactor

To evaluate the possible mass transfer limitations, an experimental approach and a theoretical calculation procedure will be presented.

III.3.5.1. Analysis of Internal Mass Transfer Effect

The rate at which the reactants diffuse into the pores within the catalyst particle is determined by internal mass transfer resistance. The reaction is considered to be under the control of internal mass transfer if the concentration of the reactants at the pore entrance is much higher than that inside the pore. The size of the catalyst particles is one of the most important factors influencing internal mass transfer resistance in catalytic reactions. Larger particles present longer pathways than smaller particles for the reactants inside the pores of the catalyst, and hence may limit the reaction. In the present study, both experimental and theoretical approaches are used to evaluate the effect of internal mass transfer on the overall rate of the reaction.

Experiments were conducted using two different catalyst particle size ranges, 45-75 micron (average size = 60 micron) and 75-150 micron (average size = 112 micron) at different hydrogen pressure and reactor temperature levels to determine the effect of catalyst particle size on the STY, and the conversion of the reactant. The feed was 1.299mol/L o-nitroanisole in methanol for all the runs. The liquid reactant solution flow rate was 0.05 ml/min, and the hydrogen gas flow rate was 5.0sccm.

Effect of particle size on the STY and conversion at different pressure levels

The effect of particle size on the space-time yield and conversion at three different pressure levels is shown in fig. 1.14. Both reactor performance parameters increase with increase in pressure but are nearly the same for the two particle sizes at all the pressure levels considered indicating that pore diffusion resistance for the reaction can be neglected in the particle size and pressure ranges utilized.

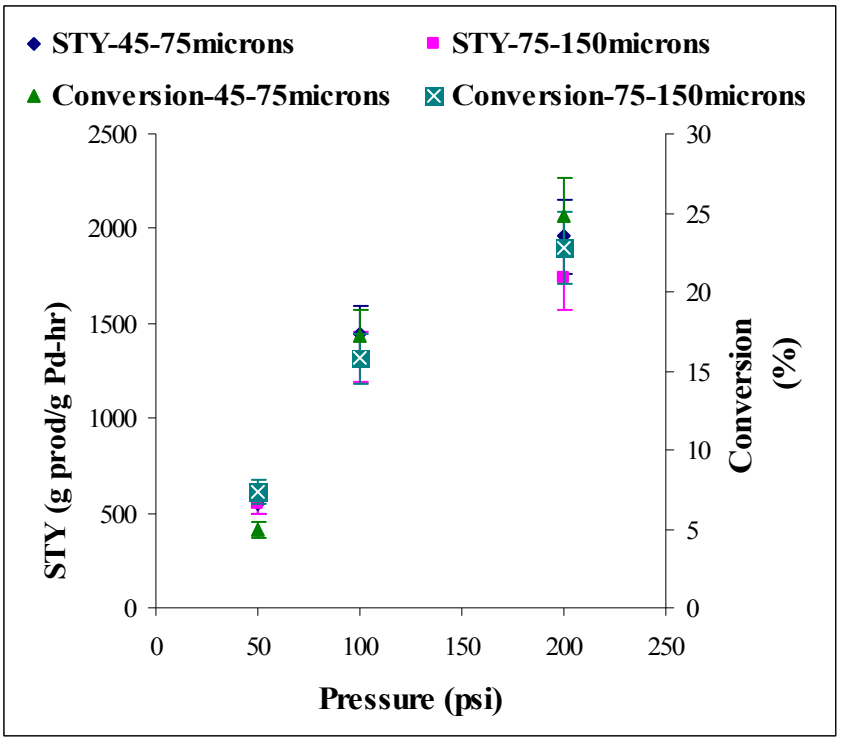

Fig. 1.14 Effect of particle size on STY and conversion at different pressures

(All runs were made with 1.299mol/L o-nitroanisole in methanol, liquid flow rate of 0.05 ml/min, H_2 flow rate = 5 sccm, 2.2 mg of 2% Pd/ Zeolite Catalyst and at 30^{o}C)

Effect of particle size on the STY and conversion at different temperatures

The effect of particle size on the STY and conversion at three different temperatures is shown in fig. 1.15. The data indicate that both reactor performance parameters at all the temperature levels considered are nearly the same for the two particle sizes utilized. Hence, pore diffusion resistance in the temperature range used can be neglected for these catalyst particle size ranges.

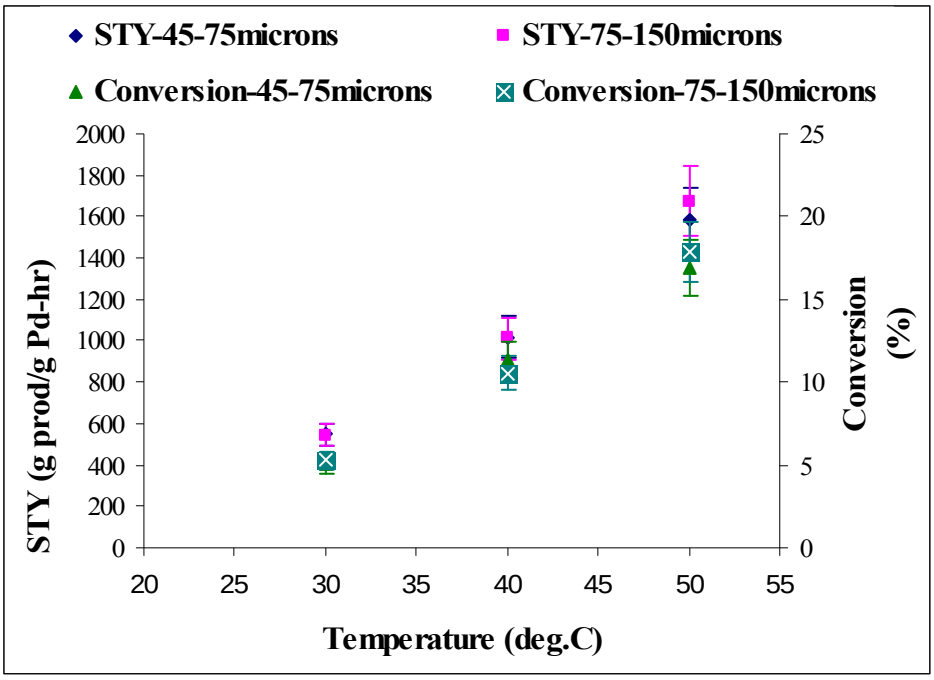

Fig. 1.15 Effect of particle size on STY and conversion at different temperature levels

(All runs were made with 1.299 mol/L o-nitroanisole in methanol, liquid flow rate of 0.05 ml/min, H_2 flow rate = 5 sccm, 2.2 mg of 2% Pd/Zeolite catalyst, at 50 psig pressure)

On the basis of the experimental data, it can be concluded that the influence of internal diffusion on the reaction rate can be neglected for the range of pressures and temperatures studied.

To further validate this conclusion, calculation of the catalyst effectiveness factor η_{eff} was performed. The magnitude of the effectiveness factor indicates the relative importance of diffusion and reaction limitations. First order approximations were used for calculating effectiveness factor for the reactant most limiting (i.e. for which the diffusivity multiplied by the driving force was smallest). Considering an irreversible reaction on a spherical catalyst particle, η_{eff} can be determined as a function of Thiele Modulus *(ϕ)* (Fogler 1992) from the following equation:

$$\eta_{eff} = \frac{3}{\phi^2}(\phi \coth \phi - 1) \tag{1.1}$$

where the Thiele Modulus is given by:

$$\phi = L\left(\frac{r_{obs}\rho_p}{C_s D_e}\right)^{1/2} \tag{1.2}$$

and L = Characteristic Length of the catalyst particle (cm)

r_{obs}= Observed reaction rate (mol/gcat-sec)

C_s =Concentration of the limiting reactant (hydrogen) on the surface of the catalyst obtained from the hydrogen solubility data (mol/cc)

ρ_p= Catalyst particle density (g/cc)

D_e= Effective diffusion coefficient of hydrogen in the particle (cm^2/sec)

The effective diffusion coefficient of hydrogen in the particle is defined as

$$D_e = D_m \frac{\delta\theta}{\tau} \qquad (4.3)$$

D_m is the hydrogen diffusion coefficient in the liquid reactant=$7.68*10^{-5}cm^2/sec$ (obtained from Wilke Chang Equation (Perry and Chilton 1973)). θ, δ and τ are the catalyst porosity, constriction factor and tortuosity factor respectively. For these parameters, the ranges are:
0.4-0.6 for θ, 0.7-0.8 for δ, and 2-8 for τ. From these ranges of values of the parameters, the Thiele Modulus and the effectiveness factors were calculated for the operating conditions used for the above experiments and the ranges are as shown in Table 1.1.

Table 1.1: Calculations for Thiele Modulus and Effectiveness Factor for the different experimental conditions

Pressure (psig)	**Temperature (deg.C)**	**Cs (mol/L)**	**STY (moles/gcat-sec)**	**$\phi_{min} \geq \phi \leq \phi_{max}$**		**$\eta_{min} \geq \eta \leq \eta_{max}$**	
				ϕ_{min}	**ϕ_{max}**	**η_{min}**	**η_{max}**
50	30	0.031301	2.47463E-05	1.78	0.68	0.837	0.97
100	30	0.0596256	6.53626E-05	2.09	0.8	0.79	0.96
200	30	0.0802689	8.84104E-05	2.1	0.8	0.791	0.96
50	30	0.031301	2.47463E-05	1.78	0.68	0.837	0.97
50	40	0.034111	4.59113E-05	2.323	0.887	0.76	0.95
50	50	0.0399577	7.15639E-05	2.68	1.02	0.71	0.936

The above calculations show that the effectiveness factor under the reaction conditions ranges from 0.7-0.97. This variation in η_{eff} can indicate the presence of some internal diffusion effects. However, this variation can also be attributed to experimental error arising from the non-uniform distribution of palladium active sites on the surface of the catalyst, when the catalyst was crushed to obtain the desired particle size. Since the effectiveness factor for these operating conditions is close to 1 ($\eta \rightarrow 1$), the calculations confirm the experimental data indicating that the hydrogen diffusion inside the catalyst pores does not affect the reaction rate.

III.3.5.2. Analysis of External Mass Transfer effect

As discussed above the external mass transfer of the reactants from the gas bulk to the surface of the catalyst takes place in a series of steps. First, the solute gas hydrogen diffuses through the gas phase to the gas–liquid interface, and then from the interface to the bulk liquid. Next the dissolved hydrogen and liquid reactant (o-nitroanisole in methanol) in the liquid phase are transferred to the external surface of the catalyst particle through the solid–liquid film. These reactants then reach the active catalytic centers where the reaction occurs, and the product diffuses out.

The gas-phase mass transfer resistance can be neglected as the gas phase is almost pure hydrogen (owing to the low vapor pressure of the solvent under reaction conditions). The gas–liquid interface is instantaneously saturated with hydrogen. The extent of resistance offered to mass transfer in the gas/liquid interface, and the transfer of dissolved hydrogen and o-nitroanisole in the liquid phase to the external surface of the catalyst particle depend greatly on the fluid velocity. An observed increase in the reaction rate with increase in the fluid velocity at constant temperature indicates that mass transfer to the catalyst is contributing significantly to

the overall reaction rate. However, if the fluid velocity is continually increased, a point is reached where the reaction becomes reaction-limited and consequently is independent of the fluid velocity. Therefore a good test for the presence of external mass transfer effects is to see if the reaction rate increases with increase in fluid velocity.

However, increasing the velocity in a packed bed reactor may be inconclusive in most cases because an increase in the flow velocity for the same length of the catalytic bed will, in addition to its effect on mass transfer increase the intrinsic rate of the reaction by increasing the average concentration (due to lower conversion at high velocities). This can be avoided by using catalyst beds of two different lengths and flow velocities, but same contact time (Satterfield 1970). At the same contact time, the linear velocity will be greater in the longer bed; and in the absence of mass transfer limitations, the concentration profile and the degree of conversion will be the same for the two cases. Therefore, experiments were conducted following the outlined approach to see the effect of overall flow velocity on the STY and determine the controlling regime in this gas-liquid-solid reaction.

Figure 1.16 shows the results obtained from these experiments which were conducted at a constant residence time by varying the gas and liquid flow rates proportionately with the catalysts amounts so as to obtain constant residence time. The data clearly show that the reaction rate is independent of the flow velocity, which indicates the absence of bulk external mass transfer limitations for the reaction under the present operating conditions.

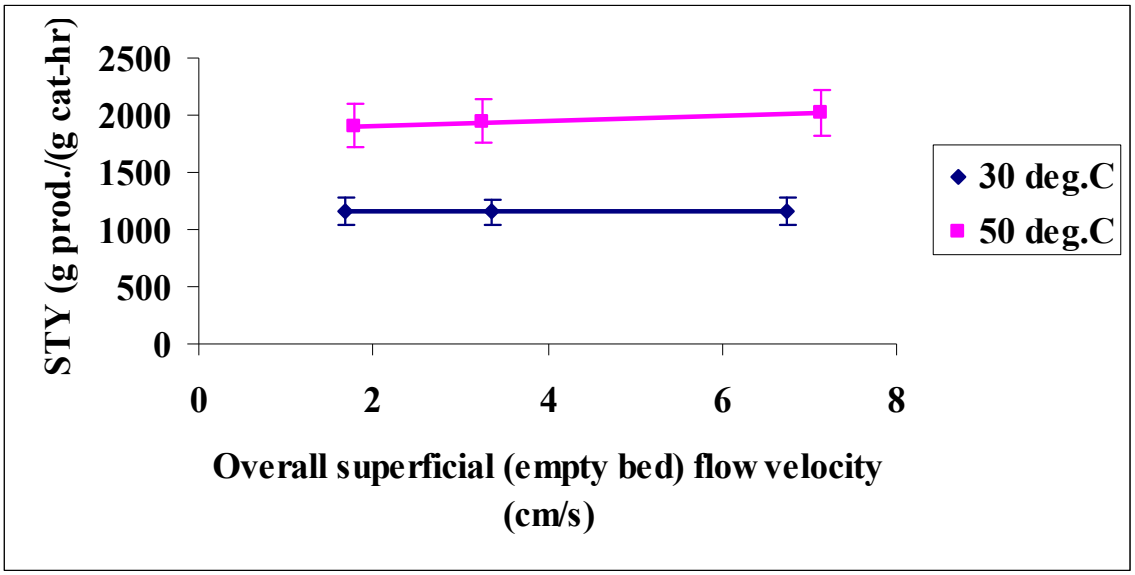

Fig. 1.16 Effect of overall flow velocity on reaction rate for the same residence time (All runs were made at reactor pressure of 100 psig and 1.299 mol/L o-nitroanisole in methanol)

To further validate this conclusion, some calculations were made to compare the observed experimental rate with the maximum mass transfer rates using known correlations in the literature for mass transfer coefficients in monolith and trickle bed reactors.

For the purpose of these calculations, the overall external mass transfer rate is split into two steps in series:

1) Gas-Liquid Mass Transfer
2) Liquid-Solid Mass Transfer

Gas-Liquid mass transfer:

The primary and the most fundamental rate process when conducting any liquid phase hydrogenation reaction is the mass transfer of the gas into the liquid reaction phase. In most industrial processes using pure hydrogen, the gas film mass transfer resistance can be ignored and mass transfer rates are dominated by liquid film resistance. The rate of the gas-liquid mass transfer can then be represented by the following expression

$$\text{Rate} = k_{gl}\, a_{gl}\, (C_{H2,\,sat} - C_{H2,\,bulk}) \qquad (1.4)$$

where k_{gl} =liquid side mass transfer coefficient (m/sec)

a_{gl}= gas-liquid interfacial area (m^2/m^3)

$C_{H2,sat}$ = Saturation concentration of hydrogen at the gas-liquid interface obtained from the hydrogen solubility data (mol/m^3)

$C_{H2,\,bulk}$ = Concentration of the hydrogen in the bulk liquid (mol/m^3)

The experimentally observed reaction rate is compared to the maximum mass transfer rate calculated from mass transfer coefficients obtained from empirical correlations in the literature, to demonstrate the impact of gas-liquid mass transfer.

The maximum rate of gas-liquid mass transfer corresponds to the case where the concentration gradient is maximum in other words $C_{H2,\,bulk}$ is essentially much smaller than $C_{H2,sat.}$ Assuming $C_{H2,sat} >> C_{H2,bulk}$, the maximum rate of mass transfer is obtained as the following expression:

Maximum Mass Transfer Rate = $k_{gl}\, a_{gl}\, C_{H2,sat}$

Three different correlations were used to estimate the value of $k_{gl}a_{gl}$

$k_{gl}\, a_{gl} = 0.05\ s^{-1}$	high estimate for mass transfer coefficient value for trickle bed reactors based on Versteeg, Visser, van Dierendonck, & Kuipers (1992) and Iliuta, Larachi, Grandjean & Wild (1999).
$k_{gl}\, a_{gl} = 0.02\ s^{-1}$	estimate for mass transfer coefficient value for trickle bed reactors based on S. Goto and J. M. Smith (1975)
$k_{gl}\, a_{gl} = 0.03\ s^{-1}$	estimate for mass transfer coefficient value for a monolith reactor based on Kreutzler, et al. (2001)

The maximum external mass transfer rate using these correlations was calculated for the reaction conditions at which the above experiments were conducted. Solubility data for H_2 in a mixture of o-nitroanisole-methanol were taken from the work of Brahme et al (1982). The saturation concentration of hydrogen in the 23% (w/w) o-nitroanisole in methanol reaction mixture at the reaction conditions of 30°C and 100psig is $59.6 mol/m^3$. Consequently, the calculated values of the maximum and minimum values of the maximum external mass transfer rate from the above correlations are $298 mol/m^3 s$ and 118 $mol/m^3 s$ respectively. The observed reaction rate at the same conditions was 24.12 $mol/m^3 s$. The comparison between the mass transfer rate values obtained from the correlations and the experimental rate may imply that external mass transfer is playing a significant role in the overall reaction rate.

However, an alternative approach was used to test if these correlations can be used to estimate the mass transfer rates for a microreactor. From the above expression of mass transfer rate, it is evident that it is dependent on the concentration gradient and the mass transfer coefficient. *Therefore a good test of the applicability of these correlations to microreactors would be to assume that the observed reaction rate is under mass transfer limited condition, calculate the concentration gradient by dividing the observed reaction rate with the mass transfer coefficients from the correlations and compare it to $C_{H2,\,sat}$, the maximum concentration*

gradient possible. The concentration gradients calculated using all the three correlations are much higher (484, 1210, 806.67 mol/m^3 respectively) than $C_{H2,sat}$ (59.6mol/m^3). An estimate of the gas-liquid mass transfer coefficient can be made from the observed reaction rate and the saturation concentration of hydrogen in the following manner:

$$k_{gl}a_{gl} = \frac{R_{obs}}{C_{H2\,sat}} = \frac{24.12}{59.6} = 0.4s^{-1}$$

This value represents the lowest value of mass transfer coefficient in the microreactor under these reaction conditions which implies that the actual mass transfer coefficient in the microreactor is much higher than the estimates (0.05s^{-1}) obtained from these correlations. Yeong et al. 2003, 2004) also showed that the standard correlations for mass transfer in conventional reactors may not always be applicable in microscale reactor configurations. Therefore, our assumption that the observed reaction rate is under mass transfer limited condition is wrong. Hence, it can be concluded that the reaction is not mass transfer limited at the gas-liquid interface.

Liquid Solid Mass Transfer:

The transfer of hydrogen from the bulk liquid phase to the surface of the catalyst is designated as Liquid Solid Mass Transfer, the rate of which is defined by the following expression:

$$\text{Rate} = k_{ls}\, a_{ls}\, (C_{H2,\,bulk} - C_{H2,\,s}) \qquad (1.5)$$

where k_{ls} =liquid/solid mass transfer coefficient (m/sec)

a_{ls}= external surface area of the catalyst particles (m^2/m^3)

$C_{H2,bulk}$ = Concentration of hydrogen in the bulk (mol/m^3)

$C_{H2,\,s}$ = Concentration of the hydrogen at the solid/liquid interface (mol/m^3)

In the kinetic region, $C_{H2,\,bulk} \cong C_{H2,\,s;}$ thus $C_{H2,\,bulk} - C_{H2,\,s} \rightarrow 0$.

The experimentally obtained rate of hydrogen consumption was 24.12 mol/m^{3}s under the experimental conditions stated above. For the calculation of mass transfer rate at the liquid-solid interface, the mass transfer coefficient is obtained from theoretical correlation. A correlation (Natividad et al. 2004) that is used to determine the liquid-solid mass transfer coefficient in a monolith reactor is:

$$k_{ls} = \frac{ShD_{H2}}{d_h} \qquad (1.6)$$

where $$Sh = 20[1 + 0.003(\frac{L}{d_h \,\mathrm{Re}.Sc})^{-0.7}]$$

Re= Reynolds number

Sc=Schmidt number

L=Slug length =0.005m (obtained experimentally)

D_{H2}= diffusivity of hydrogen in the liquid obtained from Wilke Chang equation (Perry and Chilton 1973) (cm^2/sec)

d_h= hydraulic diameter (cm)

Another correlation commonly used to determine liquid-solid mass transfer coefficient for the trickle bed reactor (Satterfield 1970) is:

$$k_{ls} = 1.64(\mathrm{Re})^{-0.331}(\frac{\rho D_{H2}}{\mu_l})^{2/3} u_l \qquad (1.7)$$

where ρ=liquid density (kg/m^3)

μ_l =Liquid viscosity (Kg-m/sec)

u_l = Liquid superficial velocity (m/sec)

Under the present experimental conditions, the liquid-solid mass transfer coefficient from both correlations was estimated to be 0.0362 and 0.0135cm/sec respectively. Considering a spherical catalyst particle of diameter 75μm, the liquid-solid interfacial area of the catalyst was calculated as 35,000 m^2/m^3. Calculation of the concentration gradient between the liquid bulk and the particle surface was obtained from the observed rate and the mass transfer coefficient as follows:

$$C_{H2,\,bulk} - C_{H2,\,s} = \text{Rate}/\, k_{ls}\, a_{ls} \qquad (1.8)$$

The concentration gradients calculated for both correlations were 1.91 and 5.14 mol/m^3 respectively. These values are compared to the value of the maximum concentration gradient possible which is $C_{H2,sat}$ (59.6 mol/m^3) to demonstrate the role of liquid-solid mass transfer. If the ratio between the observed concentration gradient and the maximum concentration gradient is less than 0.1, then the reaction is said to be in kinetic region. For the above calculated concentration gradients, these ratios are 0.03 and 0.08 respectively. Therefore, one can convincingly conclude that liquid film diffusion does not limit the reaction rate. The calculations and the experimental data confirm that the reaction is not mass transfer limited under the operating conditions utilized in the experiments.

III.3.5.3. Analysis of heat transfer effects

Apart from mass transfer limitations, heat transfer limitations can also have significant effect on the kinetics of the reaction. The intrusion of heat transfer resistances inside the reactor can lead to severe degradation in the catalyst's performance thus completely masking the true kinetics of the reaction. Efficient heat removal from the reactor is essential especially for hydrogenation reactions which are highly exothermic in nature. To ensure that the kinetic data obtained in an experimental reactor reflect only kinetic effects, the temperature gradients must be eliminated from three domains: Intraparticle within the individual catalyst particles, interphase between the external surface of the particles and fluid adjacent to them, and interparticle between the local fluid regions or catalyst particles. Certain criteria are available in the literature (Mears 1971a, 1971b) to estimate whether heat transport effects in any domain are significantly affecting the experimental results. Mears 1971a suggested that the heat transfer resistances are generally in the order of interparticle > interphase > intraparticle when the Biot number (Bi) is much smaller than 10. The Biot number expresses the ratio of thermal resistance of the particle to that of the film around the particle.

$$Bi = \frac{h d_p}{\lambda} \qquad (1.9)$$

In this calculation, d_p is the diameter of the catalyst particle ~100μm; the heat transfer coefficient (h) for the reactants is within the range of 10-100 W/m^2-K [147] and the effective thermal conductivity (λ) is in the order of 0.1 W/m-K for the porous catalyst (Ajmera et al. 2002) The calculated Biot number (0.0375) is much smaller than 10 which implies that the effect of interparticle heat transfer resistance is predominant over interphase or intraparticle heat transport resistance. Interparticle heat transport occurs both radially and axially within the reactor. Axial heat transport effect can be neglected if the ratio of axial length of the reactor is much greater (>20) than the catalyst particle size. In the present study, since the microreactor length at typical reaction conditions is much greater than the catalyst particle size (>30 times), axial heat conduction can be neglected. However, radial heat transfer effect cannot be assumed to be negligible because radial temperature gradients can lead to reaction rates several thousand folds

greater at the axis of the reactor than at the wall due to the absence of heat removal pathway from the axis of the reactor to the environment. A criterion for qualitative analysis of radial heat transport limitations is given by the Damkőhler number for heat transfer (D_a) (Mears 1971a) which is defined by the following equation:

$$D_a = \left| \frac{-\Delta H(-r_{obs})(1-\varepsilon)R_o^2}{\lambda T_w(1+b)} \right| < 0.4\frac{RT_w}{E_a} \qquad (1.10)$$

If the left hand side of the above equation is smaller than the right hand side, the radial temperature difference in the reactor would be less than 5%. In the calculations, ΔH the heat of the reaction is 536 kJ/mole; the observed reaction rate (r_{obs}) from the experiments was obtained to be 42.12mol/m^3s at a temperature (T_w) of 30°C, the radius of the tubular reactor (R_o) is 0.0003875m, ε is the bed porosity which is assumed to be 0.3 and, b is the ratio of diluent to catalyst volume which is 49. The activation energy for the reaction was obtained from the literature as 43.83 kJ/mole (Chaudhari et al. 1983). The calculations show that the left hand side (2899) is one order of magnitude smaller than the right hand side (30,500). Hence, it can be concluded that the radial heat transfer effects can be neglected in the micro reactor.

With all the above considerations, overall it can be concluded that under the present operating/processing conditions the reaction is controlled by surface kinetics and not significantly influenced by mass and heat transfer resistances.

III.3.5.4. Rate Analysis using differential method

A literature review of the intrinsic kinetics of nitro group hydrogenation presents a confusing description of the overall process kinetics, with the investigators reporting reaction orders for nitro compound and hydrogen between zero and one depending upon reaction conditions (Chaudhari et al. 1983; Hatziantoniou et al 1986; Tong et al. 1978; Acres and Cooper 1972; Hernandez and Nord 1947; Hernandez and Nord 1948; Smith and Bedoit 1951; Smith and Bedoit 1955). Most kinetic studies are based on global kinetic rate models based on hydrogen consumption and overall conversion. This does not fully explain the role of individual intermediates species involved in the reaction. As was discussed earlier, in this study the overall reaction was considered to be a process comprising two consecutive reactions, one leading to the formation of 2-methoxynitrosobenzene, and the other leading to the formation of o-anisidine. Experiments were conducted in the microreactor under different conditions to determine the kinetic rate expressions for both reactions. The conversion in the microreactor was limited to 10% so that a differential reactor can be assumed to find the dependence of the reaction rates on the reactant concentrations.

Dependence of rate of disappearance of o-nitroanisole on hydrogen concentration

The effect of hydrogen concentration on the rate of disappearance of o-nitroanisole was investigated in a range of 50-300psig, at temperatures of 30, 40 and 50°C and o-nitroanisole concentration of 1.299 mol/L in methanol. The results are presented in fig. 1.17. The rate of disappearance of o-nitroanisole increases with increase in hydrogen concentration. The slope of the line obtained by plotting log (Rate) against log (hydrogen concentration) would give the dependency of the rate on hydrogen concentration. Figure 1.18 shows the logarithmic plot of the rate against hydrogen concentration. The slopes of the lines shown in fig 1.18 represent the orders of rate dependence on hydrogen concentration. The values of the slope indicate that the

rate follows different orders with respect to concentration of hydrogen at different temperatures. This suggests that simple power law models cannot be used for the rate expression.

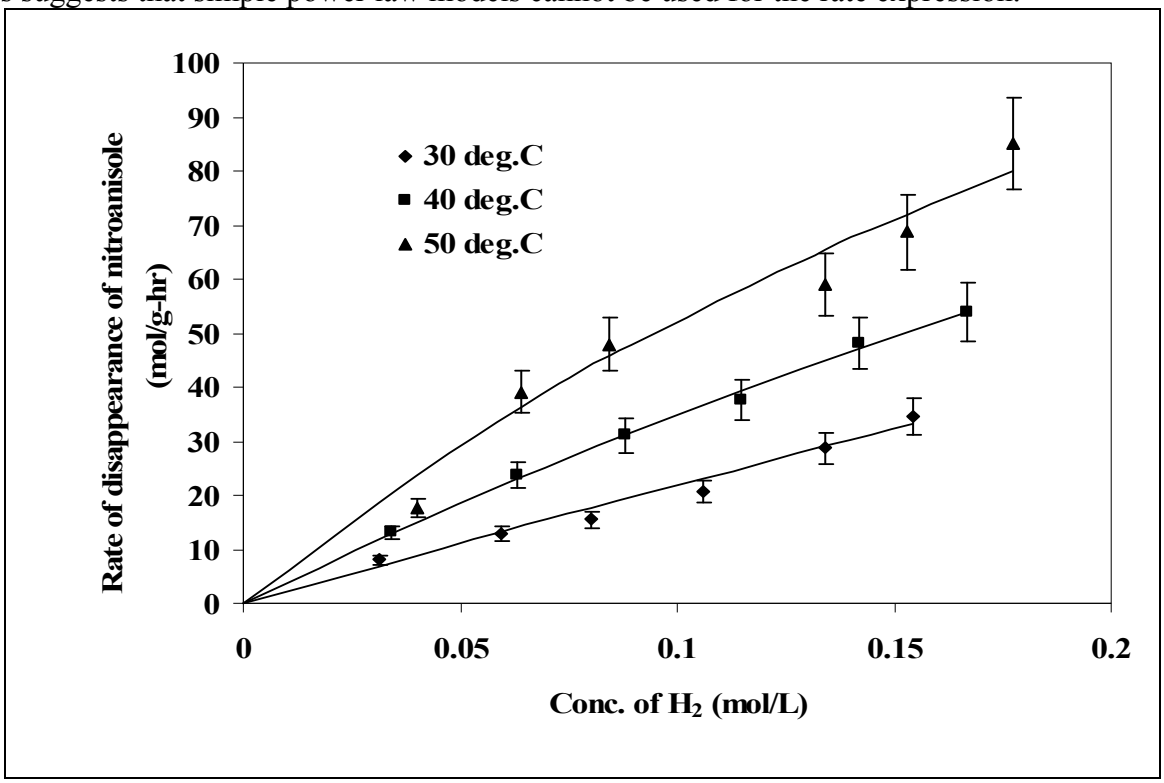

Fig. 1.17 Effect of H_2 concentration on the reaction rate of disappearance of o-nitroanisole

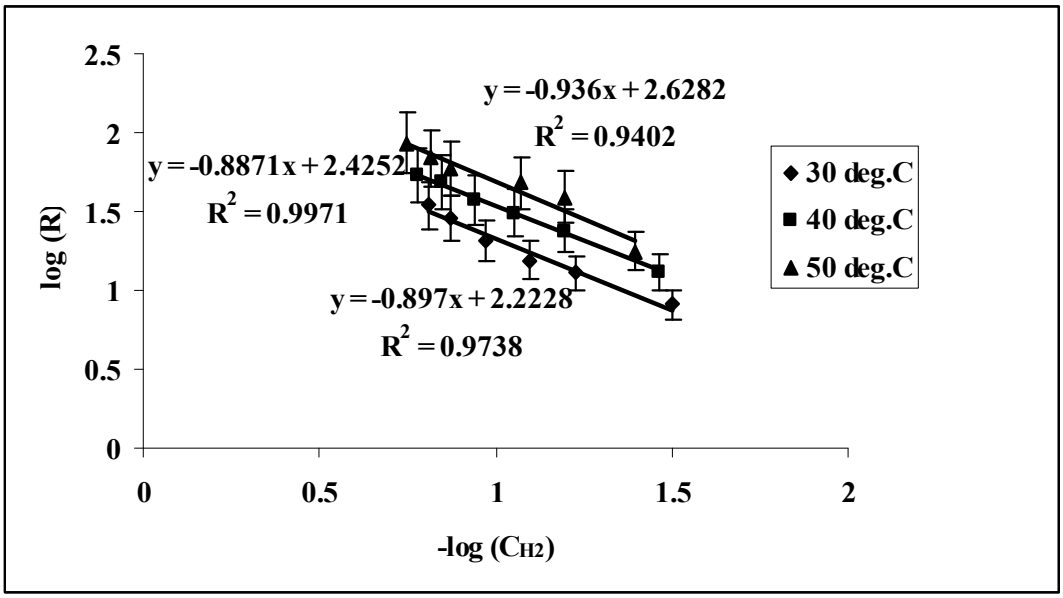

Fig. 1.18 Plot of logarithm of rate of disappearance of o-nitroanisole vs. logarithm of hydrogen concentration

Dependence of rate of disappearance of o-nitroanisole on the concentration of o-nitroanisole

The effect of o-nitroanisole concentration on the rate of disappearance of o-nitroanisole was investigated in the concentration range of 0.1 to 2 mol/L (2-30% (w/w) o-nitroanisole in

methanol) at temperatures of 30, 40 and 50°C, and a hydrogen partial pressure of 100 psig. The results are presented in fig. 1.19. The rate of disappearance of o-nitroanisole increases somewhat linearly with increase in o-nitroanisole concentration up to a certain concentration and then remains constant, for all temperatures. The order of the dependence of rate of disappearance on the o-nitroanisole concentration cannot be determined because of different trends observed at different concentration ranges for all temperatures.

Therefore the rate of disappearance of o-nitroanisole cannot be expressed as simple powers of hydrogen and o-nitroanisole concentrations. This suggests that Langmuir Hinshelwood expression should be considered for the rate equation.

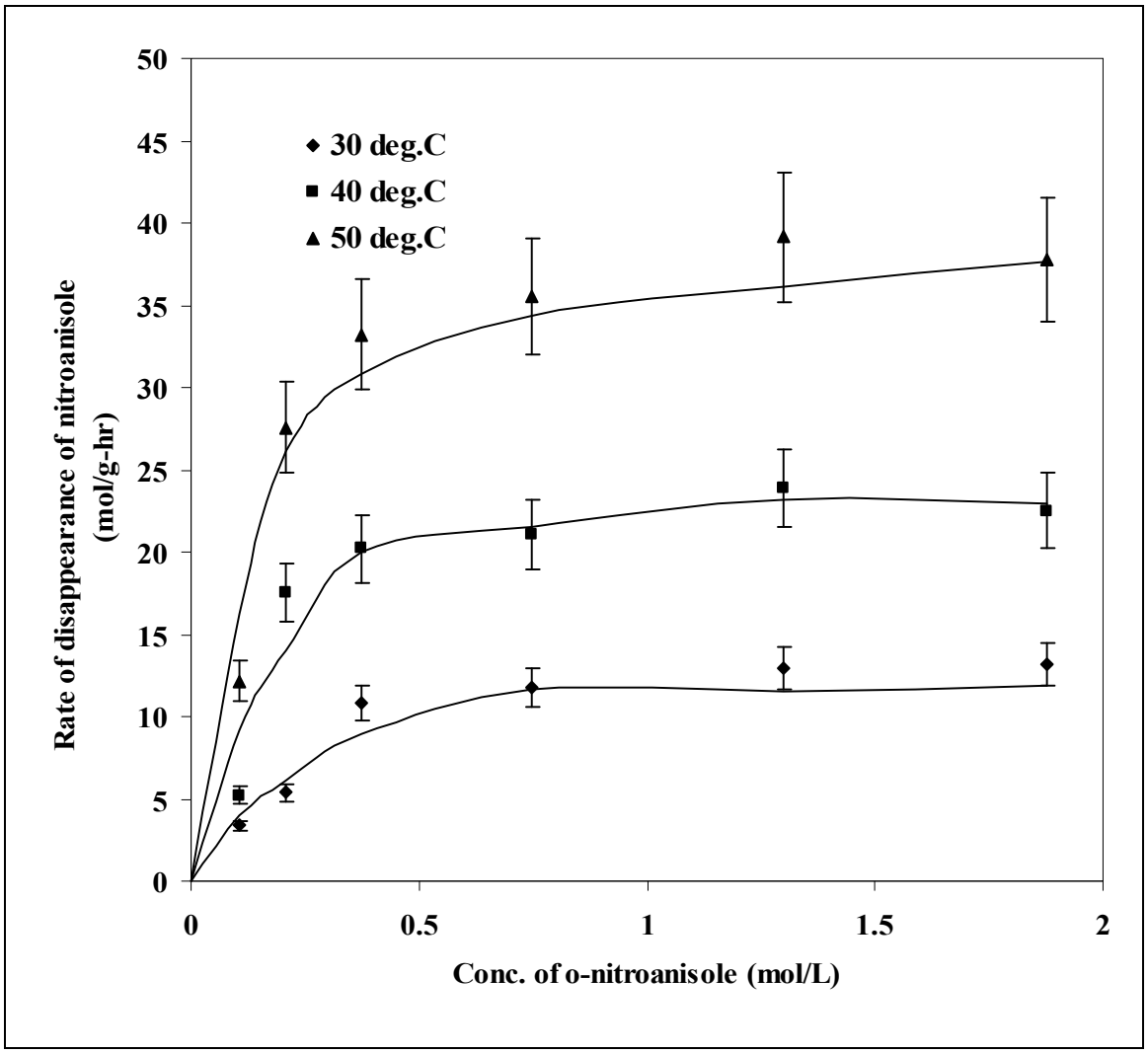

Fig. 1.19 Effect of o-nitroanisole concentration on the rate of disappearance of o-nitroanisole

Dependence of rate of formation of o-anisidine on hydrogen concentration

The effect of hydrogen concentration the rate of formation of o-anisidine was investigated in a range of 50-300psig at temperatures of 30, 40 and 50°C, and o-nitroanisole concentration of 1.299 mol/L in methanol. The results are presented in fig. 1.20. The average rate of o-anisidine formation increases linearly with increase in hydrogen concentration. To determine the dependence of the rate on the order of hydrogen concentration, a logarithmic plot of the rate

against hydrogen concentration was made as shown in fig. 1.21. The figure indicates that the rate follows different orders with respect to concentration of hydrogen at different temperatures.

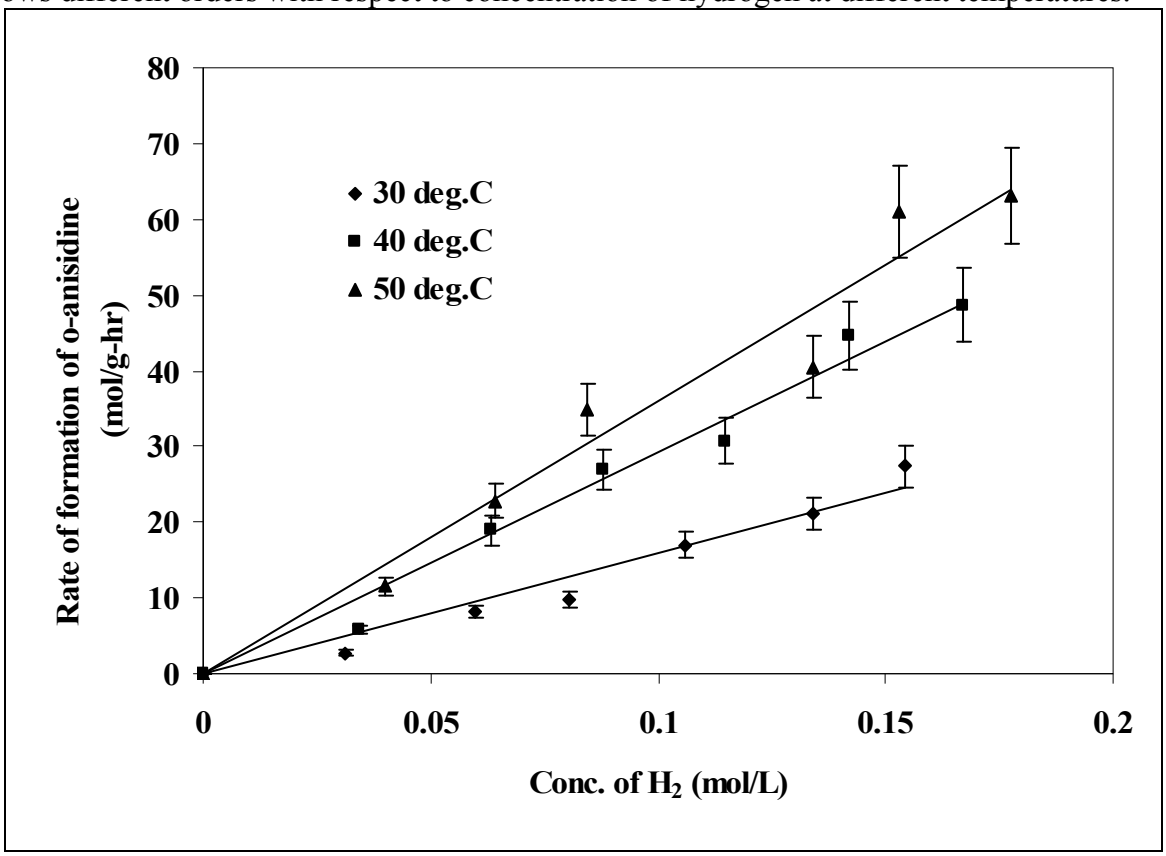

Fig. 1.20 Effect of H_2 concentration on the reaction rate of formation of o-anisidine

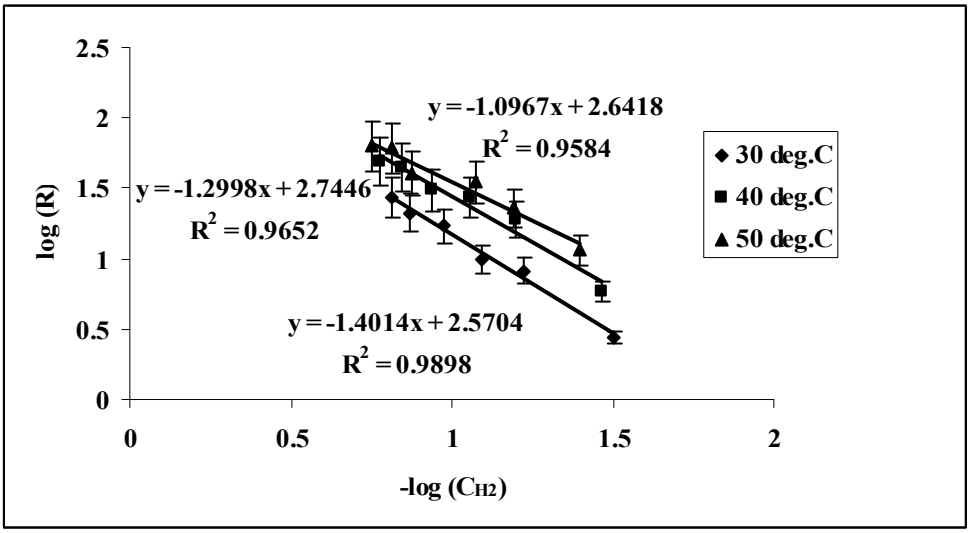

Fig. 1.21 Plot of logarithm of rate of formation of o-anisidine vs. logarithm of hydrogen concentration

Dependence of rate of formation of o-anisidine on the concentration of o-nitroanisole

The effect of o-nitroanisole concentration on the rate of formation of o-anisidine was investigated in a range of 0.1 to 2 mol/L (2-30% (w/w) o-nitroanisole in methanol), at temperatures of 30, 40 and 50^{o}C, and a hydrogen partial pressure of 100psig. The results are presented in fig. 1.22. The rate first increases with o-nitroanisole concentration, attains a maximum value and then decreases with further increase in o-nitroanisole concentration. *Comparison of fig. 1.19 and fig. 1.22 indicates that the rate of o-nitroanisole disappearance is higher than the rate of formation of o-anisidine at the same conditions.*

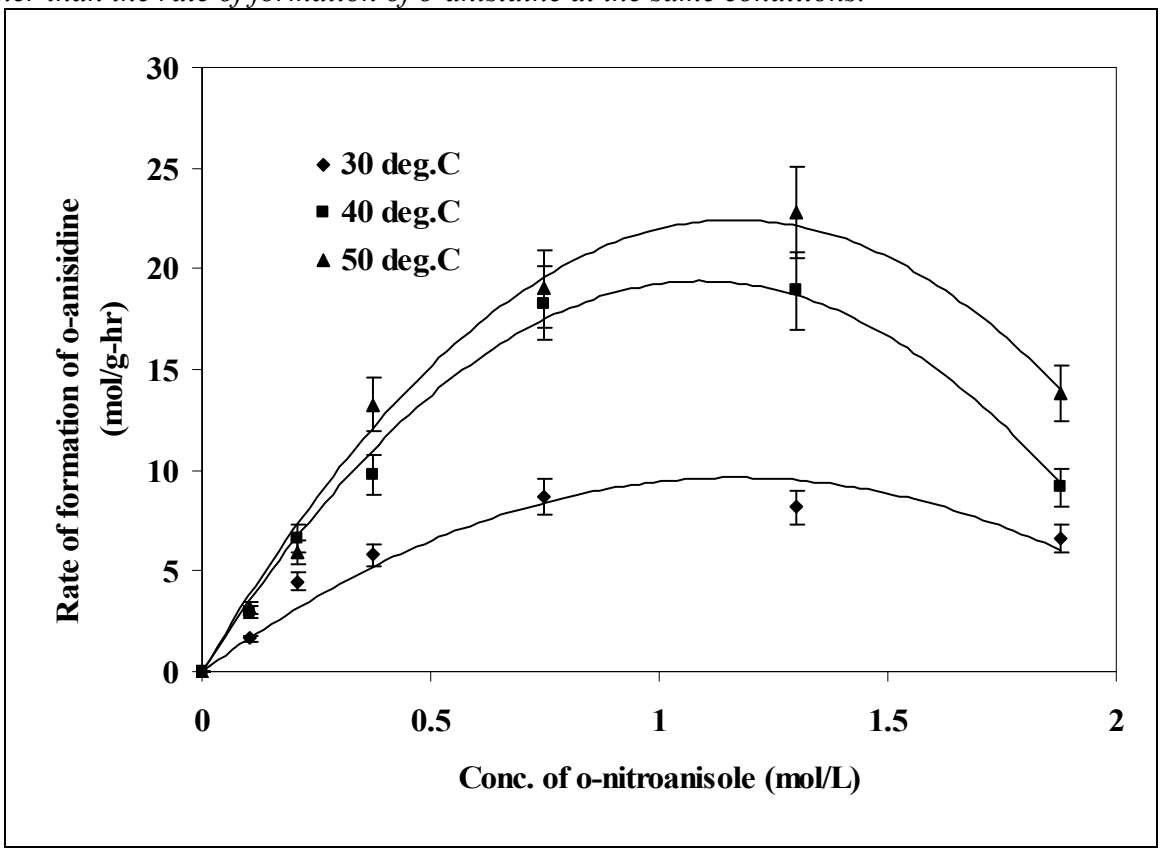

Fig. 1.22 Effect of o-nitroanisole concentration on the rate of formation of o-anisidine

The difference between the rate of disappearance of o-nitroanisole, and the rate of formation of o-anisidine at same o-nitroanisole concentration in the differential reactor is an indication of the presence of an intermediate(s). The intermediate 2-methoxy-nitrosobenzene is present in the product stream at low conversions of o-nitroanisole (fig. 1.23). Therefore the overall kinetics of o-nitroanisole hydrogenation to o-anisidine is split into two rate equations derived for the two consecutive reactions shown in fig. 1.23.

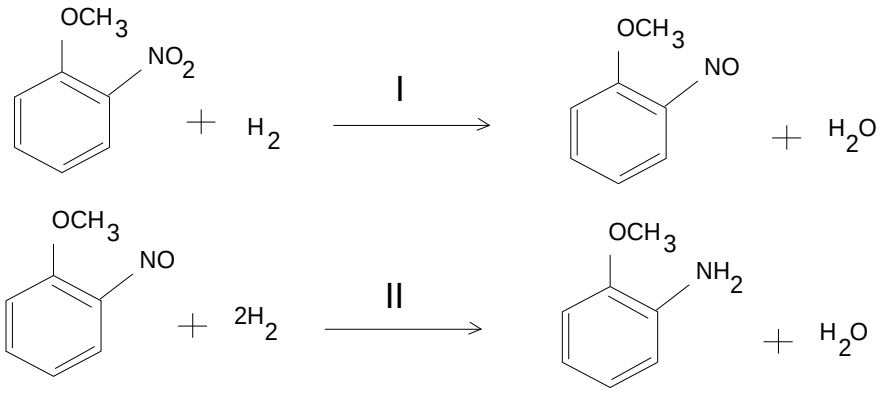

Fig. 1.23 Reaction pathway for the hydrogenation of o-nitroanisole

III.3.5.5. Kinetic modeling

The rate data obtained were fitted to different rate equations based on Langmuir-Hinshelwood (L-H) or Eley-Rideal type models. In order to estimate the kinetic constants, the individual rate equations were subjected to a nonlinear regression analysis using polymath. The non-linear regression analysis was performed to estimate the kinetic constants such that the difference between the experimental and the predicted rate has a minimum value. The regression analysis on the experimental data was performed purely on the mathematical basis and therefore did not account for the thermodynamic significance of the kinetic constants. Several models based on different mechanisms and different rate limiting steps were used for regression analysis (Chaudhari et al. 1983; Hatziantoniou 1986; Winterbottom 1981). However, some of these models involve complex rate equations which are based on complex mechanisms and hence often fail to fit the experimental data (Hatziantoniou 1986). For simple reactions like these, it is possible to formulate different rate equations using L-H approach. The L-H model for catalytic reactions typically involves a sequence of three catalytic steps:

1. Adsorption of the reactants
2. Surface reaction
3. Desorption of the products.

For each of the individual reactions shown in fig. 1.23, these steps occur on palladium sites represented by (s). The mechanistic schemes for both reactions are shown in figs. 1.24 & 1.25 respectively.

Reaction 1

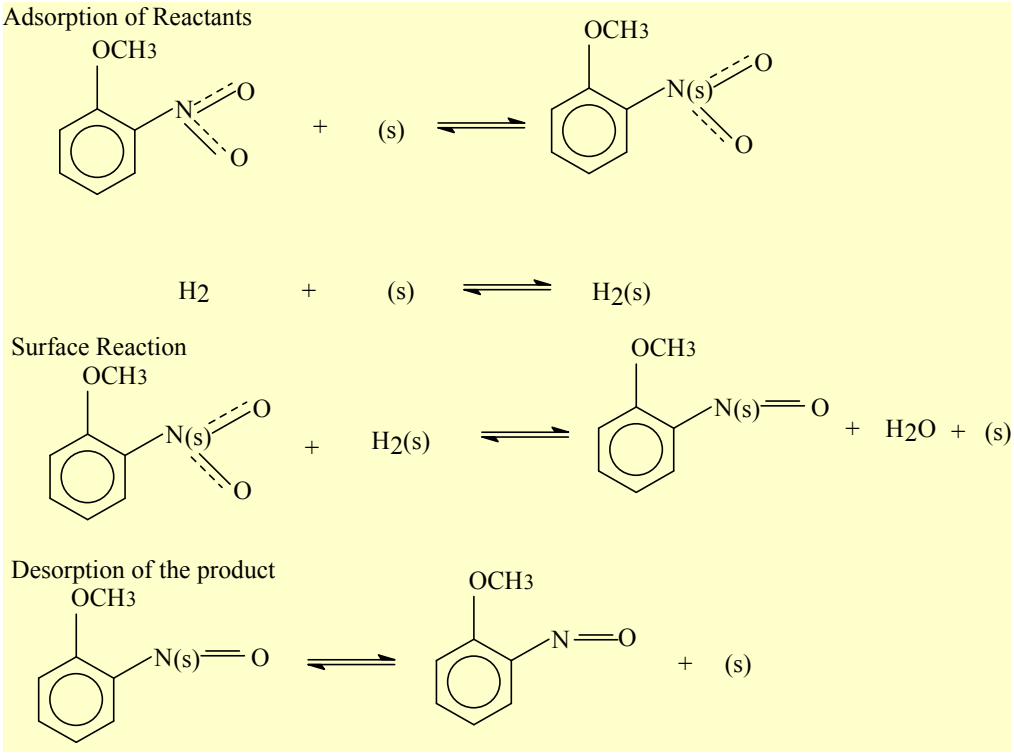

Fig. 1.24 Mechanistic scheme for Reaction 1

Although the mechanisms shown in figures 1.24 & 1.25 correspond to non-dissociative adsorption of hydrogen, dissociative adsorption of hydrogen was also considered. Based on these mechanisms, different rate equations are derived considering each step as the rate limiting step for both the reactions. These rate equations are listed in Table 1.2. The values for the kinetic constants obtained from these rate equations had to satisfy certain conditions, which are derived from the thermodynamic and optimization considerations. These constraints are

Rule 1: $k > 0$ (k should be a positive value)

Rule 2: $E_a > 0$ (Activation energy should be positive)

Rule 3: R^2 (Optimization variable) >95%

Rule 4: The confidence intervals of the parameter values should be much less than the values themselves.

Reaction 2

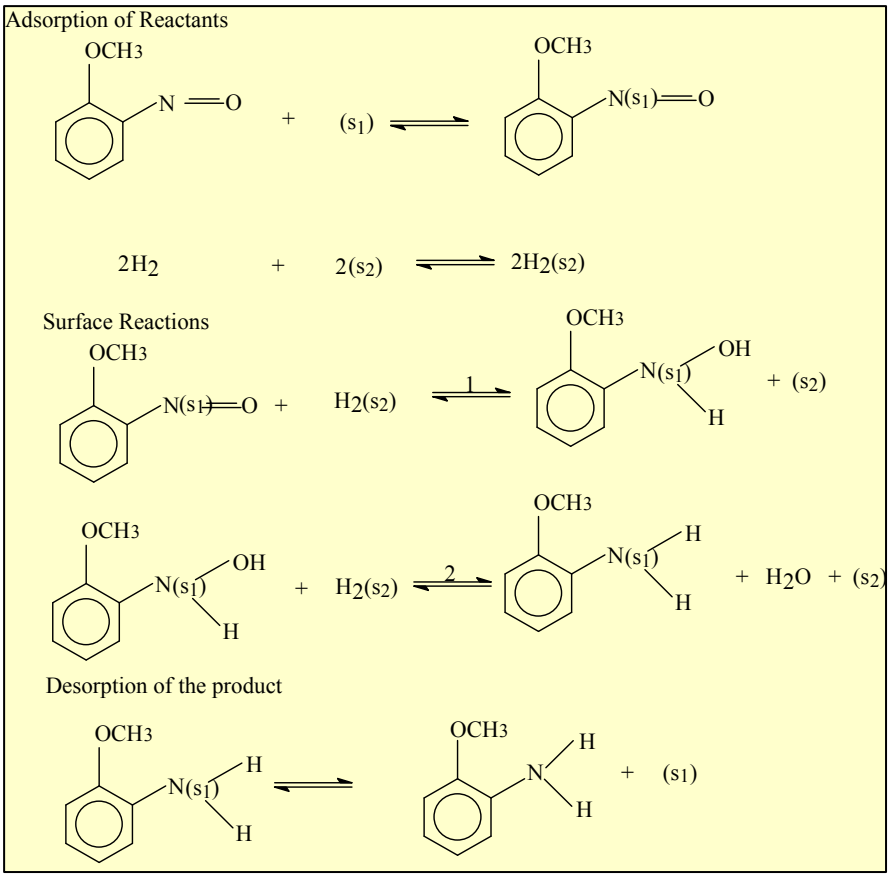

Fig. 1.25 Mechanistic scheme for Reaction 2

Based on all of the above criteria, the rate equations (from table 1.2) that best fitted the experimental data for reactions I and II are the following:

For reaction I (desorption of the product controlling)

$$r_1 = k_I(C_{H2}C_N)/((1+(K_NC_N))(1+(K_{H2I}C_{H2}))) \quad (1.11)$$

For reaction II (surface reaction controlling)

$$r_2=k_{II}(K_{H2II}C_{H2})(K_IC_I)/((1+(K_IC_I))(1+(K_{H2II}C_{H2}))) \quad (1.12)$$

where, k_I and k_{II} are the rate constants for reactions I and II respectively, K_N, K_{H2I}, K_I and K_{H2II} are equilibrium constants of nitroanisole in the presence of hydrogen, hydrogen (for reaction I) in the presence of o-nitroanisole, 2-nitrosomethoxybenzene in the presence of hydrogen and hydrogen (for reaction II) in the presence of 2-nitrosomethoxybenzene respectively. C_{H2}, C_N and C_I are concentrations of hydrogen, o-nitroanisole and 2-nitrosomethoxybenzene respectively. The concentration of hydrogen in the liquid (C_{H2}) in these expressions was calculated using hydrogen partial pressure in conjunction with the Henry's law constant obtained from the work of Brahme et al (1982).

The values of the kinetic constants obtained using the optimization program for these models are given in Table 1.3.

Table 1.2: Rate equations derived from L-H mechanism

Reaction 1- Non-dissociative adsorption of hydrogen

No.	Rate limiting step	Rate equation
1	Adsorption of o-nitroanisole	$R=k_I(C_N)/(1+(K_{H2I}C_{H2}))$
2	Adsorption of Hydrogen	$R=k_I(C_{H2})/(1+(K_NC_N))$
3	Surface Reaction	$R=k_I(K_{H2I}C_{H2})(K_NC_N)/(1+(K_NC_N)+(K_{H2I}C_{H2}))^2$
4	Desorption of 2-methoxy nitroso benzene	$R=k_I(C_{H2}C_N)/((1+(K_NC_N))(1+(K_{H2I}C_{H2})))$
Reaction 1- Dissociative adsorption of hydrogen		
1	Adsorption of o-nitroanisole	$R=k_I(C_N)/(1+(K_{H2I}C_{H2})^{0.5})$
2	Adsorption of Hydrogen	$R=k_I(C_{H2})^{0.5}/(1+(K_NC_N))$
3	Surface Reaction	$R=k_I(K_{H2I}C_{H2})^{0.5}(K_NC_N)/(1+(K_NC_N)+(K_{H2I}C_{H2})^{0.5}))^2$
4	Desorption of 2-methoxy nitroso benzene	$R=k_I(C_{H2}{}^{0.5}C_N)/((1+(K_NC_N))(1+(K_{H2I}C_{H2})^{0.5}))$
Reaction 2- Non-dissociative adsorption of hydrogen		
1	Adsorption of 2-methoxy nitroso benzene	$R=k_{II}(C_I)$
2	Adsorption of Hydrogen	$R=k_{II}(C_{H2})$
3	Surface Reaction 1	$R=k_{II}(K_{H2II}C_{H2})(K_IC_I)/((1+(K_IC_I))(1+(K_{H2II}C_{H2})))$
4	Surface Reaction 2	$R=k_{II}K(K_{H2II}C_{H2})^2(K_IC_I)/((1+(K_IC_I)+(K_aK_I K_{H2II}C_IC_{H2}))(1+(K_{H2II}C_{H2})))$
5	Desorption of o-anisidine	$R=k_{II}K(K_{H2II}C_{H2})^2(K_IC_I)/((1+(K_IC_I)+(K_aK_I K_{H2II}C_IC_{H2}(1+(K_bK_{H2II}C_{H2})))$
Reaction 2- Dissociative adsorption of hydrogen		
1	Adsorption of 2-methoxy nitroso benzene	$R=k_{II}(C_I)/(1+(K_{H2II}C_{H2})^{0.5})$
2	Adsorption of Hydrogen	$R=k_{II}(C_{H2})^{0.5}/(1+(K_IC_I))$
3	Surface Reaction 1	$R=k_{II}(K_{H2II}C_{H2})^{0.5}(K_IC_I)/((1+(K_IC_I))(1+(K_{H2II}C_{H2})^{0.5}))$
4	Surface Reaction 2	$R=k_{II}K(K_{H2II}C_{H2})(K_IC_I)/((1+(K_IC_I)+(K_aK_I C_I(K_{H2II}C_{H2})^{0.5})(1+(K_{H2II}C_{H2})^{0.5}))$
5	Desorption of o-anisidine	$R=k_{II}K(K_{H2II}C_{H2})(K_IC_I)/((1+(K_IC_I)+(K_aK_I$

		$C_I(K_{H2II}C_{H2})^{0.5}(1+(K_bK_{H2II}C_{H2})^{0.5}))$

Table 1.3: Kinetic constants and regression coefficients for the reactions

Reaction I				
Temp. (deg.C)	**k_I (L^2/g-hr-mol)**	**K_N (L/mol)**	**K_{H2I} (L/mol)**	**R^2**
30	620.15±4.06	2.00±0.018	0.24±0.006	0.97
40	1556.07± 6.67	3.14±0.017	1.38±0.04	0.984
50	3100.00±18.69	3.93± 0.03	2.61± 0.06	0.965
Reaction II				
Temp. (deg.C)	**k_{II} (mol/g-hr)**	**K_I (L/mol)**	**K_{H2II} (L/mol)**	**R^2**
30	149.1± 0.045	11.09±0.084	2.25±0.01	0.954
40	216.9±1.57	6.78±0.096	4.02± 0.04	0.972
50	404.99±3.75	3.29± 0.044	4.41± 0.06	0.957

In order to assess the adequacy of the rate equations and the accuracy of the kinetic constants, the results of the best fits were analyzed by comparing the experimental and predicted rates for both reactions as shown in figs. 1.26 and 1.27 respectively. It is evident from these figures that the predicted rates agree with the experimental rates within 10%. The activation energies and heat of adsorption of the reactants for reactions I and II were determined from the kinetic constants using the Arrhenius equations:

For rate constant

$$k = k_o e^{\frac{-Ea}{RT}} \tag{1.13}$$

For equilibrium constants

$$K = K_o e^{\frac{-\Delta H}{RT}} \tag{1.14}$$

where k is the rate constant for the reaction, k_0 is the pre-exponential factor for the reaction, Ea is the activation energy for the reaction, K is the equilibrium constant for the reactant in the presence of other reactant, K_0 is the pre-exponential factor for the reactant in the presence of other reactant, ΔH is the heat of adsorption for the reactant in the presence of other reactant and T is the temperature in Kelvin. The pre-exponential factors, activation energies and heat of adsorption of reactants calculated using the Arrhenius equations for various kinetics constants are given in Table 1.4. The values of activation energies for the two reactions compare favorably to the literature value of 43.83kJ/mol obtained from the work of Chaudhari et al 1983.

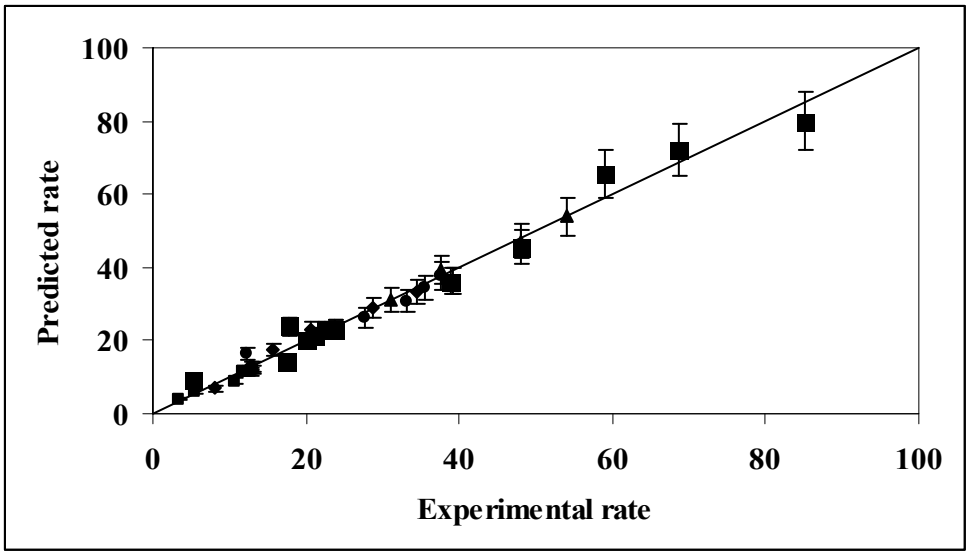

Fig. 1.26 Experimental and predicted rates for reaction I using equation (1.11)

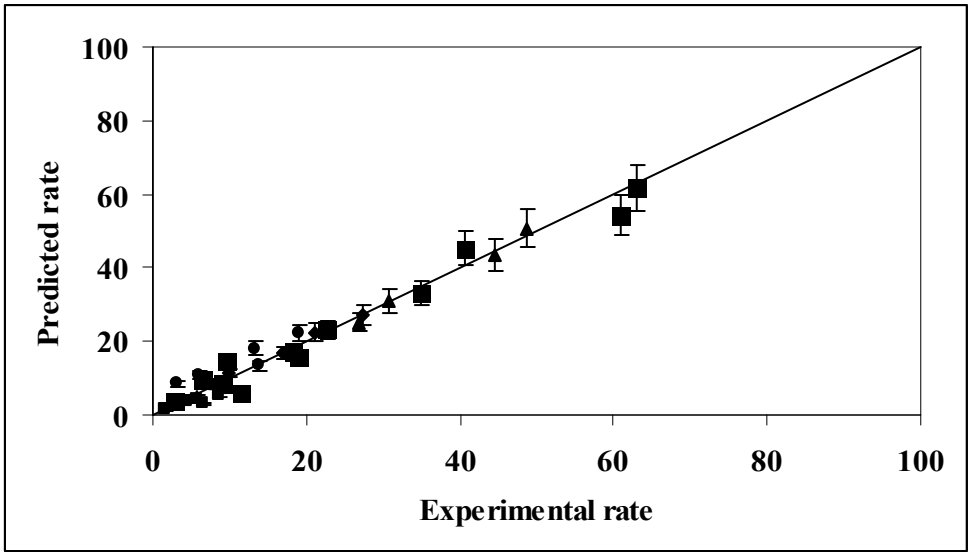

Fig. 1.27 Experimental and predicted rates for reaction II using equation (1.12)

Table 1.4: Pre-exponential factors, activation energies and heats of adsorption for the reactions

Pre-exponential factor	
Reaction I	
k_{I0} (L^2/g-hr-mol)	1.27E+14
K_{N0} (L/mol)	1.08E+05
K_{H2I0} (L/mol)	1.26E+16
Reaction II	
k_{II0} (mol/g-hr)	1.37E+09
K_{I0} (L/mol)	3.59E-08
K_{H2II0} (L/mol)	1.35E+05

Activation energy and heats of adsorption	
Reaction I	
Ea (kJ/mol)	65.55
ΔH_N(kJ/mol)	27.36
ΔH_{H2I}(kJ/mol)	96.52
Reaction II	
Ea (kJ/mol)	40.5
ΔH_I(kJ/mol)	-49.36
ΔH_{H2II}(kJ/mol)	27.53

In order to further establish the validity of the above rate equations, and associated kinetic parameters of the overall reaction, a comparison was made between the experimental data obtained in an integral reactor (where the conversion is high enough that the change in the concentration of the reactant between the entrance and the exit of the reactor is significant) and the theoretical predictions from the above rate equations. To derive the integral model based on the rate equations, the following assumptions were made: (1) isothermal conditions prevail in the reactor (2) the reaction is in the kinetic region throughout the length of the reactor without any mass transfer effects, and (3) change in the volume due to the reaction is negligible.

The rate of change of o-nitroanisole, intermediate, hydrogen and o-anisidine per unit length of the reactor are given by the following equations:

$$\frac{dF_{nitro}}{dz} = a(-r_1) \tag{1.15}$$

$$\frac{dF_{\text{int}\,ermediate}}{dz} = a(r_1 - r_2) \tag{1.16}$$

$$\frac{dF_{hydrogen}}{dz} = a(-r_1 - 2r_2) \tag{1.17}$$

$$\frac{dF_{anisidine}}{dz} = a(r_2) \tag{1.18}$$

where F_{nitro}, $F_{intermediate}$, $F_{hydrogen}$ *and* $F_{anisidine}$ are molar flow rates of o-nitroanisole, intermediate, hydrogen and o-anisidine respectively at the given instance, a is the amount of catalyst per unit length of the reactor, and r_1 and r_2 are the reaction rates for equations (1.11) and (1.12) respectively. Equations 1.15-1.18 were solved using Runge-Kutta method with the following entrance conditions: at $z = 0$, $F_{nitro} = 0.0036$ *mol/sec,* $F_{hydrogen} = 0.013$ *mol/sec,* $F_{intermediate} = 0$ and $F_{anisidine} = 0$ at a liquid flow rate of 0.05mol/min and gas flow rate of 5sccm.

Experiments were carried out with these initial conditions at different hydrogen partial pressures and different amounts of catalysts but keeping the same residence time. The model predictions and experimental data for the yield of o-anisidine under these operating conditions are shown in fig. 1.28 and are within 5-10% of each other. This excellent agreement suggests that the rate parameters determined here represent the results obtained under both differential and integral conditions. Under actual operating conditions, mass transfer effects which may be significant need to be incorporated in the analysis.

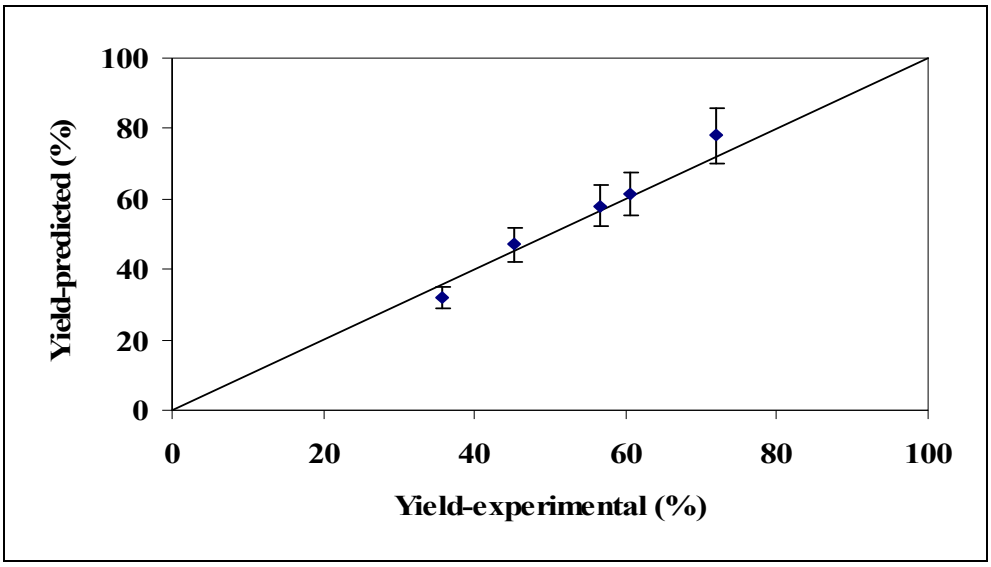

Fig. 1.28 Experimental and predicted yield of o-anisidine for an integral reactor.

III.3.6. Kinetic Study in the semi-batch reactor

In order to study the kinetics of this reaction in the semi-batch reactor, first the effect of external mass transfer was studied as a function of agitation speed to obtain the stirrer speed beyond which the reaction rate did not change. Then, the intrinsic kinetics of the reaction was investigated by studying the effect of reactants concentration on the initial rate of the reaction. Pore diffusion or internal mass transfer effect is assumed negligible based on the previous results obtained in the microreactor using particle sizes in the range 45-75µm and 75-150µm (Section III.3.5.1).

III.3.6.1. Analysis of external mass transfer effect

Experiments were done at different stirrer speeds to determine the speed at which the external mass transfer effect can be considered to be negligible. Figure 1.29 shows the effect of stirrer speed on average reaction rate and selectivity of anisidine. At low stirrer speeds, both the rate and selectivity increase with increase in stirrer speed. However, when the stirrer speed is increased beyond 600 rpm, it has no further effect on the rate and also on the selectivity. At low stirrer speeds the mass transfer effect may have some influence on the rate, while above 600 rpm stirrer speed the reaction is controlled by the intrinsic kinetics. The low selectivity values at low stirrer speeds was due to the presence of the intermediate, 2-nitrosomethoxybenzene. At high stirrer speeds the intermediate might be reacting faster, resulting in high anisidine selectivity.

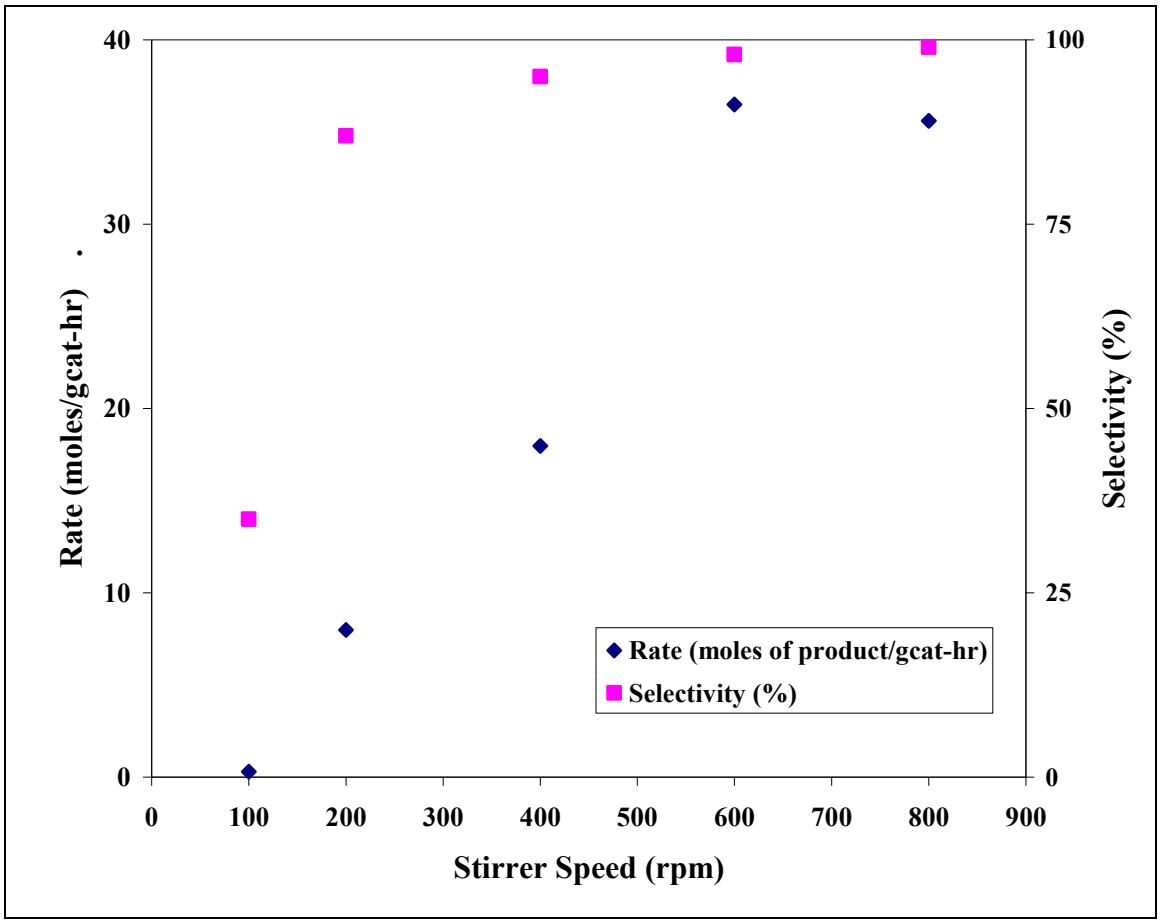

Fig. 1.29 Effect of stirrer speed on the reactor performance (20mg of 2% Pd/Zeolite catalyst, 30℃ reactor temperature, initial nitroanisole conc.=1.299 mol/L, Reactor pressure=100psig)

III.3.6.2. Initial rate analysis

Experiments were conducted at 800 rpm under different nitroanisole and hydrogen concentrations to determine the intrinsic kinetic rate expression for the reaction in a semi-batch reactor. The catalyst loading was kept small (<7mg) for all the kinetic experiments. For reproducibility purpose, all the experiments have been repeated at least twice. Figure 1.30 shows that there is a wide range of linear relationship of concentration of reactant and product vs. time close to time t=0. For the kinetic study, the initial rates of hydrogenation were calculated from the slope of these lines.

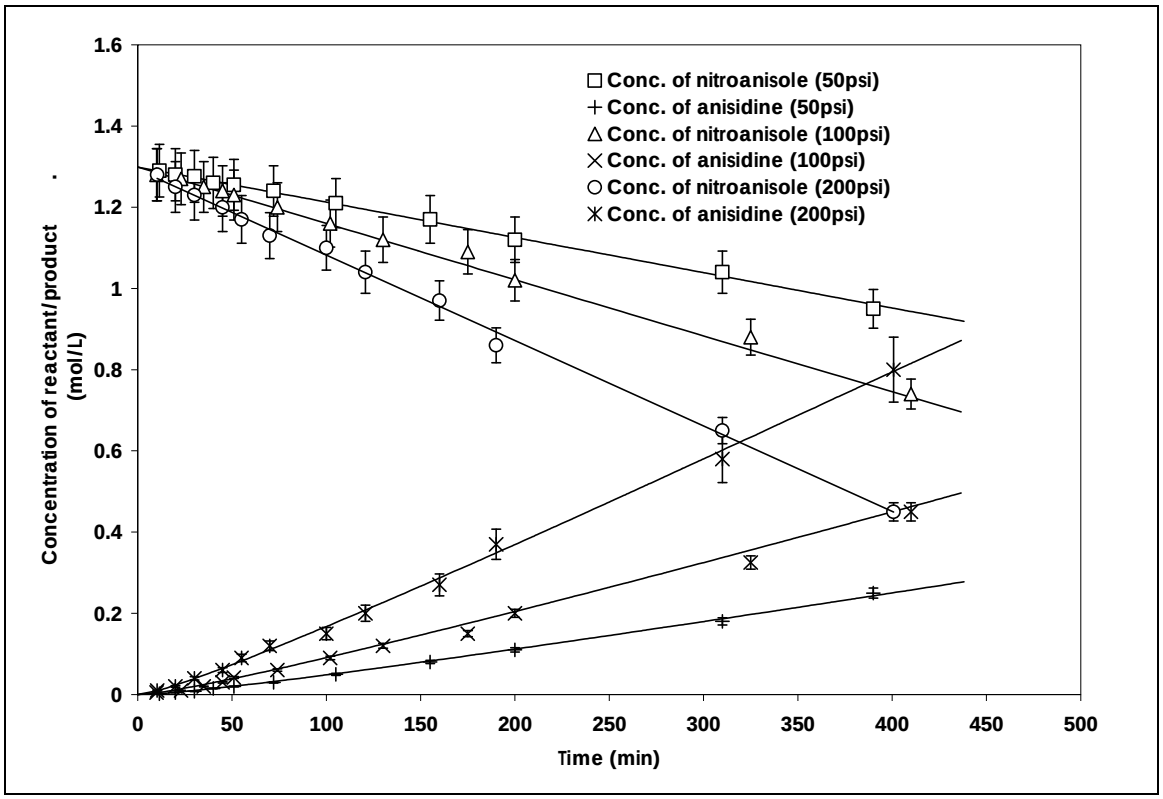

Fig. 1.30 Concentration of nitroanisole and anisidine vs. time at different hydrogen pressures

The dependence of initial rate of disappearance of nitroanisole and initial rate of formation of anisidine on hydrogen and nitroanisole concentrations is determined as follows:

Dependence of rate of disappearance of nitroanisole on hydrogen concentration:

The effect of hydrogen concentration on the rate of disappearance of nitroanisole was studied by varying the hydrogen pressure, keeping the values of the other variables including nitroanisole concentration constant. Figure 1.31 shows the effect of hydrogen concentration on the rate of disappearance of nitroanisole obtained at three temperature levels of 30, 40 and 50^{o}C, at a nitroanisole concentration of 1.29mol/L. The data show that the reaction rate increases with hydrogen concentration in the liquid. The error bars in these plots were calculated by replicating the runs at least twice. They represent the error in obtaining the initial rate data or in other words the error in being able to extrapolate the curve towards zero.

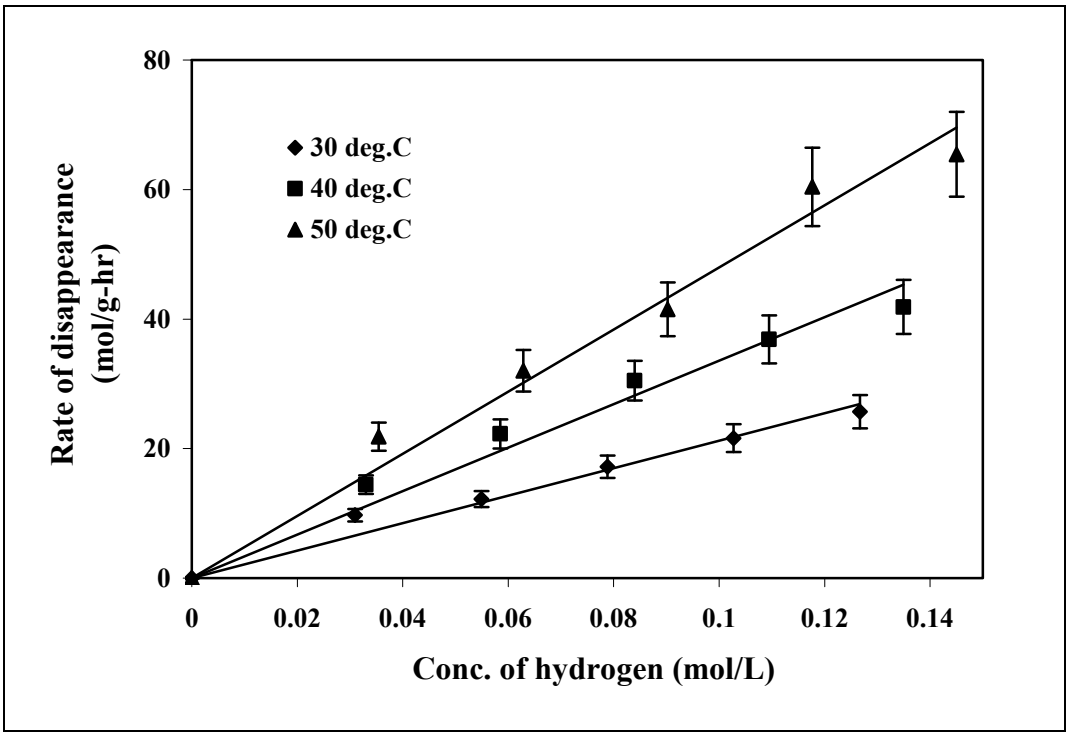

Fig.1.31 Rate of disappearance of nitroanisole with hydrogen concentration

Dependence of rate of disappearance of nitroanisole on nitroanisole concentration:
Figure 1.32 shows the rate of disappearance of nitroanisole with nitroanisole concentration keeping all variables including hydrogen pressure (100psig) or concentration constant. The rate of disappearance of nitroanisole increases with increase in nitroanisole concentration up to a certain concentration, and then remains constant for all temperatures.

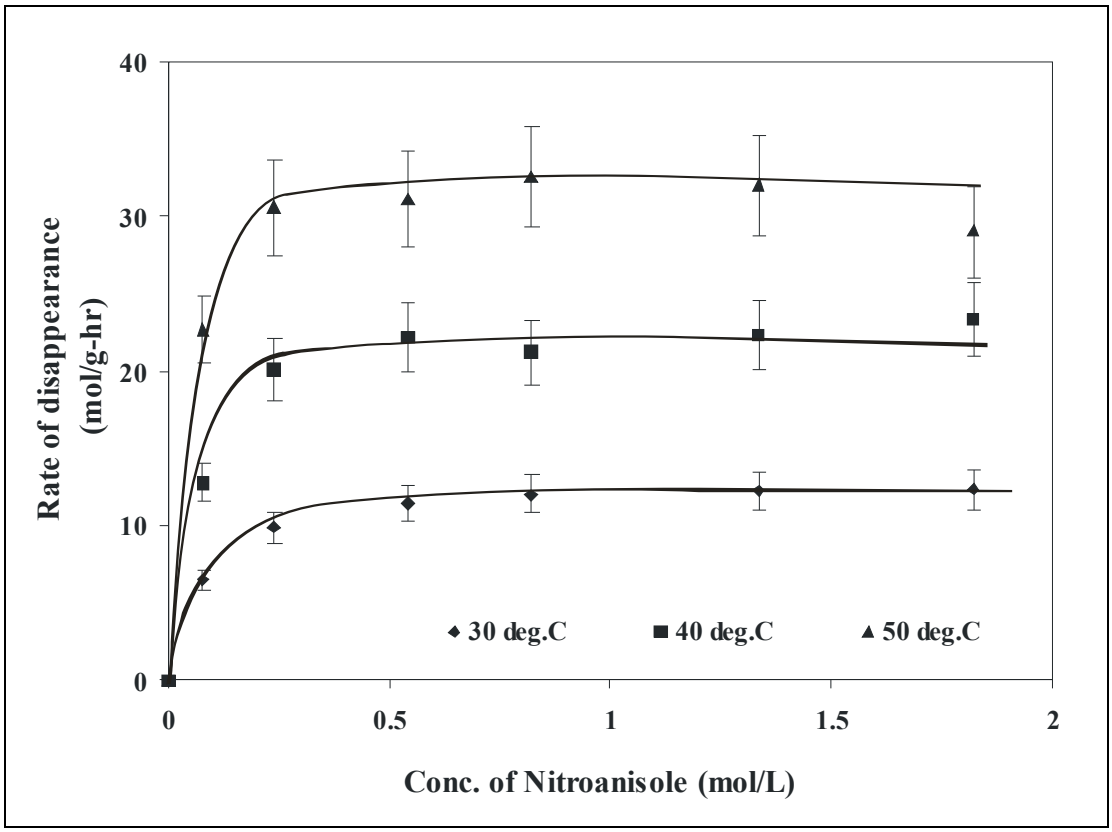

Fig. 1.32 Rate of disappearance of o-nitroanisole with o-nitroanisole concentration

Dependence of rate of formation of o-anisidine on hydrogen concentration:

Figure 1.33 shows the effect of hydrogen concentration on the rate of formation of anisidine obtained at three temperature levels of 30, 40 and 50^{o}C, keeping the values of the other variables, including nitroanisole concentration, constant. The rate increases with increase in hydrogen concentration.

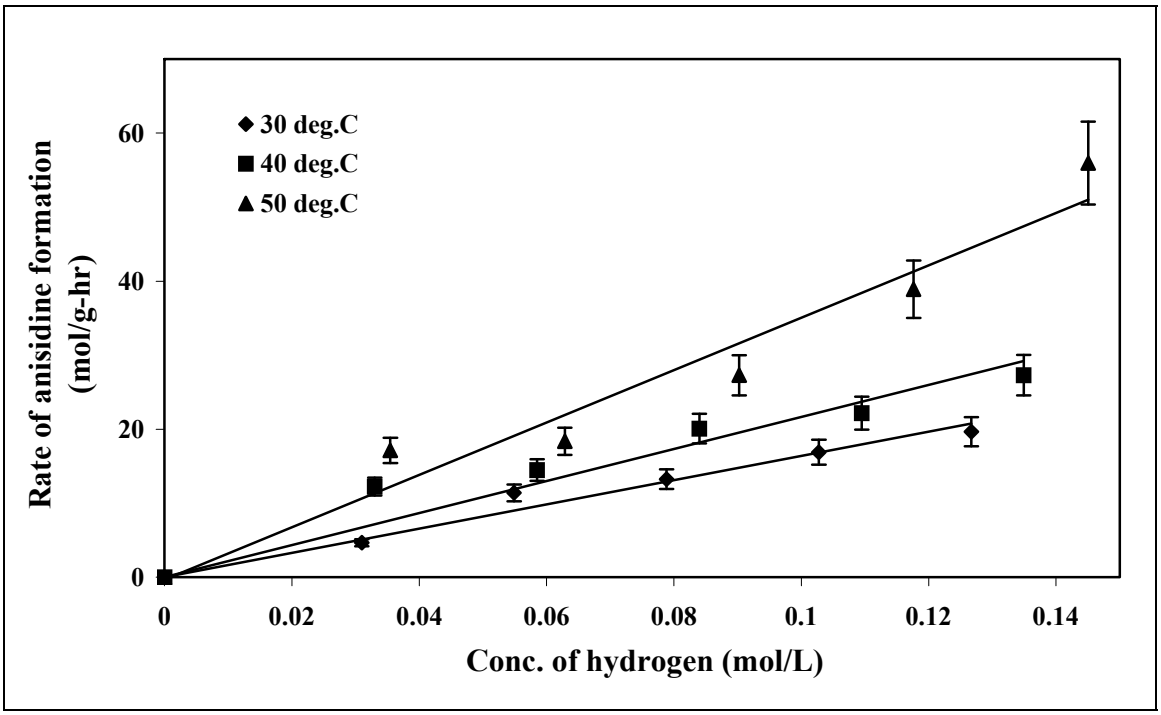

Fig. 1.33 Rate of formation of anisidine with hydrogen concentration

Dependence of rate of formation of o-anisidine on nitroanisole concentration:
Figure 1.34 shows the rate of formation of anisidine at different nitroanisole concentrations in a semi-batch reactor at constant hydrogen pressure. The rate first increases with o-nitroanisole concentration, attains a maximum value and then decreases with further increase in o-nitroanisole concentration. The decrease in the rate of o-anisidine formation at high concentrations of o-nitroanisole is due to substrate inhibition effect present at high concentrations.

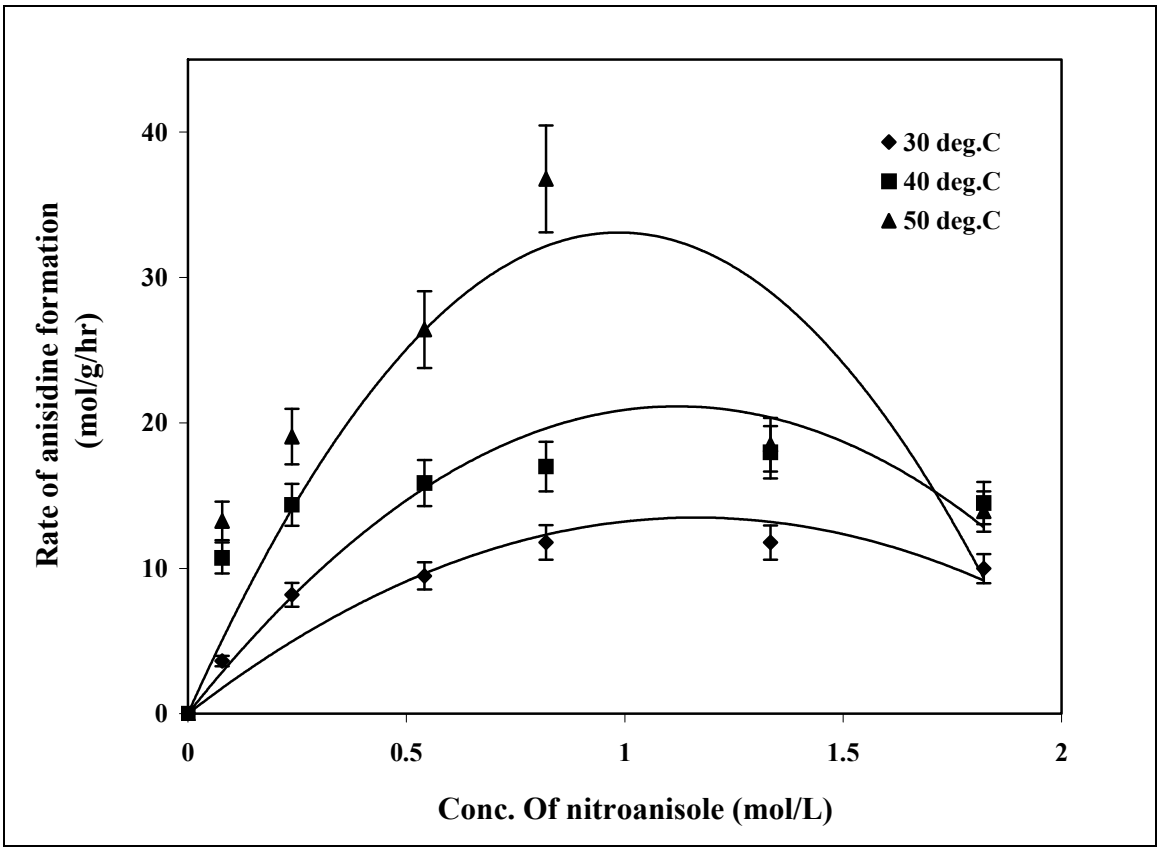

Fig. 1.34 Rate of formation of anisidine at different nitroanisole concentrations

A comparison of the data of figures 1.32 and 1.34 shows that the rate of disappearance of nitroanisole is somewhat higher than the rate of formation of anisidine at same conditions especially at high nitroanisole concentrations. This indicates that the intermediate 2-methoxy nitrosobenzene is present in the product stream as a by-product, which was also observed while conducting kinetic experiments in the microreactor (Section III.3.5.4).

III.3.6.3. Kinetic modeling

The initial rate data obtained were fitted to different rate equations based on Langmuir-Hinshelwood (L-H) or Eley-Rideal type models. A non-linear regression analysis (Levenberg-Marquardt (LM) algorithm using Polymath 5.1) was performed in order to estimate the kinetic constants for the individual rate equations. For regression analysis, the rate expressions that best fitted the micro-reactor data (Section III.3.5.5) (Eqs. 1.11& 1.12 for reactions I&II respectively) were first used to fit the semi-batch experimental data. These equations were also found to be the best fit for semi-batch data.

The values of the kinetic constants for these models are given in Table 1.5. In order to assess the adequacy of the rate equations and the accuracy of the kinetic constants, the results of the best fits were analyzed by comparing the experimental and predicted rates for both reactions as shown in figs. 1.35 and 1.36 respectively. It is evident from these figures that the predicted rates agree with the experimental rates within 10%.

Table 1.5: Kinetic constants and regression coefficients for the reactions in semi-batch reactor

Reaction I				
Temperature (deg. C)	**k_I (L^2/g-hr-mol)**	**K_N (L/mol)**	**K_{H2} (L/mol)**	**R^2**
30	2087.31±35.12	6.05±0.12	5.65±0.29	0.957
40	3766.19± 4.25	7.06± 0.01	4.01± 0.017	0.987
50	6518.78± 8.29	11.11±0.01	1.29 ±0.013	0.988
Reaction II				
Temperature (deg. C)	**k_{II} (mol/g-hr)**	**K_I (L/mol)**	**K_{H2} (L/mol)**	**R^2**
30	151.53± 0.42	98.97± 1.11	1.58±0.01	0.94
40	172.52±0.15	61.59±0.28	1.81± 0.01	0.94
50	202.99± 2.10	9.86± 0.17	7.33 ± 0.13	0.936

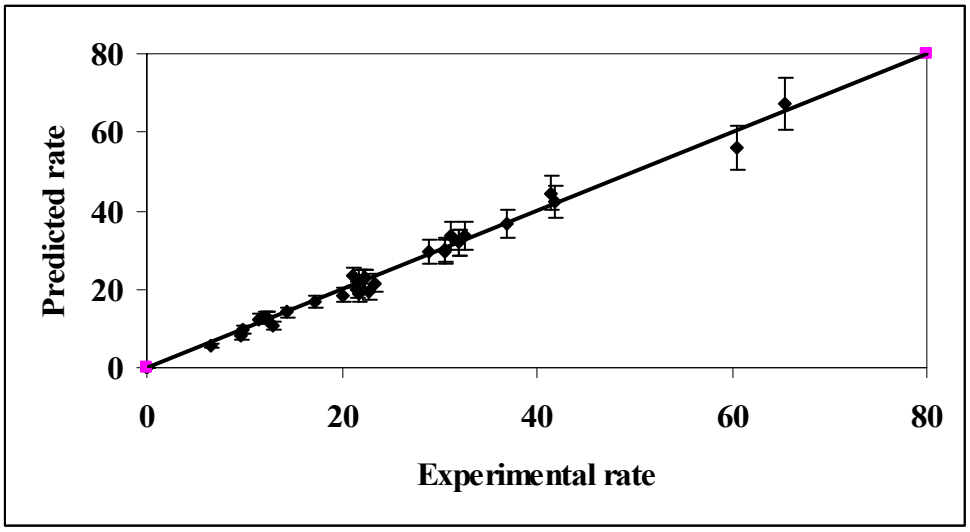

Fig. 1.35 Experimental and predicted rates for reaction I using equation (1.11)

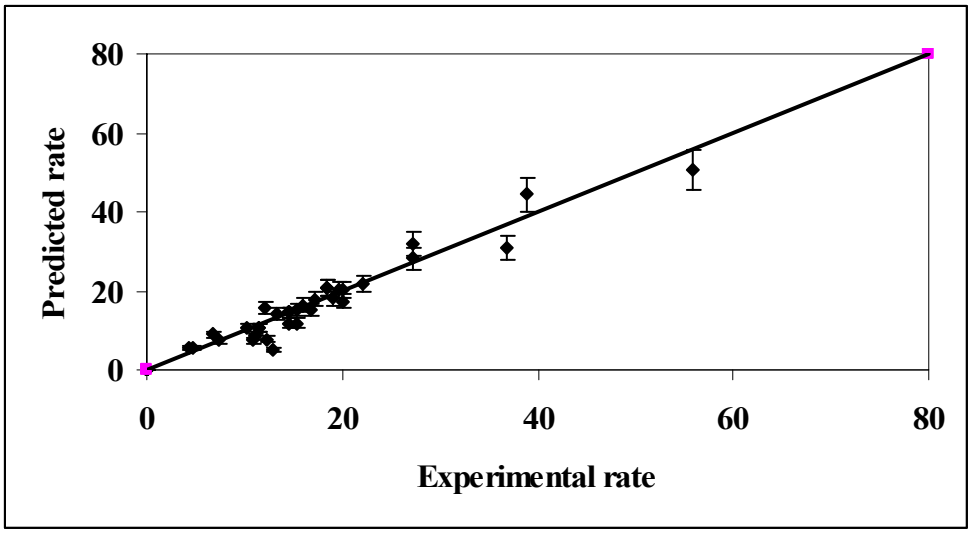

Fig. 1.36 Experimental and predicted rates for reaction II using equation (1.12)

The activation energies for reactions I and II were determined from the kinetic constants using Arrhenius equations. The values are 46.3 kJ/mol and 11.9 kJ/mol for reactions I and II respectively, which compare favorably to the literature value of 43.83kJ/mol (Chaudhari et al. 1983) for reaction I. However, there are significant differences in the activation energies obtained in the microreactor and the semi-batch reactor, especially for reaction II. This difference in the activation energy for reaction II is attributed to the difference in the concentration ranges of the intermediate 2-methoxy nitroso benzene obtained from the kinetic experiments for the same partial pressure of hydrogen used in the two reactors (fig. 1.37).

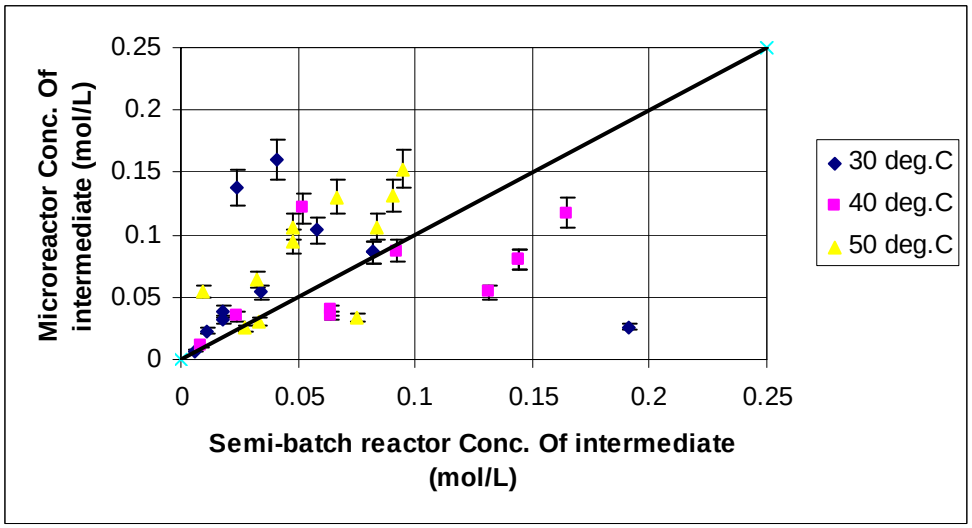

Fig 1.37 Comparison of concentration of intermediate in the microreactor and semi-batch reactor

In order to further establish the validity of the above rate equations, and associated kinetic parameters of the overall reaction, a comparison was made between the experimental data obtained under integral conditions, and the theoretical predictions from the above rate equations. To derive the integral model based on the rate equations, the following assumptions were made:

(1) there are no mass transfer limitations, and (2) change in the volume due to the reaction is negligible.

The rate of change of concentrations of o-nitroanisole, intermediate, hydrogen and o-anisidine per unit time are given by the following equations:

$$\frac{dC_{nitro}}{dt} = a_1(-r_1) \tag{1.19}$$

$$\frac{dC_{\text{int ermediate}}}{dt} = a_1(r_1 - r_2) \tag{1.20}$$

$$\frac{dC_{hydrogen}}{dt} = a_1(-r_1 - 2r_2) \tag{1.21}$$

$$\frac{dC_{anisidine}}{dt} = a_1(r_2) \tag{1.22}$$

where C_{nitro}, $C_{intermediate}$, $C_{hydrogen}$ *and* $C_{anisidine}$ are the concentrations of o-nitroanisole, intermediate, hydrogen and o-anisidine respectively at the given instance, a_1 is the density of catalyst per unit volume of the reactor, and r_1 and r_2 are the reaction rates from equations (1.11) and (1.12) respectively. Equations 1.19-1.22 were solved using Runge-Kutta method with the following initial conditions: at $t = 0$, $C_{nitro} = 1.299$ *mol/L,* $C_{intermediate}=0$ and $C_{anisidine}=0$, *temperature=30℃, pressure=100psig, catalyst loading=20mg.* The model predictions and experimental data for the conversion of o-nitroanisole under these operating conditions are shown in fig. 1.38, and are within 5-10% of each other. This excellent agreement suggests that the rate parameters determined here represent the results obtained under integral conditions.

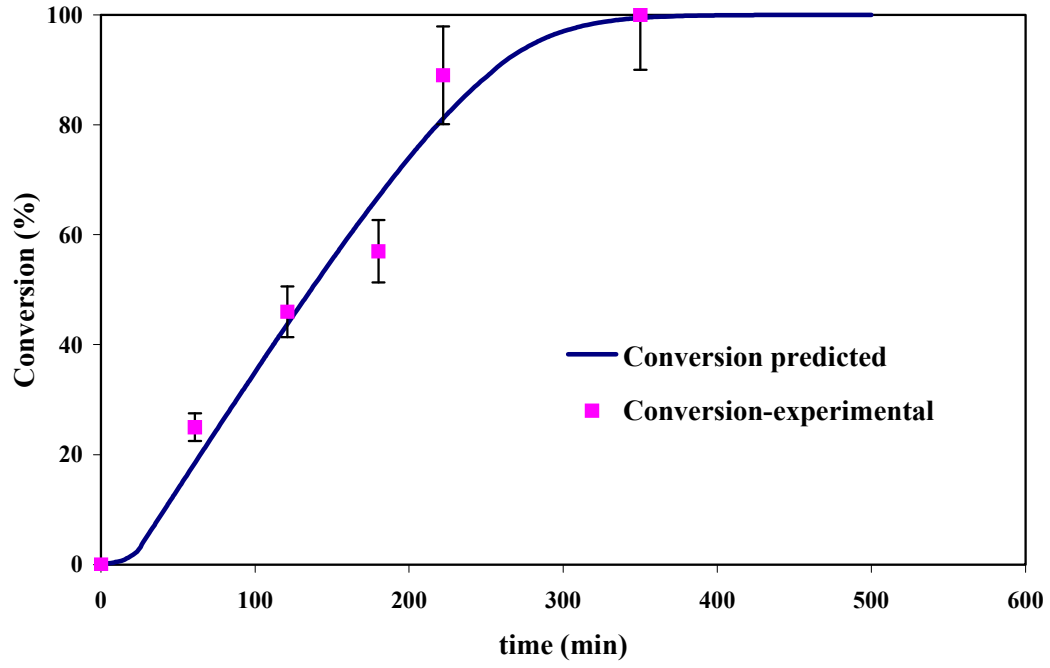

Fig 1.38 Experimental and predicted conversion of o-nitroanisole for a semi-batch reactor

III.3.7. Comparison of performance of microreactor with the semi-batch reactor

III.3.7.1. Comparison of reaction rates

A comparison between the microreactor and the semi-batch reactor was made based on the intrinsic rates obtained in two systems for this reaction. Figure 1.39 shows the comparison of initial reaction rate for the semi-batch reactor and the reaction rate obtained for a differential microreactor under similar reaction conditions. The data in fig 1.39 show that the reaction rates of both reactors are the same under similar conditions. This confirms that the kinetic data obtained in both reactors are free of any external mass transfer effects, thus indicating that the microreactor is as efficient as the semi-batch reactor in obtaining intrinsic kinetic data for this reaction. Therefore, for the range of operating conditions used for this reaction, the mass transfer limitations in the semi-batch reactor are negligible and the reaction can be assured to be controlled by intrinsic kinetics. However, it should be noted that the batch reactor used for these experiments has a volume of 25 ml. As the volume of the batch reactor increases, there is a substantial decrease in mass transfer efficiency due to in-efficient mixing in large volume of the batch reactor. Hence, it is likely that the reaction may shift from kinetic region to mass transfer region with increase in reactor volume. Therefore it is important to evaluate the mass transfer efficiency of the reactor system to determine the types of reaction that are most suited for this reactor.

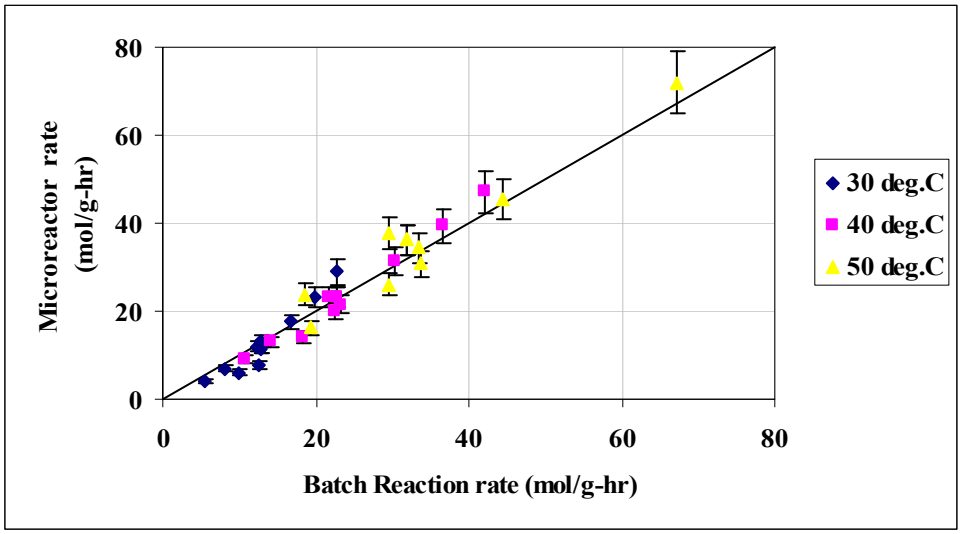

Fig. 1.39 Comparison of reaction rates of micro reactor and batch reactor

III.3.7.2. Mass transfer analysis

Using the intrinsic kinetic information and the mass transfer equations, the semi-batch reactor and microreactor were modeled. The modeling results were used to evaluate the mass transfer parameters. Unlike the modeling done in section III.3.6.3, where mass transfer effects were neglected, the modeling in this section includes different mass transfer steps of hydrogen, starting with diffusion of hydrogen from the gas phase to the liquid and from the liquid to the catalyst surface. The modeling calculations were performed using Athena Visual Workbench package (v.8.3, Stewart & Associates Engineering Software, Inc.) and these results were compared to the experimental data for an integral reactor to estimate the overall mass transfer coefficient for the two reactor systems under different reaction conditions.

Modeling of Microreactor

The microreactor model was based on the slug flow regime. With this type of flow, hydrogen from the gas phase is being depleted in two ways. From the gas slug, hydrogen is transferred to the thin film surrounding the catalyst, and also to the liquid slug through the gas-liquid interface. The schematic representation of these mass transfer steps were depicted in fig. 1.13. Following a two phase flow model, mass transfer equations for both the reactants were derived both in the gas and the liquid slugs. These equations are given below:

Two-phase flow model for microreactor

In Liquid slug

Hydrogen in bulk liquid

$$v_{gl}\varepsilon_l \frac{dC_{H,bl}}{dz_1} = k_{ls}a_{ls}\varepsilon_l(C_{H,cl} - C_{H,bl}) + k_{gl}a_{gl}\varepsilon_l(C_{H,satl} - C_{H,bl}) \tag{1.23}$$

Hydrogen at the catalyst surface

$$k_{ls}a_{ls}\varepsilon_l(C_{H,bl} - C_{H,cl}) = a_2\varepsilon_l(r_{1l} - r_{2l}) \tag{1.24}$$

o-nitroanisole in the bulk liquid

$$v_{gl}\varepsilon_l \frac{dC_{N,bl}}{dz_1} = k_{ls1,n}a_{ls}\varepsilon_l(C_{N,cl} - C_{N,bl}) \tag{1.25}$$

o-nitroanisole at the catalyst surface

$$k_{ls1,n}a_{ls}\varepsilon_l(C_{N,bl} - C_{N,cl}) = a_2\varepsilon_l r_{1l} \tag{1.26}$$

$$r_{1l} = \frac{k_1 C_{H,cl} C_{N,cl}}{(1 + K_N C_{N,cl})(1 + K_{H1} C_{H,cl})} \tag{1.27}$$

$$r_{2l} = \frac{k_2 K_{H2} C_{H,cl} K_I C_{I,cl}}{(1 + K_I C_{I,cl})(1 + K_{H2} C_{H,cl})} \tag{1.28}$$

In gas slug

Hydrogen in thin film surrounding the catalyst

$$v_{gl}\varepsilon_l \frac{dC_{H,bg}}{dz_1} = k_{gls}a_{gls}(1 - \varepsilon_l)(C_{H,cg} - C_{H,bg}) \tag{1.29}$$

Hydrogen at the catalyst surface

$$k_{gls}a_{gls}(1 - \varepsilon_l)(C_{H,bg} - C_{H,cg}) = a_2(1 - \varepsilon_l)(r_{1g} - r_{2g}) \tag{1.30}$$

o-nitroanisole in the thin film surrounding the catalyst

$$v_{gl}\varepsilon_l \frac{dC_{N,bg}}{dz_1} = k_{ls2,n}a_{gls}(1 - \varepsilon_l)(C_{N,cg} - C_{N,bg}) \tag{1.31}$$

o-nitroanisole at the catalyst surface

$$k_{ls2,n}a_{gls}(1 - \varepsilon_l)(C_{N,cg} - C_{N,bg}) = a_2(1 - \varepsilon_l)(-r_{1g}) \tag{1.32}$$

$$r_{1g} = \frac{k_1 C_{H,cg} C_{N,cg}}{(1 + K_N C_{N,cg})(1 + K_{H1} C_{H,cg})} \tag{1.33}$$

$$r_{2g} = \frac{k_2 K_{H2} C_{H,cg} K_I C_{I,cg}}{(1 + K_I C_{I,cg})(1 + K_{H2} C_{H,cg})} \tag{1.34}$$

This two phase model is complicated as it involves too many parameters and different concentrations and reaction rates of the reactants in the gas and the liquid slugs. This model was simplified by assuming a pseudo homogenous state where there is no rate oscillation between the gas and the liquid slug. The simplified mass transfer equations using this model are given below:

Pseudo Homogeneous Model for microreactor

Hydrogen concentration in bulk liquid

$$v_l \frac{dC_{H,b}}{dz_1} = k_{ls}a_{ls}(C_{H,c} - C_{H,b}) + k_{gl}a_{gl}(C_{H,sat} - C_{H,b}) \quad (1.35)$$

Hydrogen at catalyst

$$k_{ls}a_{ls}(C_{H,b} - C_{H,c}) = a_2(r_1 - r_2) \quad (1.36)$$

o-nitroanisole at the catalyst surface

$$v_l \frac{dC_{nitro}}{dz_1} = a_2(-r_1) \quad (1.37)$$

$$r_1 = \frac{k_1 C_{H,c} C_N}{(1 + K_N C_N)(1 + K_{H1} C_{H,c})} \quad (1.38)$$

$$r_2 = \frac{k_2 K_{H2} C_{H,c} K_I C_I}{(1 + K_I C_I)(1 + K_{H2} C_{H,c})} \quad (1.39)$$

For modeling of the microreactor, the intrinsic rate expressions obtained in the microreactor were used (Section III.3.5.5). The values of the kinetic constants for equations 1.38 and 1.39 are given in Table 1.3. From tables 1.3 and 1.5, it can be observed that the kinetic constants for the reactions in the two reactor systems are different. However, the reaction rates calculated from these kinetic constants are almost the same under similar conditions. Since the regression analysis does not take into account the experimental error (or error bars), it generates different kinetic constants for slight changes in the experimental data. Therefore, the difference in the kinetic constants for the reactions in the two reactor systems was attributed to regression analysis.

Equations 1.35-1.39 were further simplified by making the following assumptions:

(1) The change in the mass transfer coefficient along the reactor length is negligible.

(2) Since gas-liquid reactions are usually controlled by gas to liquid mass transfer rate, the value of the liquid to solid mass transfer coefficient was assumed to be very high (This was confirmed by calculating the $k_{ls}a_{ls}$ value using correlations in Nijhuis et al. 2003 and Kreutzer et al. 2001).

Using these assumptions, the microreactor was modeled under different reaction conditions. Figure 1.40 shows the typical modeling results obtained by solving these differential equations. The figure shows that the concentration of hydrogen in the bulk liquid as well as at the catalyst surface is close to the saturation concentration of hydrogen indicating that external mass transfer resistances are negligible and the reaction is controlled by intrinsic kinetics.

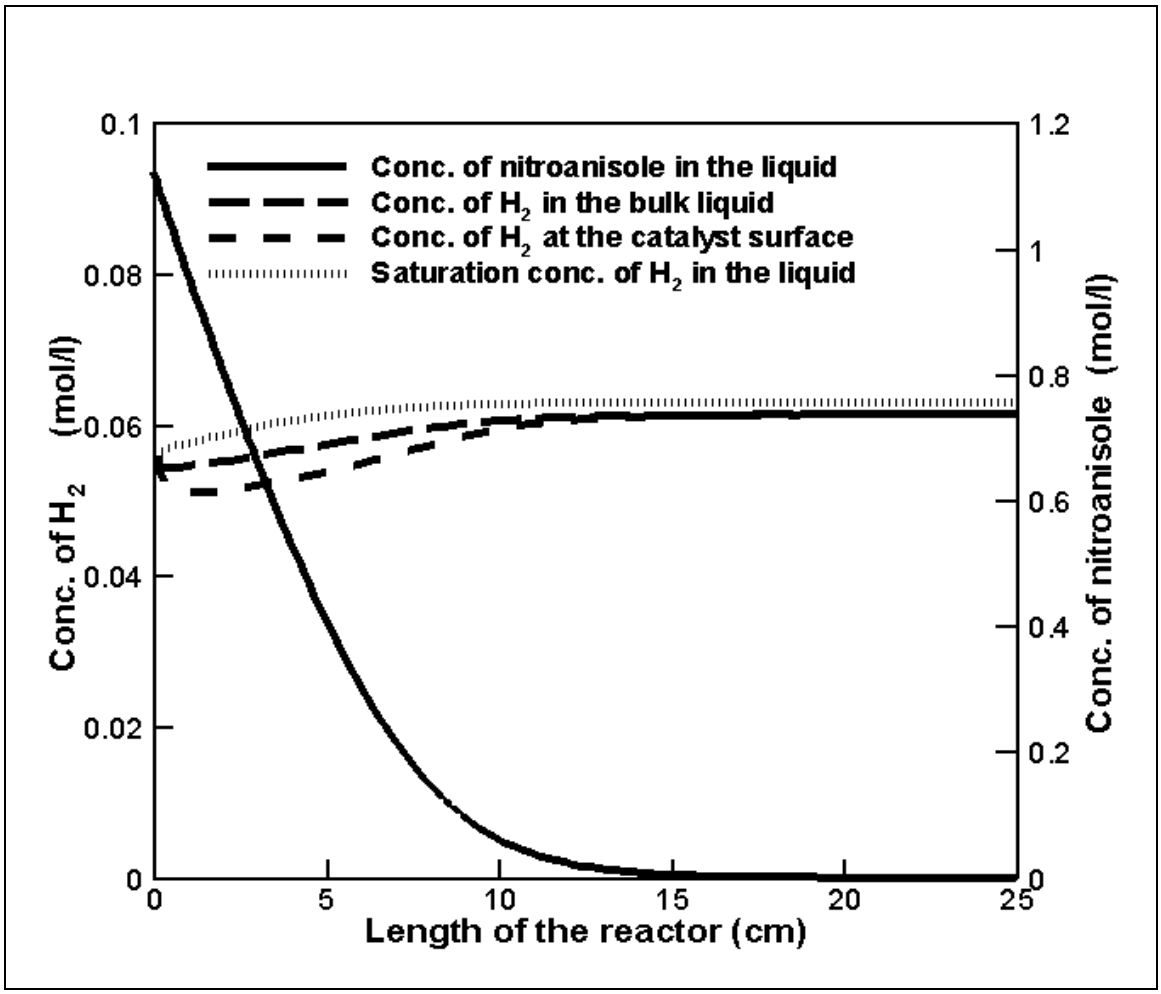

Fig. 1.40 Modeling results for a packed bed microreactor at 100 psig pressure, 30 deg. C temperature, 0.05 ml/min liquid flowrate and 5sccm gas flowrate, 1.299 mol/L nitroanisole conc., $k_{gl}a_{gl}=8s^{-1}$

Experiments were carried out in the microreactor under different operating conditions. The reaction results from these experiments were compared with the theoretical predictions from equations 1.26 and 1.27 for an integral reactor with no mass transfer effects. Most of the experimental results agree with these predictions as shown in fig. 1.28. However, some of the experiments gave lower results than those predicted from the intrinsic kinetics model. These represent the data with high catalyst loading or high conversion of hydrogen and nitroanisole. The deviations from the model predictions may be due to mass transfer limitations which were not considered in the intrinsic kinetics model. Modeling of the microreactor was done under these reaction conditions with significant mass transfer effects. The modeling results were compared with the experimental data at different velocities and catalyst loading to determine the gas-liquid mass transfer coefficient ($k_{gl}a_{gl}$). Then the overall mass transfer coefficient (K_{la}) was calculated from the following equation:

$$\frac{1}{K_{la}} = \frac{1}{k_{gl}a_{gl}} + \frac{1}{k_{ls}a_{ls}} \tag{1.40}$$

Figure 1.41 shows the overall mass transfer coefficient (K_{la}) values obtained by comparing these experimental results with the simulation results under different reaction conditions. The figure clearly shows that the mass transfer coefficient is a function of overall linear velocity, and catalyst loading. The change in the mass transfer coefficient with the catalyst loading is because of the change in the overall flow velocity along the length of the reactor. As hydrogen is consumed along the length of the reactor, the length of the gas slug decreases resulting in a decrease in the overall flow velocity. This implies that the mass transfer coefficient is invariably related to the velocity.

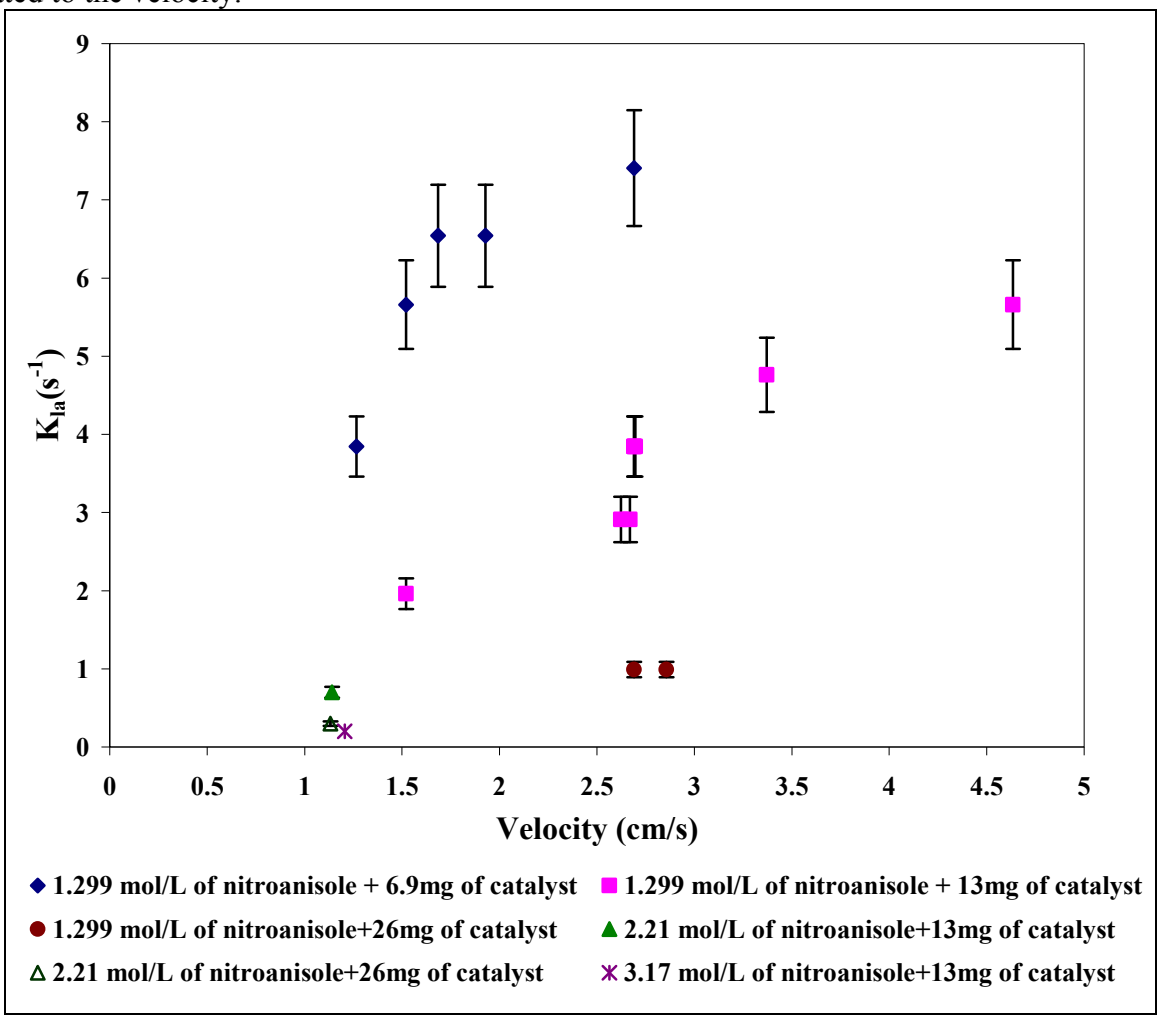

Fig. 1.41 Mass transfer coefficients in the microreactor as a function of overall velocity

Figure 1.41 shows that the mass transfer coefficients obtained in the packed bed microreactor under the present experimental conditions range between 0.2 and ~9 s^{-1}. These values compare favorably with the mass transfer coefficients obtained by Losey et al. 2001 for the hydrogenation of cyclohexene in a packed-bed microreactor under similar reaction conditions. Hence the range of mass transfer coefficient values obtained can be generalized to any hydrogenation reaction conducted in a packed-bed microreactor under these operating conditions. This range of mass transfer coefficients was used to determine the reaction times or residence times of the reactions that will be suitable for conducting kinetic study in the microreactor.

Assuming that any form of rate equation (Langmuir-Hinshelwood or power law) can be transformed into a pseudo-first order rate equation by combining all the terms in the rate expression into the rate constant, except the concentration of limiting reactant, the rate expression will be of the form:

$$r = k_r C_A \tag{1.41}$$

where, r represents the rate of the reaction, k_r represents the intrinsic rate constant and C_A represents the concentration of the limiting reactant. The mass transfer coefficient values (K_{la}) must be much higher (at least 10 times) than intrinsic rate constants (k_r) for the reaction to be controlled by true intrinsic kinetics. From the range of mass transfer coefficients obtained, it indicates that the packed bed microreactor can be used to obtain intrinsic kinetic information for hydrogenation reactions with intrinsic rate constants up to an order of magnitude of 10^0 s^{-1}, or with reaction half-life times in the order of magnitude of 10^0 s and above.

Modeling of semi-batch reactor

The modeling for a semi-batch reactor was done similar to that of the microreactor. For the modeling of a semi-batch reactor, the contributions of various mass transfer resistances were assumed to be constant with time. The model used for the semi-batch reactor assumes the liquid to be ideally mixed, so that the composition of liquid is assumed to be uniform throughout the reactor. Considering the kinetics given by equations (1.11) and (1.12) for the semi-batch reactor, the rate of hydrogenation incorporating the effect of mass transfer will be given by the following equations:

Model for semi-batch reactor

Hydrogen concentration in bulk liquid

$$\frac{dC_{H,b}}{dt} = k_{ls}a_{ls}(C_{H,c} - C_{H,b}) + k_{gl}a_{gl}(C_{H,sat} - C_{H,b}) \tag{1.42}$$

Hydrogen at catalyst

$$k_{ls}a_{ls}(C_{H,b} - C_{H,c}) = a_1(r_1 - r_2) \tag{1.43}$$

o-nitroanisole at the catalyst

$$\frac{dC_{nitro}}{dt} = a_1(-r_1) \tag{1.44}$$

In the above expressions, r_1 and r_2 are rate equations obtained in the semi-batch reactor. Using equations 1.42-1.44, the semi-batch reactor was modeled under different reaction conditions and the modeling results were compared with the experimental data obtained in the semi-batch reactor to evaluate the mass transfer coefficient. The liquid to solid mass transfer coefficient ($k_{ls}a_{ls}$) in the semi-batch reactor was calculated from the correlations in Mills and Chaudhari 1997. Figure 1.42 shows the overall mass transfer coefficient (K_{la}) values estimated by comparing the conversion from the modeling results with the experimental data under different agitator speeds. The data clearly show that the mass transfer coefficient in the semi-batch reactor increases with increase in the stirrer speed. The mass transfer coefficient in the semi-batch reactor ranges from 0.01 to 0.07 s^{-1}. These are the typical values of mass transfer coefficients reported for batch (Chaudhari 1983) and other traditional laboratory reactors (Al-Dahhan et al. 1997). This implies that such reactors can be used to obtain intrinsic kinetic information for reactions with intrinsic rates constants (k_r) up to an order of magnitude of 10^{-2} s^{-1} or with half-life times in the order of magnitude of 10^2 s and above.

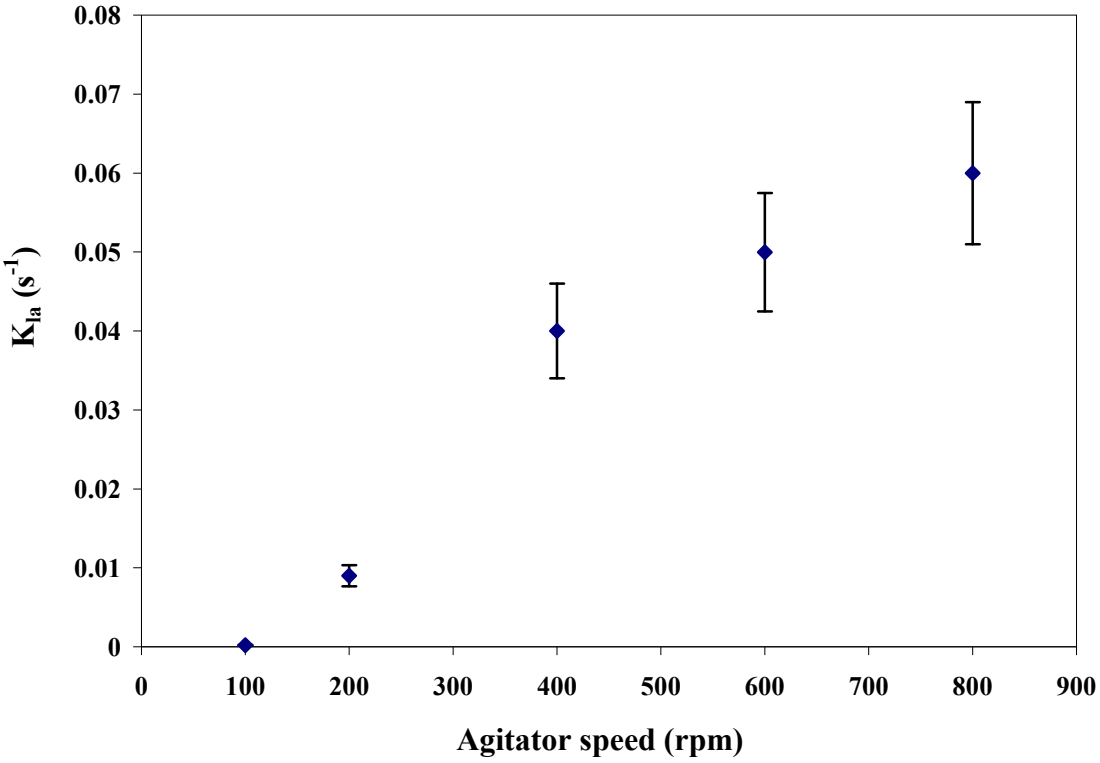

Fig. 1.42 Mass transfer coefficients in the semi-batch reactor as a function of stirrer speed

For the hydrogenation of o-nitroanisole, the half-life time was calculated to be $4.8*10^2$ s at a temperature of 30°C, pressure of 100 psig, 1.299 mol/L o-nitroanisole concentration, and catalyst loading of 20 mg in a batch reactor. Hence both batch and micro reactors are suitable for conducting kinetic studies for this reaction.

In the above analysis, the conclusions on the reaction times suited for conducting kinetic studies in the batch and the microreactor are justified only for reactions which are first order with respect to hydrogen concentration. This analysis may be inaccurate for reactions with different reaction orders for hydrogen in which case the calculation becomes even more complicated.

From the above discussion, it can be clearly seen that the mass transfer coefficient values in the micro reactor are two orders of magnitude higher than those of the semi-batch reactor. This is the result of much higher gas-liquid interfacial area in the micro reactor than in the semi-batch reactor due to the turbulence created at the gas-liquid interface in liquid slugs. This tremendous increase in the mass transfer rate in the microreactor can be used not only to increase the productivity of extremely fast reactions but also to obtain intrinsic kinetic information for such reactions. The calculations showed that both batch and microreactors are suitable to obtain intrinsic kinetic information for hydrogenation reactions with half lives in the order of magnitude of 10^2 s and above, and microreactor is better suited to obtain intrinsic kinetic information for hydrogenation reactions with half lives in the order of magnitude between 10^0 to 10^2 seconds. If a batch reactor is used to obtain intrinsic kinetic study for these reactions, the reaction data would represent a mixture of intrinsic and mass transfer effects and hence would not provide information on true intrinsic kinetics. Therefore, a microreactor is more suited than the

conventional laboratory reactors in obtaining intrinsic kinetic data for fast hydrogenation reactions because of their high mass transfer and mixing characteristics.

III.3.8. Catalyst Deactivation & Regeneration

III.3.8.1. Catalyst Deactivation

Catalyst deactivation is a problem of great concern in industrial catalytic processes. This may occur due to a number of reasons, both chemical and physical in nature. For reactions involving organic species with strong oxidizing or reducing properties or reactions involving high temperatures, catalyst deactivation is inevitable. During the hydrogenation of nitro compounds in fixed bed reactors there has always been an issue of rapid deactivation of palladium catalysts, especially with carbon supported Pd catalysts, which exhibits a rate of deactivation much faster than other supports. A few experienced researchers, (Bartholomew et al. 2001; Yeong et al. 2003) have investigated the reasons for this rapid deactivation during nitro group hydrogenation in liquid phase reaction, and they found out that depending upon the catalyst structure, deactivation could be due to three main reasons:

1. *Leaching*
2. *Sintering, and*
3. *Poisoning of active sites*.

Leaching: It has been reported by Albers et al. 2001 that leaching of palladium occurs under hydrogen starving conditions. Under such conditions, nitro compounds oxidize metal atoms on the catalyst which form complexes with amino compounds and are dissolved in the liquid. In order to prevent leaching, all the experimental runs in our study were made in hydrogen rich atmosphere. ICP analysis of the product stream to determine palladium counts revealed that palladium was not detected within the detectable range of the instrument (0.1ppm). Therefore leaching was not the reason for catalyst deactivation in the present study.

Sintering: Morphological changes of palladium due to particle growth by sintering (Albers et al. 2001) is another major cause of deactivation of palladium catalysts. Under the influence of hydrogen, particle growth of finely dispersed, palladium may occur even at temperatures as low as 50°C. In order to determine if the catalyst deactivation was a result of sintering, the dispersion of the catalyst was measured using TEM before and after the reaction. Figure 1.43 shows the TEM images of the fresh and used catalysts. The figure shows that the particle size of Pd increased after the reaction indicating agglomeration or sintering of Pd particles. This is clearly evident from Table 1.1 which shows comparison of fresh and used catalysts.

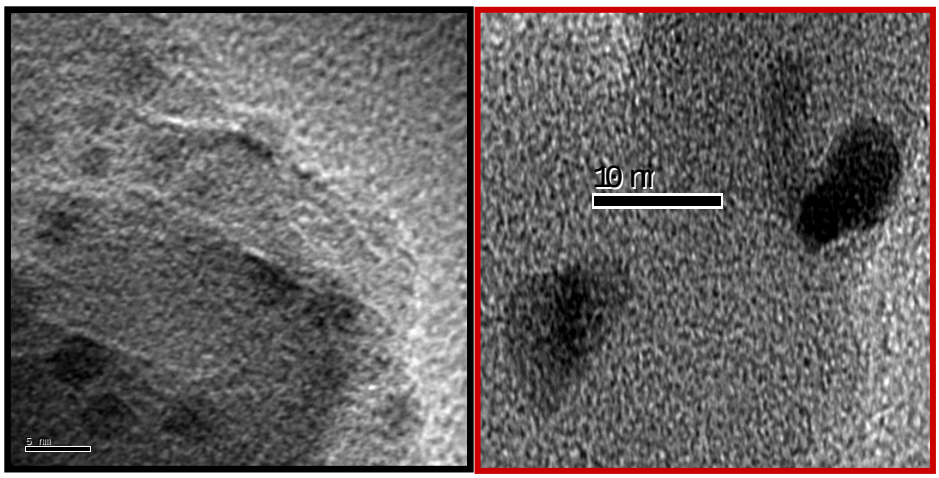

Fig. 1.43 TEM images of fresh Pd/ Zeolite catalyst (left) and used catalyst (right)

Table 1.6: Comparison of fresh and used catalyst

	Fresh	Used
Particle size [nm]	2 - 4	2 – 6
Average particle size [nm]	2.7	4.3
Dispersion	39 %	25 %

However, sintering alone cannot account for the complete loss of the catalytic activity. The rate of catalyst deactivation varies depending upon the circumstances responsible for it. Two limiting cases can be recognized. In the first, the deactivation increases with time on stream, but is independent of the feed stock composition, e.g. sintering. At the other extreme, are cases in which deactivation is caused by the adsorption of a poison, and the reduction in rate is a function of the quantity of the poison adsorbed onto the catalyst but it is independent of the time of exposure. In the present case, it was found that the decrease in catalytic activity was a function of catalyst loading, and concentration of the substrate. Figures 1.44 and 1.45 show the change in product concentration with time while conducting experiments in the microreactor with 2% Pd/ Zeolite at different catalyst loadings and concentrations of reactant respectively. The figures show that the rate of deactivation is faster for low catalyst loading, and high concentration of the substrate o-nitroanisole. Therefore both sintering and poisoning of catalyst may have significant effect on the rate of deactivation.

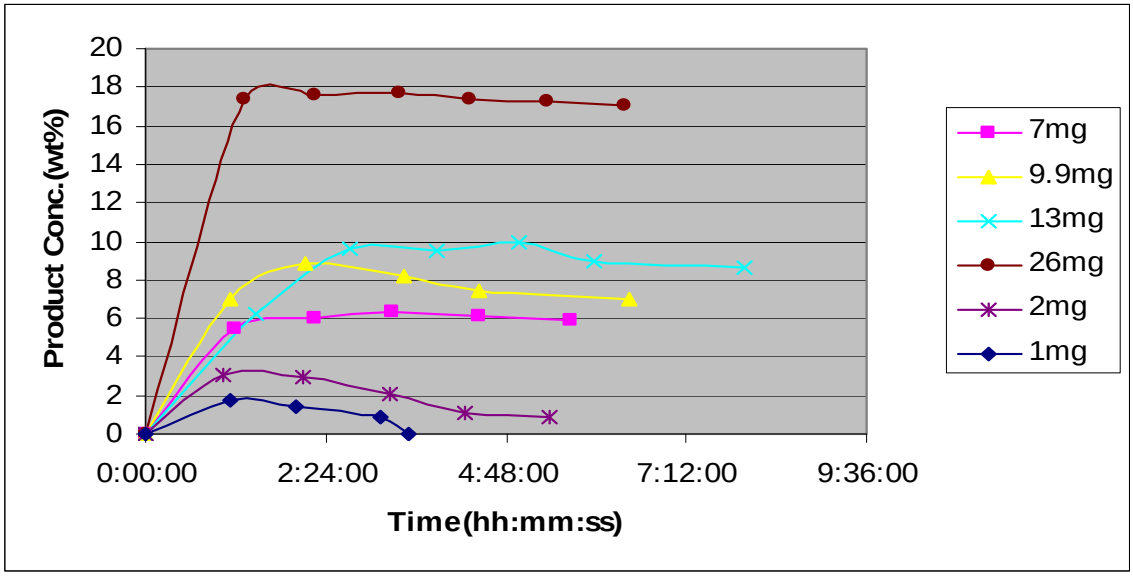

Fig. 1.44 Product concentration with time at different catalyst loading

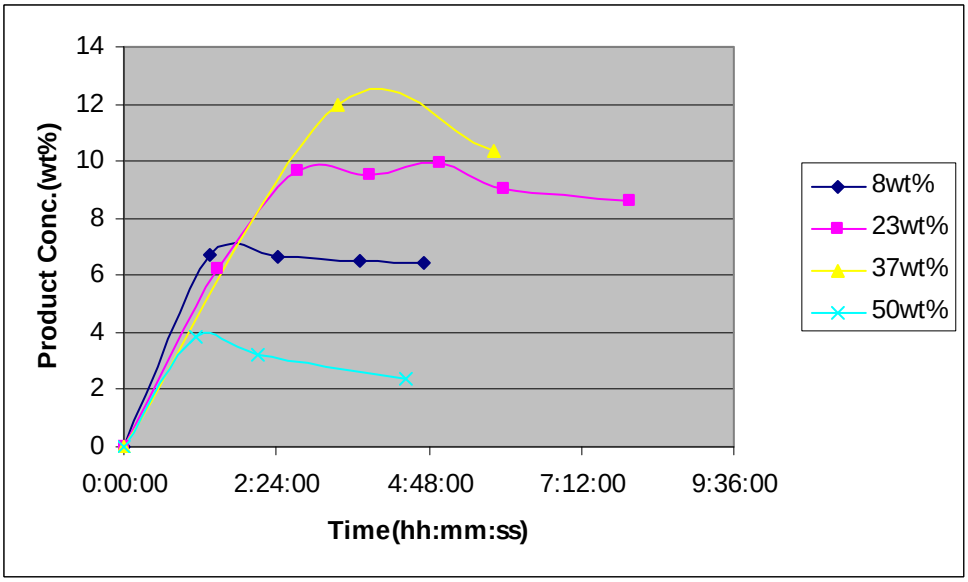

Fig. 1.45 Product concentration with time at different concentrations of reactant

Poisoning of catalysts: Metallic catalysts are particularly sensitive to poisons, especially to compounds with lone pair of electrons such as S or N-compounds, which form strong donor bonds to the surface. The poison may be the reactant, the intermediates or the product in which case it is known as self-poisoned or self-inhibited. During the hydrogenation of nitro compounds, it is most likely that the intermediate compounds i.e. nitroso, azo and azoxy compounds adsorb strongly onto the catalyst surface blocking the catalytic sites. In order to verify this, the fresh and used catalysts were analyzed using TEM. Detailed observations of the samples revealed some differences between fresh and used sample(Fig. 1.46). It appears that some whiskers comprising lighter elements such as carbon were found surrounding the Pd particles that were not observed on fresh sample. However, it is not clear which compound or molecule is actually eclipsing the Pd particle. More analysis on the poisoning of the catalyst will be done in the near future

including chemisorption to evaluate blockage of palladium atoms, and temperature programmed desorption to identify desorbing molecules.

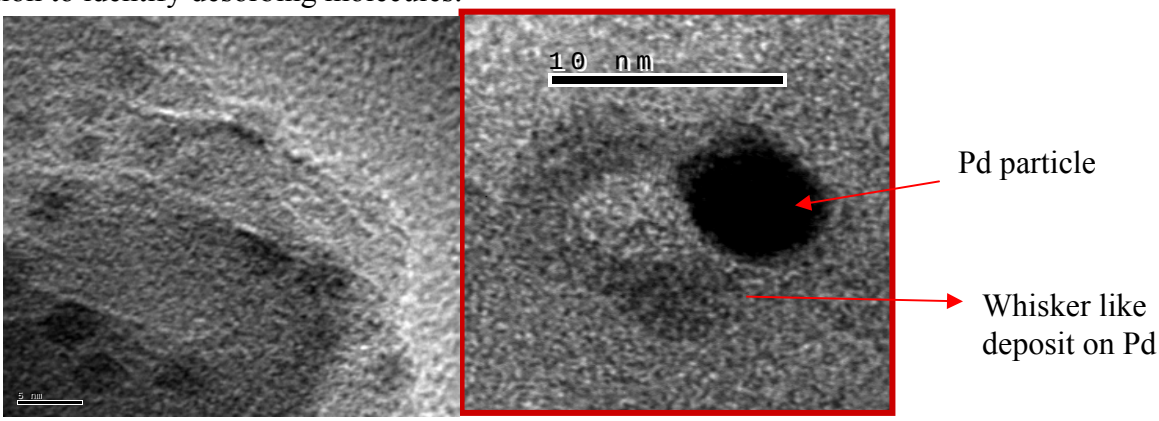

Fig 1.46 TEM images of fresh Pd/ Zeolite catalyst (left) and used catalyst (right)

III.3.8.2. Catalyst Regeneration

For an industrial catalytic chemical process to be commercially successful, it is highly important to consider means of *in situ* catalyst regeneration. Several researchers have investigated regeneration procedures of the catalysts used for nitro reduction (Yeong et al. 2003, Van Gelder et al. 1990). Van Gelder et al. 1990 observed deactivation of Pd catalyst while conducting the hydrogenation of a nitro compound. They showed that the palladium catalyst could be regenerated *in situ* by heating the catalyst in air at a temperature of 130°C, and atmospheric pressure. This process renders the catalyst activity practically equal to the initial level. Yeong et al. 2003 were also successful in removing the organic deposits on the surface of the catalyst using the same procedure. Although catalyst regeneration work has not been part of the present study, this study provides a general idea on some of the catalyst regeneration procedures described in the literature for the hydrogenation of nitro aromatics which can be implemented as part of the future work.

III.4. Conclusions

Hydrogenation of o-nitroanisole to o-anisidine was investigated in a microreactor packed with 2%Pd/Zeolite catalyst. The microreactor performance was evaluated by studying the effects of different operating conditions, intra-particle diffusion, gas-liquid and liquid-solid mass transfer, heat transfer and surface reaction kinetics. The experimental results indicate that the heat and mass transfer resistances were negligible for a wide range of operating conditions and this reaction is kinetically controlled in the microreactor. It was observed through calculations that the gas-liquid mass transfer coefficient in the microreactor is much higher than the estimates obtained from standard correlations in conventional reactors.

The rate of formation of o-anisidine was found to be lower than the rate of o-nitroanisole disappearance indicating that the intermediate 2-methoxynitrosobenzene was present in significant amount in the reactor at low conversions. Thus, two separate reaction steps were identified: the reduction of o-nitroanisole to 2-methoxynitrosobenzene and the further reduction of 2-methoxynitrosobenzene to o-anisidine. Langmuir-Hinshelwood type rate expressions were found to be suitable for these reaction steps with desorption of 2-methoxynitrosobenzene controlling the first reaction step, and surface reaction controlling the second reaction step. A set

of rate equations were obtained based on experimental kinetic data in a differential microreactor. Furthermore, the obtained kinetics were used to predict the integral reactor behavior and found to agree very well.

The kinetics of the hydrogenation of o-nitroanisole to o-anisidine was also investigated in a semi-batch reactor using 2% Pd/Zeolite catalyst. The reaction rates in the semi-batch reactor and the microreactor were found to be the same thereby confirming that the reaction is controlled by intrinsic kinetics in both reactors under similar conditions. Hence, the microreactor is as efficient as the semi-batch reactor in obtaining intrinsic kinetic data for this reaction.

The micro reactor and the semi-batch reactor were modeled using the mass transfer model approach. The simulation results showed that the mass transfer coefficients in the microreactor are two orders of magnitudes higher than those of the semi-batch reactor. Further, the calculations showed that both batch and micro reactors can be used for conducting kinetic studies for slow hydrogenation reactions with half lives in the order of magnitude of 10^2 s and above, and microreactor is better suited than the semi-batch reactor for conducting kinetic studies for hydrogenation reactions with half lives in the order of magnitude between 10^0 to 10^2 seconds.

Although several fast hydrogenation reactions have been conducted in microreactors, there are no studies on the use of microreactor for obtaining intrinsic kinetics in spite of the excellent mass transfer characteristics it offers. The present study has exploited the advantages of microreactor for obtaining the intrinsic kinetics of the hydrogenation of o-nitroanisole reaction for a wide range of operating conditions, thus extending its capability to extremely fast reactions that are controlled by mass transfer in conventional reactors.

Catalyst deactivation was observed and possible causes were identified. The most likely cause for rapid deactivation is the adsorption of reaction intermediates on the catalyst surface. Because the reaction mixture contains nitro group, partially hydrogenated nitro-groups and amino groups, it is possible that during the reaction these intermediates are formed and adsorbed or deposited on the catalyst surface. For industrial application of a catalytic chemical process it is important to devise regeneration procedures for retaining the catalyst activity. Therefore, future work will include the regeneration of the catalyst using the procedures described in the literature.

IV. Kinetics of hydrogenation of aromatic nitro ketone

IV.1. Introduction

In this section, we report on the hydrogenation of a model aromatic nitro ketone of pharmaceutical interest in a packed-bed microreactor. The amine formed from this reaction is used as an intermediate in the manufacture of a drug. In contrast to hydrogenation of o-nitroanisole investigated in section III, this reaction is extremely fast, and controlled by mass transfer limitations in industrial reactors, which makes the microreactor more suitable for conducting the kinetic studies of this reaction. The performance of the packed-bed microreactor for this reaction was evaluated by studying the effects of different processing & operating conditions e.g., reaction temperature, pressure, substrate concentration in the feed on the conversion, yield and selectivity of the product. Then, the kinetics of this reaction was studied in the microreactor so that optimum reaction conditions can be determined for the design of the multi-channel reactor. The feasibility of conducting kinetic studies of this reaction in the semi-batch reactor has been evaluated by studying the effect of different operating conditions on the reactor performance. Also, the performance of the two reactors is compared in terms of their mass transfer efficiencies and Space Time Yield or average reaction rates.

IV.2. Experimental

Here, a list of the chemicals used for the experiments, and the description of the analytical method are provided. The microreactor and semi-batch reactor experimental set-ups as well as experimental procedures were described in section II. The aromatic nitro ketone compound is a proprietary molecule of Bristol-Myers Squibb (BMS). This compound is a crystalline yellow solid. The solid substrate was dissolved in a solvent N-methyl pyrrolidone (NMP) which was obtained from Pharmco Products Inc. The hydrogen and nitrogen were purchased from Praxair. Nitrogen was used for diluting the hydrogen stream and also to flush the reactor system at the end of each experiment. Concentration of liquid product stream was determined by High Performance Liquid Chromatography (HPLC), and composition of the gas phase was measured by a Shimadzu GC-14B gas chromatograph with a Mole Sieve 5A column at 35°C and argon as carrier gas. The mobile phase used for the HPLC analysis comprised De-ionized water, methanol and Acetonitrile (HPLC grade), the latter two were purchased from Pharmco Products Inc. The catalyst used for this study was the catalyst used at BMS for conducting this reaction in batch reactors. This catalyst is 5% (w/w) Pd supported on Alumina (supplied by Johnson Matthey). The catalyst has a BET surface area of approximately 150 m^2/g, a total pore volume of approximately 0.50 cc/g, and an average pore diameter of approximately 125 Angstroms. This catalyst was sieved to obtain a particle size distribution of 45-75microns and 75-150 microns which were used for the experiments.

All the liquid product samples collected at the end of each experimental run were diluted with De-ionized water prior to being injected into the HPLC. A Diode Array detector was used for scanning so that the samples could be scanned at multiple wavelengths at the same time. A method was established in the HPLC using water, methanol, acetonitrile and ammonium acetate (buffer) as the mobile phase in conjunction with an RP C^{18} column from Phoenix. Calibration was done for both the reactant and the product using standard solutions. The concentrations of reactant and the product in the unknown product samples were determined using the calibration.

IV.3. Results and Discussion

IV.3.1. Reaction and catalyst activity

The catalytic hydrogenation of aromatic nitro ketone compound involves a three-step reduction series reaction (similar to hydrogenation of o-nitroanisole) as shown in fig 1.47. First, the reduction of the nitro group to nitroso group, then to hydroxylamine group and finally to amine group. There is no difficulty in reducing the nitro group in preference to the carbonyl (ketone group) unless these functional groups are spatially proximate, in which case ring closure may form a number of by-products along with the product of interest (Fisher and Weitz 1980). During the experiments only one intermediate was observed in the product stream along with the product and reactant at all operating conditions. This intermediate was found to be the hydroxylamine derivative by the Mass Spectrum Analysis. Hence the carbonyl group was not being reduced and only the nitro group was being reduced and the overall hydrogenation of the aromatic nitro ketone was considered as a process consisting of two consecutive reactions, one leading to the formation of the hydroxylamine derivative, and the other leading to the formation of the amine derivative.

The profitability of any heterogeneous chemical process depends often on the life time of the catalyst since short life time requires frequent regeneration or even partial or complete change of the catalyst. Catalyst deactivation is a problem of great concern in industrial catalytic processes.

The literature contains several references to the leaching of palladium catalyst in NMP (Zhao et al. 2000; Zhao et al. 2002). Leaching is especially significant for carbon supported palladium catalyst used in slurry reactors where the anchoring between palladium and the support is weak. The catalyst 5% Pd/Alumina used in the present study did not show any signs of leaching as the concentration of the product stream did not change with time at least within the 8 hours that we used to conduct the experimental run. However, the catalyst was not tested for longer time to ensure absence of leaching. This will be considered as part of the future work.

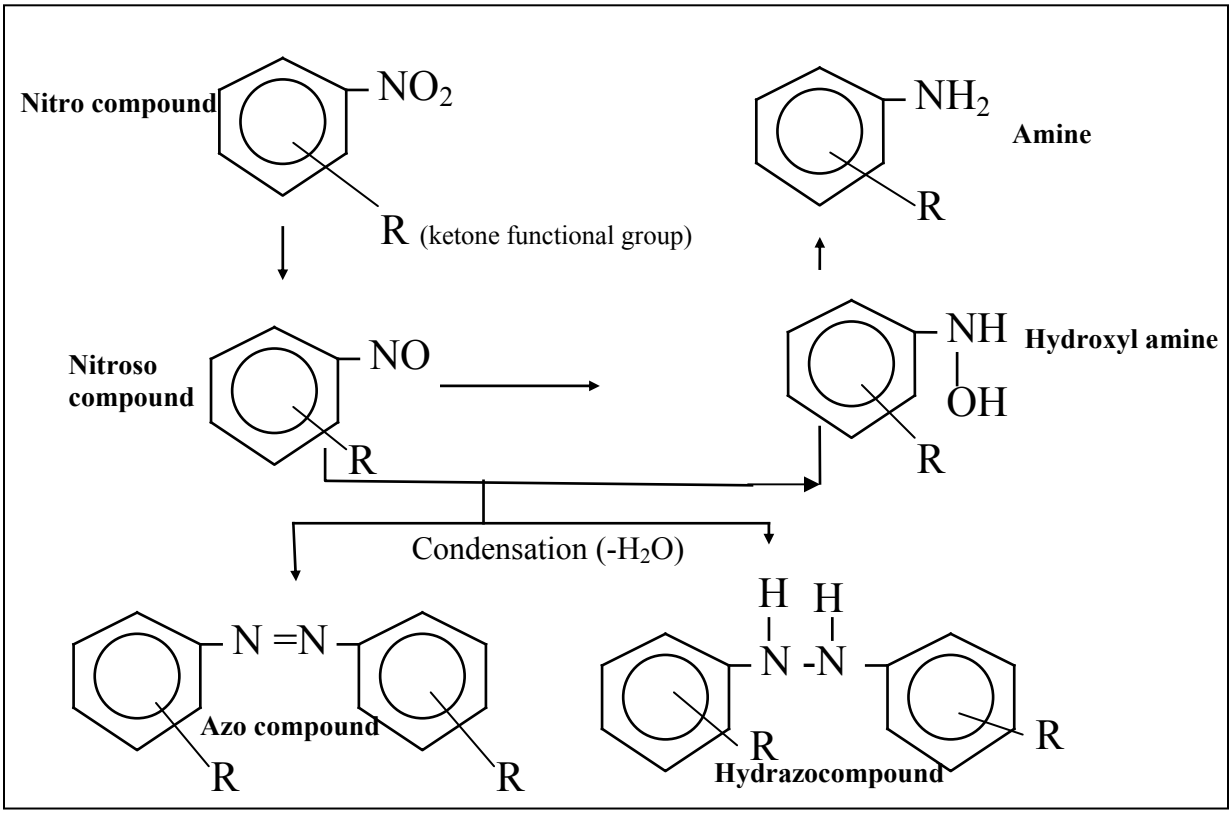

Fig. 1.47 Reaction pathways for the hydrogenation of aromatic nitro ketone.

IV.3.2. Effect of operating conditions on micro-reactor performance

The effect of operating conditions on the micro-reactor performance was studied by comparing the conversion of the reactant, selectivity and Space-Time Yield of the product (amine) under different reaction conditions.

IV.3.2.1. Effect of pressure

To study the effect of pressure on conversion, selectivity and STY, experiments were carried out in the pressure range of 50-250 psig at a substrate concentration of 1% (w/w) in NMP, temperature of 30°C and constant residence time. The residence time was kept constant by varying the catalyst loading. Figure 1.48 shows a plot of the conversion vs. pressure at a constant residence time of 0.8 seconds (inlet conditions). The data indicate that the conversion and selectivity decrease with increase in pressure, but the STY first increases and then remains constant with increase in pressure. The decrease in the conversion and selectivity with increase in pressure at constant residence time is due to the decrease in the catalyst loading with increase

in pressure to maintain constant residence time. The increase in STY with increase in pressure is attributed to the increase in the concentration of dissolved hydrogen, thereby resulting in a higher reaction rate. However, with further increase in pressure, the increase in concentration of dissolved hydrogen has negligible effect on the STY indicating that the dependency of reaction rate on hydrogen concentration is almost zero order at high pressures.

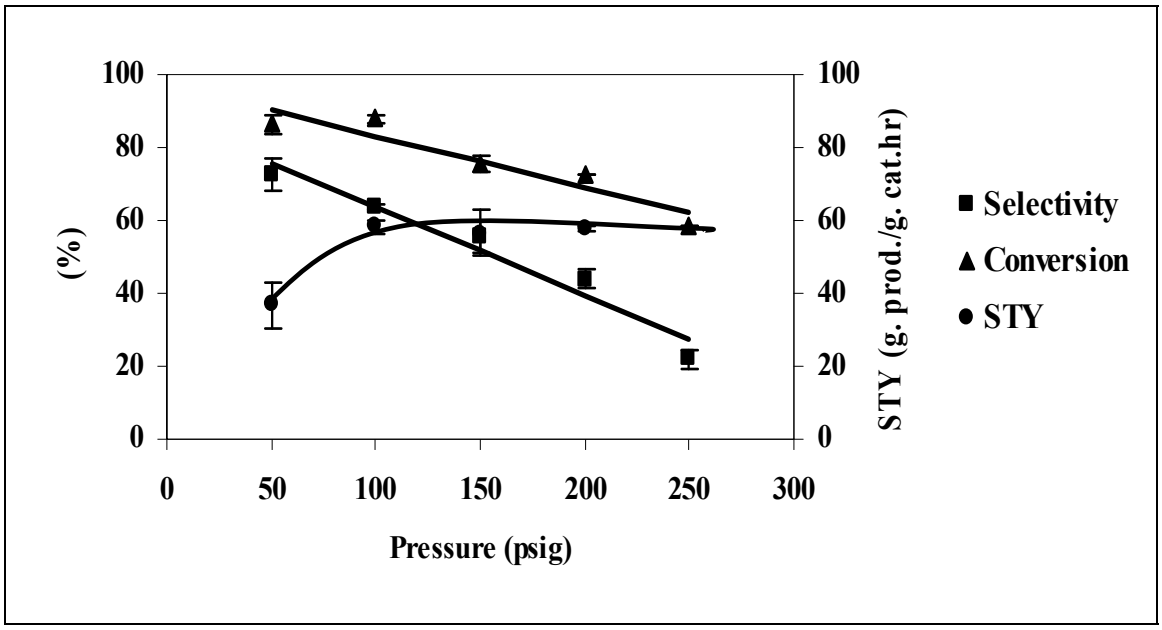

Fig. 1.48 Effect of pressure (at constant residence time) on reactor performance

(All runs were made at a temperature of 30 °C, 1% (w/w) substrate in NMP feed liquid, gas and liquid flowrate of 5sccm and 0.05ml/min respectively)

IV.3.2.2. Effect of temperature

To study the effect of temperature on conversion, selectivity and STY, experiments were carried out in the temperature range of 30-60°C, substrate concentration of 1%(w/w) in NMP, pressure of 100psig and a catalyst (5%Pd/Alumina) loading of 13mg. The liquid and hydrogen gas flow rates were 0.05ml/min and 5sccm respectively. Figure 1.49 shows that with increase in temperature, the conversion, selectivity and STY increase, and at 60°C both the selectivity and conversion were 100%. The data show that there is very slight increase in the reaction rate with increase in temperature. This may be either due to the conversion being close to 100% for the range of temperatures considered in which case the increase in reaction rate with temperature may not be significant, or it may also be that the reaction is influenced by external mass transfer under these operating conditions. This observation has been clarified in the following studies where the effect of mass transfer was studied and it was found that external mass transfer is significant in this range of temperatures considered.

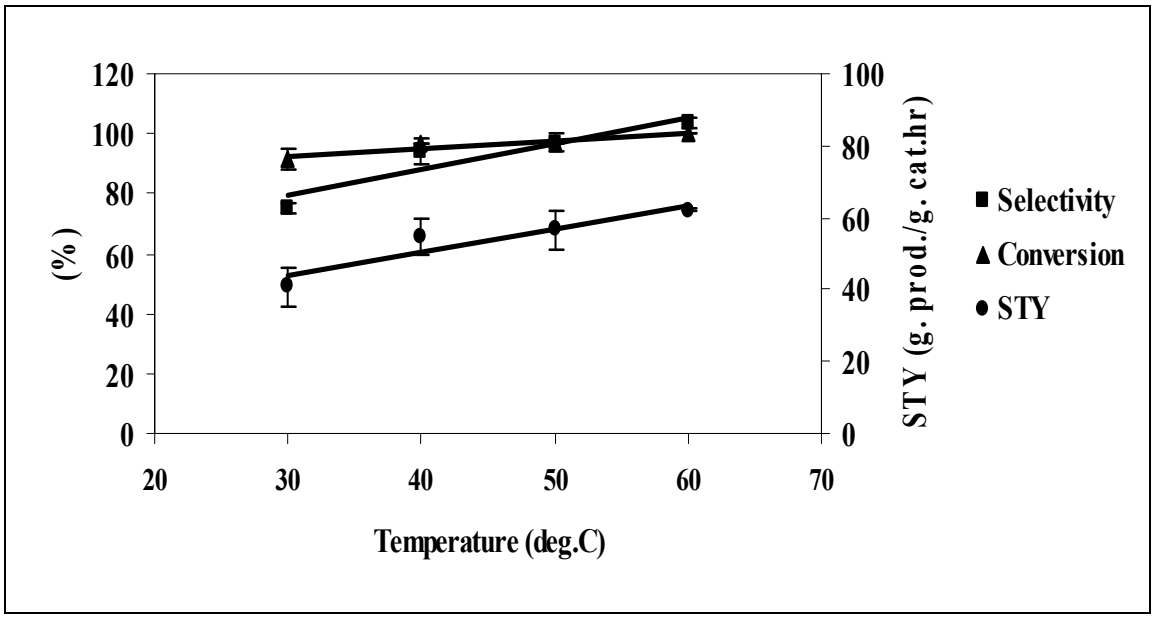

Fig. 1.49 Effect of temperature on reactor performance

(All runs were made at pressure of 100 psig, 1% (w/w) substrate in NMP feed liquid, gas and liquid flowrate of 5sccm and 0.05ml/min respectively, catalyst loading=13mg)

IV.3.2.3. Effect of residence time

Experiments for varying the residence time were done both by changing the liquid and gas flow rates, and also by changing the amount of catalyst in the reactor. Experiments for varying the liquid flow rate were conducted to study its effect on the conversion of substrate, selectivity and STY of product. All the experiments were carried out at a temperature of 30°C, substrate concentration of 1% (w/w) in NMP, pressure of 100psig and a catalyst (5%Pd/Alumina) loading of 13mg. The flow rate of the liquid was varied in the range of 0.05-0.2ml/min, and the H_2 flow rate was kept constant at 5sccm. In these experiments, the actual gas flow rate is approximately 10 times the liquid flow rate. Therefore, a change in liquid flow rate does not change the residence time significantly. Figure 1.50 shows the effect of liquid flow rate on the conversion, selectivity and STY.

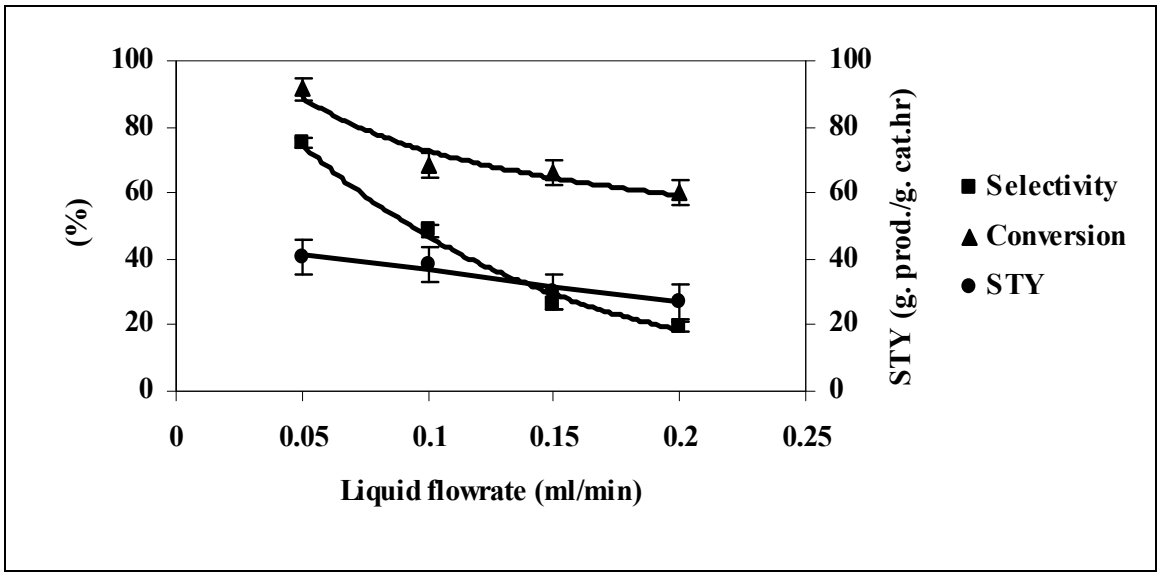

Fig. 1.50 Effect of liquid flowrate on reactor performance

(All runs were made at a temperature of 30 ℃, pressure of 100psig,1% (w/w)substrate in NMP feed liquid, gas flowrate of 5sccm, catalyst loading=13mg)

The data show that the conversion and selectivity decrease with increase in liquid flow rate while the STY or the overall reaction rate decreases very slightly with increase in liquid flow rate. In the experiments that were conducted to elucidate the effect of the liquid flow rate at constant gas flowrate, it was observed that the liquid slug length increases with increase in the liquid flow rate. As the liquid slug length increases, the rate of convective mass transfer from gas to liquid decreases [96]. Small liquid slugs enhance the mass transfer from gas to the liquid. Therefore, conversion, selectivity and STY increase with decrease in liquid flow rate (or decrease in liquid slug length).

Another method of changing the residence time is to change the gas flow rate. Experiments for varying the gas flow rate were conducted to study its effect on the conversion of substrate, selectivity and STY of product. All the experiments were carried out at a temperature of 30°C, substrate concentration of 1% (w/w) in NMP, pressure of 100psig, liquid flow rate of 0.05ml/min, and a catalyst (5%Pd/Alumina) loading of 13mg. The effect of gas flow rate on conversion, selectivity and STY is shown in fig. 1.51. The data show that the conversion, selectivity and STY are nearly unchanged with increase in gas flow rate. Although we keep the liquid flow rate constant, as we increase the gas flow rate the overall flow velocity increases thus decreasing the residence time. According to the theory, if the reaction is controlled by kinetics, the conversion, selectivity and STY should decrease with decrease in residence time; on the other hand, if the reaction is primarily controlled by mass transfer, the conversion, selectivity and STY should increase with increase in gas flow rate due to better mass transfer. However, if we assume a pseudo homogenous model for the flow, then the gas flow rate will not affect the conversion, selectivity and STY; on the other hand, if we assume a two phase flow model, then the gas flow rate affects the conversion, selectivity and STY. The present results tend to agree with the pseudo homogenous model because the conversion, selectivity and STY are unchanged with gas flow rate. However, it is not clear if the reaction is controlled both by mass transfer or intrinsic kinetics under these operating conditions. The reduction of reaction residence time and

the increase of mass transfer rate with increase in gas flow rate have an opposing effect so that the reaction performance does not change much. This observation has been clarified in the following studies by isolating the effect of residence time and mass transfer.

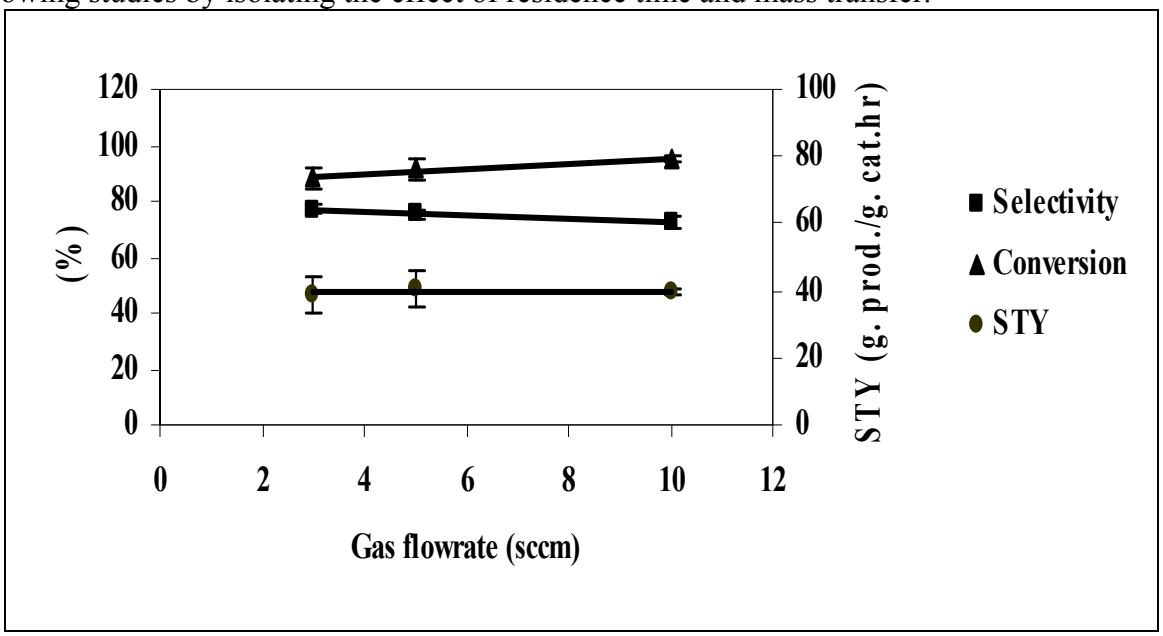

Fig. 1.51 Effect of gas flowrate on reactor performance

(All runs were made at a temperature of 30°C, pressure of 100psig,1% (w/w) substrate in NMP feed liquid, liquid flowrate of 0.05ml/min, catalyst loading=13mg)

The isolation of the effect of residence time on the conversion, selectivity and STY was achieved by varying the catalyst loading with all the other operating conditions remaining constant. All the experiments were carried out at a temperature of 30°C, substrate concentration of 1% (w/w) in NMP, pressure of 100psig, liquid flow rate of 0.05ml/min, and H_2 flow rate of 5sccm. Figure 1.52 shows the results; as expected the conversion and selectivity increase with increase in catalyst loading. The value of STY decreases with increase in catalyst loading because the average reactant concentration decreases at higher conversion.

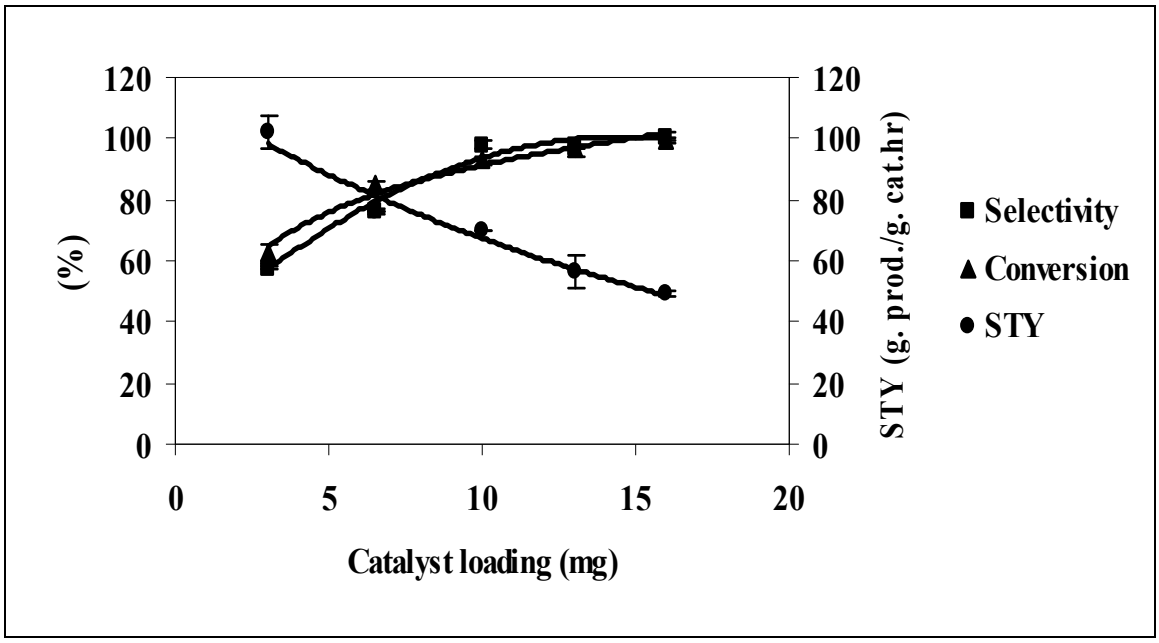

Fig. 1.52 Effect of catalyst loading on reactor performance

(All runs were made at a temperature of 30 °C, pressure of 100psig, 1% (w/w) substrate in NMP feed liquid, gas and liquid flowrate of 5sccm and 0.05ml/min respectively)

The effect of mass transfer on the STY was studied by changing the overall flow velocity at the same residence time within the range of flowrates considered. The residence time was kept constant by increasing the amount of catalyst in proportion to the increase of flow velocity. Figure 1.53 shows the effect of overall velocity on STY. The fact that the reaction rate increases with increase in flow velocity indicates that mass transfer plays an important role. Therefore we can conclude that the reaction in microreactor is controlled by both mass transfer and intrinsic kinetics under the operating conditions used for these experiments.

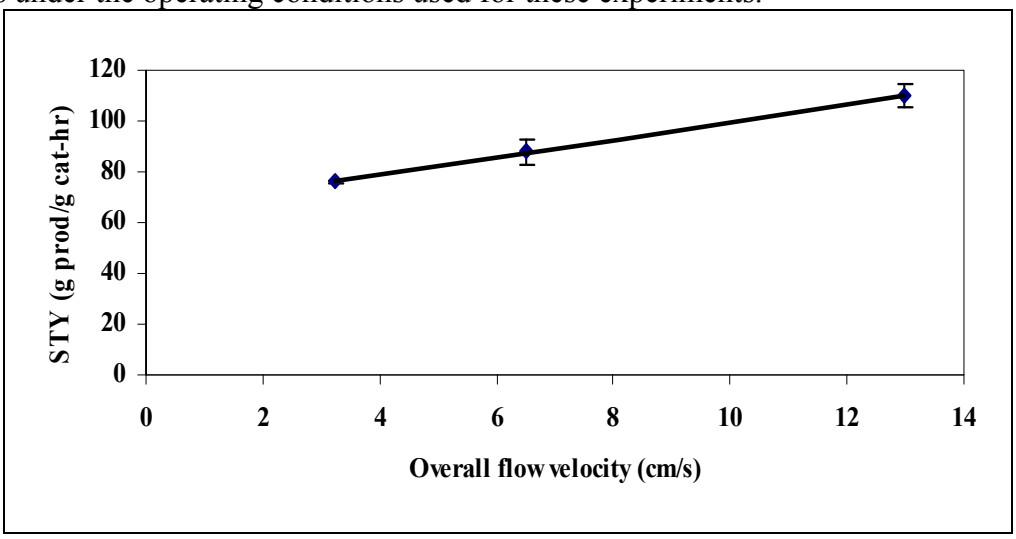

Fig. 1.53 Effect of overall flow velocity at same residence time

(All runs were made at a temperature of 30 °C, pressure of 100psig, 1% (w/w) substrate in NMP feed liquid)

IV.3.2.4. Effect of substrate concentration

To study the effect of substrate concentration on reactor performance, experiments were carried out in the concentration range of 1-10% (w/w) substrate in NMP, temperature of 50°C, 100psig reactor pressure, and a catalyst loading of 13mg of 5% Pd/Alumina. The liquid and hydrogen gas flow rates were 0.05ml/min and 5sccm respectively. Figure 1.54 shows that the increase in substrate concentration results in decrease in conversion. The selectivity is lower at higher substrate concentration indicating that the rate of intermediate formation may have a stronger dependency on the substrate concentration. The STY increases up to substrate concentration of 4% (w/w) in NMP and then starts to decrease thereafter. Similar trend was observed for the hydrogenation of o-nitroanisole at different nitroanisole concentrations (Section III). We observed that the rate of amine formation at high concentrations of o-nitroanisole is low because of substrate inhibition effect present at high concentrations as a result of weak adsorption of hydrogen on catalyst surface in comparison to nitro compound.

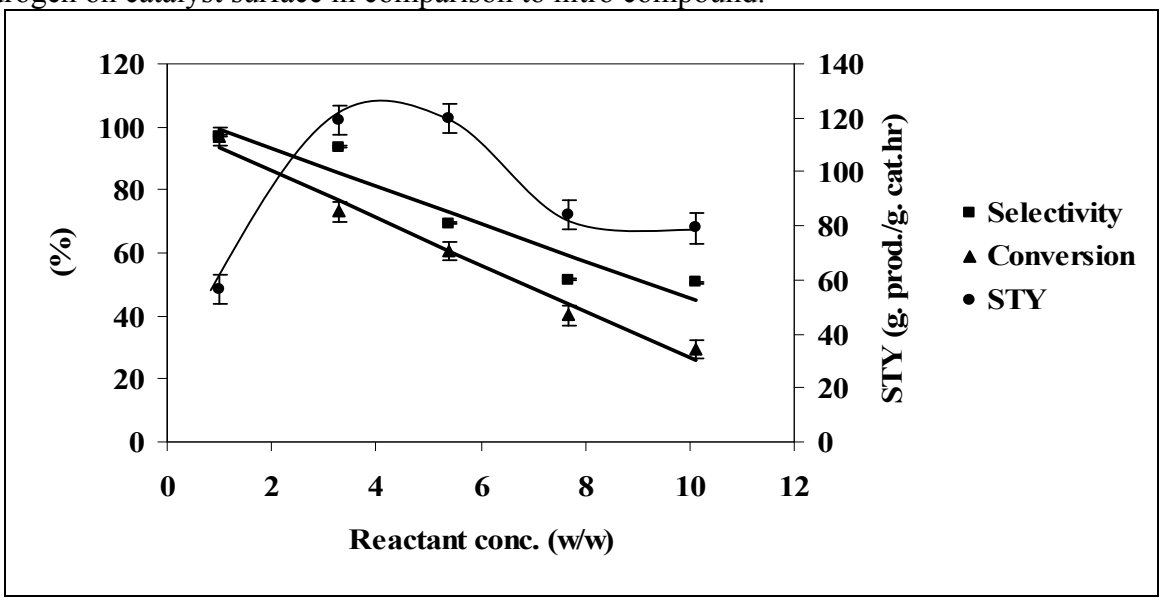

Fig. 1.54 Effect of substrate concentration on reactor performance

(All the runs were made at 30°C, 100 psig reactor pressure, liquid flowrate of 0.05 ml/min, gas flowrate of 5sccm, catalyst loading= 13 mg)

IV.3.3. Kinetic Studies in microreactor

Kinetic studies of fast hydrogenation reactions present a unique challenge because these reactions are usually limited by mass transfer steps. The surface reaction is so rapid that it is difficult to overcome the mass transfer resistances to obtain the true intrinsic kinetics of the reaction. The overall hydrogenation rate for such reactions may be influenced by transport effects such as gas-liquid, liquid-solid mass transfer and internal mass transfer. Hence, prior to determining the true intrinsic kinetics of the present reaction, appropriate conditions have to be selected where the transport effects can be considered to be negligible. The approach used for conducting kinetic studies for this reaction was similar to that used for the hydrogenation of o-nitroanisole in a microreactor (Section III). The first step in this approach is to evaluate the possible mass and heat transfer limitations within the operating conditions used for the experiments, and then study the intrinsic kinetics of the reaction.

IV.3.3.1. Analysis of internal mass transfer effect

The effect of internal mass transfer was studied experimentally by varying the catalyst particle sizes. Experiments were conducted using two different catalyst particle size ranges, 45-75 micron (average size = 60 micron) and 75-150 micron (average size = 112 micron) at different hydrogen pressure values to determine the effect of catalyst particle size on the reaction rate (STY). The effect of particle size on STY at different pressures is shown in fig 1.55. The data in this figure indicate that the values of STY at different pressure levels considered are nearly the same for the two particle size ranges utilized. Hence, it can be concluded that the influence of internal diffusion on the reaction rate can be neglected for the range of pressures and particle size ranges studied. To further validate this conclusion, calculation of the catalyst effectiveness factor η_{eff} was performed. The effectiveness factor calculated under the reaction conditions ranged from 0.8-0.99 as shown in Table 1.7. Since the effectiveness factor for these operating conditions is close to 1 ($\eta_{eff} \rightarrow 1$), the calculations confirm the experimental data which indicate that internal mass transfer does not affect the reaction rate significantly.

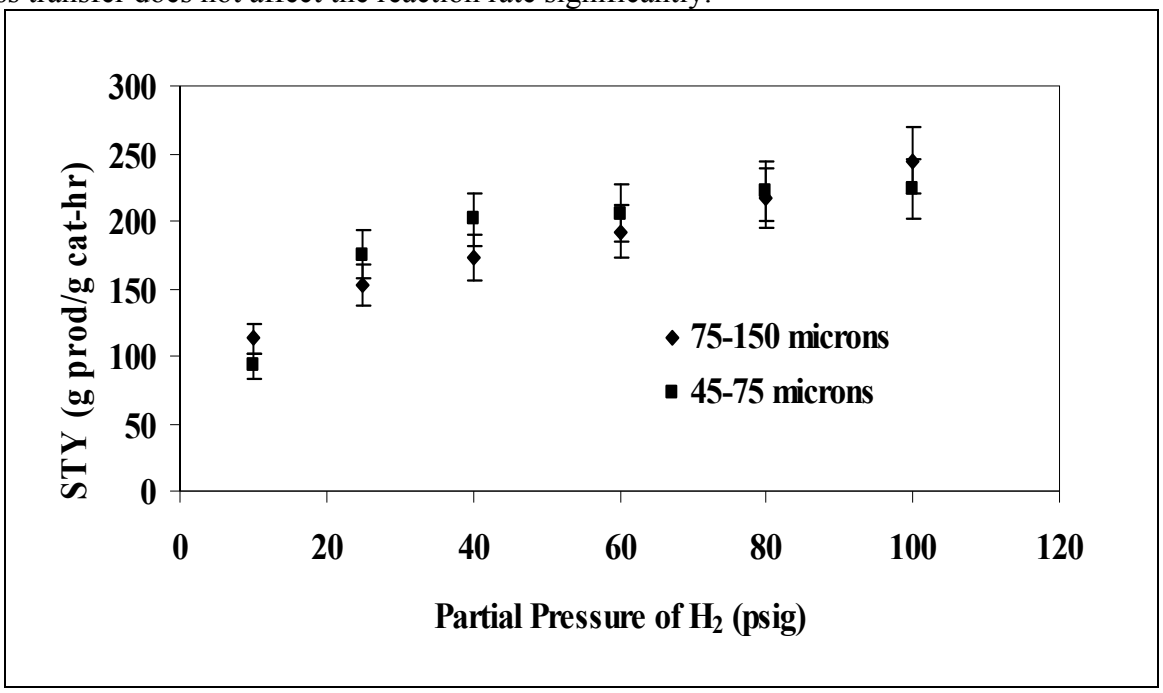

Fig. 1.55 Effect of particle size on STY at different pressures

(All runs were made at a temperature of 50 °C, 1% (w/w) substrate in NMP feed liquid, liquid flow rate of 0.4 ml/min, Overall gas flow rate = 40 sccm, catalyst loading=13mg)

Table 1.7: Calculations for Thiele Modulus and Effectiveness Factor for the different experimental conditions

Pressure (psig)	Cs (mol/L)	r_{obs} (moles/gcat-sec)	$\phi_{min} \geq \phi \leq \phi_{max}$		$\eta_{min} \geq \eta \leq \eta_{max}$	
			ϕ_{min}	ϕ_{max}	η_{min}	η_{max}
10	0.003285	4.97E-04	0.91	1.95	0.81	0.95
25	0.004615	6.71E-04	0.89	1.91	0.82	0.95

40	0.007276	8.21E-04	0.79	1.68	0.85	0.96
60	0.009936	9.20E-04	0.71	1.52	0.87	0.97
80	0.012596	1.02E-03	0.67	1.43	0.89	0.97
100	0.015256	1.08E-03	0.62	1.33	0.90	0.98

IV.3.3.2. Analysis of external mass transfer effect

The presence of external mass transfer limitation was determined experimentally by varying the flow velocity at constant residence time. At constant residence time, and in the absence of mass transfer limitations, the concentration profile and the degree of conversion will be the same for different flow velocities. In section IV.3.2.3, it was observed that the effect of external mass transfer was significant in the range of operating conditions considered. Experiments were conducted beyond this range of operating conditions to see at what overall flow velocity the reaction is controlled by true intrinsic kinetics. Figure 1.56 shows the results obtained from these experiments which were conducted at a constant residence time by varying the gas and liquid flow rates proportionately with the catalyst amounts so as to obtain constant residence time. The data show that the reaction rate increases with increase in flow velocity up to a certain velocity and then remains constant. For different partial pressures, the velocity at which the reaction rate levels off is different because of the change in the concentration of hydrogen at different partial pressures of hydrogen leading to different intrinsic reaction rates. Beyond 26 cm/s, the reaction rate is independent of the overall velocity indicating the absence of external mass transfer limitations for the reaction within the range of partial pressures considered.

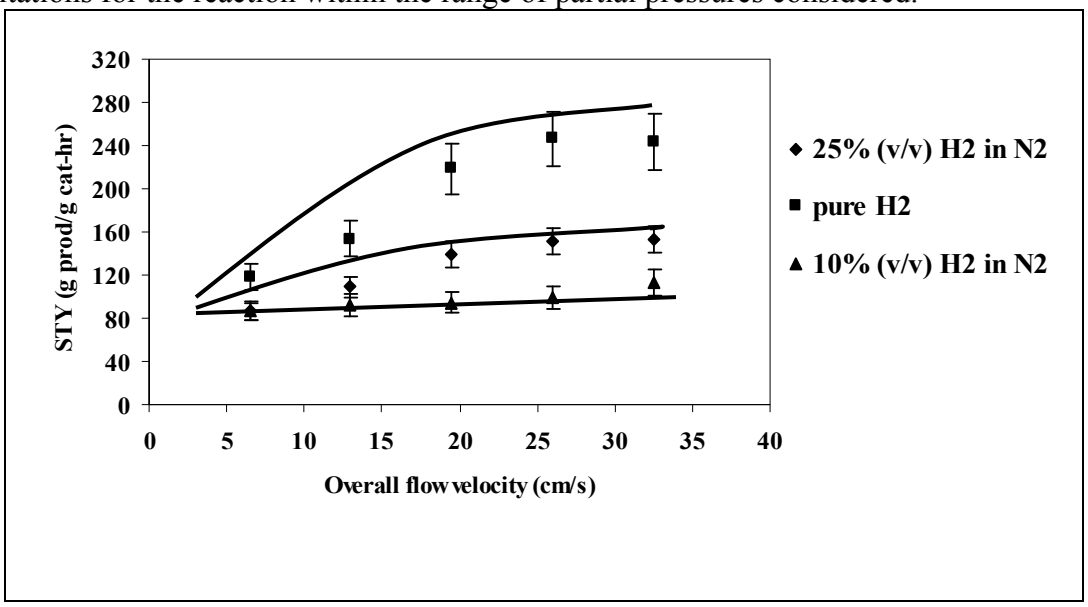

Fig. 1.56 Effect of overall flow velocity on reaction rate for the same residence time

(All runs were made at a temperature of 50 °C, reactor pressure of 100 psig and 1% (w/w) substrate in NMP)

IV.3.3.3. Analysis of heat transfer effects

Apart from mass transfer limitations, heat transfer limitations should also be considered to ensure that the kinetic data obtained in the experimental reactor reflect only kinetic effects. For this purpose, the criteria established by Mears 1971a, 1971b were used to estimate whether heat transport effects were significantly affecting the experimental results. Axial heat transport effect can be neglected if the ratio of axial length of the reactor is much greater (>20) than the catalyst particle size. In the present study, the microreactor length at typical reaction conditions is much greater than the catalyst particle size (>30 times), hence the effect of axial heat conduction can be neglected. However, radial heat transfer effect cannot be assumed to be negligible because radial temperature gradients can lead to reaction rates several thousand folds greater at the axis of the reactor than at the wall due to the absence of heat removal pathway from the axis of the reactor to the environment. A criterion for quantitative analysis of radial heat transport limitations is given by the Damkőhler number for heat transfer (D_a) (Mears 1971a) which is defined by the following equation:

$$D_a = \left| \frac{-\Delta H(-r_{obs})(1-\varepsilon)R_o^2}{\lambda T_w(1+b)} \right| < 0.4\frac{RT_w}{E_a} \tag{1.45}$$

If the left hand side of the above equation is smaller than the right hand side, the transverse temperature difference in the reactor would be less than 5%. In this case, the left hand side was found to be one order of magnitude smaller than the right hand side. Hence, it can be concluded that the heat transfer effects can be neglected in the micro reactor. With all the above considerations, appropriate reaction conditions have been obtained in the microreactor where the reaction is controlled by surface kinetics and not significantly influenced by mass and heat transfer resistances.

IV.3.3.4. Rate analysis using differential method

Experiments were conducted in the microreactor under different operating conditions to determine the kinetic rate expression for this reaction. For these experiments, the overall flow velocity was maintained above 26 cm/s to ensure the absence of external mass transfer limitations and, the conversion of the reactants was limited to 10% so that a differential reactor can be assumed to find the dependence of the reaction rates on the reactant concentrations. The high overall flow velocities used for these experiments resulted in a pressure drop between 10-25psig across the reactor. Hence, the concentration of hydrogen was calculated based on the average partial pressure of hydrogen across the reactor.

The effect of hydrogen partial pressure on the rate of disappearance of nitro compound was investigated in a range of 0-100psig, at temperatures of 30, 40 and 50^{o}C and substrate concentration of 1% (w/w) in NMP. The results are presented in fig. 1.57. The rate of disappearance of nitro compound increases almost linearly with increase in hydrogen partial pressure at constant concentration of nitro compound. The effect of concentration of nitro compound on the rate of disappearance of nitro compound was investigated in the concentration range of 1 to 10% (w/w) at temperatures of 30, 40 and 50^{o}C, and a hydrogen pressure of 100psig. The results are presented in fig. 1.58.

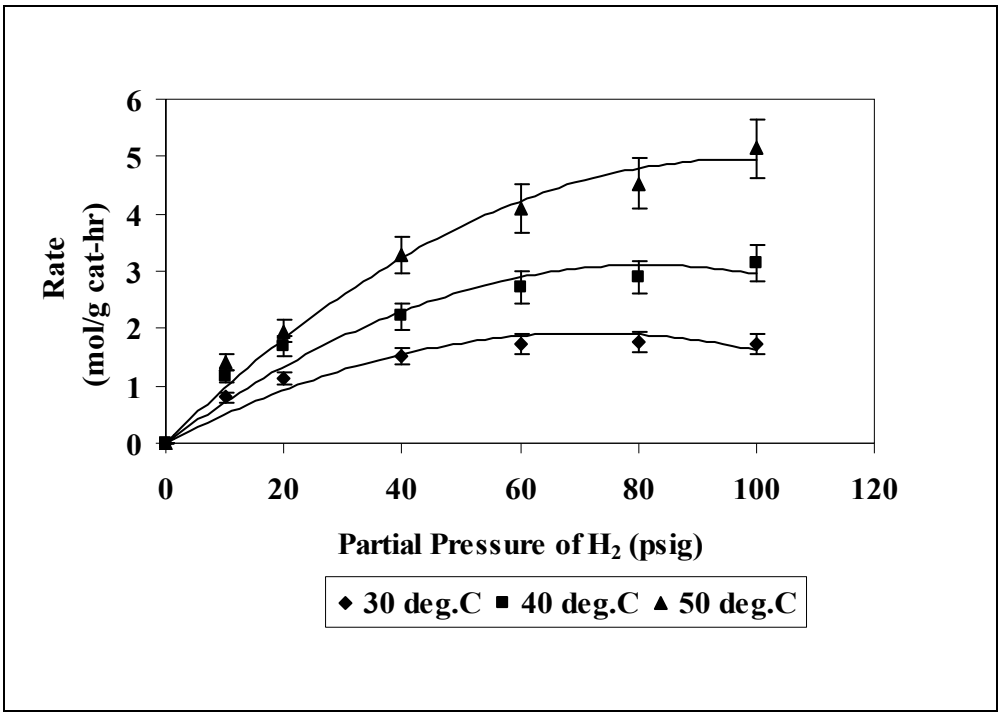

Fig. 1.57 Effect of H_2 partial pressure on the reaction rate of disappearance of nitro compound

The data show that the reaction rate first increases and then decreases with nitro compound concentration. The decrease in the reaction rate at high nitro compound concentration may be because of substrate inhibition effect present at such high concentrations as mentioned in section IV.3.2.4. This suggests that Langmuir Hinshelwood expression should be considered for the rate equation.

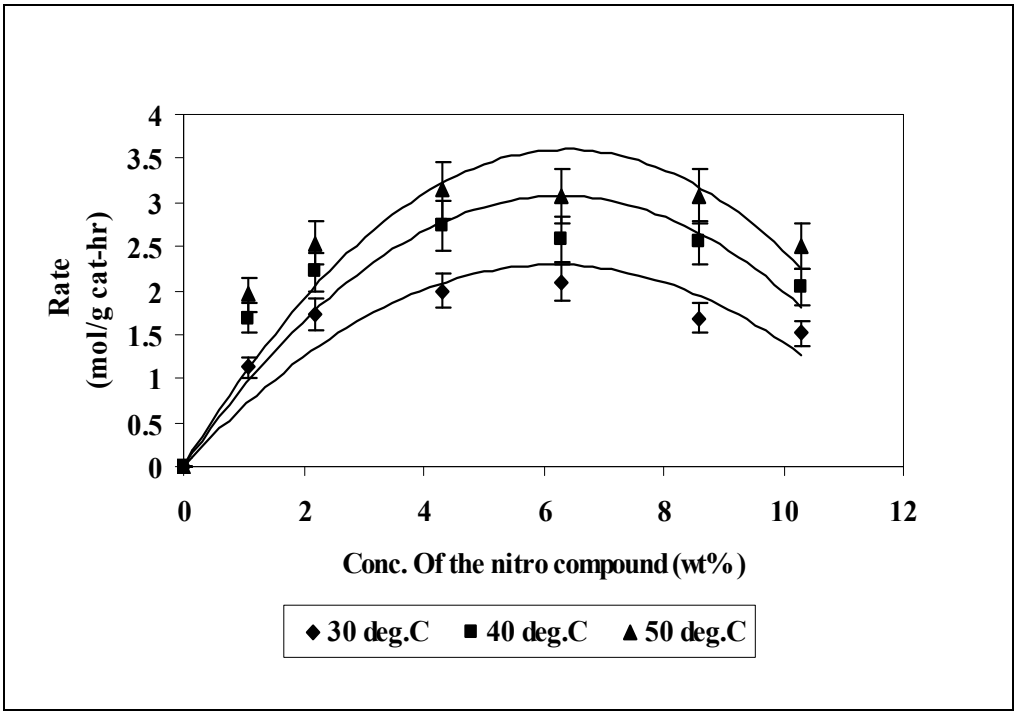

Fig. 1.58 Effect of substrate concentration on the rate of disappearance of nitro compound

The effect of hydrogen partial pressure on the rate of formation of amine was investigated in a range of 0-100psig at temperatures of 30, 40 and 50°C, and substrate concentration of 1% (w/w) in NMP. The results are presented in fig. 1.59. The data show that the rate of formation of amine at 30 and 40°C increases slightly with increase in hydrogen pressure whereas at 50°C, the rate increases almost linearly with increase in hydrogen pressure. This is due to higher adsorption affinity of the reactants at lower temperatures than at higher temperatures. Equilibrium is predominant over intrinsic kinetics at low temperatures and kinetics is more favorable than equilibrium at high temperatures. The effect of concentration of nitro compound on the rate of formation of amine was investigated in a range of 1 to 10% (w/w) (substrate in NMP), at temperatures of 30, 40 and 50°C, and a hydrogen pressure of 100psig. The results are presented in fig. 1.60.

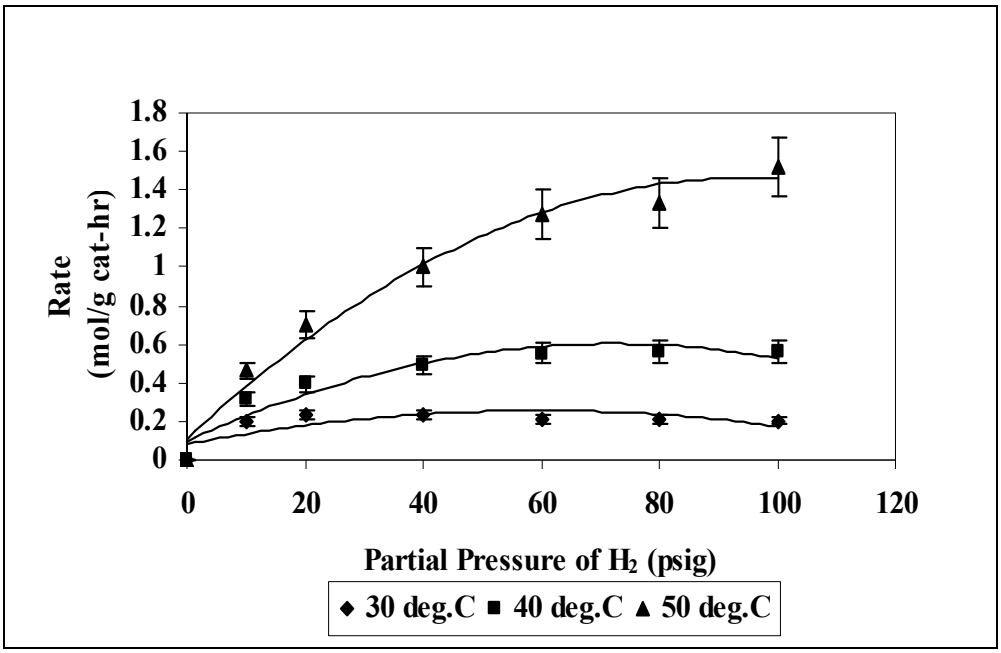

Fig. 1.59 Effect of H_2 partial pressure on the reaction rate of formation of amine

The rate first increases with increase in nitro compound concentration and then decreases slightly with further increase in concentration of nitro compound. A comparison of the data of figures 1.58 and 1.60 shows that the rate of disappearance of nitro compound is higher than the rate of formation of amine, at similar conditions. This suggests that the hydrogenation of the nitro compound to intermediate is faster than the hydrogenation of intermediate to product. For the purpose of kinetic study, the overall reaction was split into two-step series reaction as shown in fig. 1.61.

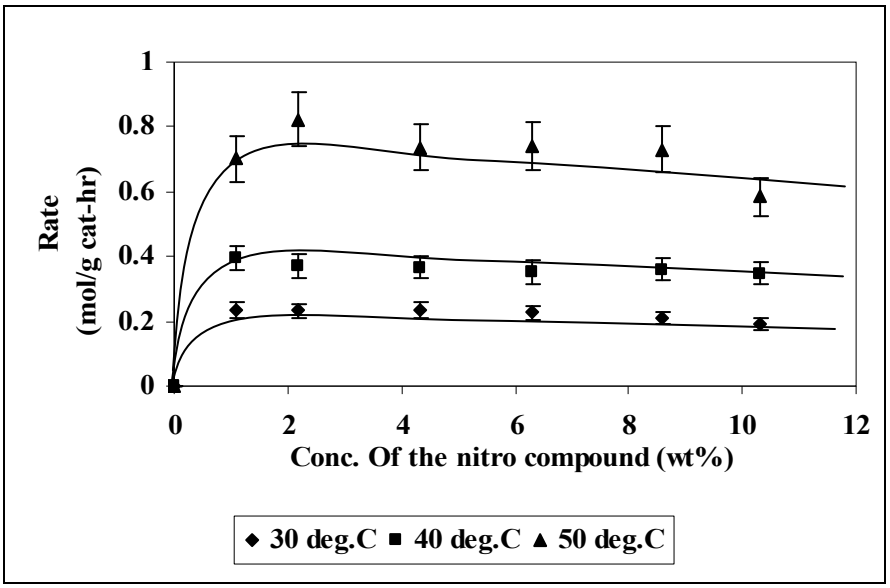

Fig. 1.60 Effect of substrate concentration on the rate of formation of amine

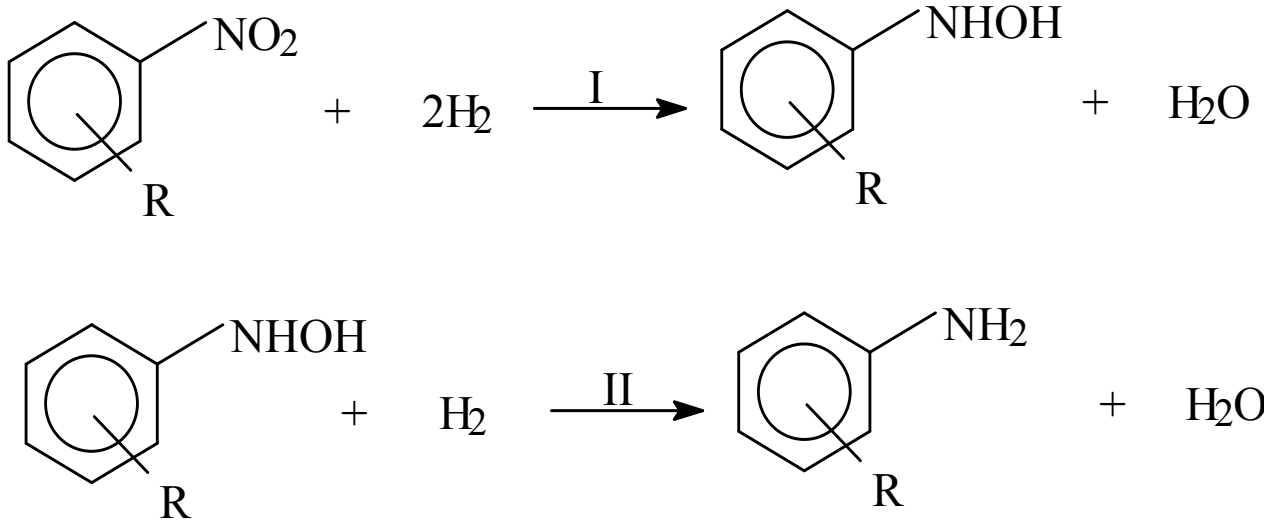

Fig. 1.61 Reaction pathway for the hydrogenation of nitro compound

IV.3.3.5. Kinetic modeling

Langmuir-Hinshelwood (L-H) model was used to develop rate equations for both the reactions. As discussed in Section III, the L-H model for catalytic reactions typically involves a sequence of three steps:

1. Adsorption of the reactants
2. Surface reaction
3. Desorption of the products.

For each of the individual reactions shown in fig. 1.15, these steps occur on palladium sites represented by '(s)'. The mechanistic schemes for both reactions are shown in figs. 1.62 and 1.63 respectively.

Reaction I- Competitive Adsorption

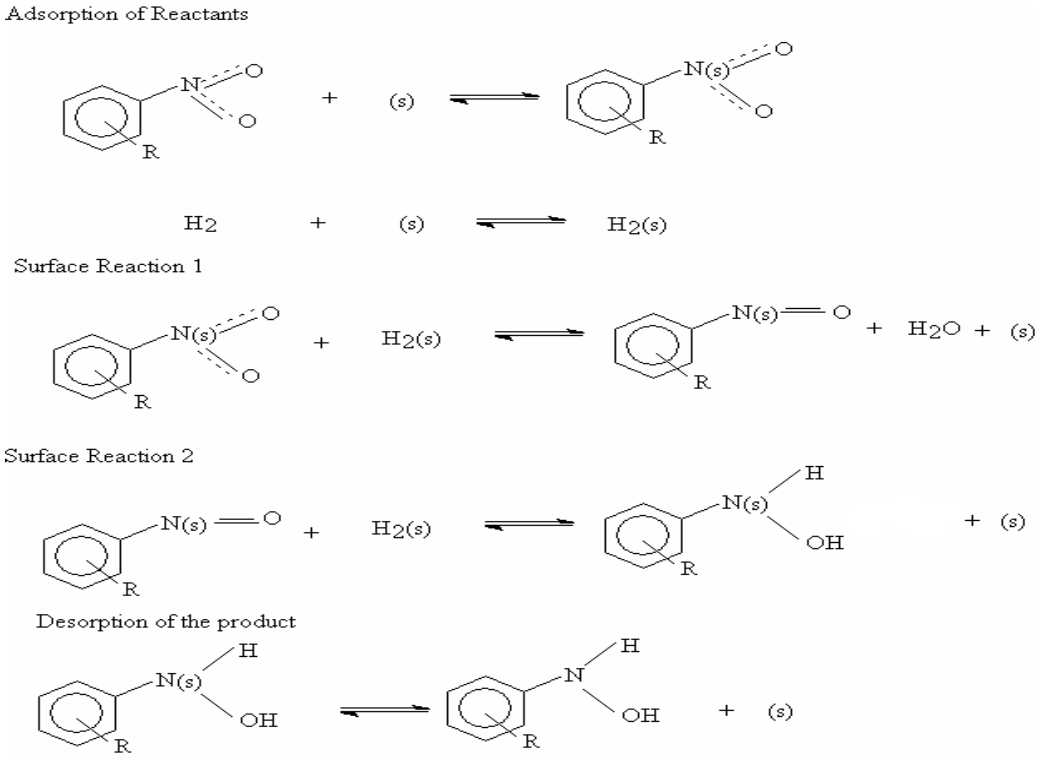

Fig. 1.62 Mechanistic scheme for Reaction 1

Reaction II- Competitive Adsorption

Adsorption of Reactants

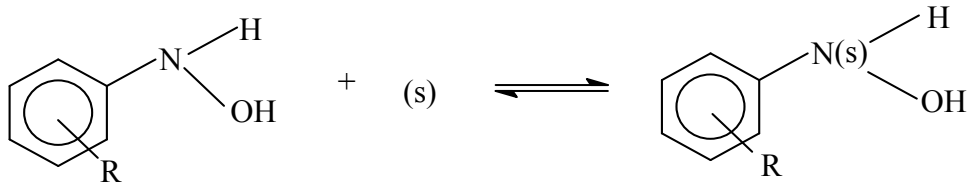

$H_2 + (s) \rightleftharpoons H_2(s)$

Surface Reaction

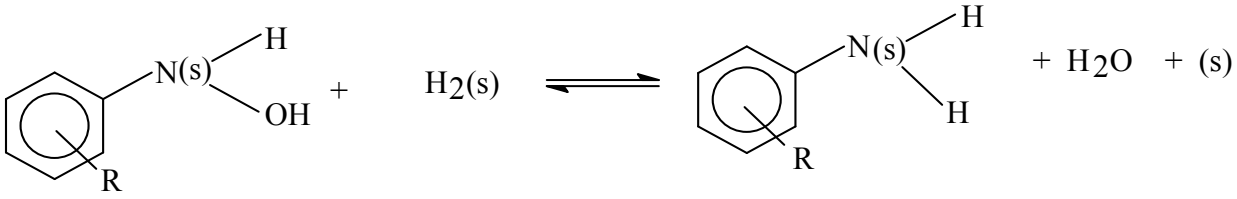

Desorption of the product

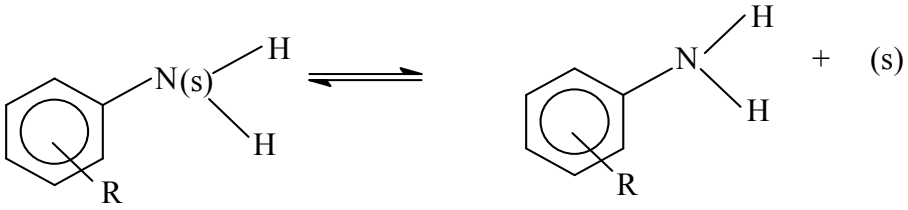

Fig. 1.63 Mechanistic scheme for Reaction 2

Although the mechanisms shown in figures 1.62 & 1.63 correspond to competitive reaction (where the two reactants compete with each other for the same site) and non-dissociative adsorption of hydrogen, other mechanisms such as non-competitive reaction/non-dissociative adsorption of hydrogen, competitive reaction/ dissociative adsorption of hydrogen, and competitive reaction/ dissociative adsorption of hydrogen are also considered. The rate equations from these mechanisms are derived considering each step as the rate limiting step for both the reactions. These rate equations are listed in Table 1.8.

Table 1.2: Rate equations derived from L-H mechanism

Competitive Reaction/ Non-dissociative adsorption of hydrogen

Reaction 1		
No.	Rate limiting step	Rate equation

1	Adsorption of nitro compound	$r_1=k_I(C_N)/(1+(K_{H2I}C_{H2}))$
2	Adsorption of Hydrogen	$r_1=k_I(C_{H2})/(1+(K_NC_N))$
3	Surface Reaction 1	$r_1=k_I(K_{H2I}C_{H2})(K_NC_N)/(1+(K_NC_N)+(K_{H2I}C_{H2}))^2$
4	Surface Reaction 2	$r_1=k_IK(K_{H2I}C_{H2})^2(K_NC_N)/(1+(K_NC_N)+(K_{H2I}C_{H2})+(KK_{H2I}K_NC_NC_{H2}))^2$
4	Surface Reaction 2 (derived by omitting the fractional coverage of intermediates and products [118])	$r_1=k_I(K_{H2I}C_{H2})^2(K_NC_N)/(1+(K_NC_N)+(K_{H2I}C_{H2}))^3$
5	Desorption of intermediate	$r_2= k_IK(K_{H2I}C_{H2})^2(K_NC_N)/((1+(K_NC_N)+(K_{H2I}C_{H2})+(K_aK_N K_{H2I}C_NC_{H2} (1+(K_bK_{H2I}C_{H2})))$
Reaction II		
1	Adsorption of intermediate	$r_2=k_{II}(C_I)/(1+(K_{H2II}C_{H2}))$
2	Adsorption of Hydrogen	$r_2=k_{II}(C_{H2})/(1+(K_IC_I))$
3	Surface Reaction	$r_2=k_{II}(K_{H2II}C_{H2})(K_IC_I)/(1+(K_IC_I)+(K_{H2II}C_{H2}))^2$
4	Desorption of amine	$r_2= k_{II}(C_{H2}C_I)/((1+(K_IC_I))(1+(K_{H2II}C_{H2}))$

Competitive Reaction/ Dissociative adsorption of hydrogen

Reaction 1		
No.	Rate limiting step	Rate equation
1	Adsorption of nitro compound	$r_1=k_I(C_N)/(1+(K_{H2I}C_{H2})^{0.5})$
2	Adsorption of Hydrogen	$r_1=k_I(C_{H2})^{0.5}/(1+(K_NC_N))$
3	Surface Reaction 1	$r_1=k_I(K_{H2I}C_{H2})^{0.5}(K_NC_N)/(1+(K_NC_N)+(K_{H2I}C_{H2})^{0.5})^2$
4	Surface Reaction 2	$r_1=k_IK(K_{H2I}C_{H2})(K_NC_N)/(1+(K_NC_N)+(K_{H2I}C_{H2})^{0.5}+(KK_NC_N(K_{H2I}C_{H2}{}^{0.5})))^2$
4	Surface Reaction 2 (derived by omitting the fractional	$r_1=k_I(K_{H2I}C_{H2})($

	coverage of intermediates and products [118])	$K_N C_N)/(1+(K_N C_N)+(K_{H2I} C_{H2})^{0.5})^3$
5	Desorption of intermediate	$r_2= k_I K(K_{H2I} C_{H2})(K_N C_N)/((1+(K_N C_N)+ (K_{H2I} C_{H2})+(K_a K_N C_N (K_{H2I} C_{H2})^{0.5} (1+(K_b K_{H2I} C_{H2})^{0.5}))$
Reaction II		
1	Adsorption of intermediate	$r_2=k_{II}(C_I)/(1+(K_{H2II} C_{H2})^{0.5})$
2	Adsorption of Hydrogen	$r_2=k_{II}(C_{H2})^{0.5}/(1+(K_I C_I))$
3	Surface Reaction	$r_2=k_{II}(K_{H2II} C_{H2})^{0.5} (K_I C_I)/(1+(K_I C_I)+(K_{H2II} C_{H2})^{0.5})^2$
4	Desorption of amine	$r_2= k_{II}(C_{H2}{}^{0.5} C_I)/((1+(K_I C_I))(1+(K_{H2II} C_{H2})^{0.5})$

Non-Competitive Reaction/ Non-dissociative adsorption of hydrogen

Reaction 1		
No.	Rate limiting step	Rate equation
1	Adsorption of nitro compound	$r_1=k_I(C_N)$
2	Adsorption of Hydrogen	$r_1=k_I(C_{H2})$
3	Surface Reaction 1	$r_1=k_I(K_{H2I} C_{H2})$ ($K_N C_N)/((1+(K_N C_N))(1+(K_{H2I} C_{H2})))$
4	Surface Reaction 2	$r_1= k_I K(K_{H2I} C_{H2})^2(K_N C_N)/((1+(K_N C_N)+(K_a K_N K_{H2I} C_N C_{H2})) (1+(K_{H2I} C_{H2})))$
5	Desorption of intermediate	$r_1=k_I K(K_{H2I} C_{H2})^2(K_N C_N)/((1+(K_N C_N)+(K_a K_N K_{H2I} C_N C_{H2} (1+(K_b K_{H2I} C_{H2})))$
Reaction II		
1	Adsorption of intermediate	$r_2=k_{II}(C_I)$
2	Adsorption of Hydrogen	$r_2=k_{II}(C_{H2})$
3	Surface Reaction	$r_2=k_{II}(K_{H2II} C_{H2})(K_I C_I)/((1+(K_I C_I))(1+(K_{H2II} C_{H2})))$

4	Desorption of amine	$r_2=k_{II}K(K_{H2II}C_{H2})(K_IC_I)/(1+(K_IC_I)+(K_aK_I K_{H2II}C_IC_{H2}))$

Non-Competitive Reaction/ Dissociative adsorption of hydrogen

Reaction 1		
No.	Rate limiting step	Rate equation
1	Adsorption of nitro compound	$r_1=k_I(C_N)$
2	Adsorption of Hydrogen	$r_1=k_I(C_{H2})^{0.5}$
3	Surface Reaction 1	$r_1=k_I(K_{H2I}C_{H2})^{0.5}$ $(K_NC_N)/((1+(K_NC_N))(1+(K_{H2I}C_{H2})^{0.5}))$
4	Surface Reaction 2	$r_1= k_IK(K_{H2I}C_{H2})(K_NC_N)/((1+(K_NC_N)+(K_aK_N C_N(K_{H2I}C_{H2})^{0.5}))(1+(K_{H2I}C_{H2})^{0.5}))$
5	Desorption of intermediate	$r_1= k_IK(K_{H2I}C_{H2})(K_NC_N)/((1+(K_NC_N)+(K_aK_N C_N(K_{H2I}C_{H2})^{0.5}(1+(K_bK_{H2I}C_{H2})^{0.5}))$
Reaction II		
1	Adsorption of intermediate	$r_2=k_{II}(C_I)$
2	Adsorption of Hydrogen	$r_2=k_{II}(C_{H2})^{0.5}$
3	Surface Reaction	$r_2=k_{II}(K_{H2II}C_{H2})^{0.5}(K_IC_I)/((1+(K_IC_I))$ $(1+(K_{H2II}C_{H2})^{0.5}))$
4	Desorption of amine	$r_2=k_{II}K(K_{H2II}C_{H2})^{0.5}(K_IC_I)/(1+(K_IC_I)+(K_aK_I C_I(K_{H2II}C_{H2})^{0.5}))$

The experimental rate data obtained were fitted to these rate equations and were subjected to non-linear regression analysis to estimate the kinetic constants. Based on the best fit in the regression analysis, it was found that surface reactions assuming competitive adsorption and non-dissociative adsorption of hydrogen were the rate controlling steps for the two reactions.

For reaction I (surface reaction 2 controlling)

$$r_1 = k_I(K_{H2I}C_{H2})^2(K_NC_N)/(1+(K_NC_N)+(K_{H2I}C_{H2}))^3 \quad (1.46)$$

For reaction II (surface reaction controlling)

$$r_2= k_{II}(K_{H2II}C_{H2})(K_IC_I)/(1+(K_IC_I)+(K_{H2II}C_{H2}))^2 \quad (1.47)$$

where, k_I and k_{II} are the rate constants for reactions I and II respectively, K_N, K_{H2I}, K_I and K_{H2II} are adsorption equilibrium constants of nitro compound in the presence of hydrogen, hydrogen (for reaction I) in the presence of nitro compound, intermediate in the presence of hydrogen and

hydrogen (for reaction II) in the presence of intermediate respectively. C_{H2}, C_N and C_I are concentrations of hydrogen, nitro compound, and intermediate respectively. The concentration of hydrogen in the reaction medium was obtained from the solubility data for H_2 in NMP from the work of Brunner 1985.

The values of the kinetic constants obtained using the optimization program for these models are given in Table 1.9. Table 1.9 shows that the equilibrium constants of hydrogen for the two reactions are different. This may be due the influence of other reactants competing for the same palladium sites as hydrogen.

Table 1.9: Kinetic constants and regression coefficients for the reactions

Reaction I				
Temperature (deg.C)	**k_I (mol/g-hr)**	**K_N (L/mol)**	**K_{H2} (L/mol)**	**R^2**
30	69.57±0.03	3.07±0.002	174.64±0.096	0.99
40	134.31± 21.89	2.73±0.36	122.59±16.71	0.97
50	296.11± 0.10	2.36±0.001	71.7±0.02	0.98
Reaction II				
Temperature (deg.C)	**k_{II} (mol/g-hr)**	**K_I (L/mol)**	**K_{H2} (L/mol)**	**R^2**
30	1.62± 0.002	203.23±0.91	303.99±1.67	0.97
40	3.96±0.003	152.49±0.66	126.09± 0.24	0.99
50	13.85±0.06	90.53± 2.46	51.15± 0.36	0.98

The rates predicted from the rate equations agree with the experimental rates within 10% error. The activation energies and heat of adsorption of the reactants for reactions I and II were determined from the kinetic constants using the Arrhenius equations:

For rate constant

$$k = k_o e^{\frac{-Ea}{RT}} \tag{1.48}$$

For equilibrium constants

$$K = K_o e^{\frac{-\Delta H}{RT}} \tag{1.49}$$

where k is the rate constant for the reaction, k_0 is the pre-exponential factor for the reaction, Ea is the activation energy for the reaction, K is the equilibrium constant for adsorption of the reactant in the presence of other reactant, K_0 is the pre-exponential factor for the adsorption of the reactant in the presence of other reactant, ΔH is the heat of adsorption for the reactant in the presence of other reactant and T is the temperature in Kelvin. The pre-exponential factors, activation energies and heat of adsorption of reactants calculated using the Arrhenius equations for various kinetics constants are given in Table 1.10. Table 1.10 shows that the heats of

adsorption of hydrogen for the two reactions are different. This difference may also be due the presence of other competitive reactants that are competing for the same sites.

Table 1.10: Pre-exponential factors, activation energies for the reactions and heats of adsorption of the reactants

Pre-exponential factor	
Reaction I	
k_{I0} (mol/g-hr)	9.46E+11
K_{N0} (L/mol)	0.045863
K_{H2I0} (L/mol)	0.000107
Reaction II	
k_{II0} (mol/g-hr)	1.57E+15
K_{I0} (L/mol)	0.000472
K_{H2II0} (L/mol)	9.86E-11
Activation energy and heats of adsorption	
Reaction I	
Ea (kJ/mol)	58.85
ΔH_N(kJ/mol)	-10.60
ΔH_{H2I}(kJ/mol)	-36.13
Reaction II	
Ea (kJ/mol)	87.11
ΔH_I(kJ/mol)	-32.78
ΔH_{H2II}(kJ/mol)	-72.47

In order to further establish the validity of the above rate equations and associated kinetic parameters of the overall reaction, a comparison was made between the experimental data obtained under integral conditions and the theoretical predictions from the above rate equations. Experiments were carried out at different hydrogen pressures and higher amount of catalyst loading under kinetically controlled conditions. The model predictions and experimental data for the yield of the product and the conversion of the reactant under these reaction conditions are shown in fig. 1.64, and are within 5-10% of each other. This excellent agreement suggests that

the rate parameters determined here represent the reactor performance data obtained under both differential and integral conditions.

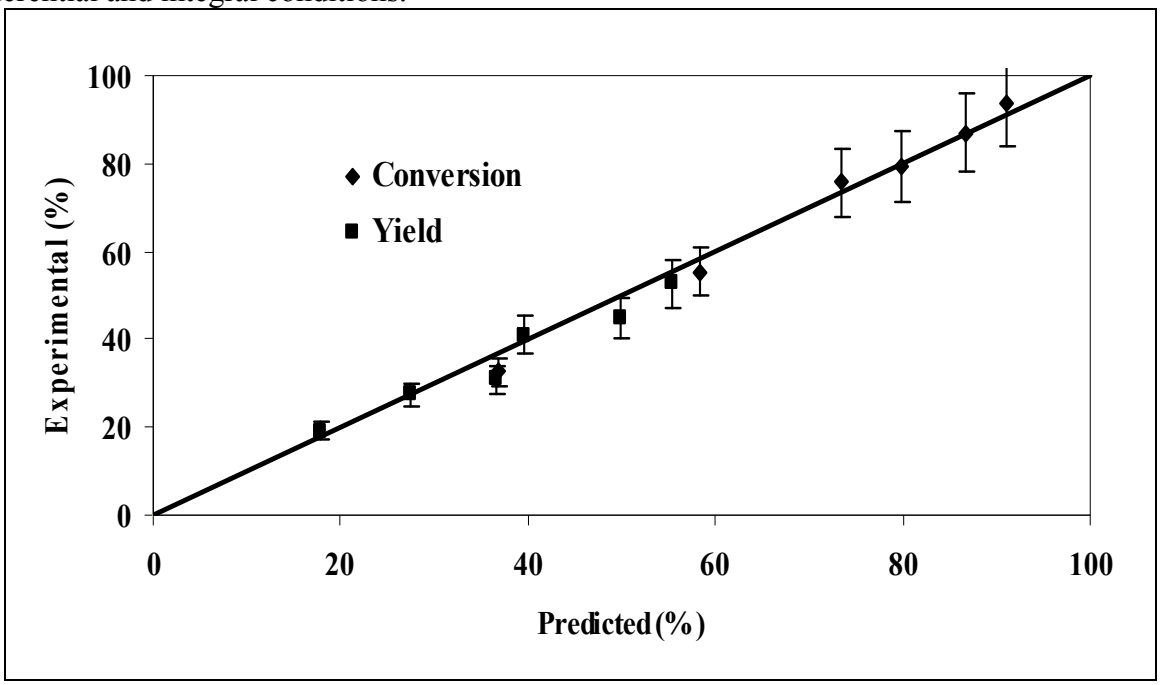

Fig. 1.64 Experimental and predicted yield and conversion for an integral reactor.

IV.3.4. Effect of operating conditions on semi-batch reactor performance

The effect of operating conditions on the performance of the semi-batch reactor was studied by comparing the conversion of the reactant, selectivity and Space-Time Yield (STY) of the product under different reaction conditions.

IV.3.4.1. Effect of pressure

To study the effect of pressure on conversion, selectivity and STY, experiments were carried out in the pressure range of 10-100 psig at a substrate concentration of 1% (w/w) in NMP, temperature of 50°C, stirrer speed of 1000rpm and a catalyst loading of 3mg. Figure 1.65 shows the experimental data obtained under these reaction conditions after a reaction time of one hour. The data show that the conversion, selectivity and STY increase with increase in pressure. This increase is attributed to the increase in the concentration of dissolved hydrogen with increase in pressure. The STY or reaction rate increases almost linearly with increase in pressure indicating that the dependence of reaction rate on the concentration of hydrogen is almost linear.

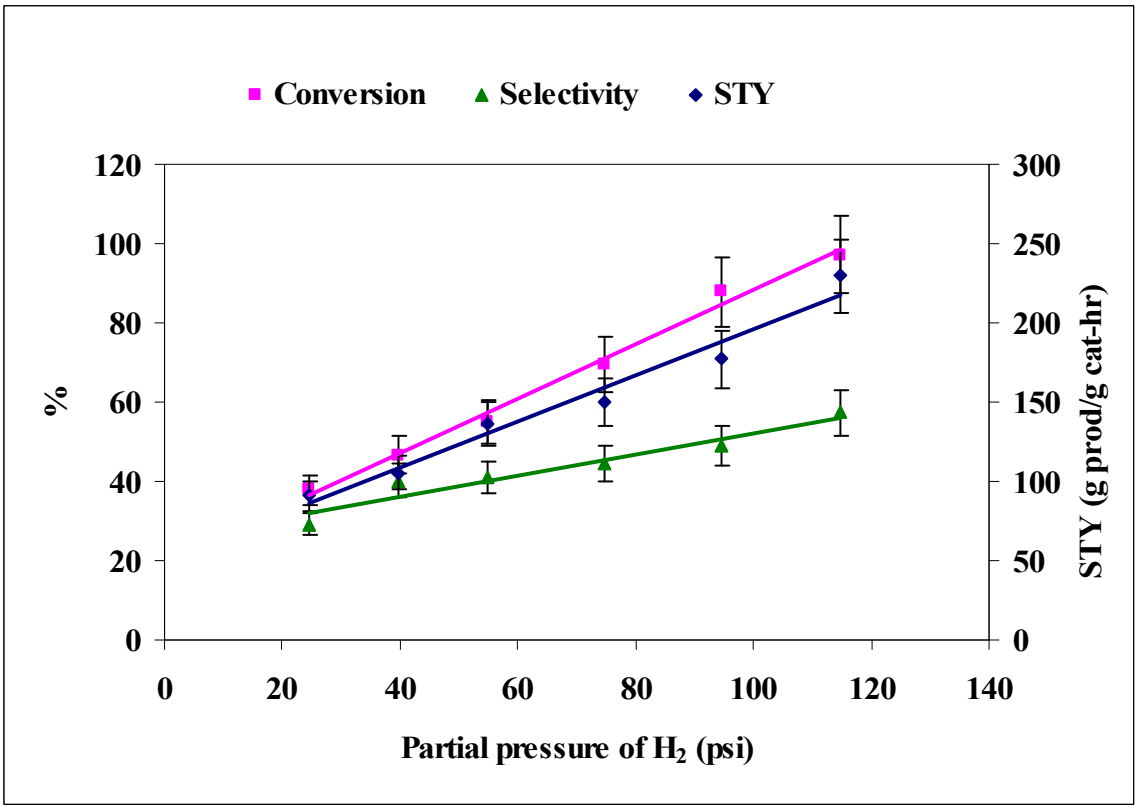

Fig. 1.65 Effect of pressure on the reactor performance

(3mg of 5% Pd/Alumina catalyst, initial substrate concentration=1% (w/w) in NMP, Reactor temperature=50°C)

IV.3.4.2. Effect of temperature

To study the effect of temperature on conversion, selectivity and STY, experiments were carried out in the temperature range of 30-60°C, substrate concentration of 1%(w/w) in NMP, pressure of 100psig and a catalyst loading of 13mg. The stirrer speed used for these experiments was 400 rpm. Figure 1.66 shows that with increase in temperature, the conversion, selectivity and STY increase. This trend in STY may suggest that the reaction is controlled by intrinsic kinetics. However, the effect of mass transfer on the reaction rate has to be studied first to see if mass transfer has a higher influence on the reaction rate than the temperature under these conditions, in which case it will be controlled by mass transfer. The effect of mass transfer was studied under these reaction conditions (discussed in section IV.3.4.3) and it was shown that at 400rpm, the reaction is controlled by mass transfer. This implies that mass transfer has a higher effect on the reaction rate than temperature under these reaction conditions indicating that the reaction is controlled by mass transfer.

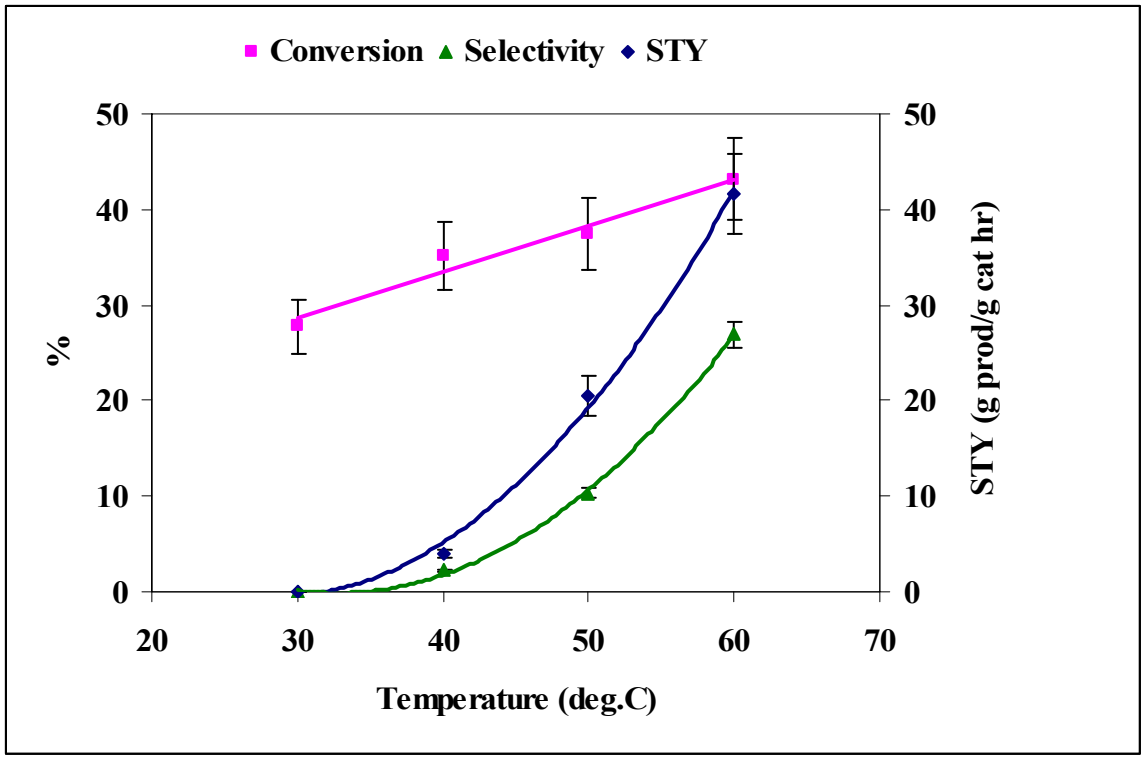

Fig. 1.66 Effect of temperature on the reactor performance

(13mg of 5% Pd/Alumina catalyst, initial substrate concentration=1% (w/w) in NMP, Reactor pressure=100psig)

IV.3.4.3. Effect of stirrer speed

The effect of external mass transfer on the rate of reaction was studied by varying the agitation speed to obtain the speed beyond which the reaction rate is no longer controlled by mass transfer i.e. the reaction rate does not change with stirrer speed. In order to study intrinsic kinetics of any reaction, it should be ensured that the effect of mass transfer resistances on the reaction rate is negligible in the range of operating conditions considered.

Experiments were conducted in the semi batch reactor at different stirrer speeds to determine the speed at which the external mass transfer effect for this reaction can be considered to be negligible. Figure 1.67 shows the effect of stirrer speed on the STY of the product. The data show that the STY keeps increasing with increase in stirrer speed even up to the maximum stirrer speed of 1000 rpm. This implies that this reaction is controlled by mass transfer even at the highest stirrer speed attainable by the batch reactor. Hence it is difficult to conduct kinetic studies in this semi-batch reactor for this reaction, and all other reactions which are much faster than this reaction. A semi-batch reactor with a higher maximum stirrer speed is required for studying the kinetics of such fast reactions.

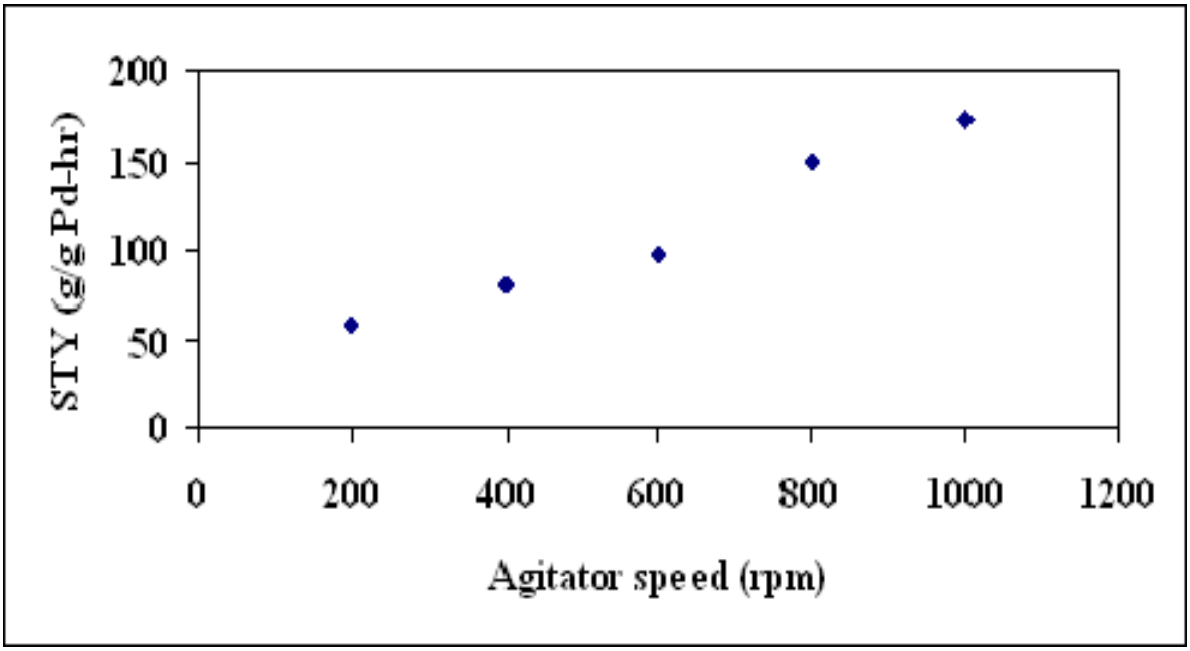

Fig. 1.67 Effect of stirrer speed on the reactor performance
(3mg of 5% Pd/Alumina catalyst, 50°C reactor temperature, initial substrate concentration=1% (w/w) in NMP, Reactor pressure=100psig)

It is clearly evident that a microreactor is more efficient than the conventional laboratory reactors in obtaining intrinsic kinetic data for fast hydrogenation reactions because of their high mass transfer and mixing characteristics. In order to better understand the mass transfer abilities of the two reactor systems, a mass transfer analysis was conducted for both reactors which will be discussed in the following section.

IV.3.5. Mass transfer analysis

An evaluation of the mass transfer characteristics of the reactor system is important in deciding which reactor system is better suited for conducting kinetic studies for different types of reactions. Especially for fast reactions, the mass transfer rate has to be high enough for the reaction to be controlled by true intrinsic kinetics. In this study, the mass transfer efficiencies of the microreactor and the semi-batch reactor have been evaluated. The approach used for evaluation was similar to that used for the hydrogenation of o-nitroanisole where the two reactors were modeled under different reaction conditions and the modeling results were compared with the experimental data to estimate the mass transfer coefficients in the two reactor systems (Section III). For modeling the two reactor systems, the intrinsic rate expressions obtained in the packed bed microreactor were used.

The experimental results in the microreactor at different overall flow velocities while keeping the residence time constant (by varying catalyst loading) are shown in Fig. 1.10. The product yields obtained from these experiments were compared with the yields obtained from simulation under similar conditions to estimate the overall mass transfer coefficients. Figure 1.68 shows the overall mass transfer coefficient (K_{la}) values estimated under the present reaction conditions. The data clearly show that the mass transfer coefficient is a function of overall linear velocity. The mass transfer coefficient values obtained in the packed bed microreactor under the present experimental conditions range between 0.2 and ~21 s^{-1}.

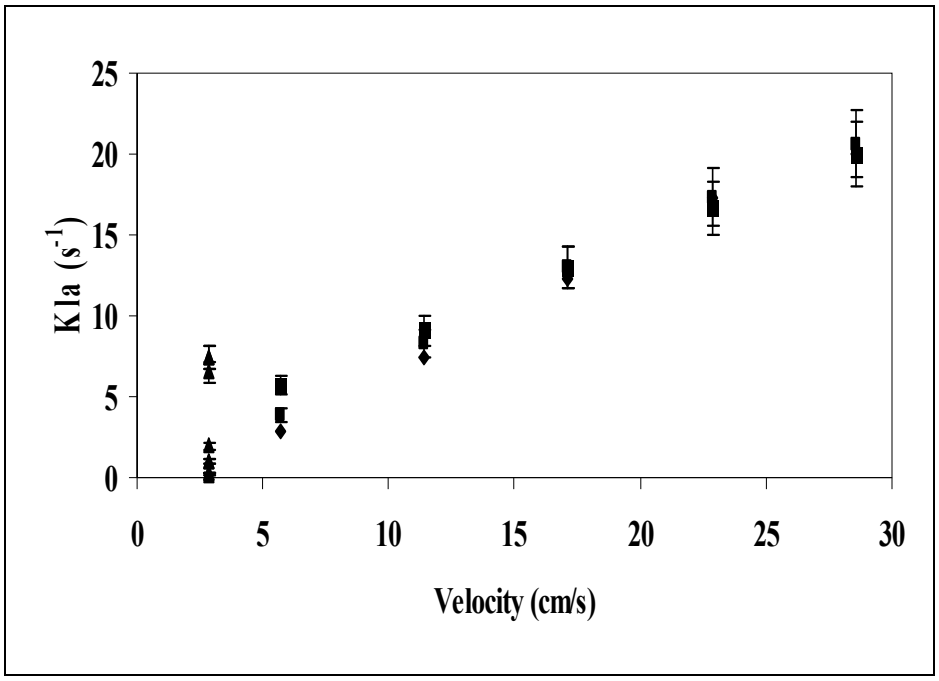

Fig. 1.68 Mass transfer coefficients in the microreactor as a function of overall velocity

The semi-batch reactor was also modeled under similar reaction conditions and the modeling results were compared with the experimental data obtained in the semi-batch reactor to evaluate the mass transfer coefficient. Figure 1.69 shows the overall mass transfer coefficient (K_{la}) values estimated by comparing the conversion from the modeling results with the experimental data under different stirrer speeds. The data clearly show that the mass transfer coefficient in the semi-batch reactor increases with increase in the stirrer speed. The mass transfer coefficient in the semi-batch reactor ranges from 0.0005 to 0.0025 s^{-1} under these reaction conditions.

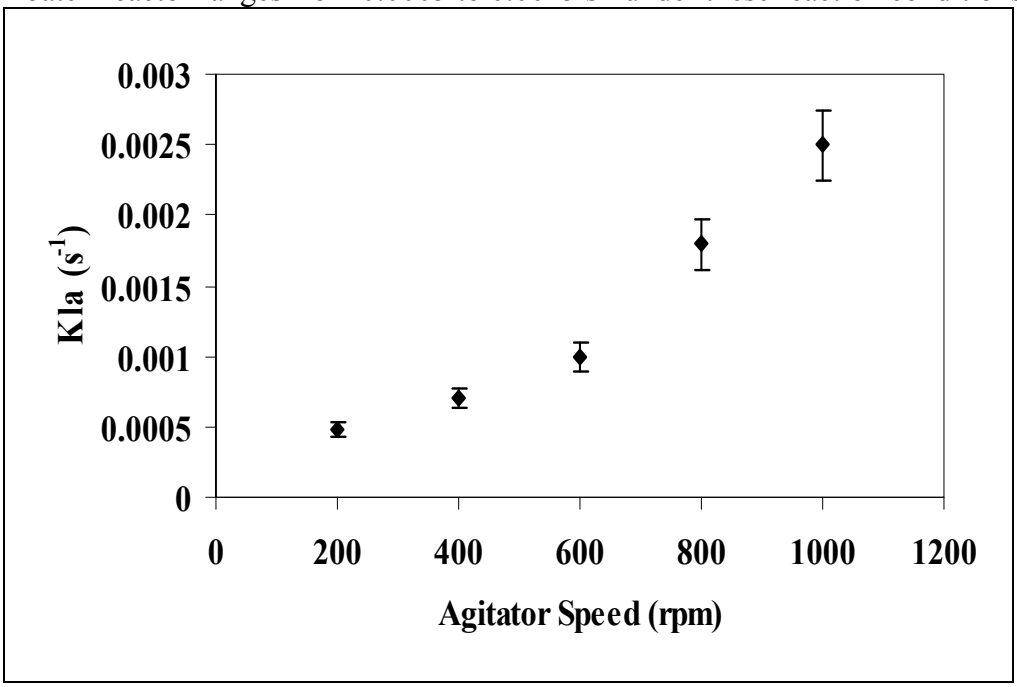

Fig. 1.69 Mass transfer coefficients in the semi-batch reactor as a function of stirrer speed

By comparing these mass transfer coefficient values with those obtained for the hydrogenation of o-nitroanisole (Section III) in the two reactor systems, it was observed that these values are an order of magnitude less than the values obtained for the hydrogenation of o-nitroanisole for similar velocities. This could be attributed to the influence of factors such as diffusivities or viscosities of the liquids that contribute to the mass transfer coefficient. For this reaction, it can be clearly seen that the mass transfer coefficient values in the microreactor are two to four orders of magnitude higher than those of the semi-batch reactor. This tremendous increase in the mass transfer coefficient values result from much higher gas-liquid interfacial area in the microreactor than in the semi-batch reactor due to higher surface to volume ratio and strong convections created at the gas-liquid interface by flow circulations in bulk slugs. This increase in the mass transfer rate in the microreactor enables the reaction to operate close to intrinsic kinetics for fast reactions. Hence, it is clearly evident that the microreactor is more efficient than the semi-batch reactor for obtaining the intrinsic kinetics for this reaction.

IV.3.6. Comparison of semi-batch reactor and microreactor data

For fast reactions, a comparison of the mass transfer rates in the two reactors is the real test of how the difference in the mass transfer coefficients translates into actual reactor performance. The mass transfer rates in the two reactors can be obtained by operating the reactor in the mass transfer controlled region. For comparison of the mass transfer rates, the reaction conditions in the two reactors were selected such that the experimental data fall under the mass transfer controlled region. Under these conditions, the STY represents the average mass transfer rates in the reactors. In the microreactor, the conditions under which the reaction is mass transfer controlled region are at an overall flow velocity of less than 5cm/s, temperature range of 30-60°C, pressure of 100psig, substrate concentration of 1% (w/w) in NMP and a catalyst (5%Pd/Alumina) loading of 13mg. Experiments were conducted in a semi-batch reactor under similar reaction conditions as the microreactor. The stirrer speed used for these experiments was 400 rpm which represents the speed in the mass transfer controlled region in the semi-batch reactor. Figure 1.70 shows the comparison of the STY and yield of the product for the two reactor systems at different temperatures. The data show that the STY and yield values in the microreactor are much higher than those of the batch especially at lower temperatures. The trend in the STY may indicate that at much higher temperatures the STY in the two systems will be the same. However, the STY at high temperatures in the microreactor represents the average reaction rate for yields which are close to 100% at which the reaction rate is the least. This implies that for the yields obtained in the semi-batch reactor the reaction rates in the microreactor will be higher than the STY reported here. Therefore, the mass transfer rates in the microreactor are much higher than those of the batch reactor. This explains why it was possible to conduct kinetic studies for this reaction in the microreactor and not in the semi-batch reactor.

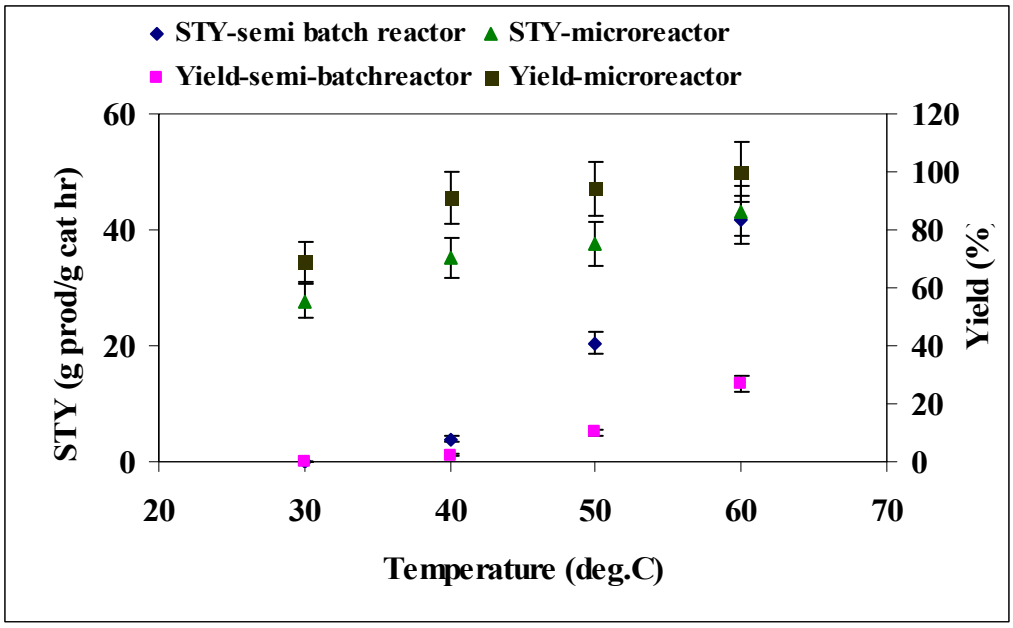

Fig. 1.70 Comparison of reactors performance
(All the runs were made at 100 psig reactor pressure, catalyst loading= 13 mg, microreactor flow velocity=3.25cm/s, semi-batch reactor stirrer speed= 400rpm)

The present reaction is a perfect example of a fast reaction where the advantages of conducting the kinetics study in the microreactor were clearly demonstrated. A batch reactor cannot be used to obtain intrinsic kinetic study for such reactions unless the reactors are designed to attain higher stirrer speeds to match the mass transfer characteristics of the microreactor. Hence, the microreactor is more efficient in obtaining intrinsic kinetics of fast hydrogenation reactions than the conventional batch reactors.

IV.4. Conclusions

A packed-bed microreactor for the hydrogenation of aromatic nitro ketone at moderate temperature and pressure has been demonstrated. The effect of different operating conditions on the reactor performance was studied using 5% Pd/Alumina catalyst. The experimental results indicate that at low overall flow velocities (<26 cm/s) the reaction is controlled by both mass transfer and intrinsic kinetics in the microreactor. Beyond 26cm/s, external mass transfer resistances were found to be negligible. Also, internal mass transfer and heat transfer resistances were established to be negligible in the microreactor. Hence, the reaction is kinetically controlled in the microreactor under these reaction conditions.

Two separate reaction steps were identified from the kinetic studies: The reduction of nitro compound to hydroxyl amine and the further reduction of hydroxyl amine to amine. Langmuir-Hinshelwood type rate expressions were found to be suitable for these reaction steps with surface reactions controlling the two reaction steps. A set of rate equations was derived based on L-H model and the kinetic rate constants were obtained from regression of the experimental data in a differential microreactor. The obtained kinetics was able to predict the integral reactor behavior under kinetic-controlled regime. In spite of the excellent mass transfer characteristics of the microreactor, there are limited studies on the use of microreactor for obtaining intrinsic kinetics of fast reactions. The present study has demonstrated the use of a packed-bed microreactor for

obtaining the intrinsic kinetics of a fast hydrogenation reaction that is controlled by mass transfer in conventional reactors.

The effects of different operating conditions on the semi-batch reactor performance were studied. The results showed that it is difficult to obtain intrinsic kinetics of this reaction in the semi-batch reactor due to mass transfer limitations even at the highest stirrer speed attainable. The mass transfer coefficients of the two reactor systems were evaluated from the simulation and experimental results. It was found that, for this reaction the mass transfer coefficient values in the microreactor were two to four orders of magnitude higher than those of the semi-batch reactor. This difference in the mass transfer coefficient values translates into a huge difference in the mass transfer rates of the two systems as evidenced by the difference in their STYs.

V. References

Acres G. J. K. and B.J. Cooper, *J. Appl. Chem. Biotechnol., 22* (1972) 769.

Ajmera S. K., C. Delattre, M.A. Schmidth and K.F. Jensen, *J. of Catal., 209* (2002) 401-412.

Albers P., J. Pietsch, and S. F. Parker, *J. Mol. Cat A: Chem, 173* (2001) 275-285.

Al-Dahhan M. H., F. Larachi, M.P. Dudukovi and A. Laurent, *Ind. Eng. Chem. Res., 36* (1997) 3292-3314.

Bartholomew C. H., *Applied Cat. A: General, 212* (2001)17-60.

Brahme P. H., H. G. Vadgaonkar, P. S. Ozarde and M.G. Parande, *J. Chem. Eng. Data., 27* (1982) 461-462.

Brunner E., *J. Chem. Eng. Data, 30* (1985) 269-273.

Chaudhari R. V., M.G. Parande, P.A. Ramachandran and P.H. Brahme, *I.Chem.E. Symposium Series No. 87,* (1983) 205-213.

Figueras F. and B. Coq, *J. of Mol. Catal. A: Chemical, 173* (2001) 223-230.

Fisher R. H. and H. M. Weitz, *Syntheses,* (1980) 261-282.

Fogler H., Elements of Chemical Reaction Engineering, 2nd edition (1992) Chapter 11, 617.

Goto S. and J. M. Smith, *AIChE J., 21* (1975) 706-713.

Hajek J. and D. Yu. Murzin, *Ind. Eng. Chem. Res., 43* (2004) 2030-2038.

Haldar P. and V.V. Mahajani, *Chem. Eng. J, 104* (2004) 27-33.

Hatziantoniou V., B. Andersson and N. Schöön, *Ind. Eng. Chem Process Des Dev., 25* (1986) 964-970.

Hernandez L. and F.F. Nord, *Experientia, 3* (1947) 489.

Hernandez L. and F. F. Nord, *J. Colloid Sci., 3* (1948) 363-375.

Iliuta I., F. Larachi, B. P. A. Grandjean and G. Wild, *Chem. Eng. Sci., 54* (1999) 5633-5645.

Kreutzer M. T., P. Du, J. J. Heiszwolf, F. Kapteijn and J. A. Moulijn, *Chem. Eng. Sci., 56 (22)* (2001) 6015-6023.

Kreutzer M. T., F. Kapteijn, J. A. Moulijn, J. J. Heiszwolf, *Chem. Eng. Sci.*, *60* (2005) 5895-5916.

Losey M. W., M.A. Schmidt and K. F. Jensen, *Ind. Eng. Chem. Res.*, *40* (2001) 2555-2562.

Mears D. E., *Ind. Eng. Chem. Process Dev. Develop. 10* (1971a) 541-547.

Mears D. E., *J. Catal., 20* (1971b) 127-131.

Mills P. L. and R. V. Chaudhari, *Catal. Today*, *37* (1997) 367-404.

Natividad R., R. Kulkarni, K. Nuithitikul, S. Raymahasay, J. Wood and J. M. Winterbottom, *Chem. Eng. Sci., 59* (2004) 5431-5438.

Nijhuis T. A., F. M. Dautzenberg and J.A. Moulijn, *Chem. Eng. Sci., 58* (2003) 1113.

Nijhuis T. A., M. T. Kreutzer, A. C. J. Romijn, F. Kapteijn and J. A. Moulijn, *Chem. Eng. Sci., 56 (3)* (2001) 823-829.

Perry R. H. and C.H. Chilton, Chemical Engineering Handbook, 5th ed., McGraw Hill, New York (1973).

Qian D., and A. Lawal, *Chem. Eng. Sci., 61* (2006) 7609-7625.

Satterfield C. N., Mass Transfer in Heterogeneous Catalysis*,* M. I. T. Press, Cambridge, England (1970) Chapter 2.

Smith H. A. and Jr. W. C. Bedoit, *J. Phys. Chem., 55* (1951)1085-1104.

Smith H. A. and Jr. W. C. Bedoit, Catalysis, Emmett, P. H., Ed., Reinhold: New York, (1955) Vol.3, 149.

Tong S. B., K.F. O'Driscoll and G.L.Rempel, *Can. J. Chem. Eng., 56* (1978) 340.

Van gelder K. B., J. K. Damhof, P. J. Kroijenga and K. R. Westerterp, *Chem. Eng. Sci., 45* (1990) 3159-3170.

Versteeg G. F., J. B. M. Visser, L. L. Van Dierendonck and J. A. M. Kuipers, *Chem. Eng. Sci., 52* (1992) 4057-4067.

Winterbottom J. M., In Catalysis and Chemical Processes; R. Pearce, W.R. Paterson, Eds. Leonard Hill: London, (1981) 318.

Yeong K. K., A. Gavriilidis, R. Zapf and V. Hessel, *Catal. Today*, *81* (2003) 641-651.

Yeong K. K., A. Gavriilidis, R. Zapf and V. Hessel, *Chem. Eng. Sci., 59* (2004) 3491-3494.

Zhao F., M. Shirai, M. Arai, *J Mol. Cat. A: Chem., 154* (2000) 39-44.

Zhao F., M. Shirai, Y. Ikushima, M. Arai, *J Mol. Cat. A: Chem., 180* (2002) 211-219.

TASK 2: Multifunctional Thin-Film Catalyst Development

Our overall approach was to develop a library of catalyst integration methods applicable to this important research project in our Center. The catalyst integration approaches that we developed include:

- Open-channel surface-selective infiltration and deposition of sol-gel catalyst coating
- Closed-channel forced-flow infiltration and deposition of sol-gel catalyst coating
- Infiltration and immobilization of commercial catalyst particles by layer-by-layer self-assembly into various microreactor geometries
- Dipping approaches for infiltrating and depositing sol-gel catalyst coating into microcellular structures
- Infiltration and synthesis of microcellular structures that fill up microchannel volume

In the following sections, we summarized mainly our research activities on surface-selective infiltration and deposition of sol-gel catalyst coating, closed-channel forced-flow infiltration and deposition of sol-gel catalyst coating, layer-by-layer self-assembly of commercial catalyst, and synthesis of cellular structure inside the microchannels.

(1) Open-channel surface-selective infiltration and deposition of sol-gel catalyst coating

We developed a procedure to prepare and selectively infiltrate Pt/Al_2O_3 thin-film into "open" microchannel Si reactors. As shown in the Figure 2.1 below, we were able to synthesize highly dispersed Pt particles into a porous Al_2O_3 thin-film by sol-gel. Based on our characterization results, the thin film was determined to possess the following characteristics: BET surface area = 480 m^2/g, average Pt particle size = 11 nm, average pore diameter = 6 nm, and crystal structure of Al_2O_3 = amorphous.

Based on this procedure, we also developed a proprietary sol-gel synthesis procedure for preparing a Pd/alumina thin-film H_2O_2 synthesis catalyst on flat Si and stainless steel (SS) substrates with a thickness of a few microns. As evident from Figure 2.2, the thin-film catalyst is uniform, microcrack-free, and adherent. We also characterized the structure, morphology, and chemical compositions of the thin-film catalyst prepared by our proprietary technique, and compared to those of conventional powder catalysts using transmission electron microscopy

(TEM), scanning electron microscopy (SEM), energy dispersive spectroscopy (EDS), X-ray diffraction (XRD), BET surface area measurements, and inductively coupled plasma (ICP). The characterization results indicated that the key characteristics of our thin-film catalyst (i.e., surface area, pore size, density, and Pd loading) compared favorably to those of commercially available powder catalyst.

An open-channel surface-selective infiltration and deposition was also developed for stainless steel-based microchannel reactors. As shown in Figure 2.2, a support stage, which provides microfluidic transitions from the reactor testing system to a T-junction metallic microreactor, was designed and fabricated. Using the T-junction reactor, we demonstrated that a thin-film catalyst could be selectively deposited into the microchannel without contaminating the top reactor surface using the special procedures that we developed and demonstrated.

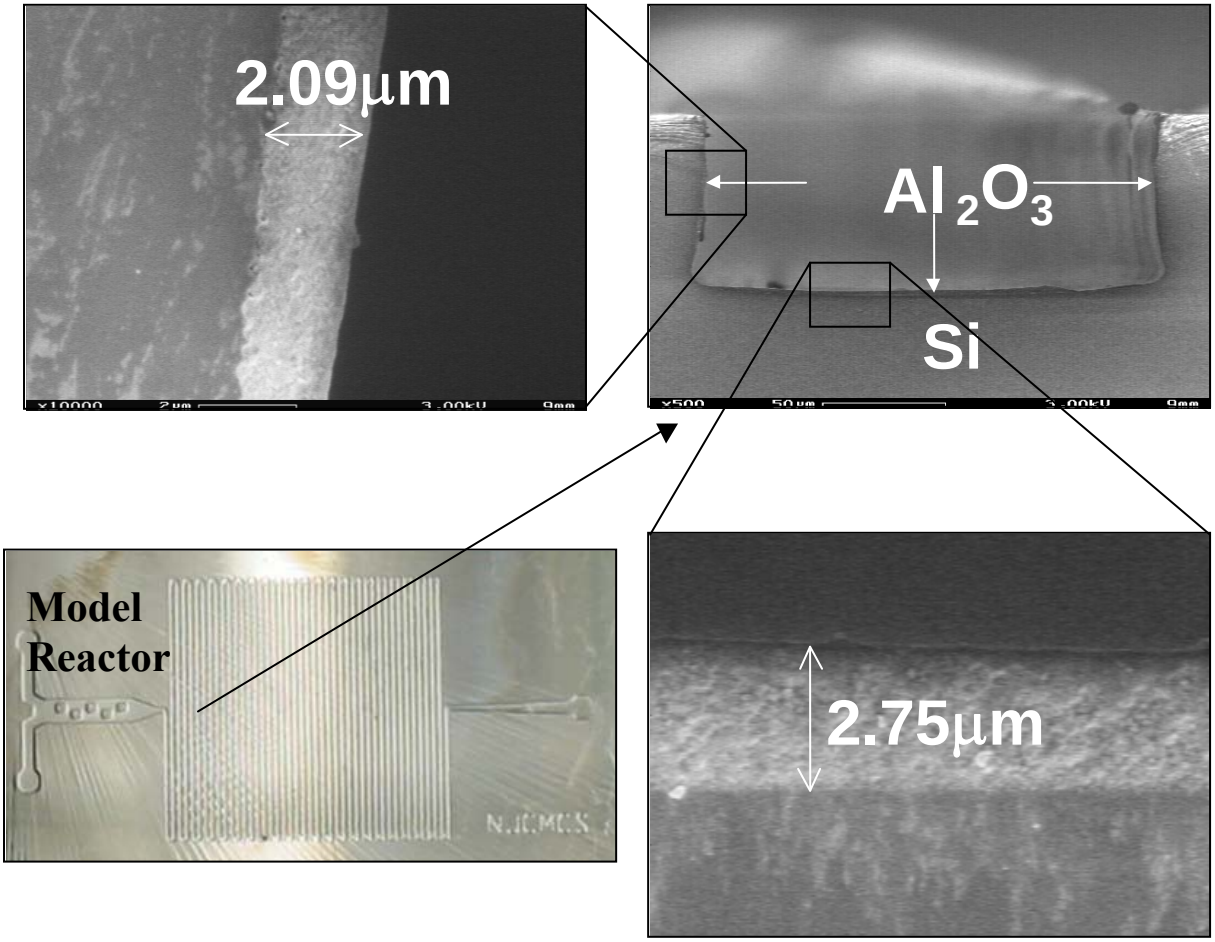

Figure 2.1: Si microchannel reactor infiltrated with Pt/Al_2O_3 thin-film. Cross-section SEM images show that the thin-film catalyst uniformly decorates the microchannel surfaces.

(2) Closed-channel forced-flow infiltration and deposition of sol-gel catalyst coating

In a parallel effort, we developed a proprietary infiltration procedure to uniformly coat the inner surface of microtube reactors with thin-film catalyst as shown in Figure 2.3. There was some localized delamination at the interface between the thin-film layer and the SS substrate surface. It appeared that the delamination occurred during our metallographic preparation of the coated microtube reactor for the cross-section analysis.

The sol-gel-based procedures were used to prepare 14 capillary tube reactors for testing under Task 1. Thickness of the thin-film catalyst was controlled to be ~0.8 μm and uniform along the 6-cm length of the capillary tube reactors.

The adhesion of the thin-film catalyst to the SS 316L substrate was evaluated by a peel test using Scotch tape on a qualitative basis. Overall, the thin-film catalyst adhered well to the substrate, except for a few local areas where some delamination was observed. For example, Figure 2.3 shows a microscopic view of the worst area. In this area, we observed that less than 10% of the thin-film under the viewing area was peeled off. The wetting behavior of the Pd/alumina thin-film catalyst on Si and SS316L substrates was studied as part of improving our infiltration procedure for 3-D microchannel reactors.

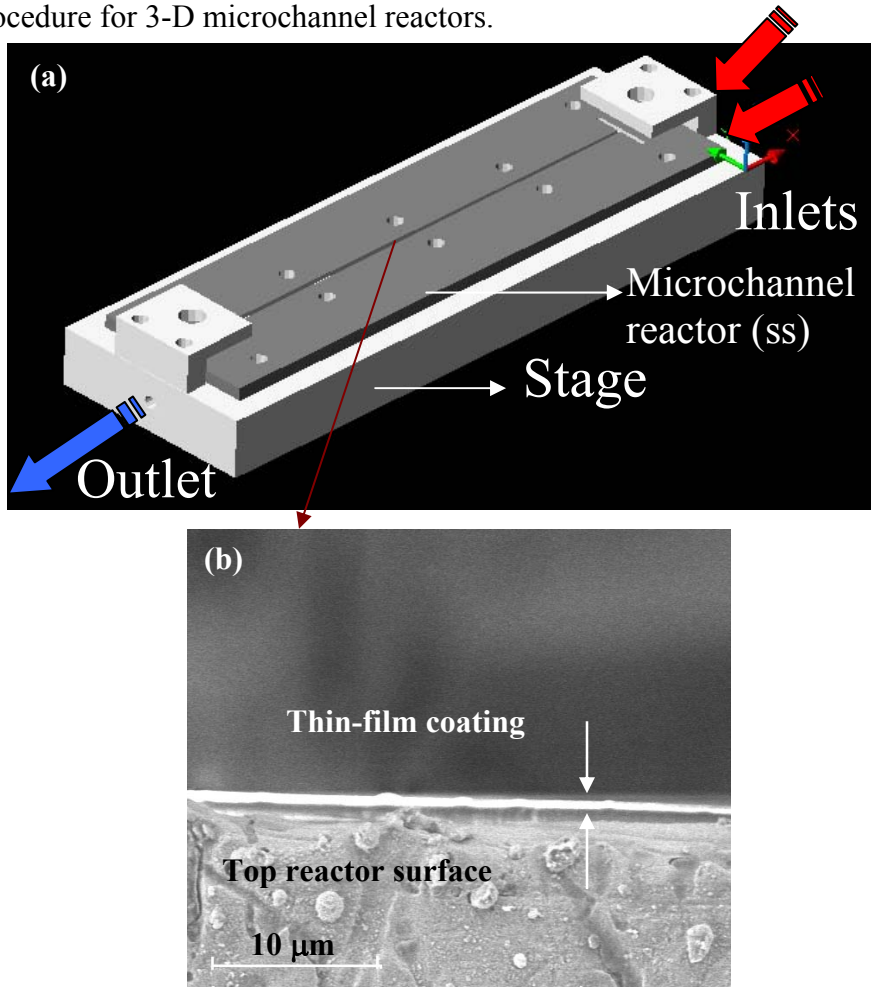

Figure 2.2: (a) T-junction reactor and the microfluidic transitions. (b) Thin-film catalyst selectively deposited on the wall of the T-junction channel.

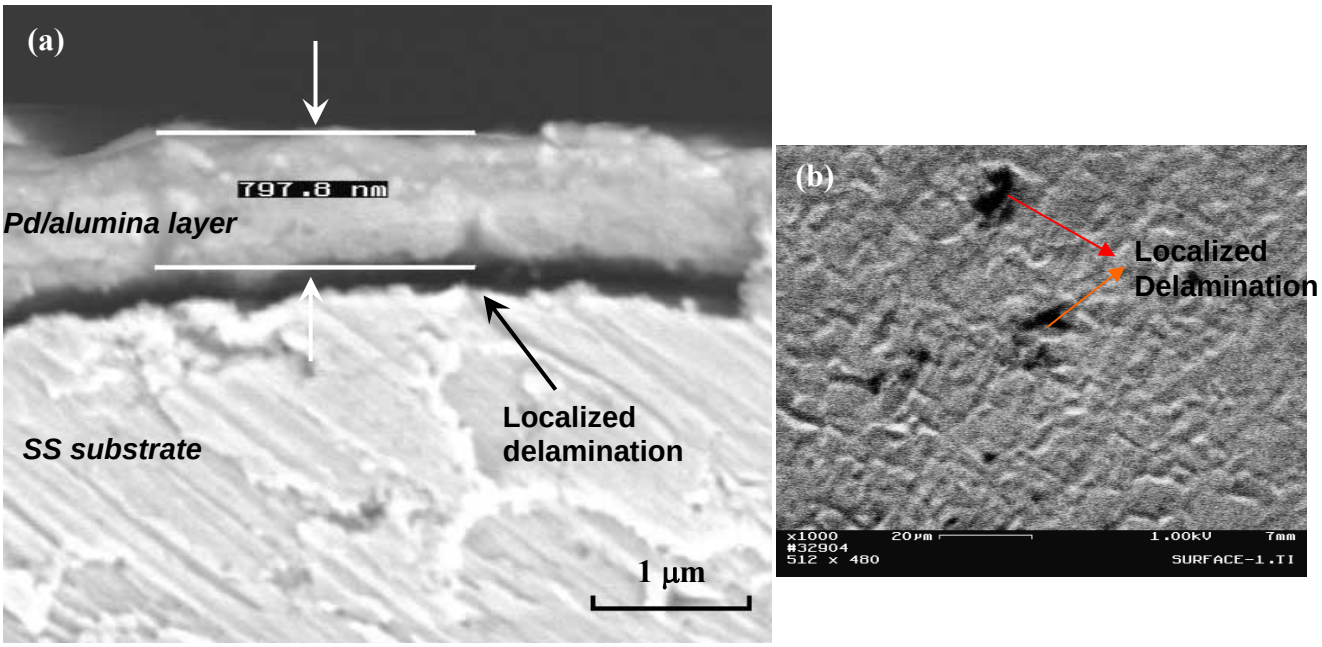

Figure 2.3: (a) Cross section view of the 6 cm long microreactor tube infiltrated. (b) Evaluation of the adhesion of Pd/alumina thin-film catalyst to the SS 316L by scotch tape test.

(3) Layer-by-layer self-assembly as a catalyst integration method

We also developed a procedure to immobilize model and catalyst particles in a thin film form on complex microstructures and building up the thickness of catalyst particles using layer-by-layer self-assembly (LBLSA).

The thickness of polyelectrolyte multilayers (PEMs) that determines the surface charge density on the surface is critical. The PEM thickness and particle surface coverage were controlled by the ionic strength of the polyelectrolyte solutions (NaCl concentration) and with the number of PEM layers (Figure 2.4). The particle surface coverage improves with increasing NaCl concentration and the number of PEM layers. However, the maximum surface coverage seems to be limited to about 70% as shown in Figure 2.5 (note that the surface coverage of 2-D close packing is ~91%) since there was no coverage increase with increased PEM thickness.

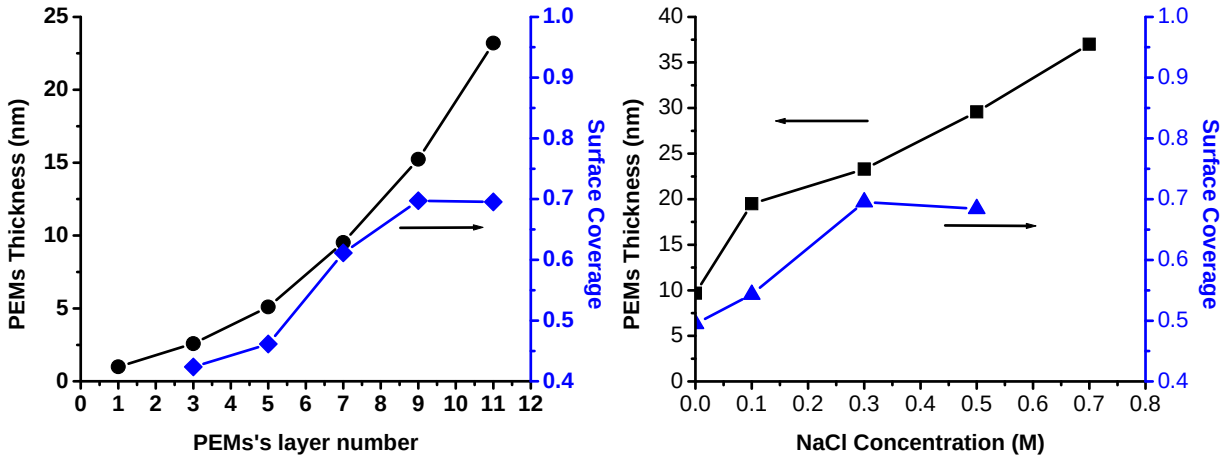

Figure 2.4: (a) Effects of the number of PEMs' layer on PEMs' thickness and the surface coverage of particles (b) effects of NaCl concentration on PEMs' thickness and the surface coverage of particles.

The layer-by-layer method was also applied to "build-up" the thickness of the particle film. By depositing repeatedly a single layer of particles, the layer-by-layer method provides a simple way of preparing relatively thick films with good uniformity. Figure 2.6 shows the SEM pictures of two and four layers of microspheres. The method was also successfully used to infiltrate and immobilize a number of commercial catalyst particles into complex cellular structures (Fig. 2.7).

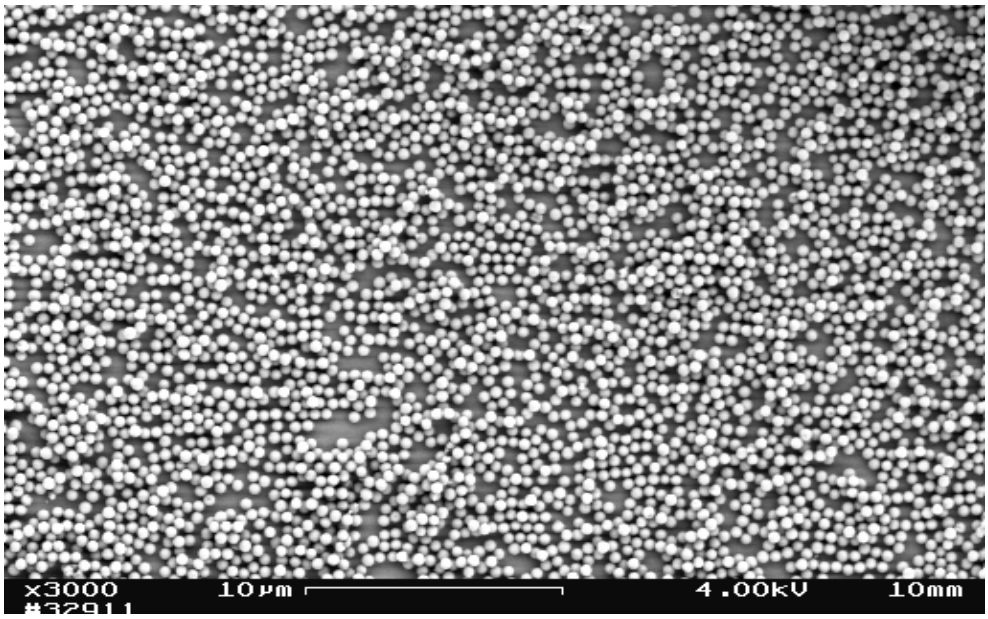

Figure 2.5: Coverage as high as 70% of single deposition of SiO_2 particles was achieved.

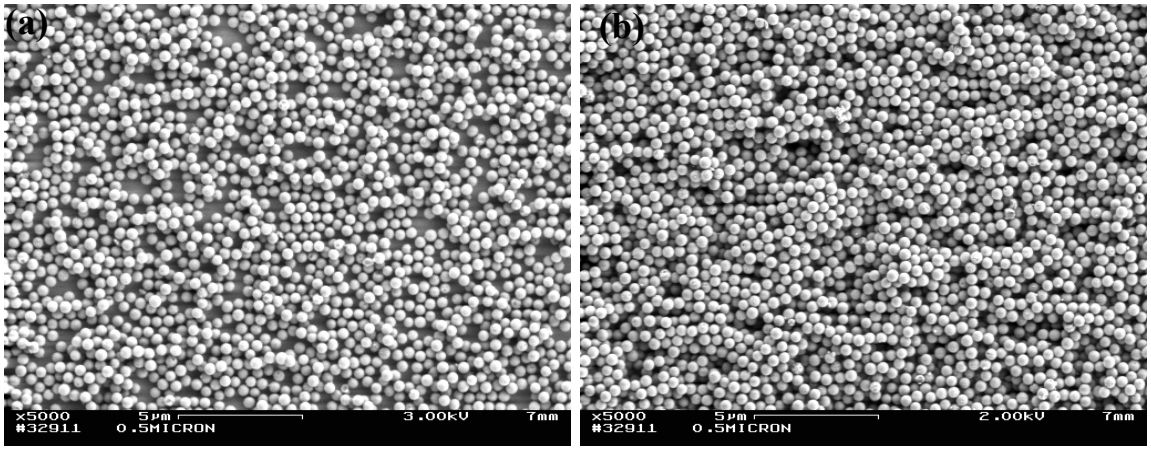

Figure 2.6: Building up the thickness of the particle thin film: (a) two and (b) four deposition cycles of silica microspheres (particle diameter - 500 nm).

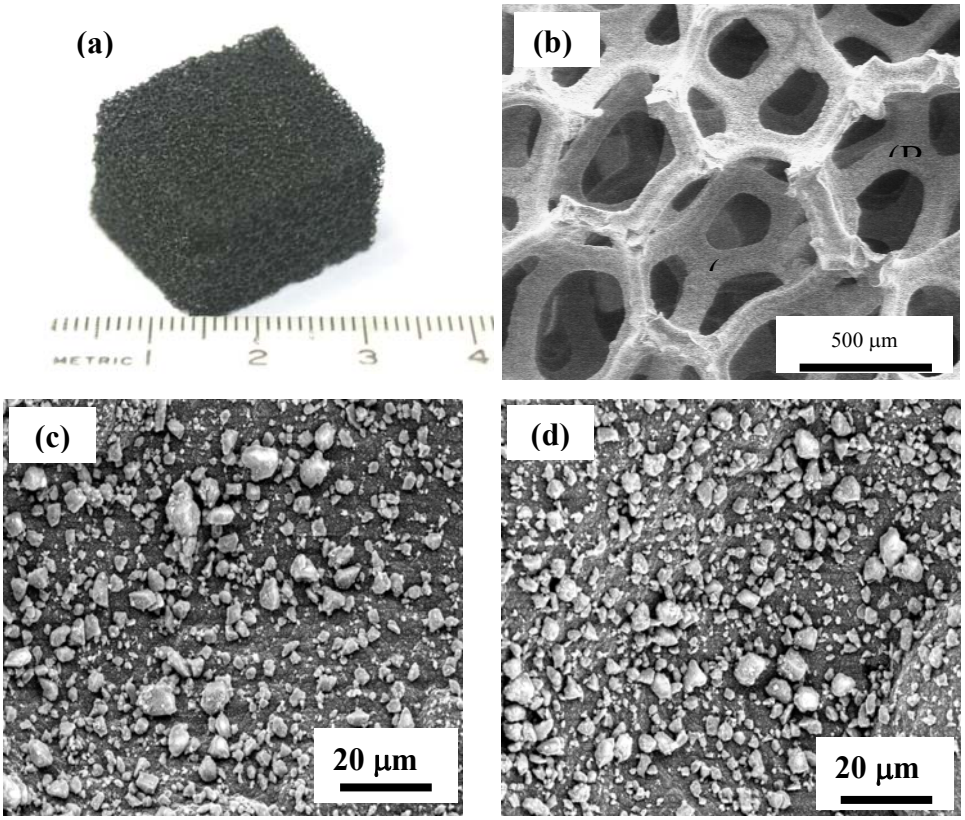

Figure 2.7: SiC cellular coupon infiltrated with the 1-layer catalyst particle assembly: (a) machined coupon with unit of the scale in cm, (b) SEM view of coated SiC skeleton, (c) and (d) SEM images of the catalyst particle assembly at points A and B in (b).

We also investigated the effects of LBL deposition on powder catalyst since it may influence the performance of the catalyst. However, any major adverse effect of the LBLSA procedures on the catalyst behavior was not evident in our study.

We evaluated the adhesion of the catalyst particle assembly deposited on flat substrates by the layer-by-layer assembly method as shown in Figure 2.8. For the evaluation, particles were assembled on model Si substrates (1.2 cm × 0.9 cm). A piece of Scotch tape was tightly attached to the top surface of the particle assembly. While the Scotch tape was being peeled off from the substrate, the force required to remove the tape was measured by a high-resolution force gauge (±0.001 N). The layer-by-layer self-assembled particles were expected to exhibit relatively poor adhesion to the substrate surface, since bonding between the particles and the substrate surface is mainly based on their weak electrostatic attractions. In order to further reinforce the immobilization of the particles on the surface, a thin layer of porous alumina was applied on the surface of the catalyst particle coating. Enhancement of the adhesion behavior by this alumina layer was observed as shown in Figure 2.8.

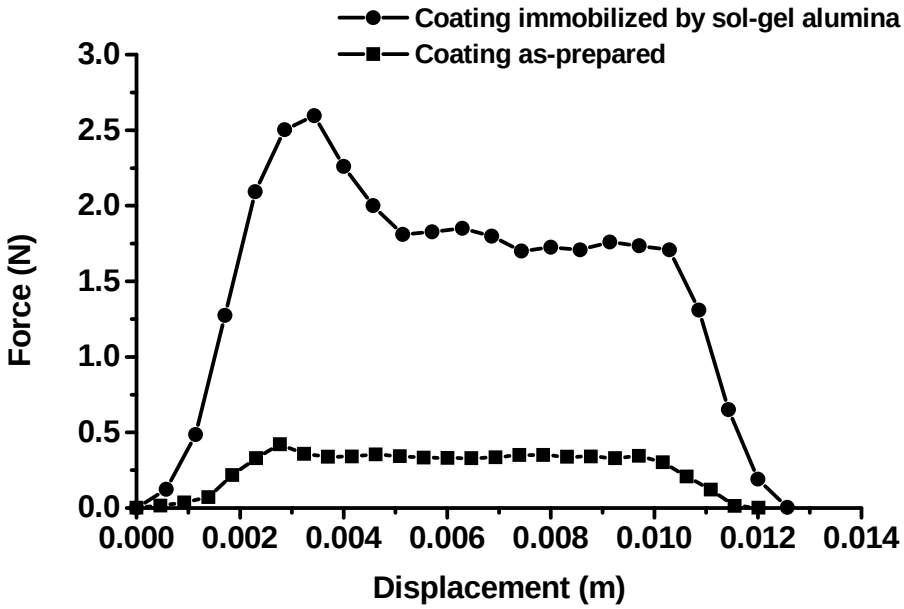

Figure 2.8: Degree of immobilization of the catalyst particle assemblies

We found that an additional thin layer of porous alumina could be used to significantly enhance the degree of adhesion if such reinforcement were desired. Adhesion behavior of the catalyst particle layer was investigated by microscopic evaluation of the delaminated surfaces resulting from the Scotch tape testing. For the catalyst layer which was not reinforced with porous alumina, the catalyst layer was mostly removed from the substrate surface. However, the catalyst layer reinforced with alumina layer was only partially removed. Figure 2.9 shows that the alumina layer diffused into the catalyst layer and formed direct contact with substrate surface.

(4) Infiltration and synthesis of microcellular structures that fill up microchannel volume

We developed a procedure to synthesize cellular structure inside microchannels to be used as a microstructure for catalyst coating (Fig. 2.10). We focused our work on optimizing the cellular structure by controlling three key structural parameters: cell size, window size, and skeleton density. Other properties of the cellular structure such as pore interconnectivity, geometrical surface area, void fraction, pressure drop and mechanical strength derive from these key parameters.

The cell size of the cellular structure was determined by the size of the microspheres used in the sacrificial template. Polystyrene microspheres with diameter in the range of 10 - 20 μm were used for the template, and the diameter of spherical cells (Figure 2.11a) in the cellular structure should be in the same range or slight smaller due to structure shrinkage during drying (Figure 2.11a). After the microspheres were packed into the microchannel using a surface-selective infiltration method they were heated at 100°C. The size of the contact area of two neighboring spheres r_N (Figure 2.11a) was controlled by the heating time, thus resulting in a certain window size in the final cellular structure. Cellular structures synthesized from template sintered after three and six minutes show some difference in cell interconnectivity (Figures 2.11c and 2.11d).

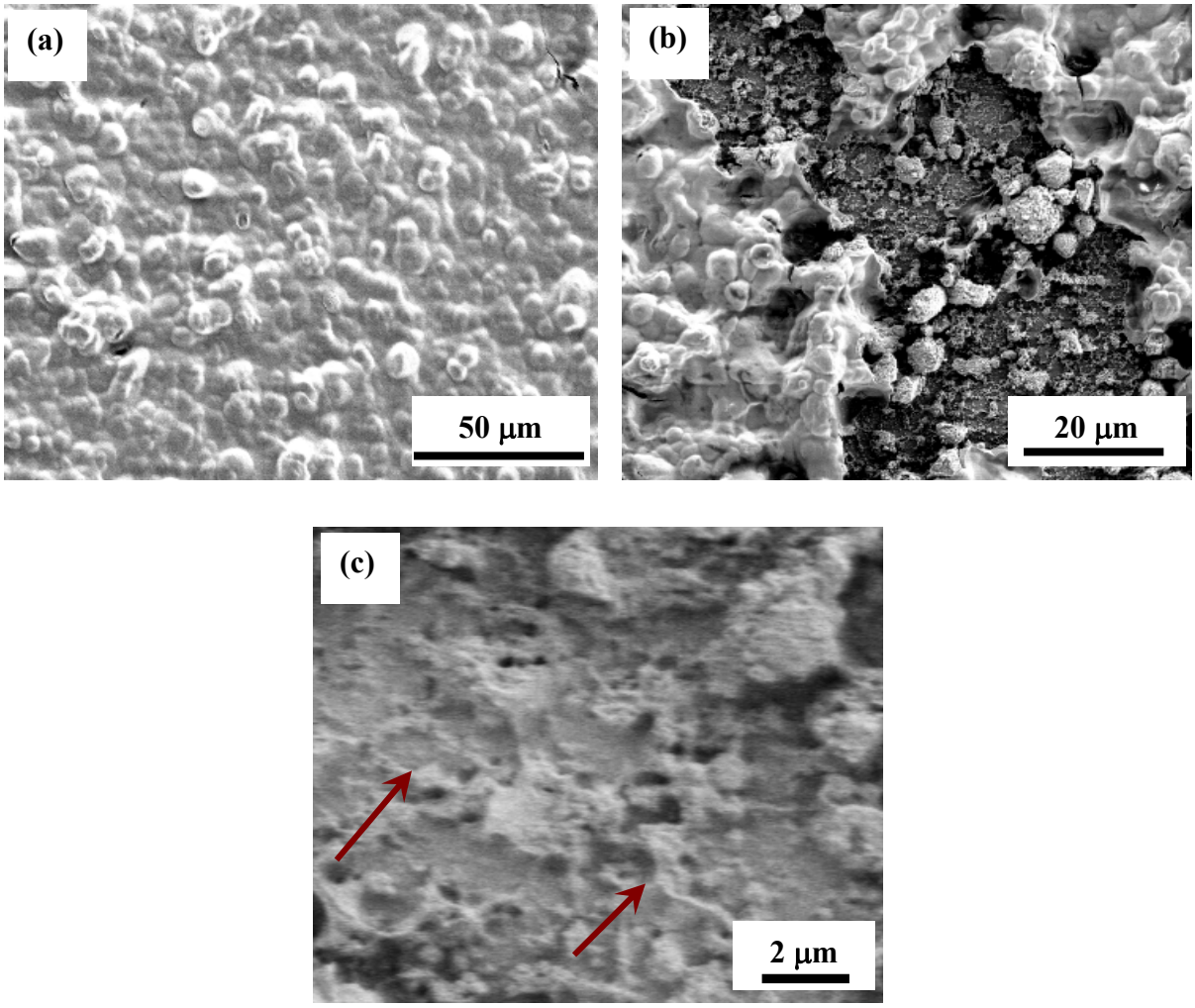

Figure 2.9: Surface scanninge electron micrographs of the catalyst particle layer reinforced with an additional layer of porous alumina: (a) before the adhesion test and (b) and (c) after the adhesion test. The arrows in (c) point indicate the alumina phase remaining on the surface.

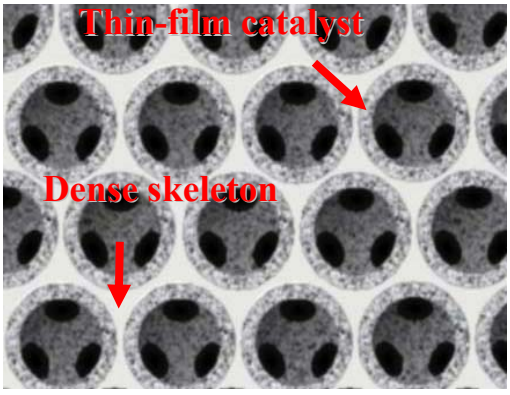

Figure 2.10: Cellular catalyst support structure.

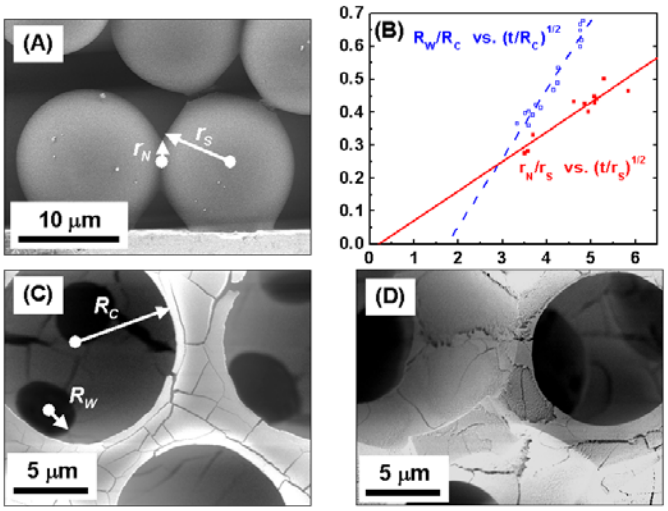

Figure 2.11: Controlling cell interconnectivity: (a) Sintering of microspheres: r_N and r_S are the radius of the contacting area between two neighboring spheres and the radius of the spheres, respectively; (b) Controlling polystyrene sintering and cell interconnectivity by changing sintering time; solid line shows the change of the polystyrene template by varying sintering time and the dotted line shows the change of cell interconnectivity of the cellular structures from sintered template; t is heating time in seconds; (c) Cellular structure from template sintered for three minutes; (d) Cellular structure from template sintered for six minutes.

We have successfully synthesized skeleton in the interstices of the microsphere template with high density and no cracks, which is a challenging task. As shown in Figure 2.12, free-standing cellular silica samples were synthesized from TEOS and Ludox®.

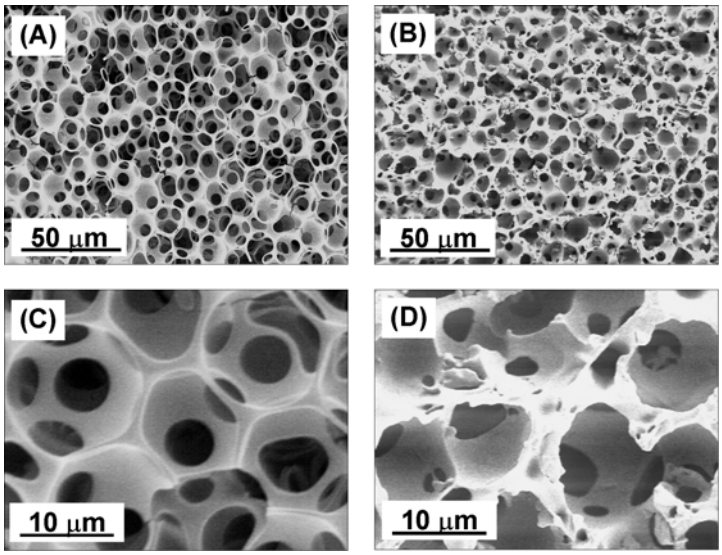

Figure 2.12: Free-standing cellular silica samples synthesized from: (A) and (C) TEOS precursor after the 500°C calcination step and (B) and (D) Ludox® precursor after the 1100°C sintering step.

The microcellular structure, combined with thin-film coating technique developed in this project provides an additional catalyst integration choice.

TASK 3: Microreactor Fabrication and Microarray Kinetic Evaluation

Summary

The purpose of the task was to adapt Si-based microfabrication to construct multiphase microchemical reactors for rapid reaction evaluation. Such evaluation could consist of screening of catalyst candidates, optimization of reaction operating parameters such as pressure, temperature, and flow rates of gas and liquid reactants. Hence the task sought to develop a methodology, rather than simply a reaction platform, for performing such characterization. Once developed as an individual reaction platform, the approach could be scaled up for rapid parallel evaluation of multiple parameter sets by incorporation of the unit into an array which could be tested simultaneously.

Multiphase (gas-liquid-solid) reaction systems such as those involved in manufacturing of pharmaceutical intermediates pose a complex problem in characterization. This is true because of the dependence on transport parameters on available interphase area. The choice of a microchemical synthesis approach (the focus of the overall project) is a sound one since this approach serves to maximize interphase surface area relative to reaction volume. Hence in designing a platform for the collection of basic reaction parameters to support this synthetic approach must also minimize transport effects, access intrinsic reaction kinetics as much as possible, and allow access to conditions similar to what will be utilized in the ultimate reaction system.

For these reasons we sought to demonstrate the feasibility of a unique microreactor concept, known as the "catalyst-trap microreactor," which accepts conventionally available particulate catalyst powders, engineers the reactor void fraction, accesses various multiphase flow regimes (including slug-like, gas-dominant, or liquid-dominant flow regimes), is easily handled, and rapidly tested. The reactor was designed by chemical engineering researchers at Stevens Institute of Technology, and was fabricated by micro/nano electrical mechanical systems (MEMS/NEMS) experts at the New Jersey Nanotechnology Consortium of Lucent (now Alcatel/Lucent) Bell Laboratories.

Summary of Technical Results

The term "microreactor" is generally used to describe devices with critical geometry ranging from tens of microns to approximately 1 mm in size. Microreactor technology possesses significant advantages over conventional macroscale reactors. Because of their small size, microreactors have inherently large surface-to-volume ratios, allowing for superior mass and heat transport. Surface-to-volume ratios of 20,000 m^2/m^3 or more are not uncommon, compared to 1,000 m^2/m^3 for a conventional reactor. Laminar flow is typically impressed by microgeometry, but because the overall heat transfer coefficient is inversely proportional to channel diameter, values for liquids are on the order of 10,000 W/m^2-K, roughly one order of magnitude higher than in conventional heat exchangers [1].

In the case of catalytic reactions, competition exists between the rate of reaction at the catalyst sites and the rate of diffusion to and from the bulk reaction medium. The small diffusion distances characteristic of microreactors are able to greatly reduce mass transport resistance, making them a useful tool for studying intrinsic reaction kinetics. Excellent heat transfer properties promote a uniform temperature throughout a microdevice and prevent the formation of

hotspots in the case of an exothermic reaction. In a stirred-tank reactor, for example, local hotspots or changes in pH can promote undesired side reactions that adversely affect product selectivity. Low residence time and ease of heat removal also make microreactors well suited for flammable service, where the potential for explosion or fire from runaway reactions is suppressed [2, 3].

In this report, we consider the effect of two-phase behavior in a microreactor for gas-liquid-solid catalytic reactions, as the rate of diffusion of gas into the bulk liquid phase tends to limit the observed reaction rate. To ensure that gas-to-liquid mass transfer effects are measurable we desire negligible resistance to intraparticle diffusion. Catalyst particles with a diameter smaller than 100 μm (1 x 10^{-4} m) generally exhibit such pore diffusion characteristics [4, 5]. The effectiveness of the bulk two-phase mass transfer is a function of the gas-liquid interfacial area and driving force for transport, both of which depend on the gas-liquid flow regime. Mass transfer in two-phase flow has been studied extensively in microchannel or capillary geometry, and here we wish to extend these principles to reactive systems.

Previous work on the characterization of two-phase flow in microchannels has identified boundaries between gas-liquid flow regimes with varying resolution [6]. For our purposes, we choose three flow regimes to generally describe the gas-liquid behavior, illustrated in Figure 3.1. Bubble flow is characterized by liquid as the continuous phase, with bubbles of gas dispersed into a fully-wetted channel. As the ratio of gas-to-liquid velocity increases, alternating segments of gas and liquid begin to occupy the channel, known as the Taylor (slug) flow regime. The relative lengths of the segments are approximately constant for a given set of inlet conditions, with gas segments increasing in size as the gas-to-liquid flow ratio increases. As gas-to-liquid velocity further increases, gas becomes the continuous phase and the liquid flows as a thin film along the channel walls. This regime is termed annular flow for a capillary or trickle flow for a wide reaction channel [6].

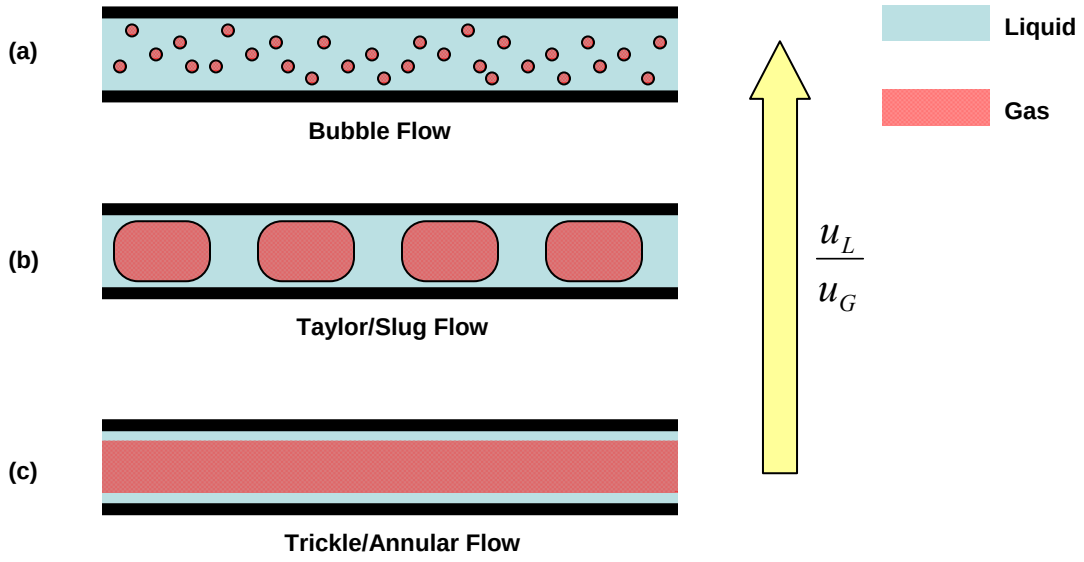

Figure 3.1- Illustration of Gas/Liquid Flow Regimes

In the context of a liquid-phase catalytic hydrogenation reaction, two characteristics are desirable pertaining to the gas-liquid flow regime. First, high liquid-solid interfacial area is beneficial to effectively utilize the catalyst bed volume. Second, good mass transport between gas and liquid,

which depends on both the concentration driving force and the gas-liquid interfacial area created, addresses the principal limitation of this reaction.

The slug flow regime in a capillary is typically associated with the best gas-liquid mass transport because of the no-slip condition at the channel walls [6], as the velocity gradient within the liquid slug promotes a chaotic mixing effect. The resultant continual refreshing of the gas-liquid interface provides a high driving force for diffusion of gas into the liquid. Bubble flow, in contrast, exhibits less turbulence within the channel, but offers higher interfacial area on both fronts. Liquid-solid interfacial area is maximized because liquid is the continuous phase with only a relatively small fraction of gas present, placing essentially all of the catalyst in contact with liquid [7]. Gas-liquid interfacial area is maximized because of the small size of the gas bubbles compared to the gas slugs.

We can generalize the tradeoff between slug and bubble flow with the statement that slug flow will possess superior gas-liquid mass transport, and that bubble flow will exhibit higher gas-liquid and liquid-solid interfacial areas. On the basis of these mass transfer arguments, we expect the best hydrogenation performance will fall in either the bubble or slug flow regimes. Likewise we suppose that the reduction in two-phase turbulence and interfacial area will render trickle flow the least effective regime for these types of reactions. We proceed to design our microreactor and subsequent experiments to investigate this premise.

Reactor Modeling, Design, and Fabrication

The reactor is designed for operation across the spectrum of flow regimes, making use of microgeometry to relieve various transport resistances for the convenience of our study. The design is pictured below in Figure 3.2.

(a)

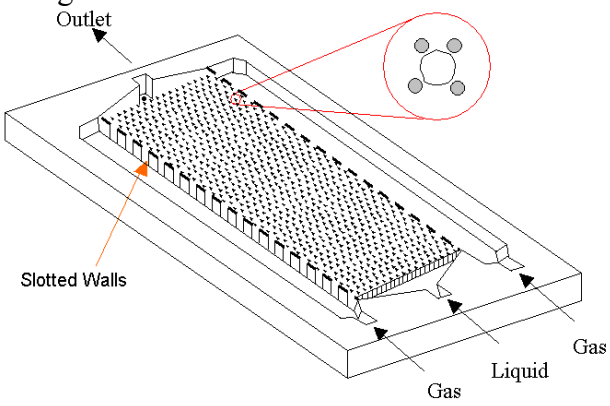

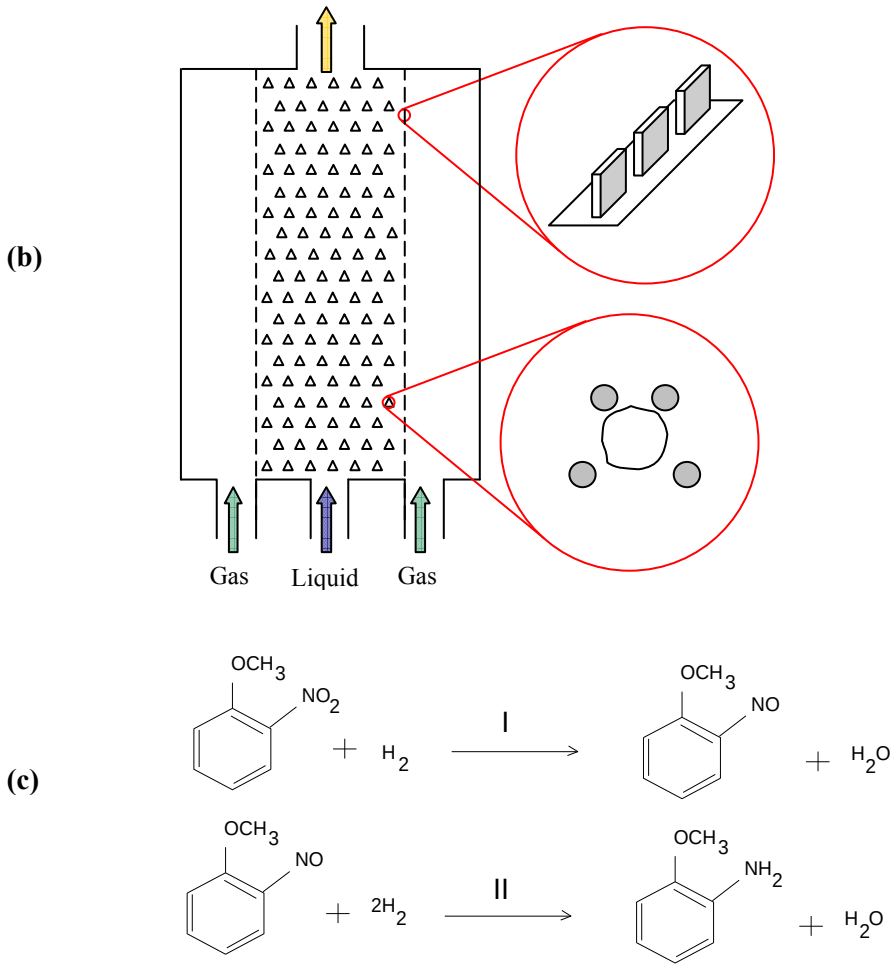

Figure 3.2- Proposed Reactor Design: (a) Three-Dimensional View; (b) Overhead View of Channels; (c) Reaction

The reaction is the liquid-phase hydrogenation of o-nitroanisole to o-anisidine in the presence of Pd catalyst, with methanol as an inert solvent. The catalyst is 5% Pd by weight on carbon support. Hydrogen enters along the two outside channels, and is allowed to diffuse into the liquid channel through perforated walls (Figure 3.2b, top inset). Liquid is introduced in the center channel, which contains a grid-like network of posts spanning the depth of the channel (Figure 3.2b, lower inset). Four such posts are arranged in a trapezoidal pattern to comprise one catalyst trap, spaced to "catch" particles approximately 50 μm in size during the catalyst loading process and hold them in place during the reaction processing, so one can imagine that the liquid sees the particles stacked single-file on top of one another as it travels down the channel.

With the assumption that the dissolution of nitroanisole occurs rapidly, the reaction is a four-step process: (1) hydrogen diffuses through the slots and dissolves in the bulk liquid; (2) the liquid, including dissolved hydrogen, disperses to the catalyst particles and diffuses within the particles to the reaction sites; (3) reaction occurs at the catalyst sites; (4) the product diffuses out of the particles and back into the bulk liquid. Our choice of catalyst particle size, wall perforation width, and reaction is intended to place no limits on the observed rate of reaction by steps (2), (3), and (4).

For design purposes, we model the liquid channel as a plug-flow reactor with a source of hydrogen available at all axial positions. In order to study the gas-liquid mass transfer represented by step (1) above, we desire that hydrogen concentration in the liquid phase is limited by diffusion across the gas-liquid interface, so we design the slotted wall to present no resistance to gas diffusion from liquid surface tension. The rate of change of liquid-phase hydrogen concentration is comprised of a gas-liquid diffusion term and a reaction term [4], with hydrogen as species A and nitroanisole as species B.

$$\frac{dc_A}{dt} = [\text{Rate of diffusion from gas into liquid}] - [\text{Rate of reaction}] \tag{3.1}$$

$$\frac{dc_A}{dz} = \frac{\varepsilon}{u_L} \cdot \left[k_L a \left(\frac{P_A}{H_A} - c_A \right) - \frac{3 w_c k c_A c_B}{(1 + K_A c_A)(1 + K_B c_B)} \right] \tag{3.2}$$

The concentration of hydrogen at the gas-liquid interface is taken to be the Henry's Law concentration for hydrogen in solutions of nitroanisole and methanol [8]. The difference between the interfacial (P_A/H_A) and bulk liquid (C_A) concentrations represents the driving force for hydrogen dissolution. Note that because liquid-solid and intraparticle transport resistances are neglected, the bulk liquid concentration of hydrogen is equal to that at the catalyst sites, and can thus be used in the reaction rate expression in equation (3.2).

The mass transfer coefficient, k_La, remains as an adjustable parameter. For reactor design purposes, we use values estimated from packed tower literature [9]. Although uncertainty exists in the application of these conventional correlations to the microreactor geometry, we can later obtain experimental k_La values from our reaction data and draw a comparison with the macroscale values in order to quantify the difference in mass transfer performance.

Finally, the reaction rate expression in equation (3.2) includes the stoichiometric coefficient for hydrogen. For the remaining species, there is no gas-liquid diffusion, so equation (3.2) contains only the reaction term with the respective stoichiometric coefficient. To obtain the outlet conversion for a given reactor geometry, the system of expressions is integrated numerically over the channel length from 0 to z. Figure 3.3 shows the final liquid channel dimensions.

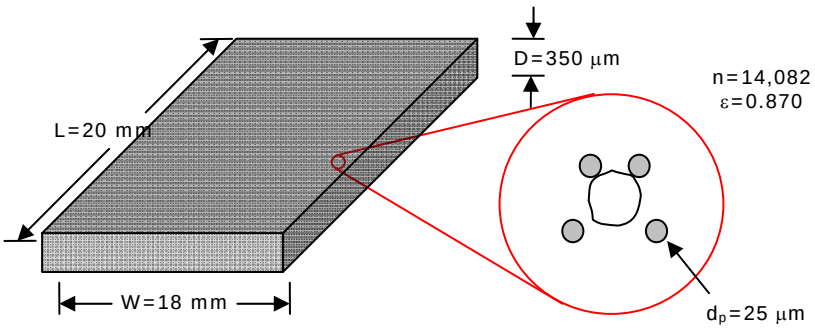

Figure 3.3- Design Parameters for Liquid Channel

Channel dimensions are chosen with the intent of yielding an appreciable conversion across our target range of experimental conditions. The channel contains approximately 14,000 catalyst traps that, when loaded, give a void fraction of 0.87. The posts are 25 μm in diameter and are spaced to hold a 35-50 μm particle. Rows of traps are staggered throughout the channel with a trap spacing, or closest edge-to-edge distance between adjacent traps, of 75 μm. The staggered arrangement facilitates catalyst loading by allowing untrapped particles to pass to the next row of traps.

The reactors are fabricated at NJNC-Bell Labs in Murray Hill, NJ using 248 nm and contact lithography and deep reactive ion etching (DRIE). After etching of the channels, traps, slotted walls, and inlet/outlet ports, the silicon wafer is diced into individual chips of dimensions 31 x 28 mm. We receive sixteen chips per eight-inch diameter wafer. Each reactor is then sealed by anodically bonding Pyrex glass to the surface of the chip. In the anodic bonding process, high voltage and temperature, typically 1000 VDC and 450-490 C, are applied to displace ions from the surface of the glass. The depletion of ions makes the glass surface highly reactive, forming a strong bond with the silicon substrate. The intent of the glass-covered reactor is both as an aid in catalyst loading and for observation of the gas-liquid flow behavior. Figure 3.4 shows the design drawing of the reactor chip, and Figure 3.5 shows Scanning Electron Microscope (SEM) images of the completed reactor.

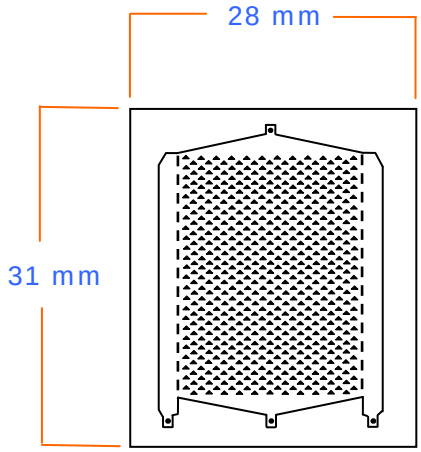

Figure 3.4- Reactor Chip

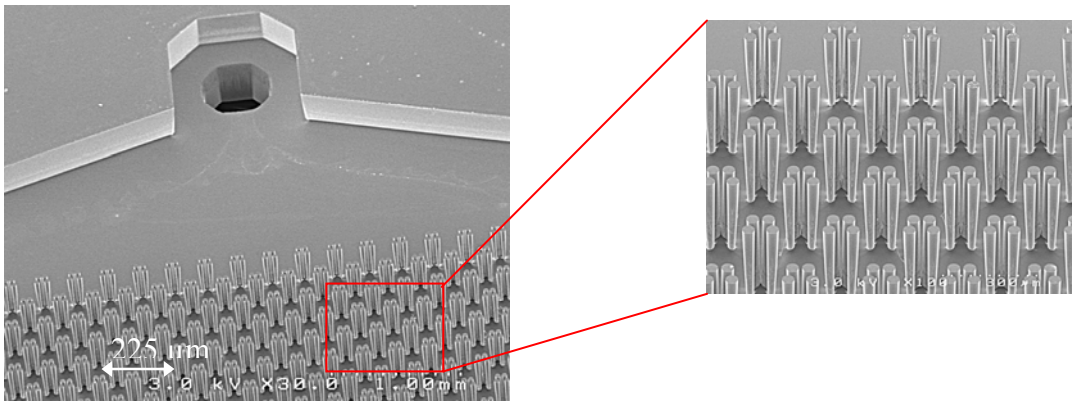

Figure 3.5- SEM Images of Microreactor

Experimental

The experimental setup is shown in Figure 3.6. For added flexibility the gas can be routed to the center channel, although this configuration was not used for experiments. The reactor itself is clamped onto a stainless steel block, through which channels are machined for gas and liquid passage. Pressure is controlled manually via a back pressure regulator at the outlet of the reactor, downstream of which a sampling line is provided. A CCD camera is used for overhead image and video capture. Throughout the setup, care is taken to minimize the internal volume of tubing and fittings so as to reduce the liquid holdup within the system, providing rapid response and stable control.

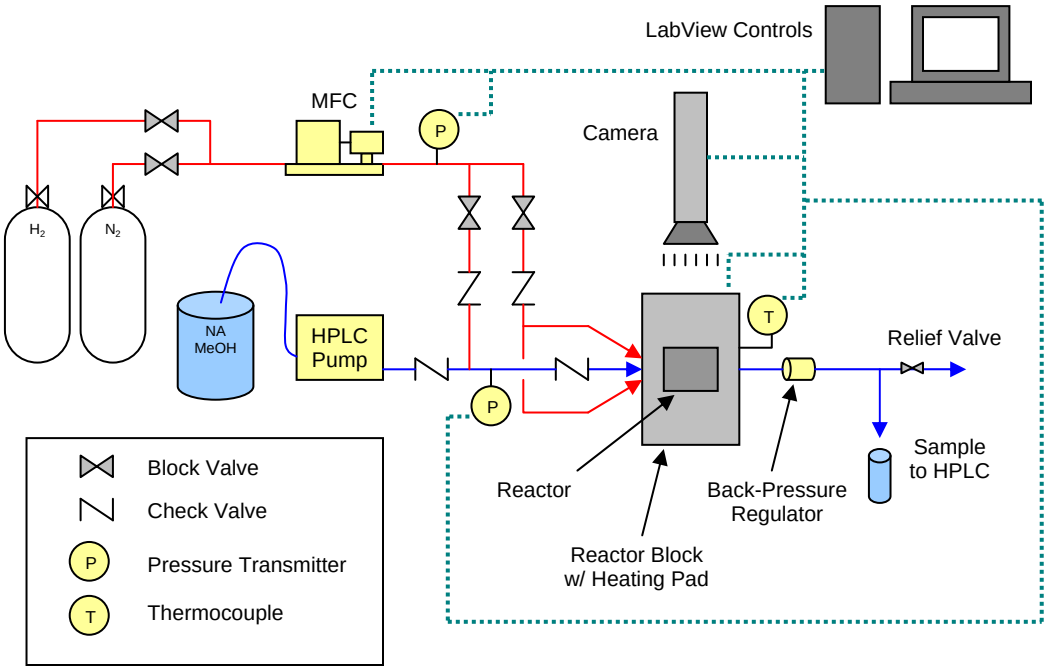

Figure 3.6- Schematic of Experimental Setup

We first performed an assessment of the gas-liquid behavior in our particular microreactor device in order to construct a "flow map" depicting the prevailing two-phase flow regimes across a range of conditions. We chose gas and liquid flow rates in accordance with the design model, from 2 to 20 sccm, and 0.06 to 0.50 mL/min, respectively. Flow map experiments were conducted in the absence of catalyst, as the small channel volume that would be occupied by catalyst particles, as well as a nearly reaction-independent liquid density, would have a negligible effect on two-phase behavior. We noted differences in the gas-liquid flow pattern with changing conditions and approximated borders between the three flow regimes, shown in Figure 3.9.

Catalyst was prepared by grinding and sieving the particles to the desired size, 38-45 μm. The resultant powder-like particles were collected and manually loaded by inverting the reactor and applying vacuum to draw the particles through the inlet port. Tapping the reactor against the countertop caused the particles to move down the channel and settle within the traps. This manual loading technique permitted coverage of 70-80% of the traps in the reactor, far better than that achieved by other methods, such as fluidization of catalyst into the reactor while online. At 70-80% coverage of the traps, approximately 6 mg of catalyst were present in the reactor.

With the flow map established, we measured reaction conversion and selectivity at each point on the map. Two sets of reaction data were obtained, the first at 30 C and hydrogen pressure of 172 kPa (25 psia), and the second at 30 C and hydrogen pressure of 689 kPa (100 psia). Operation at 689 kPa was intended to observe the effect of liquid-phase hydrogen concentration. For each experimental "run" we passed a feed solution of 10% nitroanisole by weight through the reactor at the desired gas and liquid flow rates, and then sampled the reactor outlet periodically over the course of approximately one hour. Samples were analyzed offline in an HPLC to measure the weight fractions of o-nitroanisole and o-anisidine, from which we calculated the conversion and selectivity. After each run we regenerated catalyst and evaporated any residual liquid by heating to 300 C for ten minutes.

Results and Discussion

Because this particular microchannel is rectangular-shaped with a high width-to-depth ratio, it cannot be considered a capillary or cylindrical channel. Thus, the conventional nomenclature of bubble, slug, and trickle flow discussed earlier is not entirely applicable. Instead, we choose the terms "gas-dominated," "liquid-dominated," and "transitional" flow. Figure 3.7 illustrates these flow regimes with overhead pictures of the reactor.

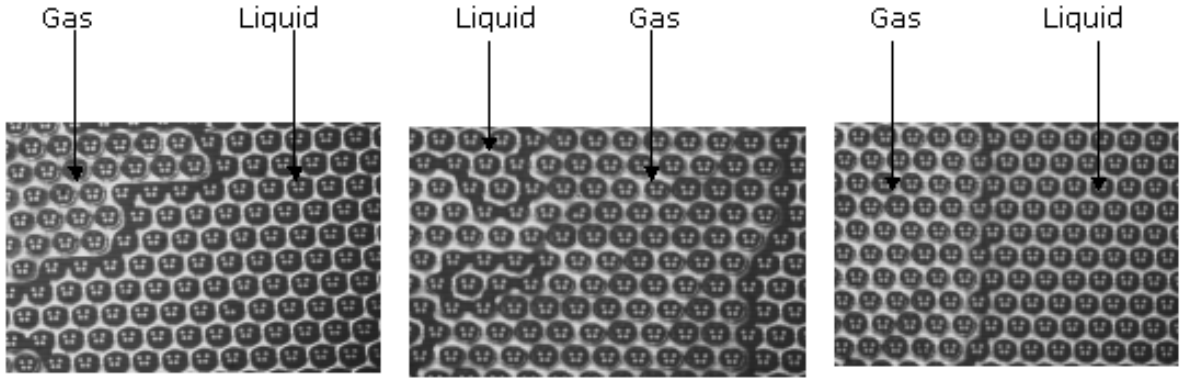

Figure 3.7- (a) Liquid-Dominated Flow Regime (b) Transitional Flow Regime (c) Gas-Dominated Flow Regime

Liquid- and gas-dominated flows are characterized by stable patterns in which the continuous phase impedes movement of the non-continuous phase throughout the channel. For example, in liquid-dominated flow, 80% or more of the channel volume is occupied by liquid, with several small pockets of gas. In gas-dominated flow, large gas pockets persist and force liquid to channel around them. The gas-liquid interfaces in these flow regimes are largely stagnant, clearly an undesirable attribute for a mass-transfer limited reaction.

Transitional flow is characterized by an unstable pattern in which gas and liquid compete for space within the channel. This competition causes a periodic refreshing of the gas-liquid pattern, so that in addition to significant interfacial area, high turbulence is exhibited within the channel. Refreshing periods are measured to be less than ten seconds for transitional flow, compared to several minutes or more for gas- and liquid-dominated flow regimes. At some gas- and liquid-dominated conditions, no refreshing at all is observed. Compared to slug flow within a capillary, the transitional flow in our microreactor manifests itself not as a recirculation within liquid slugs, but as an interface shearing throughout the entire channel, as though the gas-liquid pattern is

wiped clean and then "redrawn." Nonetheless, a significant enhancement in channel mixing is observed compared to the liquid- and gas-dominated regimes.

A second notable feature of transitional flow is that we frequently find that upon refreshing, the traps within a gas pocket are each encased in their own droplets of liquid as the small distance (~15 μm) between posts prevents gas from overcoming the liquid surface tension needed to rid the area of liquid. These "wetted" traps are a product of the continual refreshing of the gas-liquid pattern and thus are most prominent in the transitional flow regime. When extended to the entire channel, an array of several thousand traps each surrounded by liquid droplets approximately 80 μm in diameter creates extraordinary surface area. Such a cylinder itself has a surface-to-volume ratio of 50,000 m^2/m^3. If coupled with the proper cycle of gas-liquid refreshment, the traps could function as a network of miniature batch reactors, where refreshing periodically sweeps away the products and introduces new reactants. The droplets' small size would give very short diffusion distances for hydrogen, allowing for excellent transport of dissolved hydrogen throughout the liquid and high reaction conversion. Figure 3.8 shows a snapshot of the reactor in operation with areas of wetted and non-wetted traps.

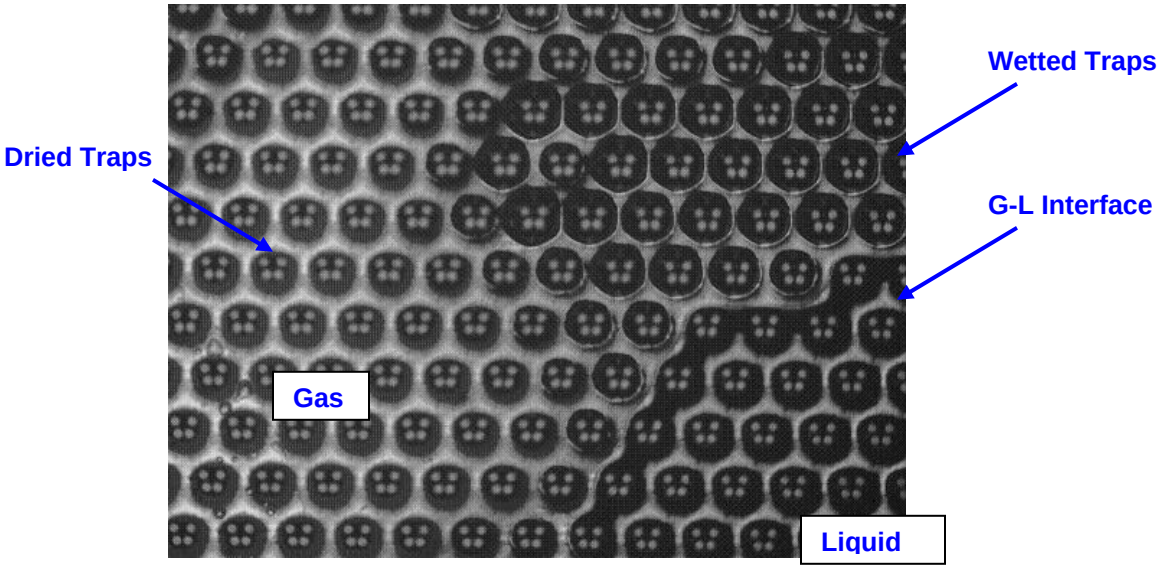

Figure 3.8- Reactor Photograph of Dried versus Wetted Traps

Our three observed flow regimes are analogous to the bubble/slug/trickle flows discussed earlier, with one outstanding exception. In the capillary example, the mass transfer characteristics of high turbulence and interfacial area that are desirable for hydrogenation performance are shared among the bubble and slug flow regimes, therefore presenting an opportunity cost for operation in either regime [2]. Because of the turbulence and presence of wetted traps in our microreactor, however, both of these critical mass transfer characteristics are common to transitional flow. Our expectation for reaction experiments is thus for transitional flow to clearly stand out as the preferred regime of operation.

Although there are no quantitative measures to determine the particular gas-liquid flow regime at hand, we identify the borders between the flow regimes based on the two reasonably reliable indicators discussed above, the refreshment frequency of the gas-liquid pattern and the presence of wetted traps. Based on our observations, the flow map is shown below.

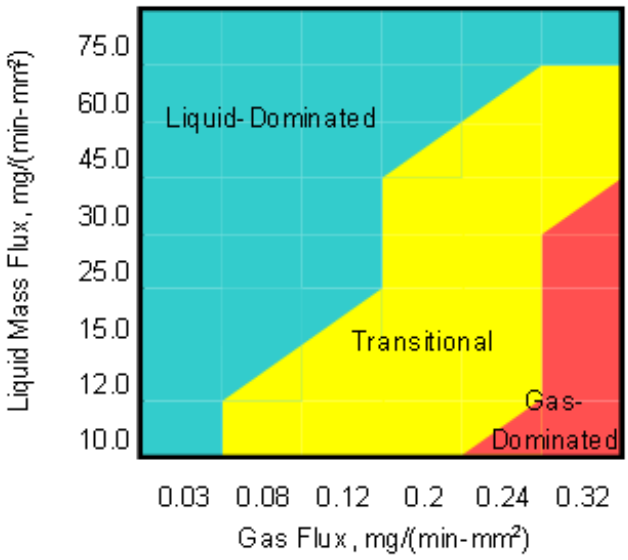

Figure 3.9- Reactor Flow Map

As we might expect, each regime extends in diagonal bands with increasing liquid and gas flow rates across our map. The liquid-dominated regime prevails to a large extent above a liquid mass flux of 45 mg/(min-mm^2) and almost exclusively for a liquid flux greater than 75 mg/(min-mm^2). The flow map at a hydrogen partial pressure of 689 kPa shows little difference, indicating that the effect of dissolved hydrogen on the flow behavior is minimal.

We obtain conversion results at both pressures for the lower portion of the flow map. No significant catalyst deactivation is observed across the one-hour time span of each run, allowing us to calculate an average conversion for each set of conditions. For all runs, the selectivity towards o-anisidine is nearly 100%, indicating that no side reactions occur. Figure 3.10 shows the conversion results.

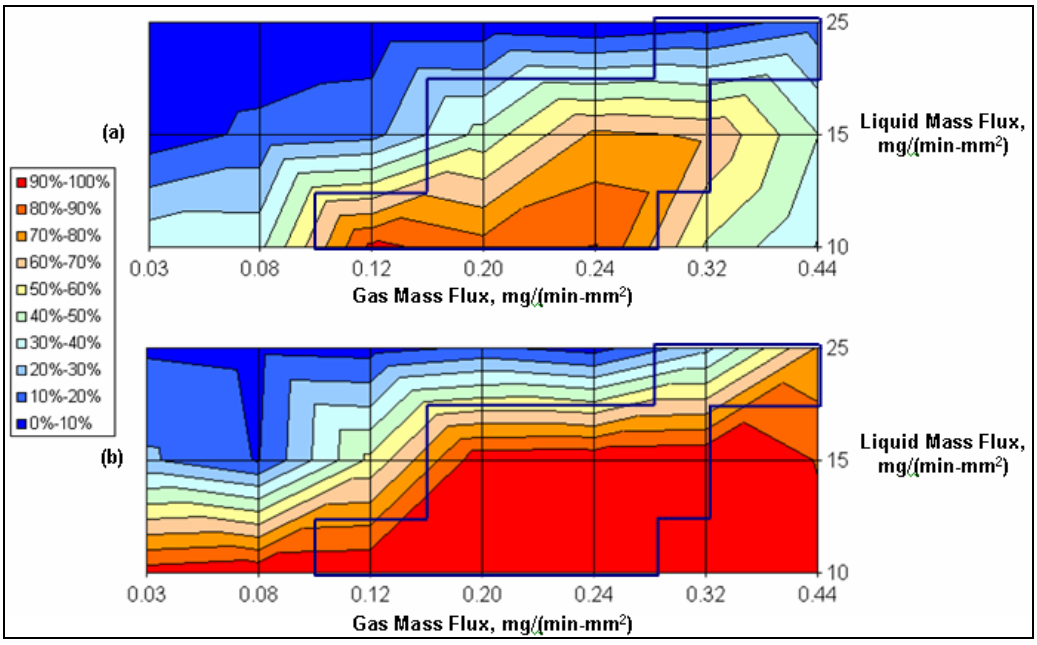

Figure 3.10- (a) Conversion Results, 172 kPa (b) Conversion Results, 689 kPa

We first note a decrease in conversion with increasing liquid flow rate, an effect attributable to liquid residence time. At each liquid flow rate we can thus draw a border around the region of highest conversion. Connecting these regions forms the highlighted ranges in Figure 3.10, which coincide with the transitional regime from our flow map in Figure 3.9. Conditions outside the transitional region experience significantly lower conversion. We can take as an example the low pressure experiments at a liquid mass flux of 10 mg/(min-mm^2) (167 kg/m^2-s): as the gas flow increases, we first observe an increase, then a decrease in conversion as the flow proceeds into, then out of, the transitional regime. Our observation that this region of highest conversion shifts upward and to the right in our plots is consistent with the notion that as liquid rate increases a corresponding increase in gas rate is required to maintain the mass transfer characteristics of transitional flow, namely continual interface shearing and high gas-liquid interfacial area, which subsequently serve to enhance reaction conversion.

As expected, the dissolution of hydrogen at a pressure of 689 kPa provides significantly higher reaction conversion across our range of conditions. Nearly complete conversion within the highlighted region is achieved for all but the highest liquid flow rate, indicating that a lower liquid residence time is necessary to obtain better resolution in the conversion results between flow regimes. Despite the lack of data at even higher liquid flow rates, at 689 kPa we observe the same shift upward and to the right in the region of highest conversion, suggesting a similar region of enhanced mass transfer behavior to that of our low pressure experiments.

In the initial design model, equation (2), we used correlations for the gas-liquid mass transfer coefficient developed for macroscale packed columns. The values of k_La applied range from 0.01-0.1 s-1, predicting conversion at 172 kPa as high as 30% across our range of gas and liquid flow rates. The design model under predicts our experimental conversion given the obvious significant difference between the two-phase behavior observed in our microreactor and that in conventional packed columns. Returning to the model and adjusting the value of k_La to match our experimental conversion data allows us to quantify the mass transfer performance in each flow regime. For this we limit our analysis to the data at 172 kPa only, as the high reaction rate at 689 kPa caused by high liquid-phase hydrogen concentration places the system outside a suitable window for representing the full effect of changing mass transfer behavior between our three flow regimes by changes in k_La, resulting in a model prediction of nearly 100% conversion even at low values of k_La.

Table 1 shows, for each flow regime at each liquid flow rate, a representative conversion. The values are derived from the bordered region in Figure 3.10a as averages of the experimental conversion in each respective flow regime. Figure 3.11 shows the values of k_La that correspond with the experimental conversion data, with error bars indicating plus/minus one standard deviation*.

Table 1- Experimental Conversion in Various Flow Regimes

	P_{H2} = 172 kPa		
Liquid Mass Flux, mg/(min-mm^2)	Liquid-Dominated	Transitional	Gas-Dominated
25.0	2%	15%	2%
15.0	11%	62%	9%
10.0	38%	89%	29%

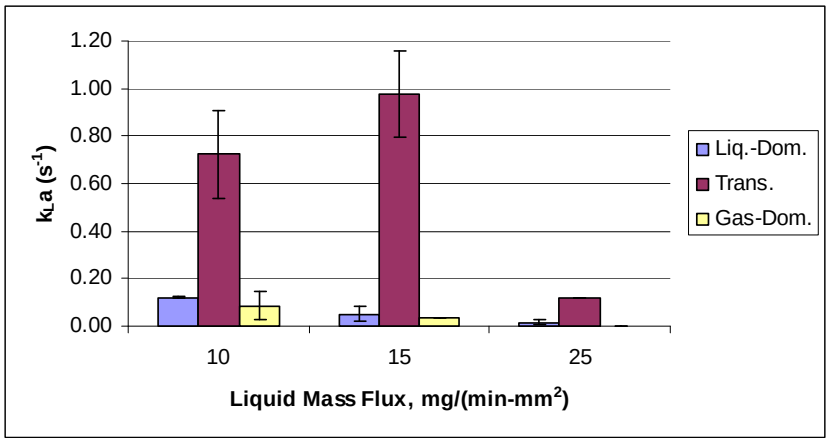

Figure 3.11- Experimental Mass Transfer Coefficient, 172 kPa

*** Points without error bars indicate only one value of k_La was measured at these conditions.**

We see that for all liquid flow rates, the value of k_La is higher in the transitional regime than in the liquid- or gas-dominated regimes. The greatest disparity in mass transfer performance between the transitional and other regimes is achieved at 10 and 15 mg/(min-mm2) liquid flux, where we calculate comparable mass transfer coefficients (k_La) of 0.72 s-1 and 0.98 s-1, respectively. Here, the transitional regime values are approximately one order of magnitude above those for liquid- and gas-dominated flows (0.04-0.12 s-1). At 25 mg/(min-mm2) the values of k_La indicate that a smaller benefit to mass transfer is realized in transitional flow. This result can be attributed to the lower conversion at lower liquid residence time, placing the system in a kinetically-controlled condition. Thus the liquid flow rates of 10 and 15 mg/(min-mm2) are the most representative conditions for quantifying the mass transfer performance in the reactor, whereby a tenfold enhancement in gas-liquid mass transfer rate is achieved in transitional flow. When compared to macroscale values of k_La, which range from 0.01-0.1 s-1 for equipment such as packed beds [1], we see that the values of k_La achieved in transitional flow are higher by approximately one to two orders of magnitude, a significant improvement in hydrogenation rate that warrants further investigation of such devices as commercial-scale production reactors.

The experimentally-derived values of k_La, combined with our observed flow patterns, suggest a two-phase behavior that can be likened to the surface renewal theory proposed by Danckwerts [10]. In the surface renewal theory, the eddy motion of the liquid brings fluid elements from the bulk to the two-phase interface, where they are exposed to the gas for a finite time before being replaced. This exposure of fresh liquid with low solute concentration offers a high local concentration gradient, a similar mechanism to the mass transport in Taylor flow discussed in the Introduction. In the case of our microreactor, the refreshing is intermittent rather than continual, but is analogous to the surface renewal theory because the periodic recreation of the gas-liquid pattern relocates the gas pockets throughout the channel, effectively bringing fresh liquid to the interface.

In proposing his model, Danckwerts assumed that every element of interfacial fluid has an equal chance of being replaced regardless of its age or position. The model relates the mass transfer coefficient to the surface renewal rate, s, defined as the fraction of the interface that is replaced per unit time.

$$k_L = \sqrt{Ds} \tag{3.3}$$

If we make the assumption in our microreactor that regardless of the type of flow regime, when refreshing of the gas-liquid pattern occurs an equal fraction of interfacial elements are replaced, then the surface renewal rate is proportional to our observed frequency of refreshing. In other words, refreshing occurs with constant magnitude but differing frequency across the three flow regimes of our microreactor due to differing levels of competition between gas and liquid flow. If the surface renewal phenomenon is at work in our system, then our observed periods of refreshing can be related to the calculated mass transfer coefficients by equation (3.3).

Characteristic mass transfer coefficients from Figure 3.11 are 1 s^{-1} for transitional flows and 0.1 s^{-1} for gas- or liquid-dominated flows. Due to the square root dependence in equation (3.3), this order-of-magnitude ratio in mass transfer coefficients translates to a two-orders-of-magnitude ratio in refreshing period between flow regimes. From our experiments, the observation in transitional flow was a gas-liquid pattern that refreshed itself every 1-10 s. Thus the surface renewal theory predicts a refreshment period of 100-1000 s in gas- or liquid-dominated flows. We did indeed observe this result, as refreshment periods of one to ten minutes or more were common for the gas- and liquid-dominated conditions which produced the mass transfer coefficient values in Figure 3.11. These results indicate that the Danckwerts model can explain the two-phase behavior in the microreactor, as differences in the refreshing period cause differences in the gas-liquid mass transfer rate due to more or less fluid elements being replaced at the interface per unit time.

It should be noted that the mass transfer rate in equation (3.3) is represented by k_L, and not k_La. Thus the above analysis assumes a constant interfacial area between all flow regimes, although certainly the total mass transfer rate receives a contribution from both the inherent mass transfer coefficient and from the interfacial area. The agreement between our observed behavior and the surface renewal theory indicates that the refreshing of the bulk gas-liquid pattern, and not the magnitude of local interfacial area, is likely the dominant mechanism in enhancing mass transfer rates in transitional flow. Such a conclusion underscores the potential benefits of a well-designed device which one can operate in a precise region of the flow map for this type of application.

Conclusions

We define two-phase regimes of liquid-dominated, gas-dominated, and transitional flow in our microreactor based on certain key aspects of the gas-liquid behavior. We measure conversion and selectivity of the heterogeneous catalytic reacting system across the flow map at both low and high hydrogen partial pressure. We find that the highest conversion falls within the transitional regime due to two prevailing mass transfer characteristics. First, the two-phase competition induced by transitional flow provides a constant interface shearing across the gas-liquid pattern, generating high driving force for gas-liquid mass transfer. Second, the presence of wetted traps results in a large interfacial area for hydrogen dissolution. Experimental conversion is higher than predicted by our design model due to the use early on of macroscale values of the gas-liquid mass transfer coefficient. When the mass transfer coefficient is calculated from the experimental conversion in each flow regime, we find an order-of-magnitude improvement in mass transfer rates in transitional flow over the liquid- and gas-dominated regimes, with our observation of pattern refreshment supported by Danckwerts' theory of mass transfer by surface renewal. The enhanced mass transfer coefficient quantifies the effects of the refreshing pattern and wetted traps that are prominent in the transitional regime, emphasizing

that a reactor design maximizing the region of transitional flow is well-suited for this type of reaction.

To this end, future work should experiment with the reactor design in the context of large-scale chemical production. Specifically, operation in the transitional regime with a high liquid flow rate is desirable in order to maximize product throughput. Central to this is a thorough understanding of the interaction between the aspects of transitional flow, namely the refreshing frequency and the extent of wetted traps, for use, for example, of the wetted traps as a network of miniature batch reactors. An optimized design may result in the possibility of microreactors as a beneficial alternative to conventional reactors in fine chemical and other industries.

Notation

c_i	liquid-phase concentration of species i
c_{i0}	initial liquid-phase concentration of species i
D	liquid-phase diffusivity
ε	reactor void fraction
H_i	Henry's Law constant for species i
k	reaction rate constant
k_L	gas-liquid mass transfer coefficient
k_La	volume-specific gas-liquid mass transfer coefficient
K_i	absorption constant for species i
N_{eff}	effective number of batches
P_i	partial pressure of species i
s	surface renewal rate, fraction of surface per unit time
t	time
τ	residence time in batch reactor
u_L	liquid superficial velocity
w_c	weight of catalyst per unit volume of reactor bed
z	length coordinate

References

1. Ehrfeld, W.; Hessel, V.; H. Lowe, H. *Microreactors: New Technology for Modern Chemistry*; Wiley, 2000.
2. Tadepalli, S.; Halder, R.; Lawal, A. Catalytic hydrogenation of o-nitroanisole in a microreactor: Reactor performance and kinetic studies. *Chemical Engineering Science*. 2007, 62, 2663-2678.
3. Surangalikar, H.; Ouyang, X.; Besser, R.S. Experimental study of hydrocarbon hydrogenation and dehydrogenation reactions in silicon microfabricated reactors of two different geometries. *Chemical Engineering Journal*. 2003, 93, Issue 3, 217-224.
4. Chaudhari, R.V.; Parande, M.G.; Ramachandran, P.A.; Brahme, P.H. Kinetics of hydrogenation of o-nitroanisole to o-anisidine. *I. ChemE Symposium Series No. 87*.
5. Chaudhari, R.V.; Jaganathan, R.; Vaidya, S.H.; Chaudhari, S.T.; Naik, R.V.; Rode, C.V. Hydrogenation of diethyl maleate in a fixed-bed catalytic reactor: kinetics, reactor modeling and pilot plant studies. *Chemical Engineering Science*. 1999, 54, 3643-3651.

6. Kreutzer, M.; Kapteijn, F.; Moulijn, J.; Heiszwolf, J. Multiphase monolith reactors: Chemical reaction engineering of segmented flow in microchannels. *Chemical Engineering Science*. 2005, 60, 5895-5916.
7. Heiszwolf, J.; Kreutzer, M.; van den Eijnden, M.; Kapteijn, F.; Moulijn, J. Gas-liquid mass transfer of aqueous Taylor flow in monoliths. *Catalysis Today*. 2001, 69, 51-55.
8. Brahme, P.H.; Vadgaonkar, H.G.; Ozarde, P.S.; Parande, M.G. Solubility of hydrogen in o-nitroanisole, o-nitroanisole-methanol mixtures, and o-anisidine. *Journal of Chemical Engineering Data*. 1982, 27, 461-462.
9. Seader, J.D.; Henley, E.J. *Separation Process Principles;* Wiley, 1998.
10. Danckwerts, P.V.; Significance of liquid-film coefficients in gas absorption. *Industrial & Engineering Chemistry*. 1951, 42, 1460.
11. Losey, M.; Jackman, R.; Firebaugh, S.; Schmidt, M.; Jensen, K.F. Design and fabrication of microfluidic devices for multiphase mixing and reaction. *Journal of Microelectromechanical Systems*. 2002, 11, Issue 6, 709-717.
12. Fogler, H.S. *Elements of Chemical Reaction Engineering, 4th Ed.*; Prentice Hall, 2006.
13. Moore, W.J. *Physical Chemistry, 4th Ed.*; Prentice Hall College Division, 1972.
14. Bird, R.B.; Stewart, W.E.; Lightfoot, E.N. *Transport Phenomena, 2nd Ed.*; Wiley, 2002.
15. Jensen, K.F; Microreaction engineering—is small better? *Chemical Engineering Science*. 2001, 56, 293-303.
16. Jensen, K.F.; Chemical kinetics: smaller, faster chemistry. *Nature*. 1998, 393, 735.
17. Ehrfeld, W.; Hessel, V.; Mobius, H.; Russow, K. Microsystem technology for chemical and biological microreactors. *DECHEMA-Monographs*. 1996, 132, 1-28.
18. AlDahhan, M.H.; Larachi, F.; Dudukovic, M.P.; Laurent, A. High-pressure trickle-bed reactors: a review. *Industrial and Engineering Chemistry Research*. 1997, 36, 3292-3314.
19. Xu, J.L.; Cheng, P.; Zhao, T.S. Gas-liquid two-phase flow regimes in rectangular channels with micro/mini gaps. *International Journal of Multiphase Flow*. 1999, 25, 411.
20. Gavriilidis, A.; Angeli, P.; Cao, E.; Yeong, K.K.; Wan, Y.S.S. Technology and applications of microengineered reactors. *IChemE*. 2002, 80, 3-30.
21. Worz, O.; Jackel, K.P.; Richter, T.; Wolf, A. Microreactors, a new efficient tool for optimum reactor design. *Chemical Engineering Science*. 2001, 56, 1029-1033.
22. Srinivasan, R.; Hsing, I.M.; Berger, P.E.; Jensen, K.F.; Schmidt, M.A.; Harold, M.P.; Lerou, J.J.; Ryley, J.F. Micromachined reactors for catalytic partial oxidation reactions. *AIChE Journal*. 1997, 43, 3059.
23. Ajmera, S.K.; Losey, M.W.; Jensen, K.F.; Schmidt, M.A. Microfabricated packed-bed reactor for phosgene synthesis. *AIChE Journal*. 2001, 47, 1639.
24. Watts, P.; Haswell, S.J. The application of microreactors for small scale organic synthesis. *Chemical Engineering & Technology*. 2005, 28, 290-301.
25. Mills, P.L.; Chaudhari, R.V. Mulitphase catalytic reactor engineering and design for pharmaceuticals and fine chemicals. *Catalysis Today*. 1997, 37, 367-404.
26. Mishima, K.; Hibiki, T. Some characteristics of air-water 2-phase flow in small-diameter vertical tubes. *International Journal of Multiphase Flow*. 1996, 22, 703.
27. Triplett, K.A.; Ghiaasiaan, S.M.; Abdel-Khalik, S.I.; Sadowski, D.L. Gas-liquid two-phase flow in microchannels Part I: two-phase flow patterns. *International Journal of Multiphase Flow*. 1999, 23, 377.
28. Akbar, M.K.; Plummer, D.A.; Ghiaasiaan, S.M. On gas-liquid two-phase flow regimes in microchannels. *International Journal of Multiphase Flow*. 2003, 29, 855.

29. Chen, W.L.; Twu, M.C.; Pan, C. Gas-liquid two-phase flow in microchannels. *International Journal of Multiphase Flow*. 2002, 28, 1235.
30. Kapteijn, F.; Nijhuis, T.A.; Heiszwolf, J.J.; Moulijn, J.A. New non-traditional multiphase catalytic reactors based on monolithic structures. *Catalysis Today*. 2001, 66, 133-144.
31. Kovacs, G.T.; Maluf, N.I.; Petersen, K.E. Bulk micromachining of silicon. Proceedings of IEEE. 1998, 86, 1536.
32. de Carvalho, R.F.G.; Alves, A.M. Mass transfer and dispersion around active sphere buried in a packed bed. *AIChE Journal*. 1999, 45, 2495-2502.
33. Stitt, E.H. Alternative multiphase reactors for fine chemicals- A world beyond stirred tanks? *Chemical Engineering Journal*. 2002, 90, 47-60.

TASK 4: Model-based Concept Microreactor Design and Demonstration

Multiphase reactions in microchannels find applications in many industrially important chemical processes such as the direct synthesis of hydrogen peroxide, hydrogenation of liquid substrates, and immiscible liquid-liquid nitration. The hydrodynamic characteristics of the flow play a very important role in reactor design. Since the flow in a microchannel is typically laminar, the mass transfer between the phases is mainly dominated by diffusion, and turbulent convective flow normally relied upon for rapid and effective mixing in macroreactors is non-existent. Mixing is therefore a critical issue in the design of multiphase microreactors. Many investigators have characterized gas-liquid flows in a microchannel (Chen et al. 2002, Chung & Kawaji 2004, Triplett et al. 1999, Yang & Shieh 2001, Fukano & Kariyasaki 1993, Coleman & Garimella 1999, Akbar et al. 2003). Bubbly, slug, churn and annular flow are among the observed flow regimes. However, over a wide range of operating conditions, the flow in a multiphase microchannel is typically the so-called Taylor flow regime (Heiszwolf et al. 2001). The Taylor flow is a special case of slug flow where the bullet-shaped bubbles (Taylor bubbles) are separated by free-gas-entrained liquid slugs. The elongated bubble has a characteristic capsular shape with equivalent diameter larger than the channel width. There is a very thin film between the gas bubble and the channel wall. Taylor slug flow has been shown to increase transverse heat and mass transfer compared to single phase laminar flow because of the recirculation within the liquid slugs and the reduction of axial mixing between the liquid slugs (Bercic & Pintar 1997, Kreutzer et al. 2001, Irandoust & Andersson 1989, Thulasidas et al. 1997).

All the results available in the literature indicate that mass transfer, pressure drop and residence time distribution for slug flows in microchannels are highly dependent on the thin liquid film and slug length. Unlike other flow parameters such as superficial velocities and fluid properties, the liquid film thickness and the slug length cannot be determined a priori. Flow visualization, conductivity, or other advanced tomography techniques like magnetic resonance imaging are commonly used to determine these quantities. While the film thickness has been extensively studied experimentally and numerically, there are limited studies on the slug length, an important parameter for Taylor flows. However, there is significant inconsistency in the literature, therefore a systematic study on the gas and liquid slug lengths in microchannels is warranted. As Kreutzer et al. (2005a) pointed out in their review CFD studies will provide the mechanistic insight for the slug flow in microchannels. Current CFD studies mainly focus on one unit slug cell, which presume that the gas and liquid slug lengths are known. Researchers either used single phase model with void gas (van Baten & Krishna 2004, van Baten & Krishna 2005, Kreutzer et al. 2005b, Irandoust & Andersson 1989a) or implemented two phase VOF

model (Taha & Cui 2004, 2006a, 2006b) to investigate bubble shape, bubble velocity, film thickness, mass transfer, pressure drop and velocity profile inside the liquid slug. Some commercial CFD packages such as FLUENT, FIDAP and CFX have proven to be appropriate to perform these studies. The most important objective of this task was to study numerically the gas and liquid slugs for Taylor flow in microchannels. A T-junction microchannel serves as model geometry. The development of the gas and liquid slugs in the geometry with different inlet configurations at various operating and fluid conditions was investigated.

The hydrodynamic characteristics of the flow in microchannels are different from those encountered in ordinarily large-size channels. The threshold of hydraulic channel diameter is about 1mm with fluid properties similar to air and water (Akbar et al. 2003). In microchannels, the buoyancy effect is negligible in comparison to surface tension, which in effect renders the flow characteristic independent of channel orientation with respect to gravity (Triplett et al. 1999). In the studies of chemical reaction in microchannels, a T-junction microreactor with millimeter to submillimeter range is typically chosen to investigate the hydrodynamics or kinetics for multiphase reactions. We consider an empty T-junction microchannel reactor (not packed with catalyst) with cross-sectional width of 0.25, 0.5, 0.75, 1, 2 and 3 mm for the studies of gas-liquid hydrodynamics. This type of reactor is applicable to homogeneous reaction or surface reaction with thin-film catalyst coated on the wall.

Figure 4.1 is the model T-junction microchannel reactor used in our simulation. The microchannel reactor comprises a vertical inlet mixing zone and a horizontal reaction zone. A stream of water and a stream of air are fed separately into the two inlets of the mixing zone, and then enter the reaction zone. The cross-sectional dimensions of the channel are the same, which are represented by d. The mixing zone has a length of 6d while the reactor zone has a length of 60d. "Cold" flow without any chemical reaction is considered. The whole system is maintained at room temperature, and the pressure is atmospheric at the exit. The superficial gas velocity as well as superficial liquid velocity varies from 0.01 to 0.25 m/s. According to the flow regime maps by Chung & Kawaji (2004), Triplett et al. (1999), Yang & Shieh (2001), Fukano & Kariyasaki (1993), Coleman & Garimella (1999) and Akbar et al. (2003), at these operating conditions, the flow falls within the Taylor slug regime in microchannels.

A finite volume based commercial CFD package, FLUENT (Release 6.1.22, 2003), was used to perform the numerical simulations, and typical results are presented in Figs. 4.2 – 4.12. The results show that the slug length is not uniform throughout the channel especially for channel cross-sectional dimensions exceeding 1 mm. When the gas or liquid flow rate increases, the slug non-uniformity becomes more pronounced. The slug length is also highly dependent on the inlet configuration. From the studies of gas and liquid slugs in a T-junction microchannel at various operating conditions, the following conclusions are drawn:

- The gas slug length increases with increase in superficial gas velocity, and decrease in superficial liquid velocity.
- The liquid slug length increases with increase of superficial liquid velocity, and decrease of superficial gas velocity.
- The dimensionless slug length is mainly determined by the phase hold-up, with a slight effect of Re and Ca. Therefore, wider channels have longer slug length at the same superficial gas and liquid velocities.
- Gravitational effects can be ignored in microchannels.
- The effects of fluid density and viscosity are also negligible.

- The surface tension and wall surface adhesion moderately impact the slug lengths.

Based on the equations of conservation of mass and momentum, the associated boundary conditions, and simplifying assumptions, the dimensionless slug length will have the following dependence:

$$L^* = L^*(\mathrm{Re}, Ca, \varepsilon_G) \tag{4.1}$$

Regression of the simulation data provides the following correlations for the dimensionless slug length:

$$(L_G + L_L)/d = 1.637\varepsilon_G^{-0.893}(1-\varepsilon_G)^{-1.05}\,\mathrm{Re}^{-0.075}\,Ca^{-0.0687} \tag{4.2}$$

$$L_G/d = 1.637\varepsilon_G^{0.107}(1-\varepsilon_G)^{-1.05}\,\mathrm{Re}^{-0.075}\,Ca^{-0.0687} \tag{4.3}$$

$$L_L/d = 1.637\varepsilon_G^{-0.893}(1-\varepsilon_G)^{-0.05}\,\mathrm{Re}^{-0.075}\,Ca^{-0.0687} \tag{4.4}$$

A total of 148 sets of numerical simulation data were correlated with channel width 1 mm and less for parameter values in the range: $0.09 < \varepsilon_G < 0.91$, $15 < \mathrm{Re} < 1500$, $0.000278 < Ca < 0.01$. Eq. (4.3) is obtained by multiplying Eq. (4.2) by ε_G, while Eq. (4.4) is obtained by multiplying Eq. (4.2) by $1-\varepsilon_G$, for $L_G/(L_G+L_L) \approx \varepsilon_G$ and $L_L/(L_G+L_L) \approx 1-\varepsilon_G$ in our simulation conditions. The average difference between the correlated data and the simulated data is about 10%. These correlations show that the dimensionless slug length is mainly determined by the phase hold-up, while the Re and Ca have a slight effect. This result can explain why the dimensionless slug length falls within a narrow range even for wide operating conditions.

These correlations can be used to predict the slug length based on the operating conditions, and subsequently some important transport parameters such as pressure drop, heat transfer and mass transfer coefficients can be estimated. Based on this numerical study of Taylor flow in microchannels, we can begin to understand, and quantify heat and mass transfer enhancement in microchannels. Further details about this task can be found in Qian and Lawal (2006).

Finally we investigated the two phase flow in a packed bed. In our simulation region, the gas-liquid flow in a microchannel is also a slug flow. This was confirmed by our flow visualization experiments. Figure 4.13 shows the simulation results of the gas and liquid slug lengths in 0.25, 0.50, and 0.75 mm packed bed with 50 micron particles at different void fraction values. Here the gas and liquid velocities were based on real void volume (physical velocity). We can see that as the particles become more densely packed, the slug length decreases.

Notation

d	internal channel width, m
f	apparent friction factor
L	mean slug length, m
t	time, s
U	superficial velocity, m/s
U_{TP}	unit cell velocity (=U_G+U_L), m/s
v	velocity, m/s
V_b	gas slug velocity (≈U_G+U_L), m/s

Greek letters

ε hold-up
μ molecular viscosity, kg/m s
θ contact angle, ^{o}
ρ density, kg/m^3
σ surface tension, N/m

Dimensionless numbers
Ca Capillary number ($=\mu U/\sigma$)
Re Reynolds number ($=\rho Ud/\mu$)

Subscripts & superscripts
G gas
L liquid
* dimensionless value

REFERENCES

Akbar, M.K., Plummer, D. A., Ghiaasiaan, S.M., 2003. On gas-liquid two-phase flow regimes in microchannels. International Journal of Multiphase Flow. 29, 855-865.

Bercic, G., Pintar, A., 1997. The role of gas bubbles and liquid slug lengths on mass transport in the Taylor flow through capillaries, Chemical Engineering Science 52(21/22), 3709-3719.

Chen, W.L., Twu, M.C., Pan, C., 2002. Gas-liquid two-phase flow in micro-channels. International Journal of Multiphase Flow 28, 1235-1247.

Chung, P.M.-Y., Kawaji, M. 2004. The effect of channel diameter on adiabatic two-phases flow characteristics in microchannels. International Journal of Multiphase Flow 30, 735-761.

Coleman, J. W., Garimella S., 1999. Characterization of two-phase flow patterns in small diameter round and rectangular tubes. International Journal of Heat and Mass Transfer 42, 2869-2881.

FLUENT 6.1 documentation, 2003. Fluent Incorporated, Lebanon, New Hampshire.

Heiszwolf, J.J., Kreutzer, M.T., van den Eijnden, M.G., Kapteijn, F., Moulijn, J.A., 2001. Gas-liquid mass transfer of aqueous Taylor flow in monoliths. Catalysis Today 69, 51-55.

Fukano, T., Kariyasaki, A., 1993. Characteristics of gas-liquid two-phase flow in a capillary tube. Nuclear Engineering and Design 141, 59-68.

Irandoust, S. , Andersson, B., 1989. Simulation of flow and mass-transfer in Taylor flow through a capillary. Computers Chemical Engineering 13(4/5), 519-526.

Jensen, K.F., 2001. Microreaction engineering — is small better? Chemical Engineering Science 56, 293-303.

Kreutzer, M.T., Du, P., Heiszwolf, J.J., Kapteijn F., Moulijn J. A., 2001. Mass transfer characteristics of three-phase monolith reactors. Chemical Engineering Science 56, 6015-6023.

Kreutzer, M.T., Kapteijn F., Moulijn J. A., Heiszwolf, J.J., 2005a. Multiphase monolith reactors: Chemical reaction engineering of segmented flow in microchannels. Chemical Engineering Science 60, 5895-5916.

Kreutzer, M.T., Kapteijn F., Moulijn J. A., Kleijn C. R., Heiszwolf J. J. 2005b. Inertial and interfacial effects on pressure drop of Taylor flow in capillaries. AIChE Journal 51(9), 2428-2440.

Qian, D., Lawal, A., 2006 Numerical Study on Gas and Liquid Slugs for Taylor Flow in a T-junction Microchannel. Chemical Engineering Science 61, 7609-7625.

Tata, T., Cui, Z.F., 2004. Hydrodynamics of slug flow inside capillaries. Chemical Engineering Science 59, 1181-1190.

Tata, T., Cui, Z.F., 2006 (a). CFD modelling of slug flow in vertical tubes. Chemical Engineering Science 61 (2006) 676 – 687.

Tata, T., Cui, Z.F., 2006(b).CFD modelling of slug flowinside square capillaries. Chemical Engineering Science 61 (2006) 665 – 675.

Thulasidas, T.C., Abraham, M.A., Cerro, R.L., 1997. Flow patterns in liquid slugs during bubble-train flow inside capillaries. Chemical Engineering Science 52 (17), 2947–2962.

Triplett, K.A., Ghiaasiaan, S.M., Abdel-Khalik, S.I., Sadowski, D.L., 1999. Gas-liquid two-phase flow in microchannels Part I: two-phase flow patterns. 25, 377-394.

Van Baten, J.M., Krishna, R., 2004. CFD simulation of mass transfer from Taylor bubbles rising in circular capillaries. Chemical Engineering Science 59, 2535-2545.

Van Baten, J.M., Krishna, R., 2005. CFD simulation of wall mass transfer for Taylor flow in circular capillaries. Chemical Engineering Science 60, 1117-1126.

Yang, C.-Y., Shieh, C.-C., 2001, Flow pattern of air-water and two-phase R-134a in small circular tubes. International Journal of Multiphase Flow 27, 1163-1177.

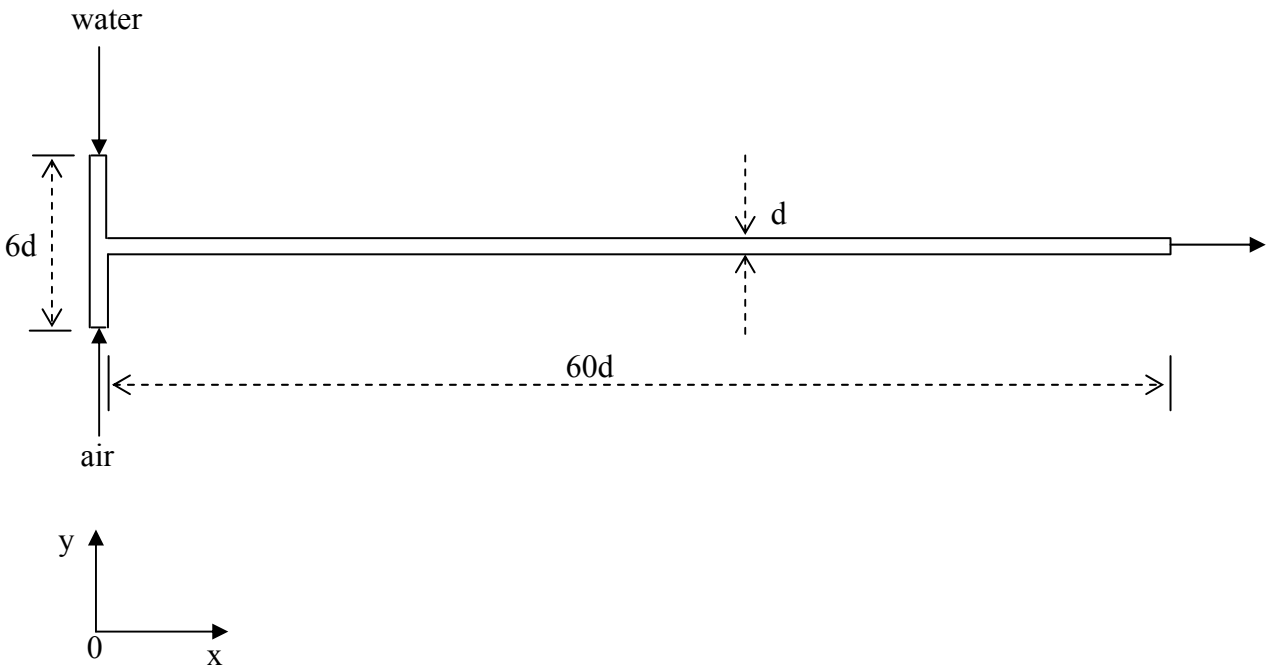

Figure 4.1: Model T-junction microreactor used in the simulation.

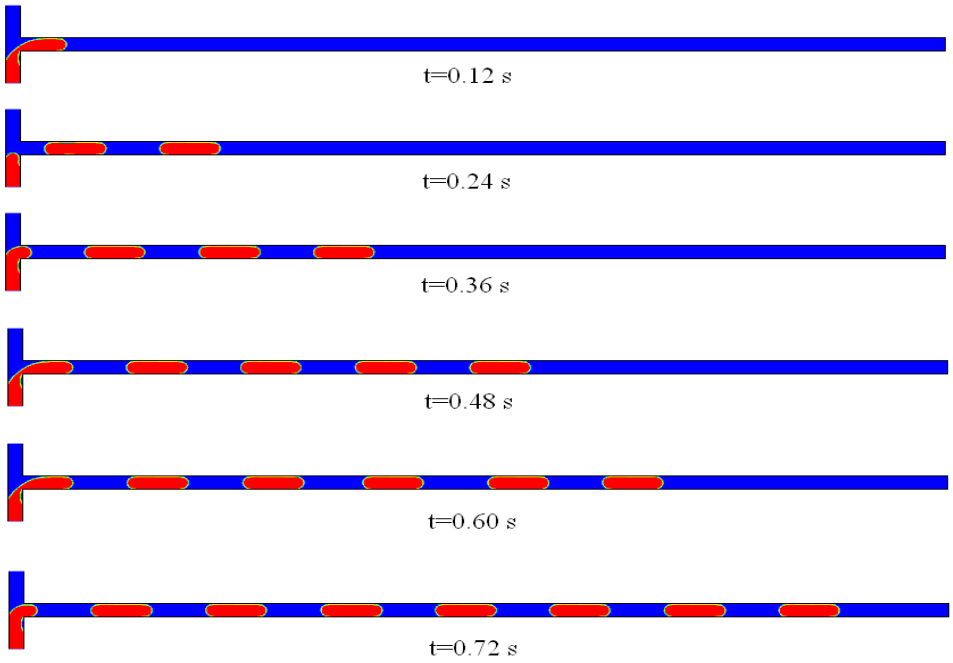

Figure 4.2: Slug flow development in the model geometry. (red —— gas slug, blue —— liquid slug d=0.5 mm, U_G=U_L=0.02 m/s).

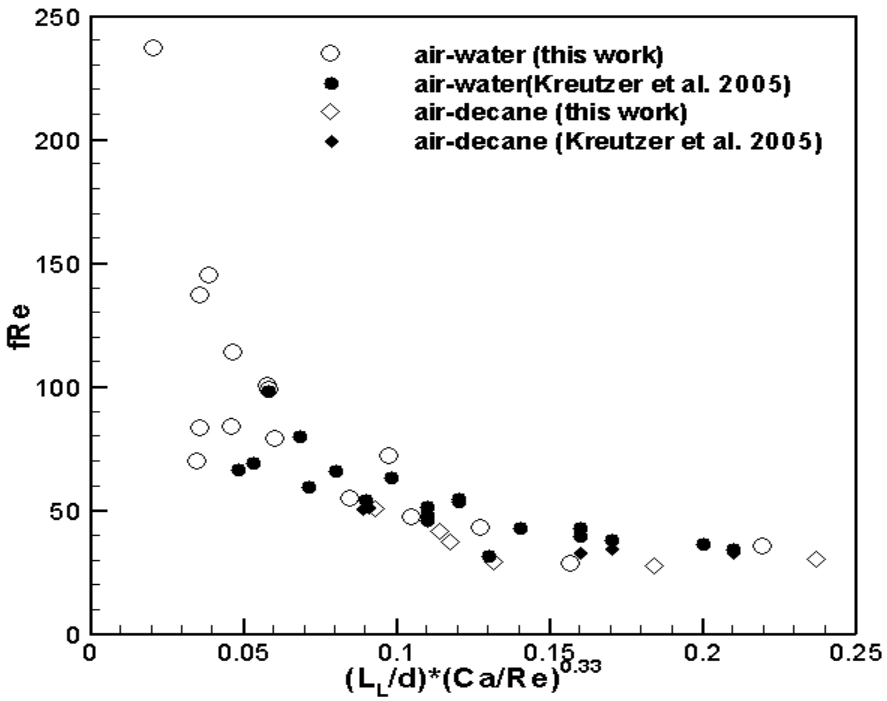

Figure 4.3: (f Re) as a function of the dimensionless group $(L_L/d)*(Ca/Re)^{0.33}$.

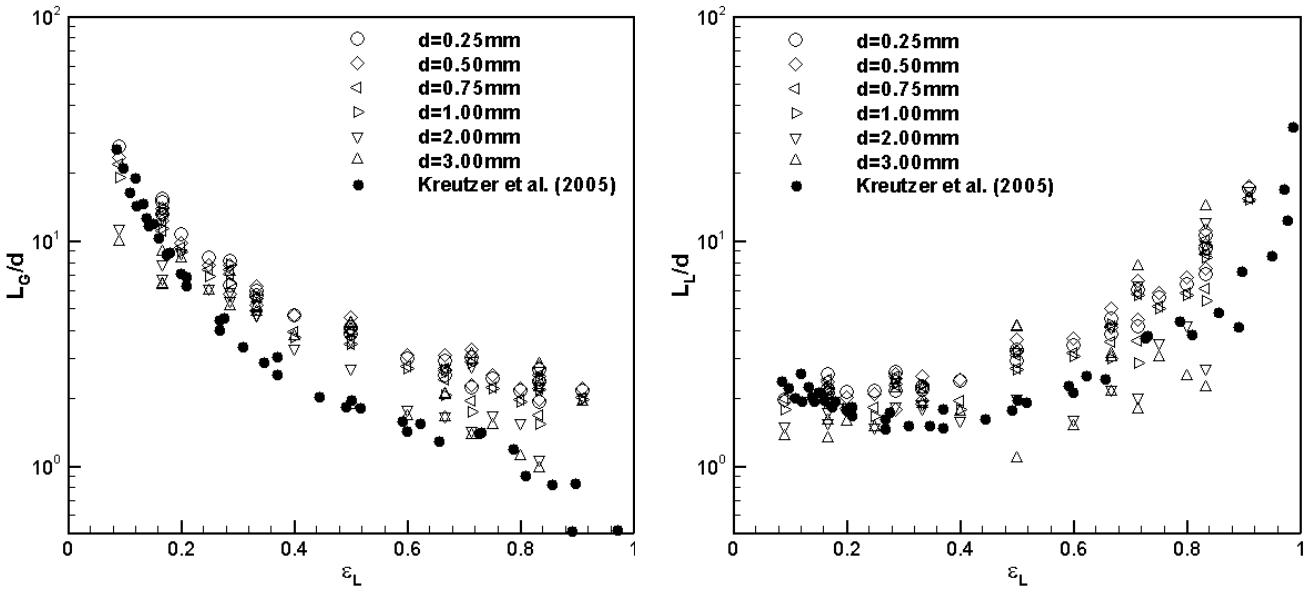

Figure 4.4: Dimensionless slug length against liquid hold-up.

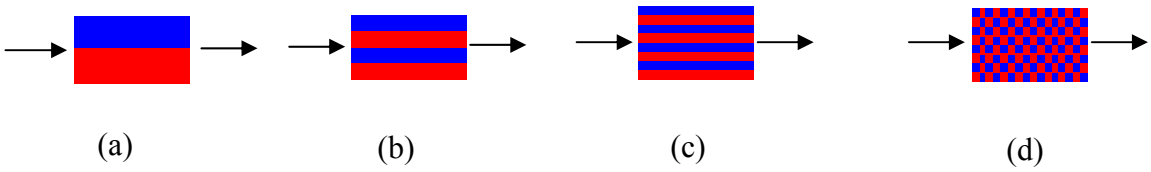

(a) L_G=5.75 mm, L_L=4.88 mm

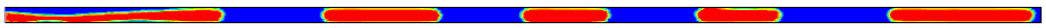

(b) L_G=3.24 mm, L_L=2.80 mm

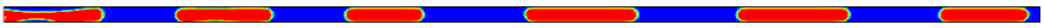

(c) L_G=3.10 mm, L_L=2.50 mm

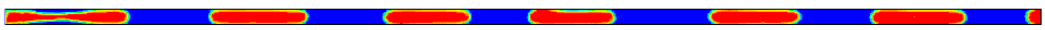

(d) L_G=2.61 mm, L_L=2.11 mm

Figure 4.5: Gas and liquid slugs at different inlet mixing levels. (d= 0.5 mm, U_G=U_L=0.02 m/s)

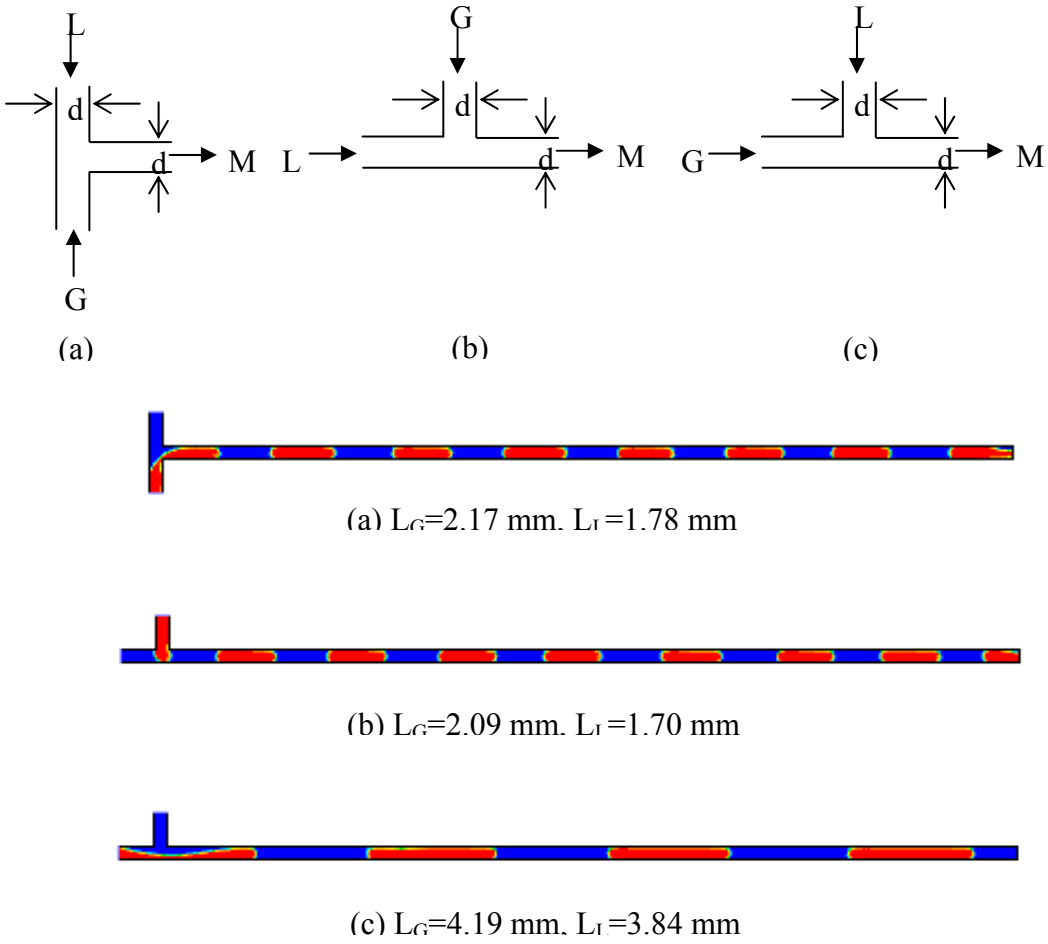

Figure 4.6: Gas and liquid slugs at different tee orientations. (d= 0.5 mm, U_G=U_L=0.02 m/s)

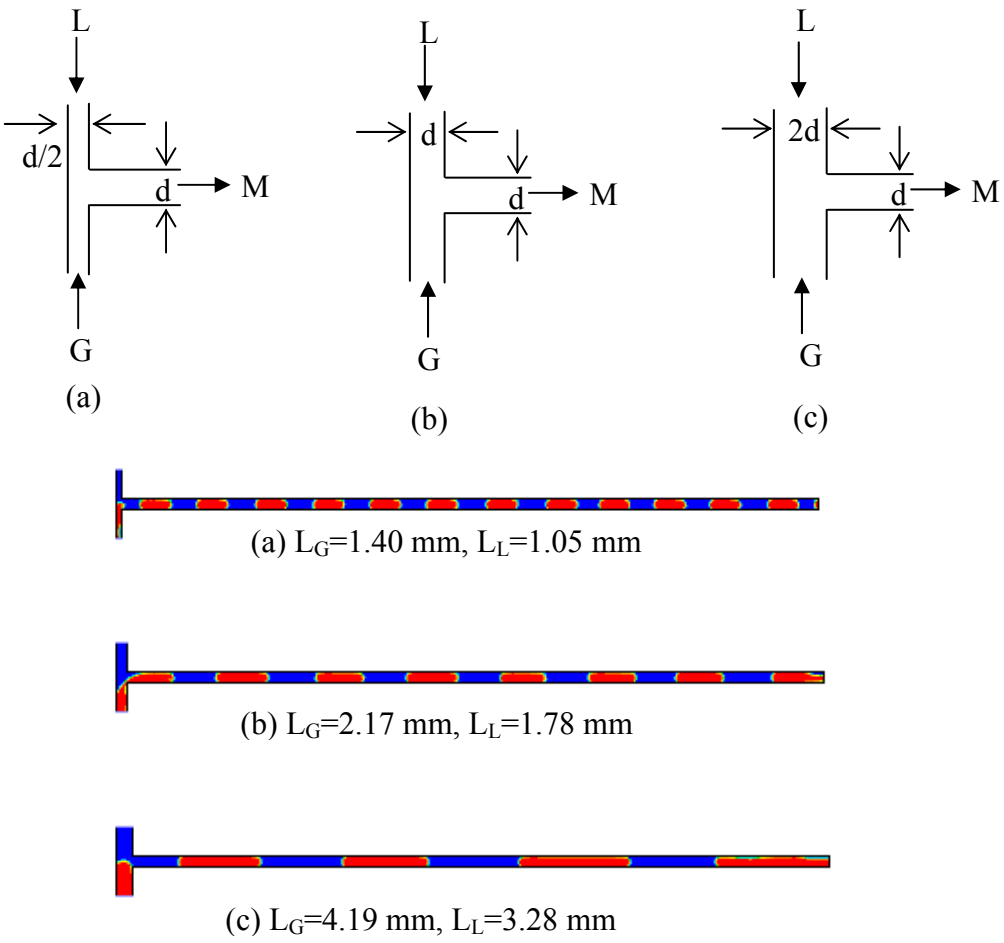

Figure 4.7: Gas and liquid slugs at different inlet tee sizes. (d=0.5mm, U_G=U_L = 0.02 m/s)

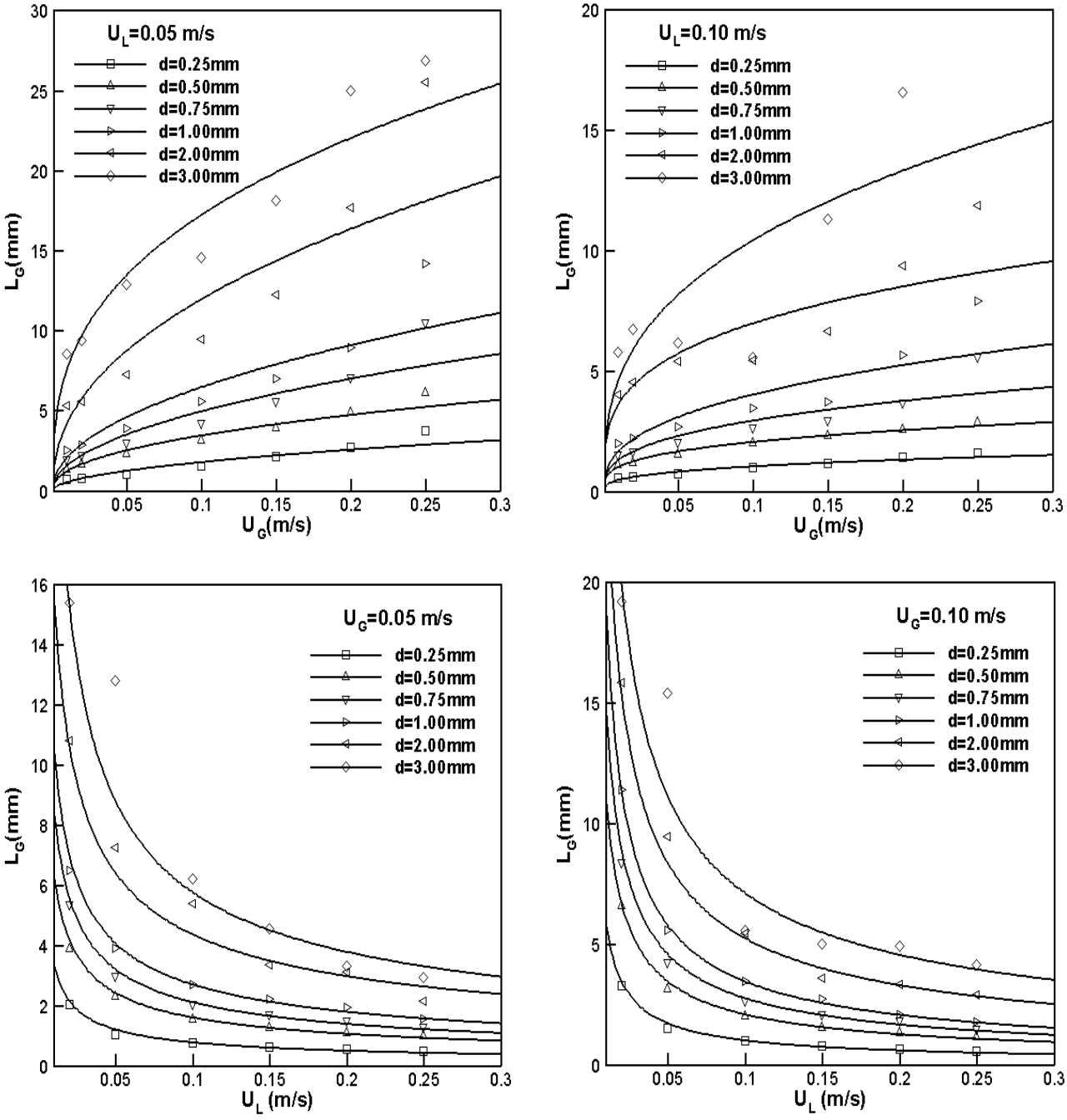

Figure 4.8: Influence of gas and liquid superficial velocities on gas slug length.

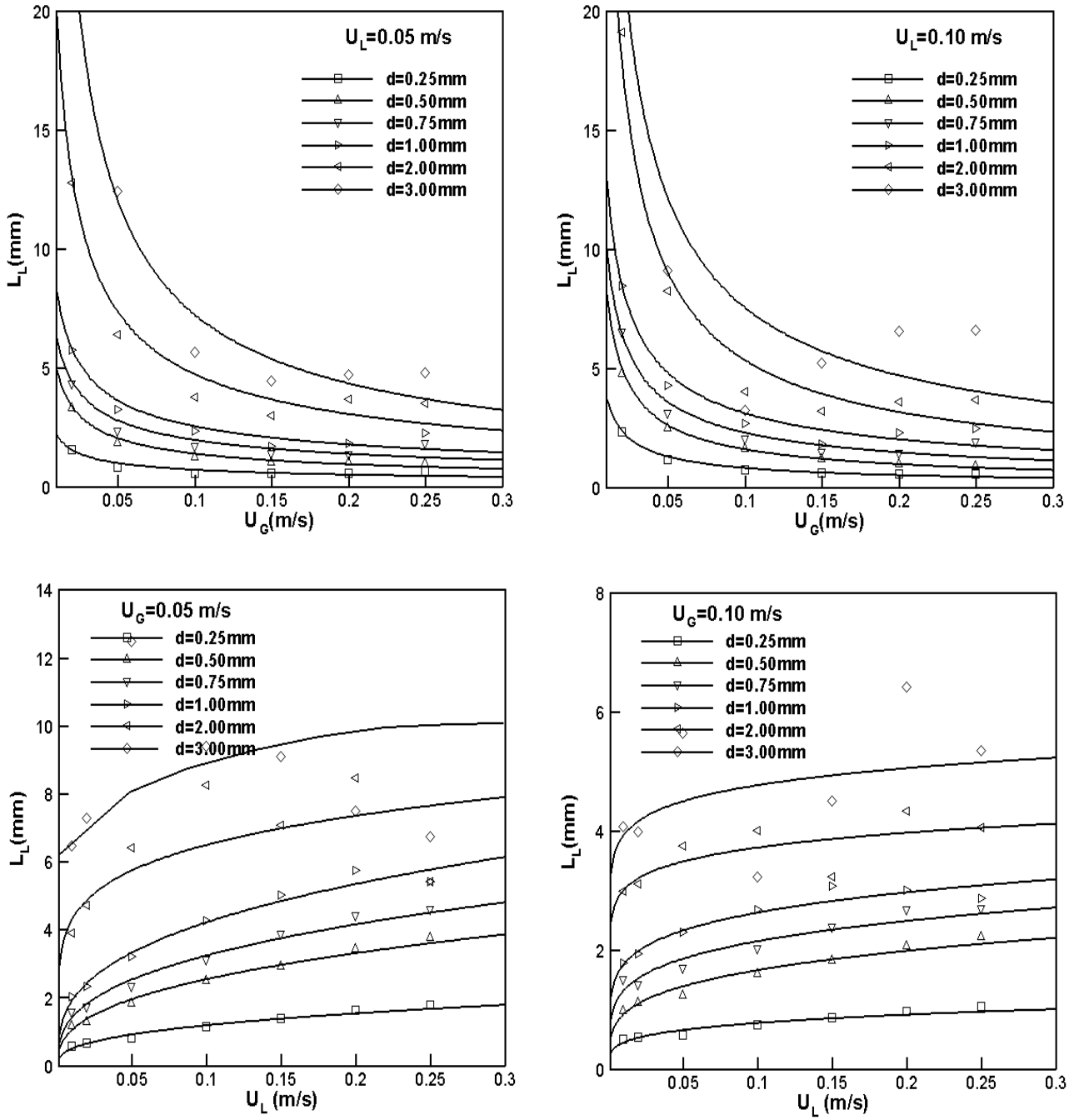

Figure 4.9: Influence of gas and liquid superficial velocities on liquid slug length.

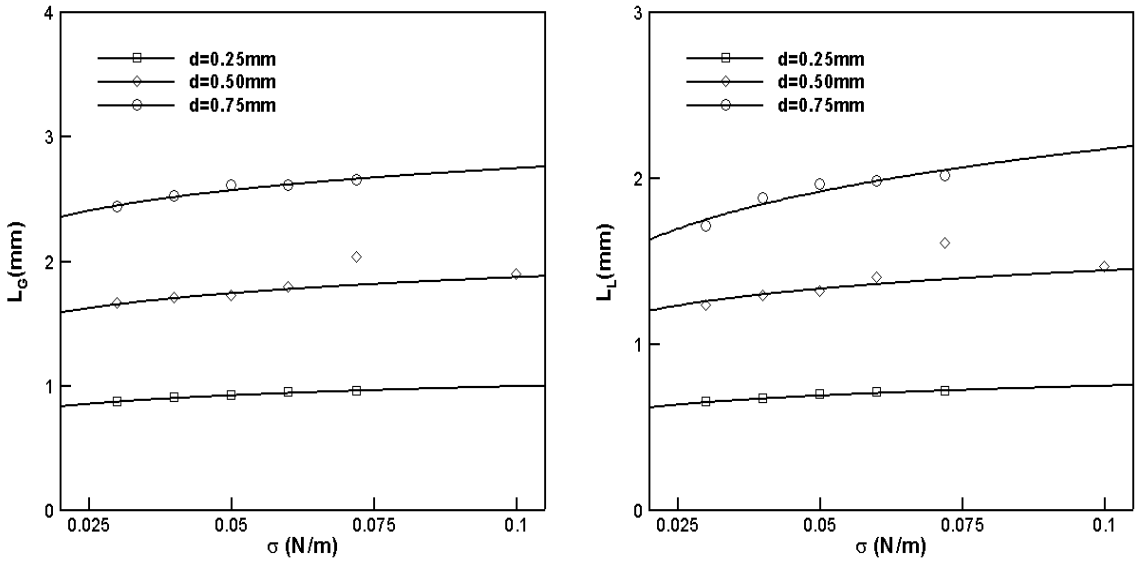

Figure 4.10: Influence of surface tension on gas and liquid slug length. (U_G=0.1 m/s, U_L=0.1 m/s)

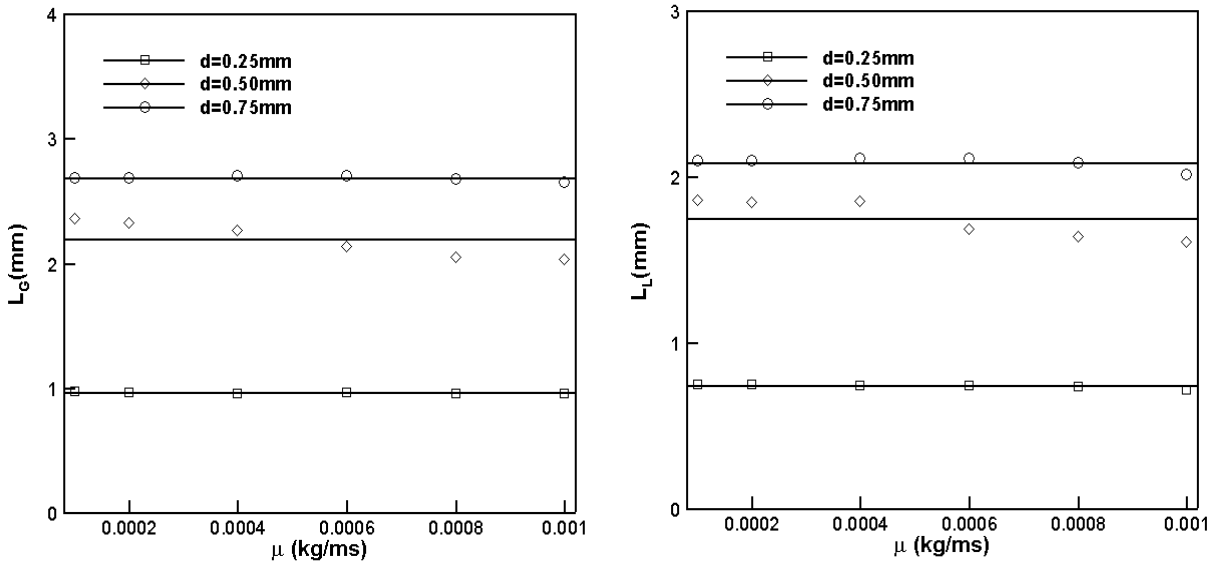

Figure 4.11: Influence of liquid viscosity on gas and liquid slug lengths. (U_G=0.1 m/s, U_L=0.1 m/s)

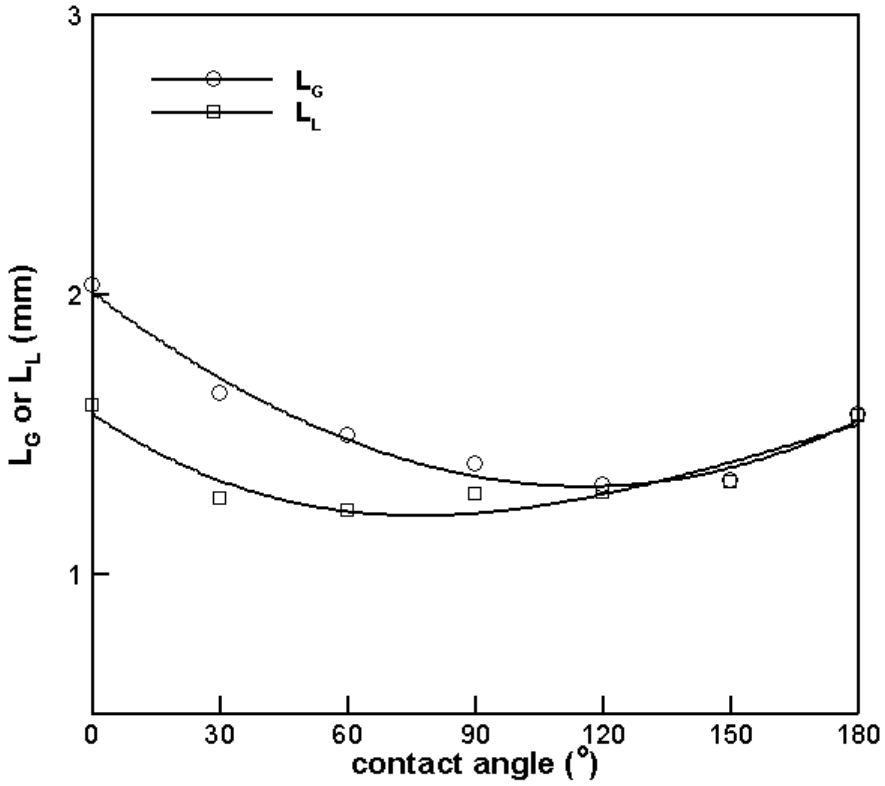

Figure 4.12: Influence of contact angle on gas and liquid slug lengths.
(d=0.50mm, U_G=0.1 m/s, U_L=0.1 m/s)

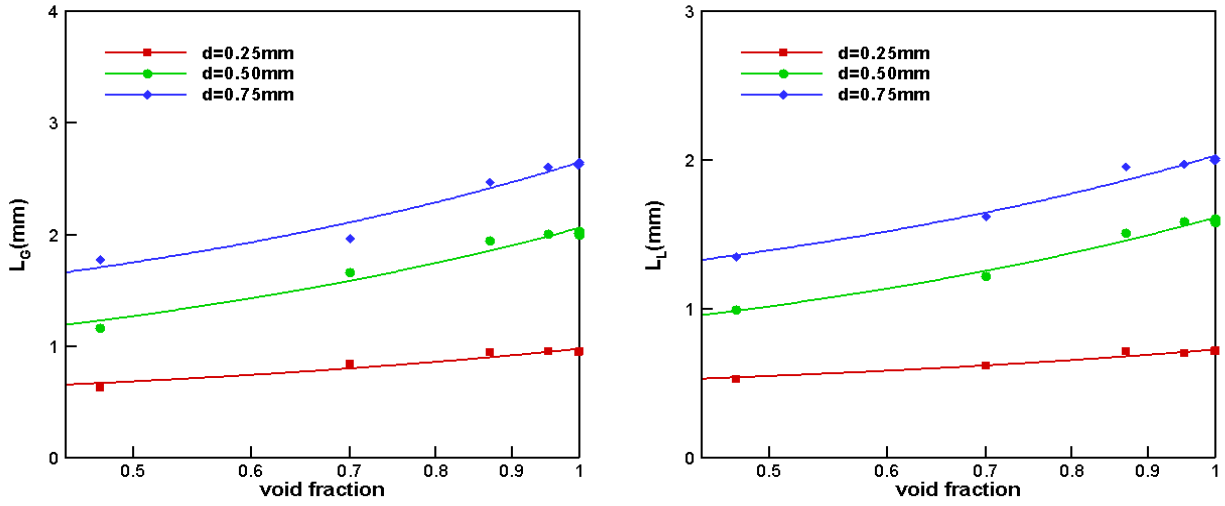

Figure 4.13: Slug length in a bed packed with 50 micron particles at different void fraction
(U_G=0.1 m/s, U_L=0.1 m/s)

TASK 5: Laboratory Reactor System Optimization

The modeling and simulation work in Task 4 focussed principally on the flow characteristics in microchannels. The flow behaviour plays a very important role in reactor design. We established that the gas-liquid flow in microchannels is mainly the Taylor slug flow. The gas and liquid slug lengths depend on superficial velocity, channel diameter, fluid property and inlet geometry. From this activity, we learned how to design a multiphase micro-reactor such that the gas and liquid slug lengths are minimized and consequently mass transfer between the phases is enhanced.

We next incorporated reaction kinetics into the modeling and simulation of two phase flows. This multiphase flow with chemical kineitcs was quite challenging because it involved momentum, heat and mass transfer as well as chemical reactions. Furthermore, the use of solid catalyst makes the problem more complicated because the actual flow has three phases in addition to the gas and liquid phases. It is very difficult to determine in which of the phases the reaction exactly takes place, is it in liquid slugs, or in gas slugs, or between the gas and liquid phases? This is the key question that needs to be addressed for this type of reactor before any meaningful simulation can be carried out. However, the answer was not readily available, hence we expected that CFD would throw some light on the question.

The verison of our CFD software had the capability to deal with multiphase species transport. However, the user has to simplify the physical problem, choose an appropriate model, and then incorporate some user-defined functions. Here we still used the VOF two phase model with chemical reactions. We selected the o-nitroanisole hydrogenation reaction as the model reaction since we had obtained experimentally the rate expressions for this reaction in addition to the one that was available in the literature.

The first step in the CFD simulation was to assume that the reaction involved both the gas and liquid phases. Since the model reactor was a packed bed, and there is a thin liquid film on the catalyst surface, we made the assumption that the reaction occurred inside the whole volume, both gas and liquid. Figure 5.1 shows the mass fraction of o-nitroanisole along the reactor length, and Figure 5.2 shows the mass fraction of anisidine along the reactor length. One can clearly see the change of the reactant and product concentrations inside the reactor.

Another objective of this activity was to study the mass transfer between the phases. From the species concentration distribution, the mass transfer coefficient can be computed and compared with our experimental value and that in the literature.

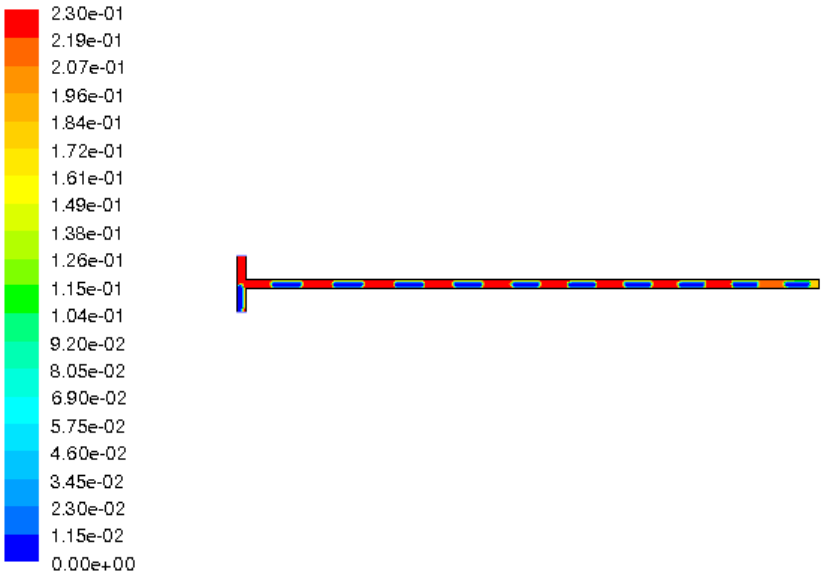

Figure 5.1: **Mass fraction of o-nitroanisole (reactant) along the reactor**

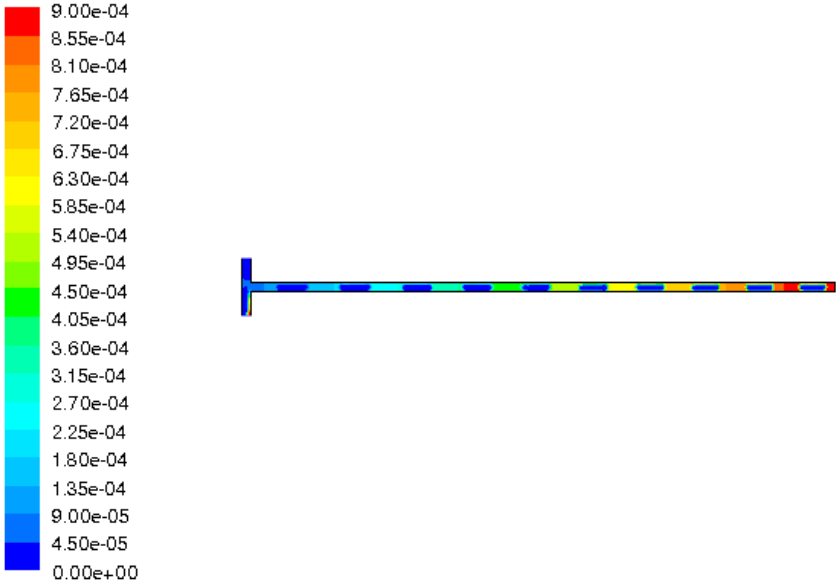

Figure 5.2: **Mass fraction of anisidine (product) along the reactor length**

As a first step, we applied the simple 1D model for the kinetic analysis. We assumed values for the mass transfer coefficients, and predicted the effluent product concentration. When the predicted and measured effluent concentrations agreed, the correct mass transfer coefficient had been selected. We next predicted reactant and product concentration profiles along the reaction length. However, no detailed information about slug length and its variation with reaction extent could be obtained from the 1D analysis. Also, with the 1-D analysis, the question as to whether the reaction took place predominantly in liquid or gas phase could not be unanswered. Inherent in the 1-D analysis is that the reaction occurs at the interface between the gas and liquid.

The predicted reaction extent from the simulation was much smaller than that obtained from the experimental data. We next assumed that the reaction took place in the liquid, because the substrate was in the liquid phase. Hydrogen from the bulk gas transfers across the interface, dissolves in the liquid, and then reacts with the reactant. Although the catalyst was packed in the bed, the model treated the solid only as a momentum sink. The VOF two phase model was still used in the simulation. A gas to liquid mass transfer mechanism was superimposed on the simulation and a mass transfer parameter of 5 s^{-1} was assumed.

Figure 5.3 shows the slug lengths inside the reactor; liquid slug is shown in red while the gas slug is in blue. One can see that, as the reaction proceeds down the reactor length, the gas slug is getting shorter because of the consumption of hydrogen; at the same time, the liquid slug is getting longer because of the liquid product. Figure 5.4 is the mass fraction of o-nitroanisole along the reactor length which as expected should reduce since the reactant is being consumed by the reacton. Figure 5.5 is the mass fraction of hydrogen dissolved in liquid. The concentration of hydrogen in the liquid is very small because of its low solubility. There is a distribution of hydrogen concentration inside the liquid slug because of the diffustion and reaction effects. Near the interface, hydrogen concentration in the liquid is larger for there is a direct contact between the gas and liquid phase.

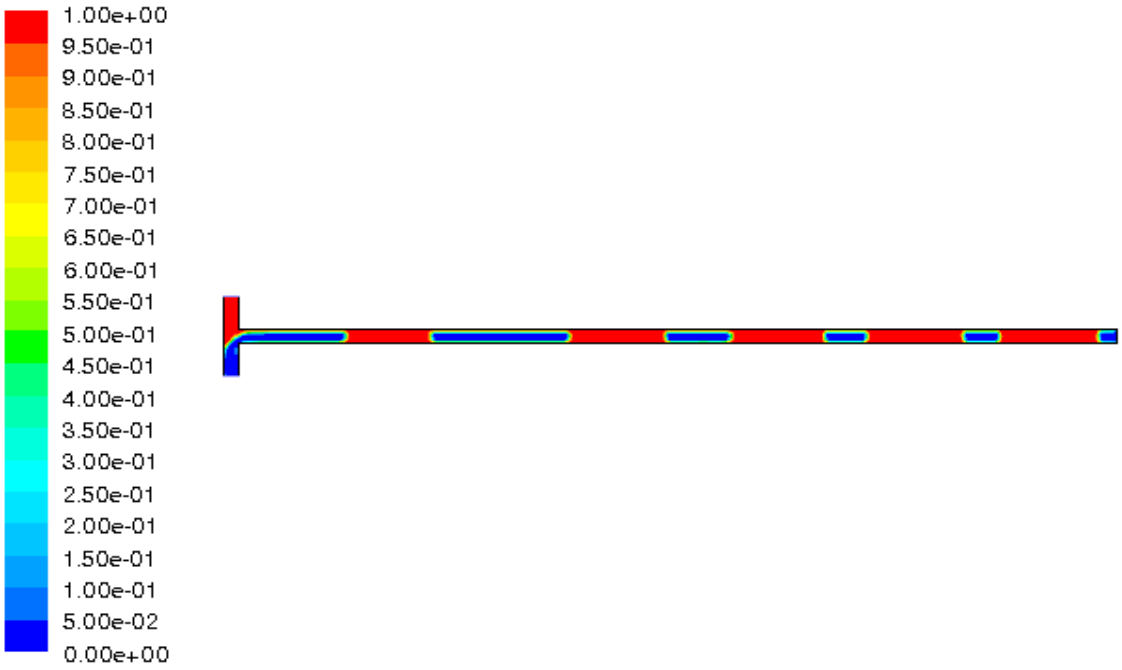

Figure 5.3: Gas (blue) and liquid (red) slugs inside the reactor

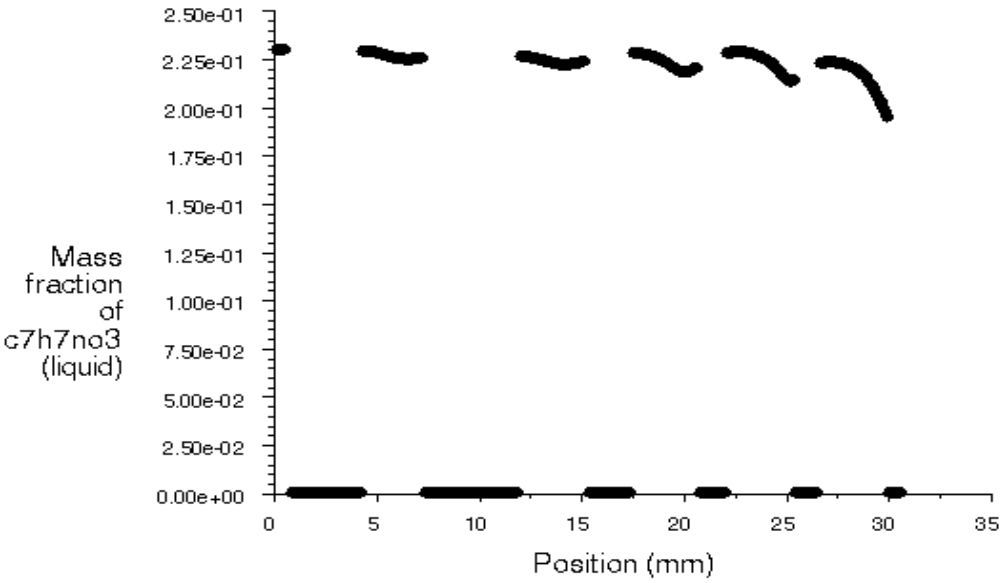

Figure 5.4: Mass fraction of o-nitroanisole (reactant) along the reactor

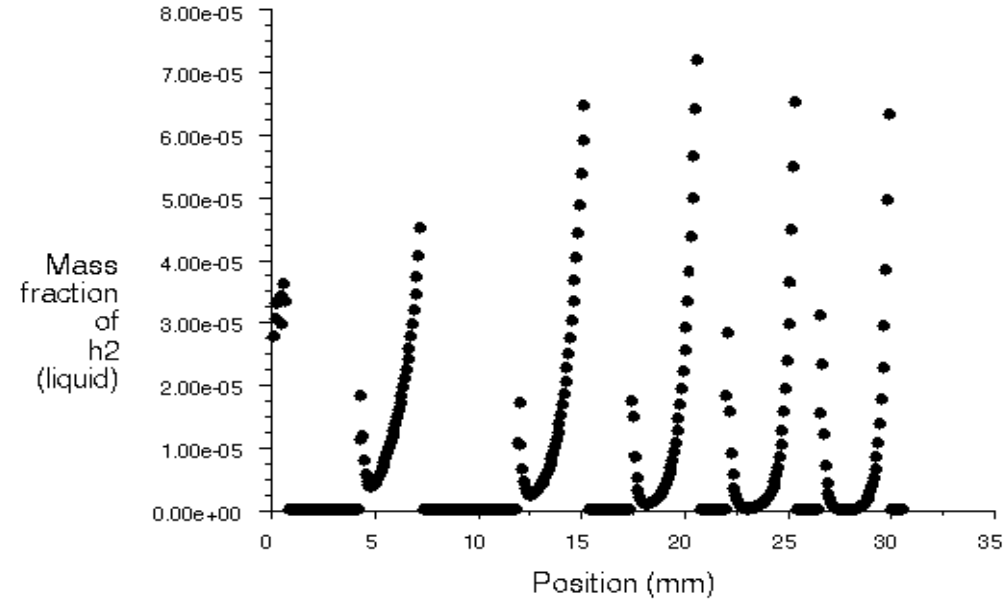

Figure 5.5: Mass fraction of hydrogen in the liquid phase (reactant) along the reactor

The mass transfer parameter from gas to liquid was an adjustable parameter in the model we used. According to the literature, the mass transfer coefficient in microreactors is 2 orders of magnitude larger than that in standard laboratory scale reactors. The significant increase of mass transfer coefficient is the primary advantage of microreators over conventional reactors. Many fast reactions which are hitherto difficult to conduct in conventional reactors due to poor mass transfer will be much easier to perform in microreactors. Losey et al., 2001 used micro-fabricated packed bed reactors for the hydrogenation of cyclohexene and obtained the mass transfer parameter in the range of 5 to 15 s^{-1}. The mass transfer parameter of 5 s^{-1}, which was used in previous simulations was changed to 10 s^{-1} and the simulations repeated. The results are shown in Figures 5.6 – 5.8. When the mass transfer rate of hydrogen into the liquid becomes faster, the reduction of gas slug length along the reactor is faster, and so is the increase of liquid slug length. This also results in more consumption of o-nitroanisole, which implies that more substrate is converted to the product in the reactor. However, the hydrogen concerntration in the liquid phase is much higher compared to the previous result due to the faster rate at which it is replenished. This higher level of hydrogen concentration enables a higher reaction rate than in the previous model. Applying this model, the gas-liquid mass transfer parameter in the microreactor can be obtained by fitting the model results with the experimental data.

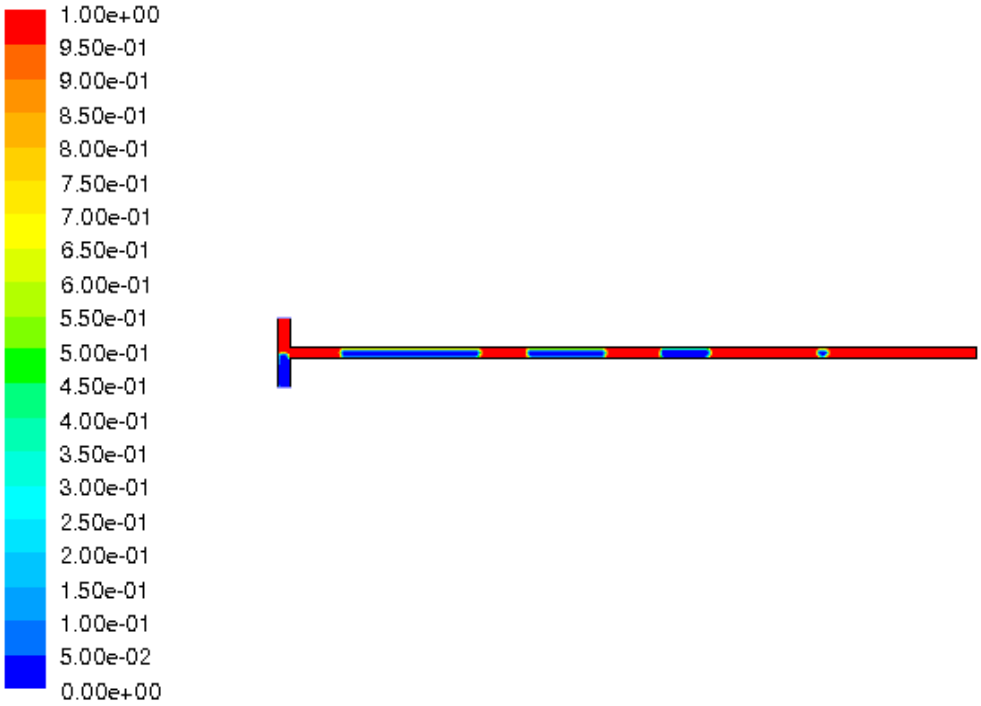

Figure 5.6: Gas (blue) and liquid (red) slugs inside the reactor

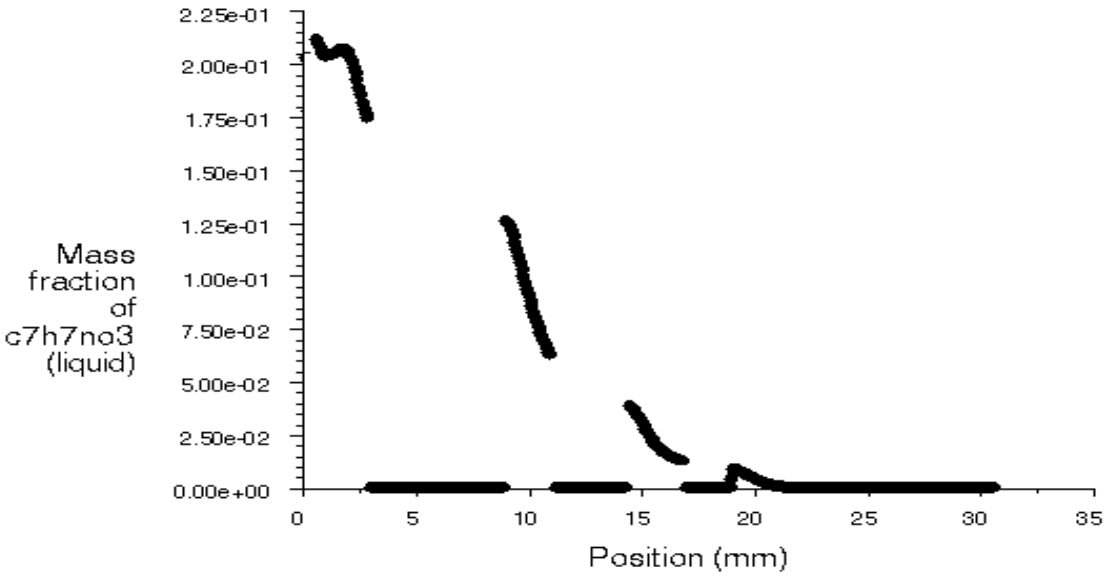

Figure 5.7: Mass fraction of o-nitroanisole (reactant) along the reactor length

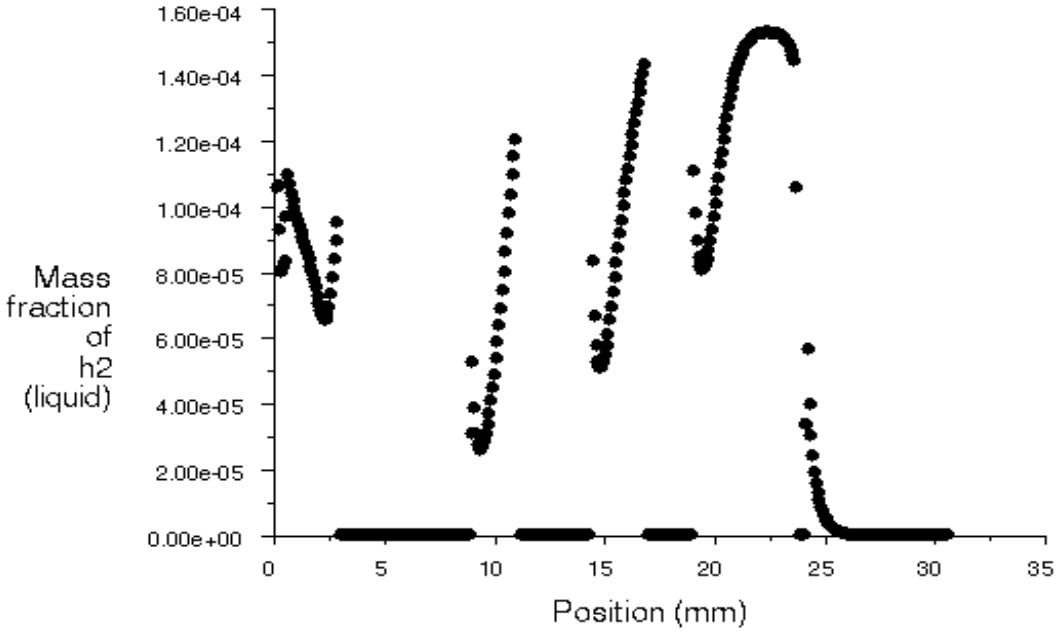

Figure 5.8: Mass fraction of hydrogen in the liquid phase (reactant) along the reactor length

The second hydrogenation reaction considered in this activity was that of the BMS proprietary molecule, a nitro ketone. The reaction pathway for this molecule was identified and the corresponding kinetics determined. Compared to the previous model reaction − hydrogenation of

o-nitroanisole to o-anisidine, this reaction had some distinct features: the concentration of the substrate was much smaller in the reaction solution because the substrate was solid; the reaction was much faster so a higher process flow rate was generally required to eliminate the mass transfer effect.

Similar to the simulation of the previous model reaction, the model we used for hydrogenation of BMS molecule is also multiphase reaction VOF model: hydrogen passes through gas-liquid inteface, dissolves into the liquid, and then reacts with the substrate. The chemical reaction only takes place in the liquid phase, and the gas is transferred into liquid by gas-liquid mass transfer process. In this simulation, the chemical kinetics used was that obtained in our lab, and the mass transfer parameter from gas to liquid was $10s^{-1}$.

Figure 5.9 shows the slug lengths inside the reactor; liquid slug is in red and gas slug is in blue. One observes that, as the reaction proceeds downstream of the reactor, the gas slug length is becoming shorter and shorter because of the consumption of hydrogen; at the same time, the liquid slug is getting longer because of the liquid product. Figure 5.10 presents the mass fraction of nitro compound along the reactor length which reduces with reactor length since it is being consumed by the reacton. Figure 5.11 is the mass fraction of hydrogen dissolved in liquid. The concentration of hydrogen in the liquid is very small because of its low solubility in the substrate. It's observed that there is a hydrogen concentration distribution inside the liquid slug because of the interplay between diffusion and reaction effects. At the interface on the liquid side, hydrogen concentration is higher than in the bulk liquid because there is a direct contact between the gas and liquid phase. Along the reactor length, average hydrogen concentration in the liquid increases, which indicates that the diffusion rate is faster than the reaction rate.

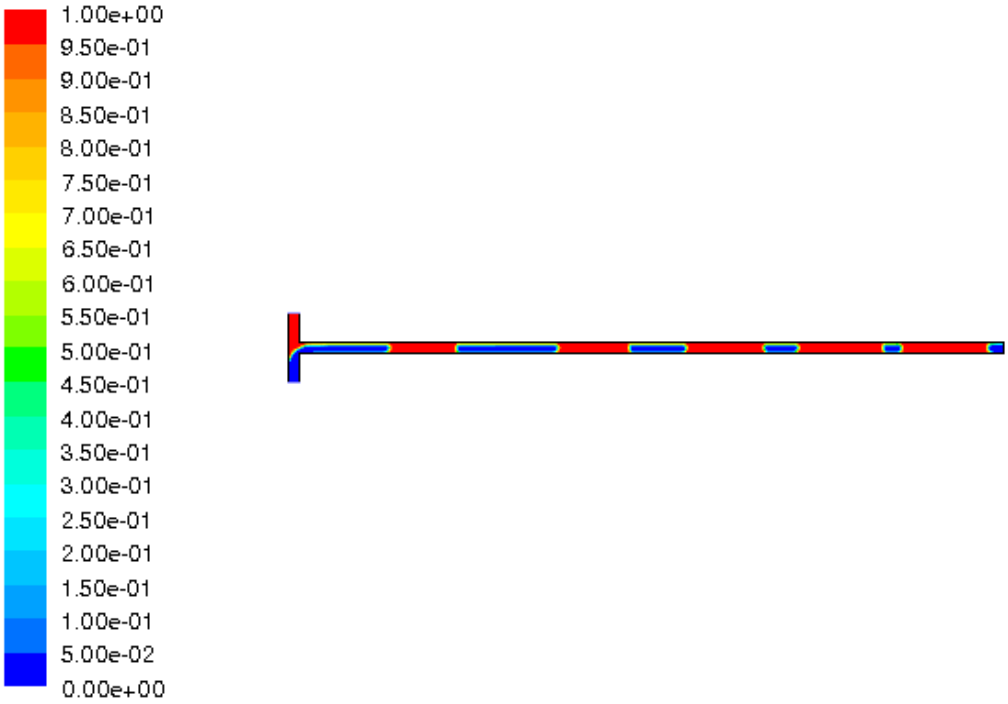

Figure 5.9: **Gas (blue) and liquid (red) slugs inside the reactor**

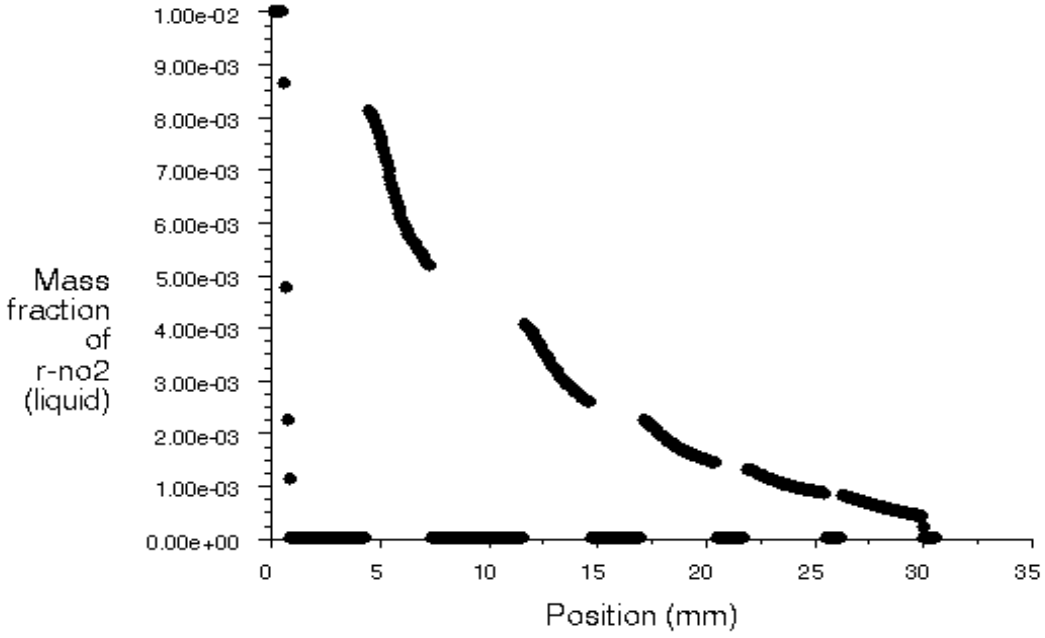

Figure 5.10: **Mass fraction of nitro compound (reactant) along the reactor length**

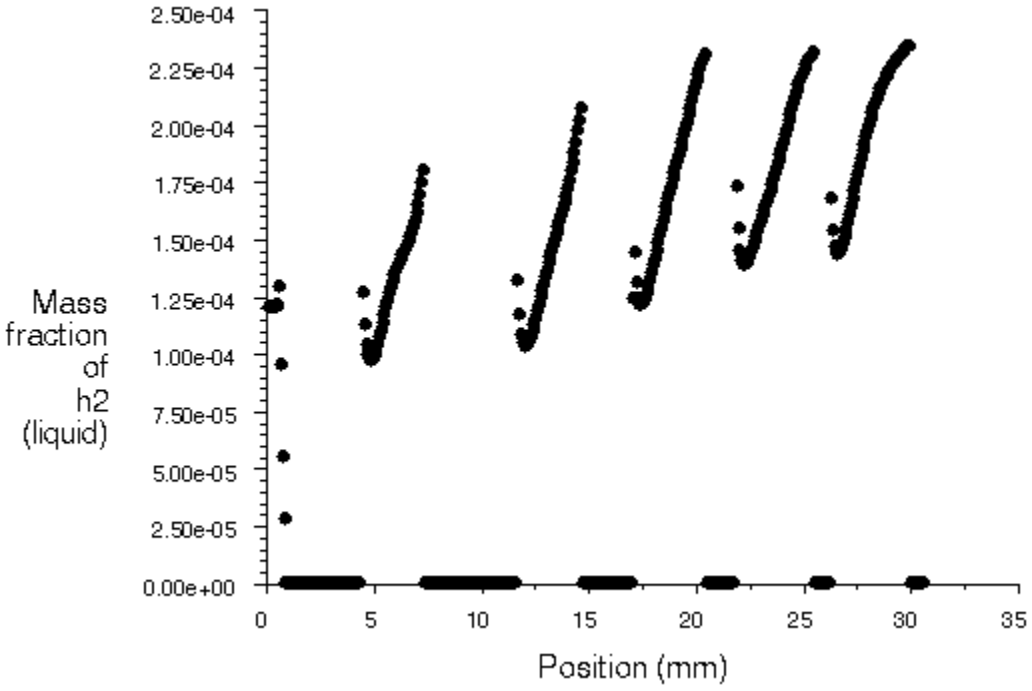

Figure 5.11: Mass fraction of hydrogen in the liquid phase (reactant) along the reactor length

TASK 6: Production Plant Design (ChemProcess Technologies, LLC)

EXECUTIVE SUMMARY

The total world annual capacity of cyclohexane is about 1,800 million gallons of which the U.S. capacity is about 600 million gallons. Chevron Phillips is the world's largest producer and marketer of cyclohexane with a total worldwide annual supply capacity of about 300 million gallons. Cyclohexane is generally used as an intermediate chemical where about 54 percent of its production is used in the production of adipic acid for nylon-6/6, 39 percent for caprolactam for nylon-6, and 7 percent for miscellaneous including solvents, insecticides and plasticizers. The demand for nylon (and hence cyclohexane) in engineering thermoplastics in resins and films is growing at about 6% annually.

The production of cyclohexane from hydrogenation of benzene and hydrogen is a highly exothermic reaction where the reactor temperature control is very critical. Consequently, in most conventional commercial cyclohexane processes, multi-stage reactors involving recycling of cyclohexane, inter-reactor cooling to allow efficient removal of the heat of hydrogenation, and staged addition of the benzene feed are employed. In our design, we have taken advantage of the efficient and rapid heat removal characteristics of microreactor system which are more than two orders of magnitude better than conventional reactors, to provide for a compact microreactor that achieved efficient heat removal and safe process where the reactor temperature is well controlled. The main reactor is a 200-micro-channel reactor, each with dimension (500 micron x 500 micron x 6 in). The reactor will operate at a combined space-time yield of 500g cyclohexane/g cat.h and produce 10kg/h of cyclohexane with 99 wt% purity. Our design also achieved minimal benzene, methylcyclopentane and other impurities (by-products) in the product thus making less impact on the environment compared with the conventional process.

The production cost of hydrogenation of benzene to cyclohexane using microreactor technology has been estimated to be 50.5 cents/lb of cyclohexane. The costs are based on 10 kg/hr (0.18 million lbs/yr) of cyclohexane at 8,000 on stream hours per year, and $200,000.00 fixed capital cost. The hydrogen and benzene raw materials account for about 96% of the production costs. One of the key advantages of this production scale using microreactor technology is the process intensification that makes it possible to have modular units at considerably low fixed capital and provides for a very efficient heat transfer scheme.

The work accomplished in this Task 6 of the DOE project, "**Microchannel Reactor System for Catalytic Hydrogenation**" gives some generalization of the best practice for potential companies that may be interested in the application of the outcome of our development of the microreactor to the production of cyclohexane with application to other similar commodity chemicals as an economical and safer route than the conventional technology.

1. INTRODUCTION

In view of the importance of the technical and economic feasibility of the proposed catalytic hydrogenation concept in this project, a conceptual plant design of catalytic hydrogenation of benzene to cyclohexane on a basis of 10 kg/hr of cyclohexane product as a test case of relevance of the microreactor technology to the chemical industry as Task 6 was carried out. The goal of this Task 6 is to carry out production scale plant design including process creation, synthesis and integration, equipment sizing and cost estimation, profitability analysis and optimization, and overall energy requirements. Environmental issues and safety concerns were emphasized in the plant design. The results of the design will in our view serve as a bench mark for the plant design and commercialization of the microchannel reactor-based process intensification technology across the chemical and pharmaceutical industries.

Both patents and technical literature on conventional production of cyclohexane from hydrogenation of benzene have been reviewed. The available processes are very similar but influenced by the choice of catalysts to ensure high degree of hydrogenation activity to meet product specifications. The major by-products of hydrogenation of benzene to cyclohexane are n-hexane, methyl-cyclopentane, methyl-cyclohexane, methyl-pentane, n-pentane, and methane. The control of the reactor's temperature and maintaining it at a certain level minimizes the by-products formation. One of the major problems encountered in the production of cyclohexane is the deactivation of the reactor's catalyst bed by the CO in the hydrogen source necessitating a pre-treatment reactor unit (methanator) that converts the CO to methane and water before the hydrogen is fed into the main reactor. We have adopted in this project, the recent concept of a compact reactor design (US patent Application # 0030114723) that uses a two-stage catalyst bed where at the first stage, the bed is packed with catalyst that converts CO to methane and water, and the second stage is packed with catalyst that minimizes the formation of the by-products and gives efficient conversion of benzene to cyclohexane with minimum recycling of the hydrogen. A sensitivity analysis on the temperature control was carried out to investigate the best phase to carry out the reaction. The results are included in this report.

Although production of cyclohexane is mainly carried out in the vapor phase but there are claims in the open literature that the mixed-vapor (liquid and gas mixture) phase gives the best reactor temperature control. However, when the temperatures and pressures are carefully chosen with the right catalyst, a liquid phase reaction minimizes by-products and gives a good reactor temperature control.

2. MARKET PRODUCTION AND IMPACT OF CYCLOHEXANE

Chevron Phillips is the world's largest producer and marketer of cyclohexane with a total worldwide annual supply capacity of about 300 million gallons. Its most recent plant is located in Al Jubail in Saudi Arabia with 20 million gallons annual capacity. UOP, an important player in the cyclohexane production technology, has patents in innovative reactor designs for cyclohexane production.

We have reviewed the worldwide production and marketing of cyclohexane to estimate its energy impact. Cyclohexane is generally used as intermediate chemical where about 54 percent of its production is used in the production of adipic acid for nylon-6/6, 39 percent for caprolactam for nylon-6, and 7 percent for miscellaneous including solvents, insecticides and plasticizers. The demand for nylon (and hence cyclohexane) in engineering thermoplastics in resins and films is growing at about 6% annually. Engineering thermoplastics are noted for their outstanding properties of high tensile strength, excellent abrasion, and chemical resistance and

heat resistant. They have particular and growing demand in performing mechanical duties that traditionally relied on metal parts. The total world annual capacity of cyclohexane is about 1,800 million gallons of which the U.S. capacity is about 600 million gallons with the U.S. annual production of Chevron-Phillips of 205 million gallons as shown in the below table 2.1. Cyclohexane growth rate is estimated to average about 2 percent annually. The demand for cyclohexane in Japan has decreased due to a new production route to adipic acid via cyclohexene rather than cyclohexane.

Table 2.1: U.S. Production of Cyclohexane

Company and Plant Location	Annual Capacity	
	Thousand Metric Tons	Millions of Gallons
Chevron Phillips, Port Arthur, TX	148	50
Chevron Phillips, Borger, TX	118	40
Chevron Phillips, Guayama, PR	399	135
Chevron Phillips, Sweeny, TX	340	115
CITGO, Corpus Christi, TX	118	40
ExxonMobil, Beaumont, TX	192	65
Huntsman, Port Arthur, TX	266	90
Koch, Corpus Christi, TX	74	25
Sun Refining, Marcus Hook, PA	104	35
Total	1760	595

In view of the fact that the demand for cyclohexane in Japan has decreased due to a new production route to adipic acid via cyclohexene rather than cyclohexane, we have investigated the impact of other new routes to adipic acid which do not use cyclohexane to assess their impact on the worldwide demand for cyclohexane especially in the U.S. The use of cyclohexene route to adipic acid is currently limited to Japan with low production capacity. About 54 percent of cyclohexane produced worldwide is generally used in the production of adipic acid for nylon-6/6. Other than cyclohexene route to adipic acid, the other routes to adipic acid are cylohexanone, and cyclohexanol (US patent 2,316,543; US patent 4,649,217; US patent 6,521,789 B1; and US patent 6,822,117 B1) that are considered to be more environmental-friendly than the direct route using cyclohexane. Since cyclohexanone and cyclohexanol are

derivatives of cyclohexane and also the use of cyclohexene is limited to Japan, to that extent, in our opinion, those alternative routes to adipic acid do not significantly impact the demand for cyclohexane worldwide. We have concluded our investigation of an alternative route to adipic acid via cyclohexene rather than cyclohexane. The impact is very minimal on the world demand for cyclohexane. Thus, our developed microreactor technology concept on industrial scale production of cyclohexane remains very attractive as it provides an economical and safer route than the conventional technology used by Chevron Phillips and other producers of cyclohexane.

3. PRELIMINARY DESIGN OF CONVENTIONAL PRODUCTION OF CYCLOHEXANE

A preliminary design of the reactor for the production of 10 kg/hr of cyclohexane from hydrogenation of benzene has been carried out. The design of the reactor is the key to the production of cyclohexane where the temperature control of this highly exothermic reaction is an important determinant in the reactor configuration. We have done extensive literature search on many of the industrial processes and find out that most of the processes for production of cyclohexane were carried out in the vapor phase. Table 3.1, reveals the reactor operating conditions for different phases (liquid, liquid + vapor, and vapor). Our results are consistent with the studies reported by John McKetta and William Cunningham, Vol. 14 of Encyclopedia of Chemical Processing and Design. Although most industrial processes for the production of cyclohexane are carried out in the vapor phase, McKetta and Cunningham discussed that a mixed phase (liquid + vapor) has the advantage of considerable flexibility. In addition to this flexibility, a more relevant application of the reactor design to the overall goal of this DOE project especially Task 2 where nitro-anisole (liquid) in a given solvent (methanol) is hydrogenated presents a situation involving mixed phase. In view of these facts we have chosen to design the reactor for a mixed phase.

The operating conditions (temperature of about 200°C, and pressure of about 40 atms) that we have selected for the mixed phase reactor design are very similar to the IFP (US patent 3,202,723, August 24, 1965 assigned to Institut Francais du Petrole, "Process for the Catalytic Hydrogenation of Aromatic Hydrocarbons"). At these operating conditions, the principal side reaction of isomerization of cyclohexane to methyl cyclopentane is minimized. The mixed phase presents a great challenge for the reactor design that we have modeled into separate liquid and vapor phases and applied different kinetics equations to each phases. From our extensive literature search, we have found the work of Konyukhov, et al., "Kinetics of Liquid-Phase Hydrogenation of Benzene on Palladium Catalyst and Hydrogenation of Toluene on Palladium and Catalysts" (Kinetika, Vol. 28, No 2, pp. 360-365, 1987) to be one of the best referenced liquid phase kinetics studies of hydrogenation of benzene to cyclohexane. We have also found the work of Kehoe and Butt, "Kinetics of Benzene Hydrogenation by Supported Nickel at Low Temperature" (Journal of Applied Chem. Biotechnol. 1972, 22, 23-30) as the most relevant vapor phase kinetics studies of hydrogenation of benzene to cyclohexane. The work of Konyukhov, et al., and the work of Kehoe & Butt have reconciled the many variations of the literature kinetics results in the liquid and vapor phases respectively. In particular, Kehoe and Butt have shown that for a commercial nickel on kieselguhr, Harshaw Ni-0104 P, supplied as a powder and containing 58% wt Ni, the following kinetic equation derived from the experimental results is applicable:

$$\text{Rate} = \{vKP_BP_{H2} \exp[(-Q-E)/RT]\}/\{1 + KP_B\exp(-Q/RT)\}$$

Where v = 0.1774 mol/g catalyst s Torr

K = 0.000008905 $Torr^{-1}$ (or 8.905 $X10^{-6}$ $Torr^{-1}$)

Q = -8.26 kcal/mol (Heat of adsorption)

E = 12.29 kcal/mol (activation energy)

P_B = Partial Pressure Benzene, Torr

P_{H2} = Partial Pressure Hydrogen, Torr

T = Temperature, deg K

R = 1.987 cal/gmol K (gas constant)

Torr = (101.325/760) kN/m^2

The combined kinetics results from work of Konyukhov et. al (liquid phase) and Kehoe/Butt (vapor phase) were used for the preliminary reactor design.

A modified generic reactor model (ASPEN's RSTOIC reactor model) of feed benzene has been developed. Typically, hydrogen and benzene are fed into the reactor maintained at 392 ^oF and 315 psia where the main reaction of $C_6H_6 + 3H_2 = C_6H_{12}$ takes place. The effluent from the reactor is flashed to separate the liquid product. The low boiling point by-products such as methane and unreacted H_2 are recycled into the reactor. A split fraction of the liquid product is also recycled into the reactor and the rest is further flashed to have a high purity (more than 99.7 %) cyclohexane product. The major by-products of hydrogenation of benzene to cyclohexane are n-hexane, methyl-cyclopentane, methyl-cyclohexane, methyl-pentane, n-pentane, and methane. The control of the reactor's temperature and maintaining it at a certain level minimizes the by-products formation. One of the major problems encountered in the production of cyclohexane is the deactivation of the reactor's catalyst bed by the CO in the hydrogen. In this model we have included a pre-treatment reactor unit (methanator) that converts the CO to methane and water before the hydrogen is fed into the main reactor.

We have also carried out sensitivity analysis on the operation of the reactor for different phases. Our results (see Table 3.1) show that the molar ratio of hydrogen to benzene (HBR) fed into the reactor is the key determining factor for the reactor's operating phase. In particular, if HBR > 3.5, the reactor will only operate in the gas phase irrespective of the reactor's operating pressure. The reactor temperature is effectively controlled by the amount of liquid recycled to the reactor.

Table 3.1 Reactor Operating Conditions

Temperature (F)	**Pressure (Psia)**	**H_2/C_6H_6 (HBR)**	**Reactor Phase**
350 – 500	250 – 500	≥3.5	Vapor
350 – 500	350 – 500	3.05 – 3.5	Vapor + Liquid
350 – 400	≥2500	3.05 – 3.2	Liquid

Figure 3.1. Impact of Liquid Recycle on Reactor Heat & Reactor Liquid

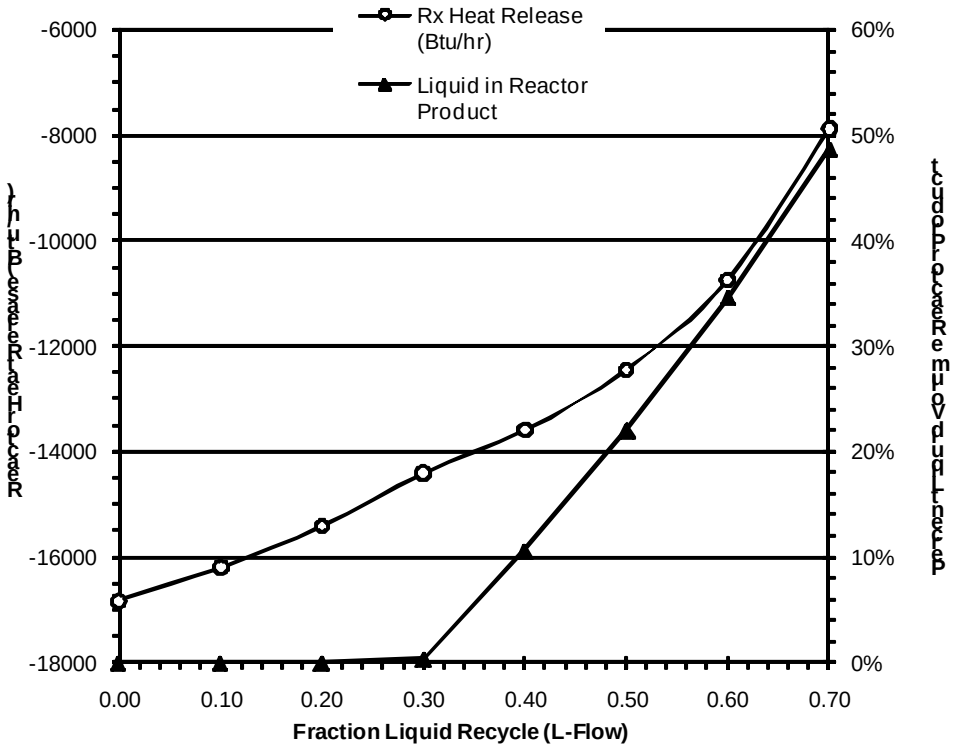

Figure 3.2. Impact of Purge on Inerts in Reactor Feed

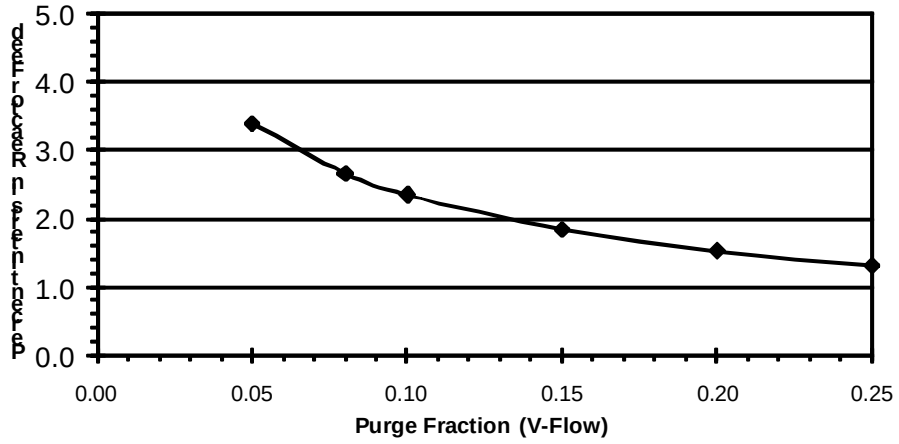

Figure 3.3. Reactor Liquid vs Reactor Pressure & H2/Benzene Ratio (HBR)

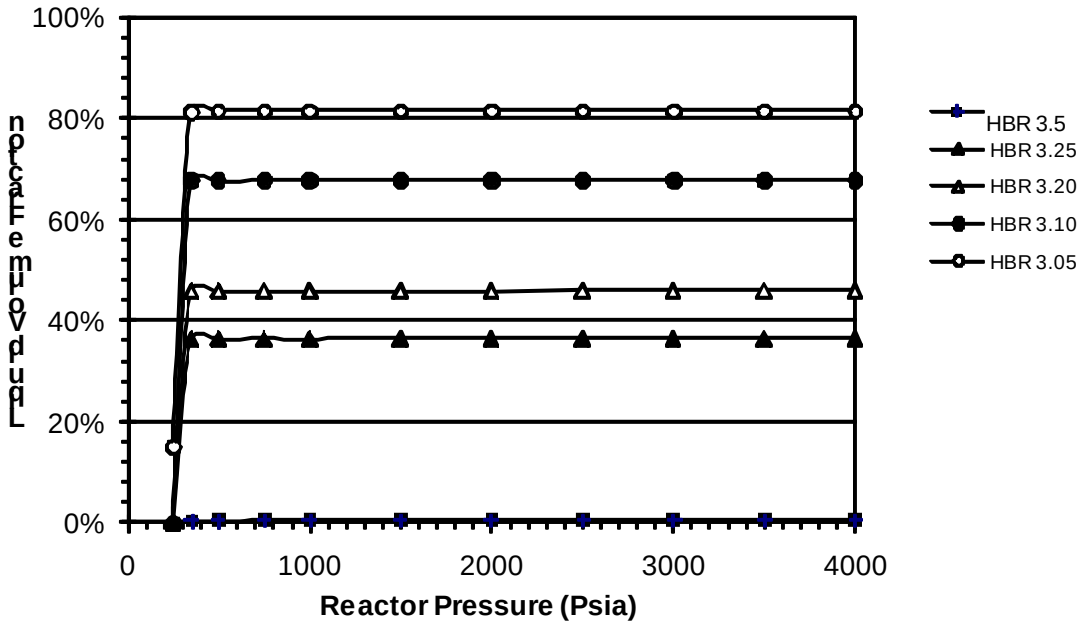

Figure 4. Reactor Heat vs Pressure & H2/Benzene Ratio (HBR)

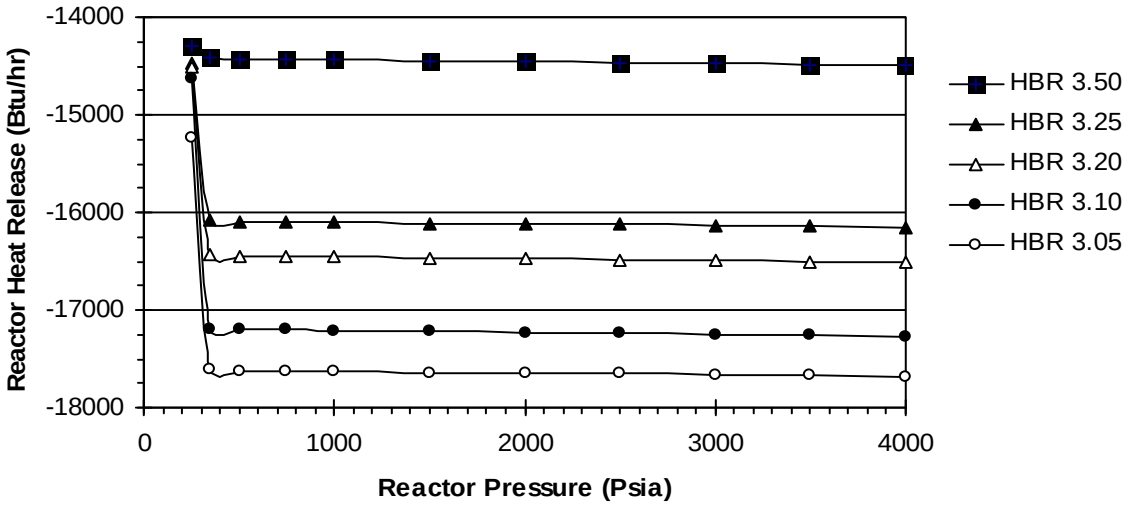

Figure 3.5: Updated ASPEN Simulation Flowsheet of Hydrogenation of Benzene to Cyclohexane
Basis: 10kg/hr Production

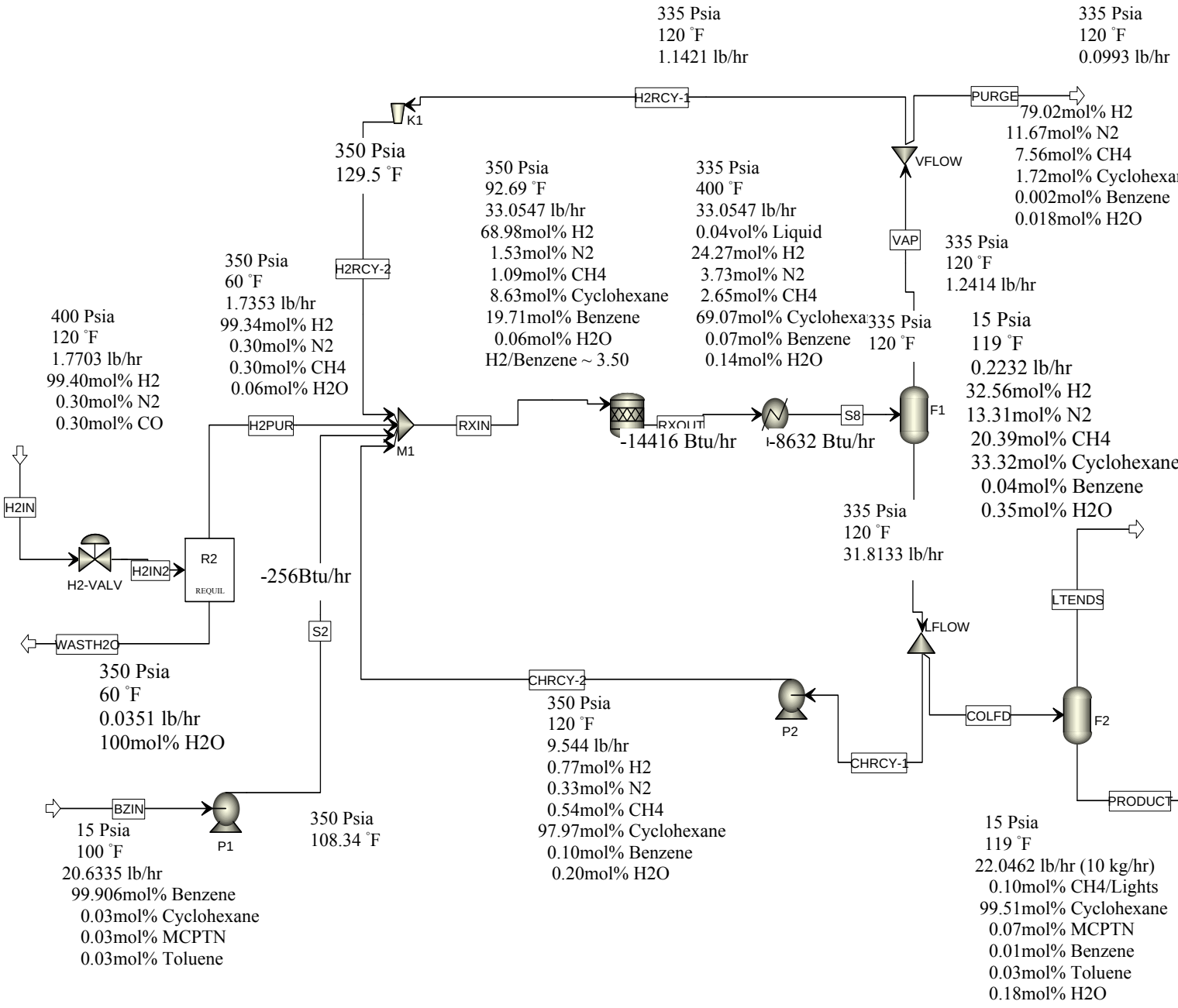

We have carried out detailed analysis of the reactor space-time yield. The result shown in Figure 3.6 will be used to design the microreactor for the 10 kg/hr cyclohexane product. A commercial nickel catalyst such as the kieselguhr, Harshaw Ni-0104 P, supplied as a powder and containing 58% wt Ni will be used. From our result and available literature, on how the space-time yield is affected by the reactor operating conditions, we have determined that our optimum operating conditions are 35 atm. and 400^{o}F. At this condition, the space time yield is 1200 g of cyclohexane/g catalyst/hr, and the benzene conversion is about 38% per pass.

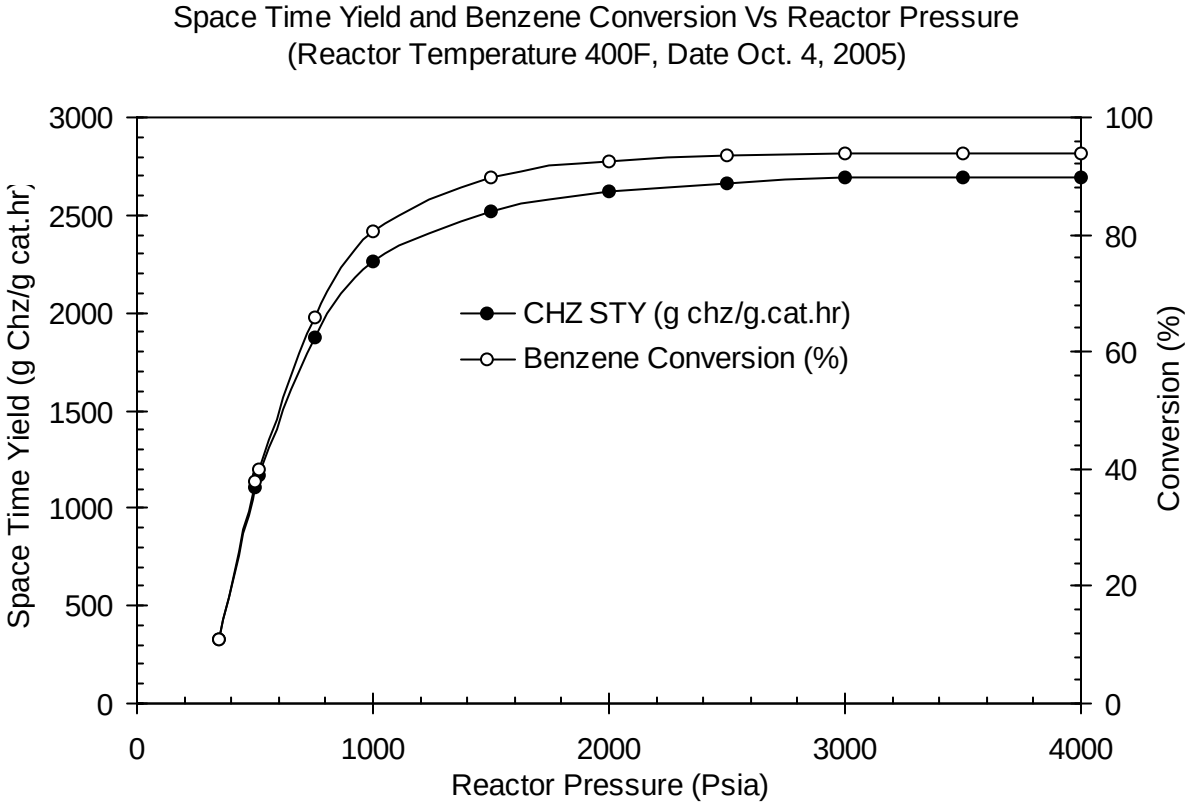

Figure 3.6: Sensitivity Analysis of the Reactor Space Time Yield

4. PROCESS OPTIMIZATION FOR THE DESIGN OF PRODUCTION OF CYCLOHEXANE

The proper design of the miroreactor is the key to Task 6. We made a determination, therefore, to take a more critical review of our analysis of the space-time yield and expand the analysis to include other factors to ensure that we have investigated all the feasible parameters for the success of the design of the microreactor. From this analysis, we concluded that for optimum performance, the reactor will be operated at 35 atm pressure and 400 deg F with the space time yield of ~ 1949 g cyclohexane/g cat.hr, space velocity ~ 0.80 g feed/g cat.s, and HBR (Hydrogen to Benzene Ratio) approximately 3.5. These parameters will be used to design the reactor and detailed cost analysis of the major components of the plant design for the production

of 10 kg/hr cyclohexane will be carried out. The following gives the summary of the space-time yield analysis that we carried out.

Figure 1 shows the impact of pressure on space-time yield of cyclohexane and the conversion of benzene for reactor for gas phase operation. As expected, the space-time yield and benzene conversion increase with pressure because reaction rate is directly influenced by reactor pressure as implied by equation 1. It is important to note that the results in Figure 1 were generated for the reactor condition: molar ratio feed hydrogen to benzene (HBR) ~ 3.5, temperature ~ 400^{o}F, catalyst weight ~ 5.25g (catalyst density ~ 2.1g/cc Kieselguhr support) and product ~ 10kg/hr cyclohexane.

At these conditions the space velocity of the reactor is 0.80g feed/g cat.s on average. Also at 35atm (or 514.4 Psi) reactor pressure, the space-time yield for cyclohexane is 1949g/g cat.hr and conversion for benzene is 68.6% per pass.

Figure 1. Impact of Pressure on STY (CHZ) and Conversion (BZ)
Reactor Temp = 400F, HBR = 3.50, SV = 0.80 g/g cat.s

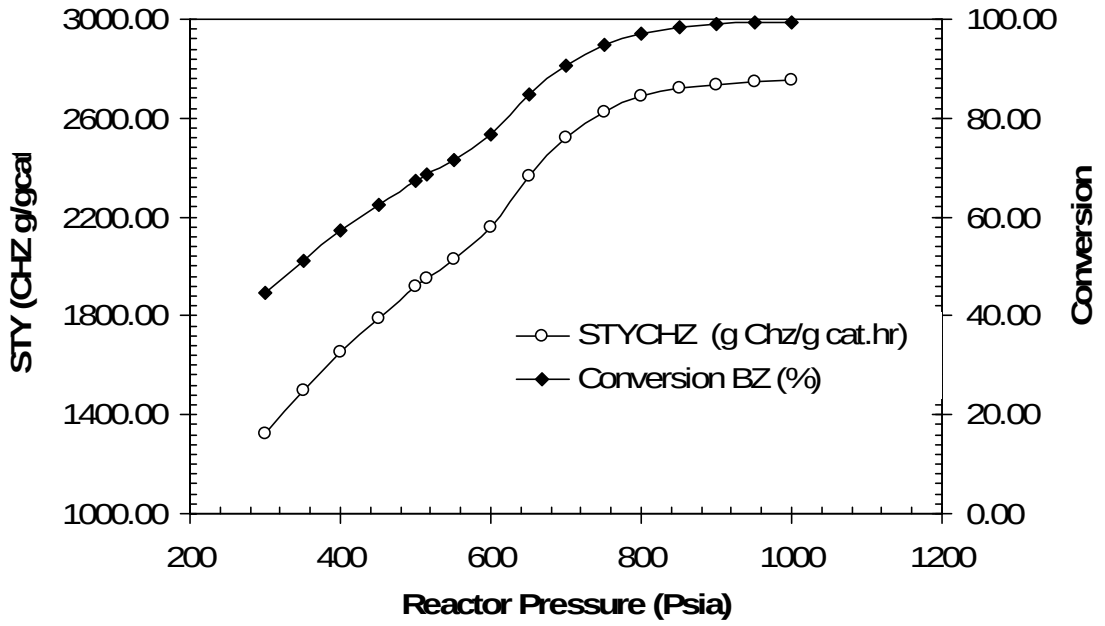

Figure 2 shows the impact of temperature on cyclohexane space-time yield and benzene conversion for the reactor. Again, both parameters increase with temperature as the reaction is exothermic with rate described by Arrhenius kinetics, which increases rapidly with temperature. For Figure 2 the reactor was maintained at 35 atm pressure and at Figure 1 conditions except temperature, which was varied.

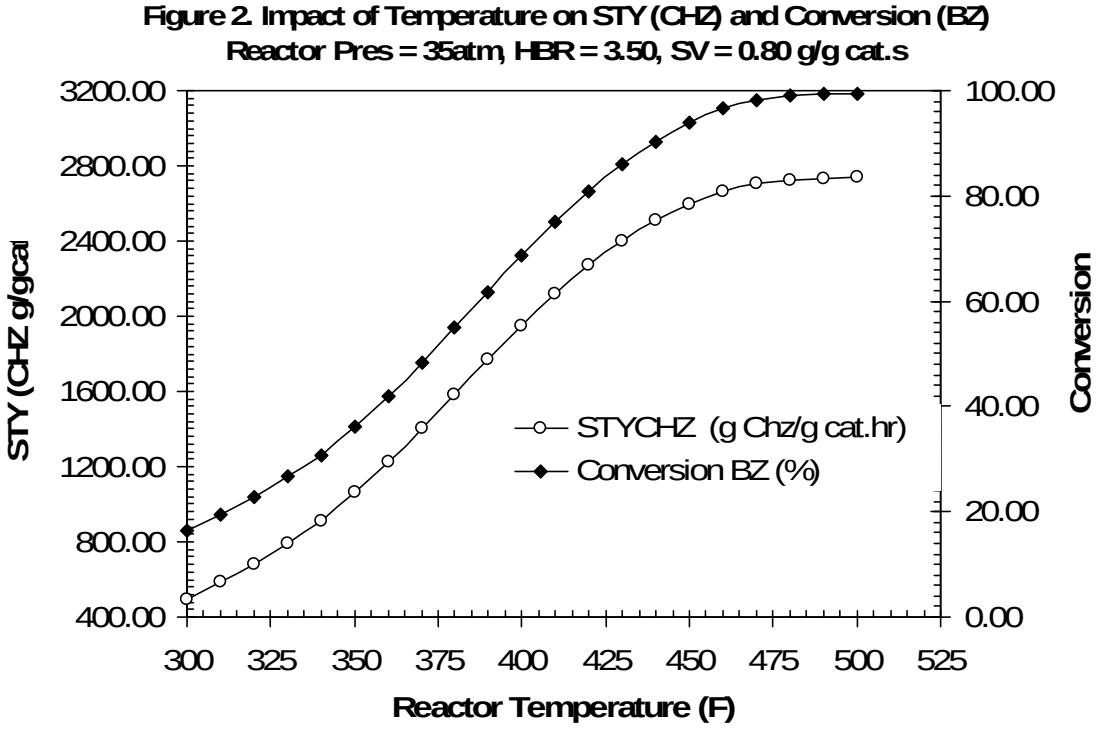

Figure 3 shows the effect of space velocity on the space-time yield of cyclohexane and benzene conversion. This figure was obtained by maintaining reactor temperature at 400 deg F, reactor pressure at 35 atm, and using 5.25g catalyst. The variation in space velocity was achieved by varying reactor feed rate to obtain 5kg/hr to 100kg/hr cyclohexane production targets.

Because catalyst weight or volume is fixed, increase in space velocity means a reduction in reactor residence time and consequently decline in benzene conversion as shown in Figure 3. Figure 3 also shows that the conversion will level off to about 8.4% at high space velocities (>8). As expected, the space-time yield of cyclohexane increases with space velocity, rapidly at low values, but gradually at high space velocities, leveling off at about 2560g/g cat.hr.

Figure 3. Impact of Space Velocity on STY (CHZ) and Conversion (BZ)
RxTemp = 400F, Reactor Pres = 35atm, HBR = 3.50

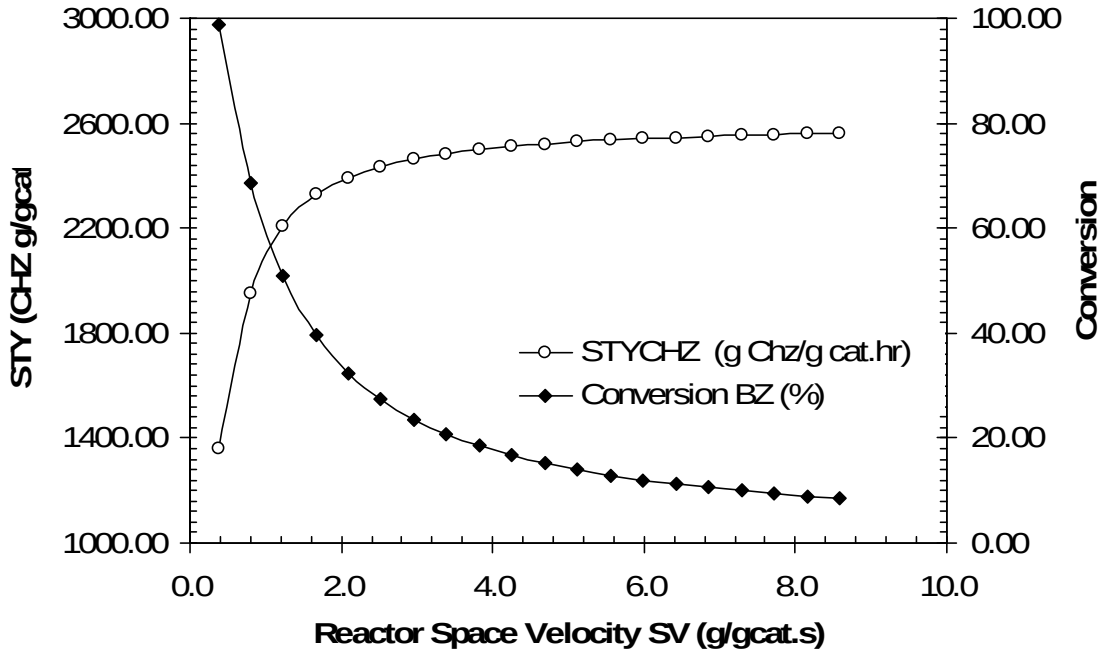

Finally, Figure 4 shows the effect of HBR on the space-time yield of cyclohexane and the conversion of benzene. It shows that benzene conversion will increase for high HBR values, since this will lead to high hydrogen partial pressure, resulting in high reaction rate from equation 1. Also, high reaction rate will lead to high values of cyclohexane space-time yield.

Figure 4. Impact of HBR on STY (CHZ) and Conversion (BZ)
RxTemp = 400F, Reactor Pres = 35atm, SV = 0.80g/gcat.s

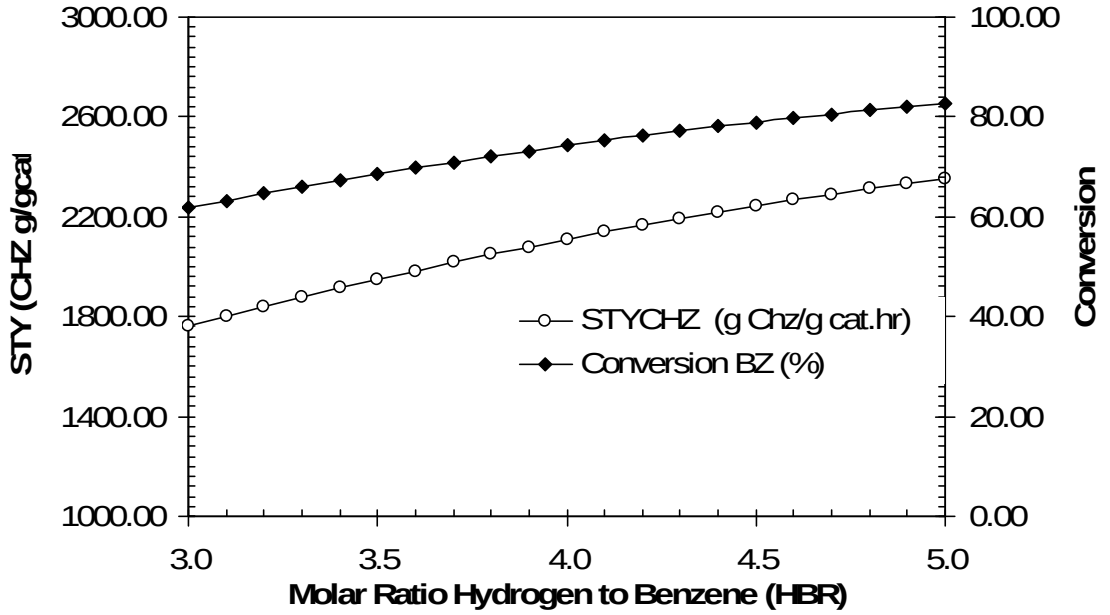

4.1 Re-EVALUATION OF OPTIMIZATIONAND SENSITIVITY ANALYSIS

We completed the re-evaluation of the impacts of sensitivity analysis and optimization previously carried out for the two separate reactors system for the compact two-stage single reactor system. The compact microreactor combines the hydrogenation of the benzene in the main microreactor and pre-treatment reactor unit (methanator) that converts the CO to methane and water before the hydrogen is fed into the main reactor. This compact system gives efficient conversion of benzene to cyclohexane with minimum recycling of the hydrogen. The goal is to make 10 kg/h product with high purity (99 wt %).

Since unreacted benzene is the main impurity of the product, the primary focus of this work is reducing benzene in the product and minimizing the energy requirement of the process. The distillation option for final product purification is avoided to obviate the need for high utilities consumption in the process inherent in this option which is primarily duties for heating and cooling for distillation. Therefore, instead of a distillation option, a flash vessel is used for final product purification and recovery. With this constraint, the recourse for increasing the purity of the product is by increasing the benzene conversion in the reactor in the process.

Two methods were explored in the study for increasing the benzene conversion in the process as follows: (1) Increasing reactor volume or reducing the space-time yield of the reactor, and (2) Increasing hydrogen to benzene ratio (HBR). The results are shown in Figures 1 and 2 and the simulation results are given in Figure 3.

4.2.1 Impact of Reactor Volume on product Purity

Without doubt, raising reactor volume increases the residence time of the reactor thus allowing more benzene to be converted in the reactor. The trend in Figure 1 confirms this fact, showing that a reactor with space-time yield of 600 g Cyclohexane (CHZ)/g cat.h or less is needed to achieve 99wt% or more product purity. Benzene conversion is also high for this reactor (>99%). It is worth noting that molar ratio of hydrogen to benzene (HBR) was held at 3.2 in this study, a recommended value in the literature for this process. The number of micro-reactor channels is also shown in figure 1. About 200 or more channels are needed to deliver 99 wt% product purity. Each channel is assumed to be of dimensions 500 micron x 500 micron x 6 in.

Figure 1. Impact of Space Time yield on Product Purity
Production~10kg/h Cyclohexane (CHZ), HBR~3.2

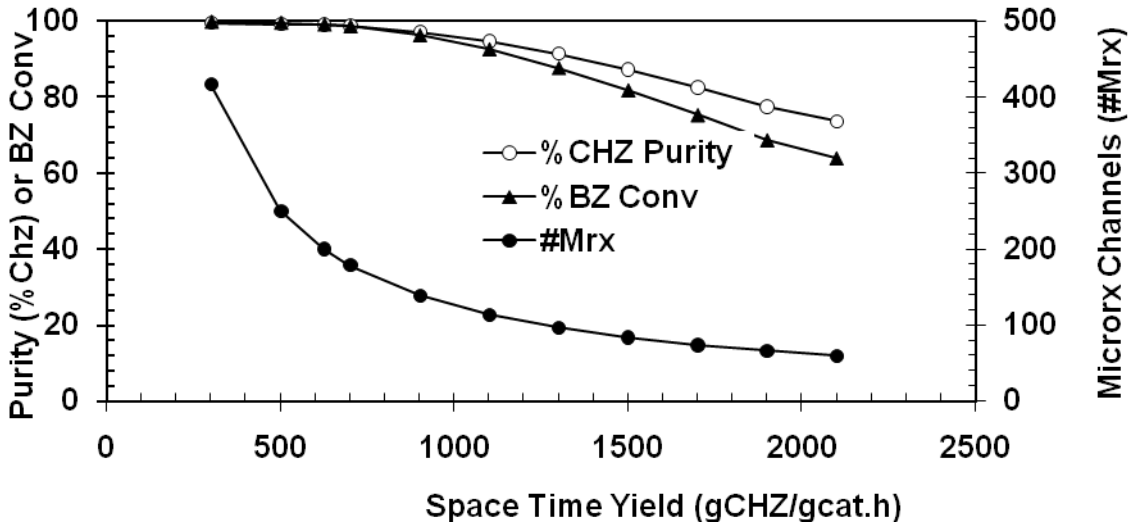

4.2.2 Impact of Hydrogen-Benzene Ratio on Product Purity

Figure 2 shows that for all space-time yield values, increasing the hydrogen-benzene ratio will result in higher product purity. As expected, a reactor with moderate to large volume (e.g. 500 - 800 g CHZ/g cat.h (STY) yields high purity product (>99wt %) with moderate amount of hydrogen (3.2- 4.0 HBR). Also, a reactor with small volume (1100-2100 g CHZ/g cat.h STY) will need moderate to large amount of hydrogen (>4.5 HBR) to attain the same product purity.

The only drawback of this option is the large amount of hydrogen needed for small reactors and the high compression cost that will be required for the hydrogen and circulating gases in the process. However in spite of the high compression cost for this option, this mode of operation could be desirable for all reactor capacities to maintain benzene conversion and product purity during inevitable catalyst deactivation.

Figure 2. Impact of HBR on Product Purity Production~10kg/h Cyclohexane (CHZ)

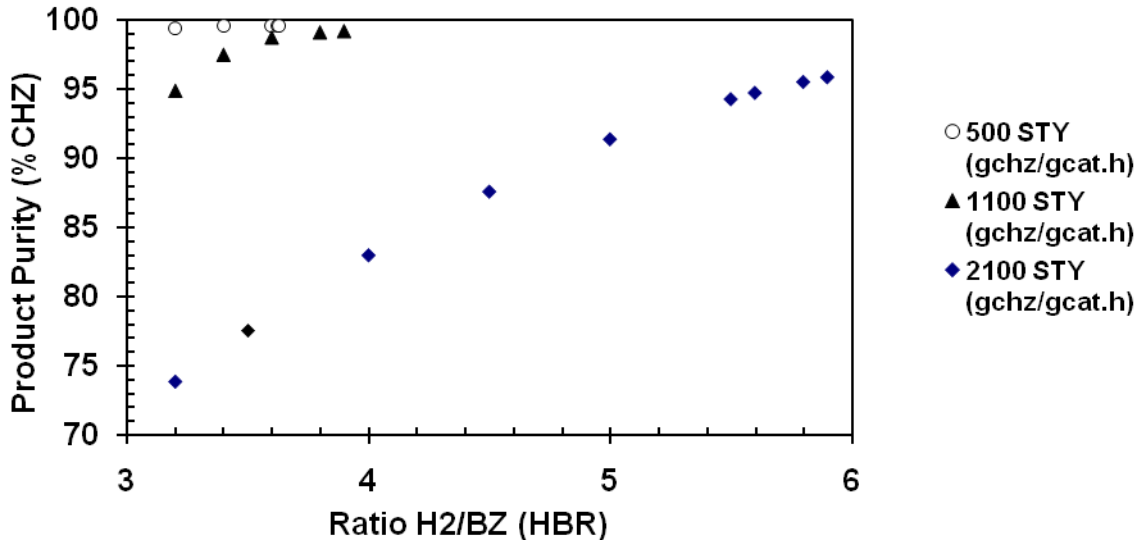

Based on the above analysis, we conclude that for the production of the cyclohexane:

1. The cyclohexane process should be designed for a 200-micro-channel reactor, each with dimension (500 micron x 500 micron x 6 in). The reactor will operate at a combined space-time yield of 500g cyclohexane/g cat.h and produce 10kg/h of cyclohexane with 99wt% purity.
2. The process should utilize a flash drum for final product purification, thus avoiding the use of distillation and its high utility consumption for product purification. The purity of the product would be 99wt% cyclohexane or higher.
3. The process should be operated around 3.2 molar ratio of hydrogen to benzene. This ratio could be raised during catalyst deactivation to enhance benzene conversion in the reactor and product purity in the process.

5.1 PRODUCTION COST ESTIMATE

We have considered compact microreactor that combines the hydrogenation of the benzene in the main microreactor and the pre-treatment reactor unit (methanator) that converts the CO to methane and water before the hydrogen is fed into the main reactor. This is similar to the recent concept of a compact reactor design (US patent Application # 0030114723) that uses a two-stage catalyst bed where at the first stage, the bed is packed with catalyst that converts CO to methane and water, and the second stage is packed with catalyst that minimizes the formation of the by-products and gives efficient conversion of benzene to cyclohexane with minimum recycling of the hydrogen.

Using the optimum reactor performance at 35 atm pressure and 400 deg F with the space- time yield of ~ 1949 g cyclohexane/g cat.hr, space velocity ~ 0.80 g feed/g cat.s, and HBR (Hydrogen to Benzene Ratio) ~ 3.5 (Figure 5.1), there is no significant change in the system flow but there is a tremendous advantage from cost point of view and operation of the system to have a compact microreactor system that will have a direct application to this project especially Task 2. Microreactor system being specialized, the traditional cost estimate tools are not directly applicable. We have carried out some preliminary cost estimates for the plant design for the production of 10 kg/hr of cyclohexane considered in this project using traditional cost estimate tools.

We have completed the detailed design of the 12 major equipment units for the production of 10 kg/hr of cyclohexane as shown in Table 5.1. A unique design for this plant is the compact microreactor that combines the hydrogenation of the benzene in the main microreactor and the pre-treatment reactor unit (methanator) that converts the CO to methane and water before the hydrogen is fed into the main reactor. This is similar to the recent concept of a compact reactor design (US patent Application # 0030114723) that uses a two-stage catalyst bed where at the first stage, the bed is packed with catalyst that converts CO to methane and water, and the second stage is packed with catalyst that minimizes the formation of the by-products and gives efficient conversion of benzene to cyclohexane with minimum recycling of the hydrogen. We consulted with Bayer Corporate and Business Services (BCBS) LLC, Baytown, TX to give us reasonable cost estimates for the installation of the plant per the design in Table 5.1. BCBS is a division of Bayer Corporation that specializes in microreactor technology services. The results of the installed cost from BCBS are as provided below.

TABLE 5.1: SUMMARY OF THE MAJOR EQUIPMENT UNITS

UNIT	DESCRIPTION
MR	Combined Microreactor, 6 mL reactor, rated 500 deg F, 1000 psia with 150 microchannels, each channel with dimension 0.5 cm by 0.5 cm by 6 inches.
H1 & CWP	Heat Exchanger, H1 Surface Area 0.5 sq ft, heat duty 9000 Btu/hr with 2 gpm (10 lpm) cooling water pump, CWP
F1	0.5 liter pressure vessel at 300 psia, 200 deg F
F2	Product receiver/storage tank, 100 gallons 50 psia, 200 deg F rated vessel with an inlet pressure valve reducer and a top vent.
PP	The product pump, a 1 gpm centrifugal type pump.
T-Bz	Benzene storage tank, T-Bz is a 100 gallons atmospheric tank.
P1	Benzene feed pump, a 200 mL/min positive displacement type pump at 0.1 HP
P2	Cyclohexane recycle pump, a 100 ml/min positive displacement

	type pump at 0.1 HP.
K1	H2 Recycle compressor for a 3 scfm (or 60 slpm), 0.5 HP rating, 1000 psia.
M1	Gas liquid mixer, a 200 SLPM, rated at 1000 psia, 300 deg F.
VFLOW	Gas splitter, a 100 SLPM rated 500 psia, 200 deg F with 0 to 20% split capacity.
LFLOW	Liquid splitter, 1 LPM unit rated 500 psia, 200 deg F with a 0 to 50% split capacity.

Note: All materials of construction are 316 SSL/compatible

Figure 5.1: ASPEN Flowsheet for the Modified Production of Cyclohexane

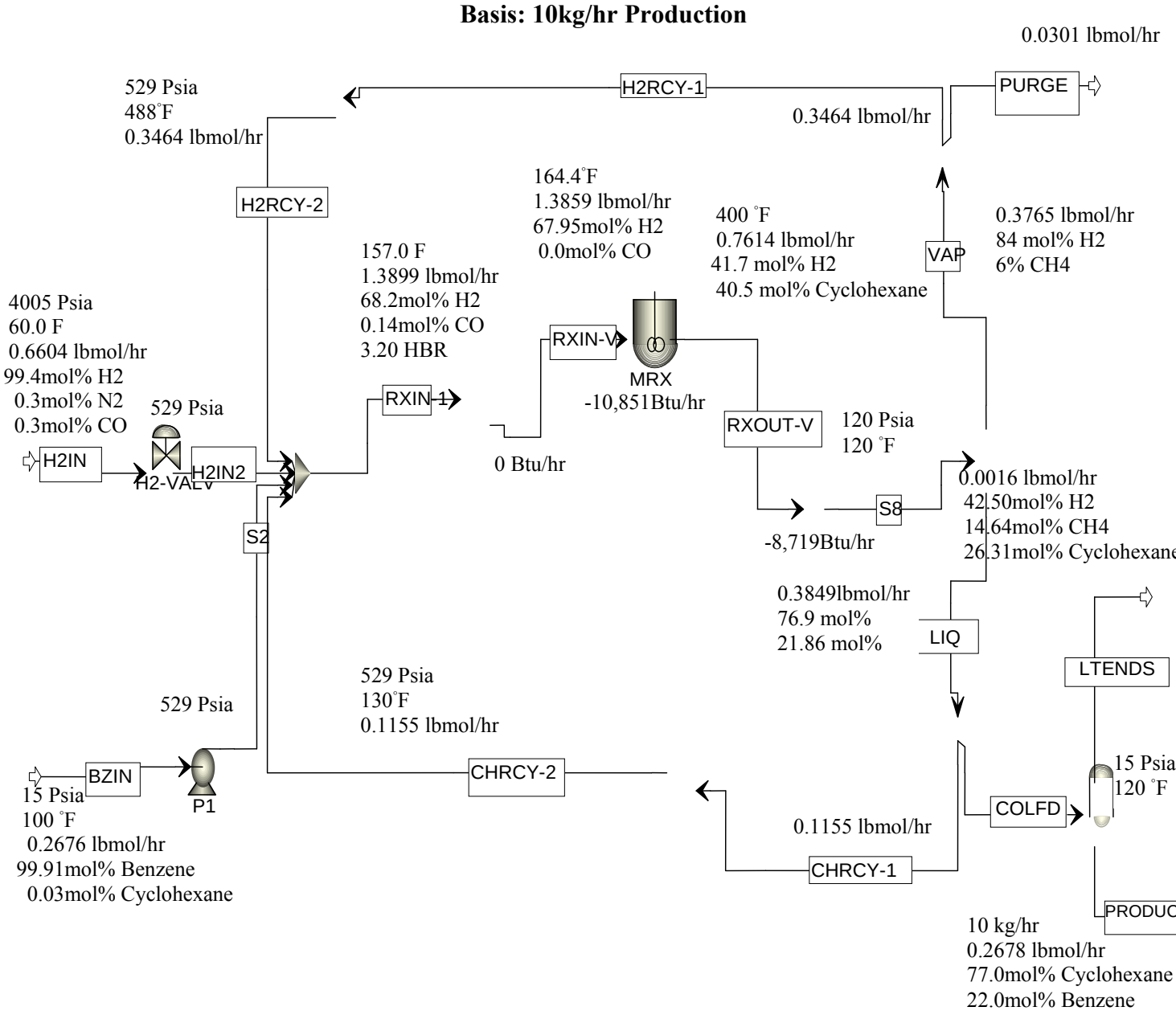

In consultation with Bayer Corporate and Business Services (BCBS) LLC, Baytown, TX we have obtained the cost estimate for 12 major equipment units for the production of 10 kg/hr of cyclohexane. We have complemented the cost estimates from BCBS with other resources to estimate the cost of the major equipments as detailed in Table 5.2. The total costs of the major equipment have been estimated to be $100,000.00. The cost of some of the equipment suffered from economics of scale in that for example the cost of a pressure rated vessel of 100 gallons is almost the same as the cost of a 500 gallons pressure rated vessel. However, the total installed cost of this mini-pilot plant is estimated to be $200,000.00 which is about twice the cost of the major equipment because the equipment is envisaged to be installed as modular units unlike

conventional large scale plant that installed cost can be as high as five times the cost of the major equipment.

TABLE 5.2: SUMMARY OF THE COST OF THE MAJOR EQUIPMENT UNITS (2006)

UNIT	DESCRIPTION	COST
MR	Combined Microreactor, 6 mL reactor, rated 500 deg F, 1000 psia with 150 microchannels, each channel with dimension 0.5 cm by 0.5 cm by 6 inches.	$20,000
H1 & CWP	Heat Exchanger, H1 Surface Area 0.5 sq ft, heat duty 9000 Btu/hr with 2 gpm (10 lpm) cooling water pump, CWP	$9,500
F1	0.5 liter pressure vessel at 300 psia, 200 deg F	$800
F2	Product receiver/storage tank, 100 gallons 50 psia, 200	$1,300
PP	The product pump, a 1 gpm centrifugal type pump	$1,500
T-BZ	Benzene storage tank, T-BZ is a 100 gallons atmospheric tank.	$700
P1	Benzene feed pump, a 200 mL/min positive displacement type pump at 0.1 HP	$3,500
P2	Cyclohexane recycle pump, a 100 ml/min positive displacement type pump at 0.1 HP.	$3,500
K1	H2 Recycle compressor for a 3 scfm (or 60 slpm), 0.5 HP rating, 1000 psia.	$19,500
K2	H2 Feed compressor for a 6 scfm (or 120 slpm), 1.0 HP rating, 1000 psia.	$22,000

M1	Gas liquid mixer, a 200 SLPM, rated at 1000 psia, 300 deg F.	$6,500
OW	Gas splitter, a 100 SLPM rated 5 psia, 200 deg F with 0 to 20% sp capacity.	$370
LFLOW	Liquid splitter, 1 LPM unit rated 500 psia, 200 deg F with a 0 to 50% split capacity.	$350
MISC. **	Pressure Transducers, Mass Flow Meters, sensors, etc.	$10,000
Total		$99,520

**: Continuation of Table 5.2

The production costs of hydrogenation of benzene to cyclohexane has been estimated to be 50.5 cents/lb of cyclohexane as shown in the below table. The costs are based on 10 kg/hr (0.18 million lb./yr) of cyclohexane at 8,000 on stream hours per year, and $200,000.00 fixed capital cost. With this relatively low production capacity, the by-product credits for steam and fuel gas are not applicable and we have assumed that the mini-plant will share operator with other operating units within the plant facility. The hydrogen and benzene raw materials account for about 96% of the production costs. One of the key advantages of this production scale using microreactor technology is the process intensification that makes it possible to have modular units at considerably low fixed capital and provides for a very efficient heat transfer scheme. A cost comparison of this unit on both a stand-alone facility and extrapolated to a mega capacity with conventional production at a larger scale of about 2 to 250 million lb/year has been investigated.

TABLE 5.3 PRODUCTION COSTS FOR BENZENE HYDROGENATION TO CYCLOHEXANE

Capacity: 10kg/hr (0.18 million lb/yr) Cyclohexane at 8,000 hr/yr On-stream

	UNIT OF USAGE	UNIT OF PRICE	PRICE	USAGE	Cost, c/lb
Raw Materials:					
Benzene	gal/lb	$/gal	3.85	0.11	42.40
Hydrogen	KSCF/lb	$/KSCF	5.35	0.011	5.75
Catalyst	lb/lb	$/lb	4	0.00001	0.004
Fuel gas	million Btu/lb	$/ million BTU	9.58	0.00123	1.18
Total Materials					49.34
Utilities:					
Cooling water	gal/lb	$/1000 gal	0.719	2	0.14
Steam (250 psig)	lb/lb	$/1000lb	8	0.2	0.16
Process Water	gal/lb	$/1000 gal	5.5	0.1	0.06
Electricity	kwh/lb	c/kwh	6	0.04	0.24
Total Utilities					0.60
TOTAL VARIABLE COST					49.94
Labor:					
Operators	man yr	k$/yr	55	0.5	0.16
Supervision	man yr	k$/yr	75	0.1	0.04
Maintenance	% of fixed capital			2	0.02
Laboratory Charges	Man Yr	k$/yr	55	0.1	0.03
Total Labor Cost					0.25

****	UNIT OF USAGE	UNIT OF PRICE	PRICE	USAGE	Cost, c/lb
Supplies:					
Operating	% of fixed capital			0.5	0.01
Maintenance	% of fixed capital			0.5	0.01
Total Supplies Cost					0.01
TOTAL DIRECT COST					50.20
INDIRECT:					
Administration	% of labor			5	0.01
Taxes and Insurance	% of fixed capital			2	0.02
Plant Overhead	% of labor			10	0.03
Depreciation	% of fixed capital			10	0.11
Interest on Working Capital	% of 50% of fixed capital			10	0.06
Miscellaneous	%(labor + supplies)			10	0.03
TOTAL INDIRECT COST					0.26
TOTAL PRODUCTION COST					50.46
By-Product Credits (N/A)					
Fuel Gas					
Steam					
Total By-Product Credits					0
NET PRODUCTION COST					50.46

****: Continuation of Table 5.3

5.2 COMPARISON OF CYCLOHEXANE PRODUCTION COST OF THE CONVENTIONAL AND MICROREACTOR TECHNOLOGY

As shown in the appendix, from SRI, Process Economics Program Report No 7B, Supplement B on Caprolactam by Ken K. Ushiba (January 1976), the total fixed capital cost of a 220 million lb/yr conventional cyclohexane production from hydrogenation of benzene at 8,000 on stream hours per year was estimated at $2.78 million based on a CE Index of 150. Note that the principal feedstock for the manufacturing of caprolactam (the monomer for nylon 6) is cyclohexane. We extrapolated the fixed capital cost of the conventional mega plant to 2006 (same year of the estimated microreactor miniplant total fixed capital cost estimate) based on the CE Index 499.6 (year 2006 CE Index) to $9.26 million. From this result, we estimated the fixed capital cost of a scaled down conventional miniplant of 10 kg/hr (0.18 million lb/yr) at 8,000 on stream hours using a cost scaling factor of 0.6 as $130,000.000 ($0.13 million).

We are of the opinion that the grass root estimate of the microreactor miniplant fixed capital cost of $0.20 million will be cheaper than a grass root conventional miniplant currently estimated at $0.13 million via a cost scaling factor (0.6) and CE Index (from 1976 to 2006, about 30 years different) and capacity escalation of 220 million lb/yr to 0.18 million lb/yr (a scaled down factor of more than 1,200). However, the results showed that our estimated microreactor miniplant total fixed capital cost is very realistic and comparable to the conventional miniplant. The advantages of using microreactor over the conventional technology include an efficient heat removal of more than two orders of magnitude better than conventional reactor that provides for a better safe process than the conventional route.

6. TECHNOLOGY TRANSFER AND COOPERATION

The planned technology presentation round table on Task 6 to potential companies that may be interested in the application of the outcome of our development of the microreactor to the production of cyclohexane with application to other similar commodity chemicals as an economical and more safe route than the conventional technology was postponed to avoid potential conflict of interest between Stevens and one of the companies. At the AIChE Spring meeting in New Orleans, April 2008 we met with our contact person in UOP to discuss the interest of UOP in the technology. UOP holds the patent to the most used conventional technology on hydrogenation of benzene to cyclohexane. No specifics were discussed but just in general terms on cyclohexane production.

The results of this work will be used to leverage discussion with UOP, Chevron Phillips and other potential partners especially the commodity chemical companies interested in the microreactor technology. We have not been successful to get a high commodity industrial partner that can collaborate with us on using our developed microreactor technology concept on industrial scale production of cyclohexane. We plan to continue to talk to UOP, LLC and seek other chemical companies that may be interested to partner with us.

7. ENVIRONMENTAL AND SAFETY ISSUES

We have looked into the environmental issues and safety concerns in the plant design. The production of cyclohexane from hydrogenation of benzene and hydrogen is a highly exothermic reaction where the reactor temperature control is very critical. Consequently, in most conventional commercial cyclohexane processes, multi-stage reactors involving recycling of cyclohexane, inter-reactor cooling to allow efficient removal of the heat of hydrogenation, and staged addition of the benzene feed are employed. In our design, we have taken advantage of the

efficient and rapid heat removal characteristics of microreactor system which are more than two orders of magnitude better than conventional reactor, to provide for a compact miroreactor that achieves efficient heat removal and safe process where the reactor temperature is well controlled. Our design also achieves minimal benzene, methylcyclopentane and other impurities (by-products) in the product thus making less impact on the environment compared with the conventional process. Overall, the compactness of our design reduces product inventory making the facility a less threat to terrorism and reduces liability risks in case of an accident and/or spillage. We have also looked into the issue of health and safety of the cyclohexane product. Cyclohexane is not a highly toxic chemical. It has been reported that workers exposed to 600 to 700 ppm by volume did not suffer any chronic effects. The threshold limit for cyclohexane in human being is about 300 ppm. The acceptable explosive limits of cyclohexane in air are 1.31 to 8.35 %. Our design took into consideration the need to maintain the vapor phase of the cyclohexane product well below the acceptable explosive limits of cyclohexane in air.

8. CONCLUSION

We have completed Task 6 of the microchannel reactor system for catalytic hydrogenation project on the plant design and commercialization of the microchannel reactor-based process intensification technology across the chemical and pharmaceutical industries with specific reference to the production of cyclohexane from hydrogenation of benzene. The main reactor is a 200-micro-channel reactor, each with dimension (500 micron x 500 micron x 6 in). The reactor will operate at a combined space-time yield of 500g cyclohexane/g cat.h and produce 10kg/h of cyclohexane with 99 wt% purity. The highlights of this report include the adoption of a novel compact two-stage reactor that combines both the methanation and hydrogenation reactions in one single reactor that minimizes by- products and ensures efficient conversion of benzene to cyclohexane.

The production cost of hydrogenation of benzene to cyclohexane has been estimated to be 50.5 cents/lb of cyclohexane. The costs are based on 10 kg/hr (0.18 million lbs/yr) of cyclohexane at 8,000 on stream hours per year, and $200,000.00 fixed capital cost. With this relatively low production capacity, the by-product credits for steam and fuel gas are not applicable and we have assumed that the mini-plant will share operator with other operating units within the plant facility.

We have emphasized in this work, environmental issues, and safety concerns that are very critical especially in this process that involves large and rapid heat transfer for process control and safety. Microreactors with large surface to volume ratio provide better heat transfer than conventional reactors. This study gives some generalization of the best practice (blue-print) for potential companies that may be interested in the application of the outcome of our development of the microreactor to the production of cyclohexane with application to other similar commodity chemicals as an economical and safer route than conventional reactor technology.

9. ACKNOWLEDGMENT

ChemProcess Technologies (CPT), LLC would like to acknowledge the contributions of Dr. Emmanuel Dada, Dr. Luke Achenie, and Dr. Timothy Odi to this project.

10. REFERENCES

Amend, William J., "Catalytic Oxidation", US Patent 2316543 assigned to DuPont, April 14, 1943

Clement, Thonon, “Process for the Catalytic Hydrogenation of Aromatic Hydrocarbons”, US patent 3,202,723, August 24, 1965 assigned to Institut Francais du Petrole.

Felix, Albert; Roques, Yves, "Method of making adipic acid", US patent 6822117 assigned to Rhodia, Fiber and Resin Intermediates (Courbevoie, FR), November 23, 2004

John McKetta and William Cunningham, Vol. 14 of Encyclopedia of Chemical Processing and Design.

Kehoe and Butt, “Kinetics of Benzene Hydrogenation by Supported Nickel at Low Temperature”, Journal of Applied Chem. Biotechnol. 1972, 22, 23-30

Kirk-Othmer Encyclopedia of Chemical Technology, Vol. 12, John Wiley & Sons, 1980.

Konyukhov, et al., “Kinetics of Liquid-Phase Hydrogenation of Benzene on Palladium Catalyst and Hydrogenation of Toluene on Palladium and Catalysts”, Kinetika, Vol. 28, No 2, pp. 360-365, 1987

Sanderson, John Ronald, et al.," Manufacture of cyclohexane from benzene and a hydrogen source containing impurities”, US patent application # 20030114723, June 19, 2003

Srinivas, Darba; Chavan, Suhas; Ratnasamy, Paul, "Process for the preparation of adipic acid", US Patent 6521789 assigned to Council of Scientific and Industrial Research (New Delhi, IN) February 18, 2003

Ullmann's Encyclopedia of Industrial Chemistry, 2005

Ushiba, Kenk, K. "Process Economics Program Report No 7B", Supplement B on Caprolactam, January 1976

Zhou Zhi-ming, Cheng Zhen-min, Yuan Wei-kang, "Advance in the reaction kinetics of benzene hydrogenation to cyclohexane"**,** UNILAB Research Center of Chemical Reaction Engineering, East China University of \Science and Technology, Shanghai 200237, China.

11. APPENDIX

Process Economics Program Report No 7B, Supplement B on Caprolactam by Ken K. Ushiba, January 1976

Table 4.4

BENZENE HYDROGENATION PROCESS

TOTAL CAPITAL INVESTMENT

Capacity: 220 Million lb/yr (100,000 Metric Tons/yr)
Cyclohexane at 8,000 hr/yr Onstream
CE Index: 150

	Cost	Capacity Exponent Up	Capacity Exponent Down
Battery limits equipment, f.o.b.			
Reactors	$ 74,300	0.71	0.70
Columns	9,000	0.42	0.39
Vessels and tanks	32,100	0.60	0.58
Exchangers	60,000	0.76	0.66
Compressors	222,300	0.76	0.76
Pumps	17,000	0.46	0.38
Total	$ 414,700	0.71	0.69
Battery limits investment	$1,741,700	0.64	0.62
Utilities and tankage			
Cooling water	118,800	0.34	0.28
Process water	3,900	0.77	0.77
Steam	95,000	0.80	0.80
Refrigeration	37,600	0.72	0.69
Tankage	296,500	0.65	0.65
Total	$ 551,800	0.62	0.59
Utilities and tankage investment	676,000	0.59	0.56
BATTERY LIMITS & UTILITIES INVESTMENT	2,417,700	0.63	0.60
General service facilities	362,600		
TOTAL FIXED CAPITAL	$2,780,300		
Interest on construction loan @ 10%/yr*	127,400		
Start-up cost	1,410,000		
Working capital	2,015,000		
TOTAL CAPITAL INVESTMENT†	$6,205,300		

*Construction period of 11 months, financed loan on $2.672 million for average of half of construction period assumed.

†Not including the land cost.

TASK 7: Reactor System Analysis, Optimization, Integration and Evaluation (Phase 2)

I. Design and Construction of the Skid-mounted Microreactor System

At the end of Phase I of the project, we reviewed the go/no-go criteria for Phase 2, and based on the outcomes of Tasks 1 to 6, the criteria were met, therefore we embarked on Phase 2. Based on Aspen Plus process simulations, we designed a comprehensive process flow diagram along with balance of plant (BOP) and process controls for a two-phase gas-liquid hydrogenation reaction with a liquid product rate of about 1.0 – 10 kg/hr. Hydrogen is compressed to the reaction pressure through a H_2 mini-compressor. The compressed gas stream then goes into a gas pre-heater where it is heated to the reaction temperature. The liquid reaction medium, comprising the substrate and the solvent is prepared through a batch process, and stored in a batch tank from where it is fed to a tank. The liquid feed stream is then pumped through a mini-pump into a liquid pre-heater where it is heated to the reaction temperature. The preheated gas stream and liquid stream enter separately the multichannel microreactor unit where both the reaction, and heat exchange with the cooling stream take place. The product stream from the microreactor passes through a two-stage gas-liquid flash separation, a high pressure separator and a low pressure separator, to separate the gas and liquid. The liquid product is collected from the 2nd stage separator. Part of the gas stream from the 1st stage separator goes back into the system through a gas mini-compressor, and the other part combines with the gas stream from the 2nd stage separator before being vented into the atmosphere. The microreactor is the main processing unit in the system; it integrates a reactor and a heat exchanger. There is a cooling water loop in the system for heat exchange. The cooling water is pumped into the microreactor cooling side for effective removal of the heat liberated by the exothermic reaction from the reaction plates. The cooling stream is then passed through the gas pre-heater and the liquid pre-heater for initial heat recovery and the remaining heat is finally rejected through a mini heat exchanger. The cooled water returns to the cooling loop. Heating tape is wrapped around the gas and water inlets for system startup. The reaction conditions are based on our lab test result, and both the conversion and selectivity are 100%. Total energy usage per pure liquid product is approximately 9.12 Btu/lb.

There are a number of controlling points in the process: pressure controllers and mass flow controllers in the gas feed, mass flow controller in the liquid line, liquid level controller in the liquid feed tank, liquid level controller in the 1st stage separator and temperature controller in the cooling water heat exchanger. Other auxiliary equipment includes pressure, flow rate, and temperature indicators, check valves, frame arresters, and liquid traps. All the main pieces of equipment comprising the pilot plant except the reactor/heat exchanger were selected off-the-shelf. The microreactor and the associated manifolds were fabricated from titanium using precision-machining. There were altogether 10 cooling plates and 9 reaction plates alternately stacked and bonded together. Each reactor plate has 73 channels while there are 153 channels on each cooling plate. The off-the-shelf components include H_2 generator, HPLC pumps, gear pump, air-driven gas compressors, liquid mass flow controllers, gas mass flow controllers, temperature sensors, pressure transducers, feed and storage tanks, finned-tube heat exchangers, and gas-liquid separators. The equipment was professionally assembled in a skid-mounted pilot plant system in accordance with the process P&ID design. A computer data acquisition and control system was installed to facilitate process control and data acquisition (see Figure 7.1).

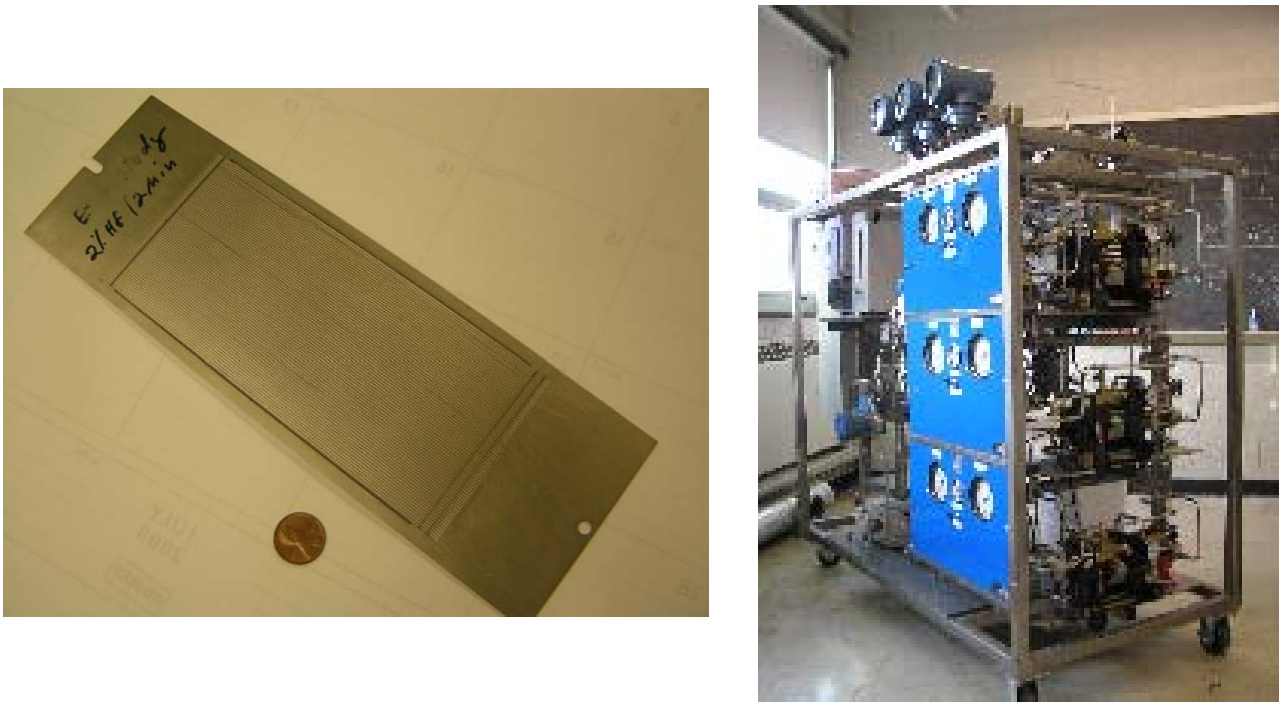

Figure 7.1: (a) Multi-channel microreactor plate (b) Compact Skid-mounted Micro-reactor-based Distributed Production Plant (1 – 10 kg/h)

International Flavors and Fragrances (IFF), a world leader and valuable partner in the creation of consumer-preferred flavors and fragrances expressed strong interest in the adoption of our microreactor technology for the production of some of their fine chemicals. If the demonstration of the production unit at Stevens was successful, IFF would like to evaluate a two-phase reaction in this system, and eventually commercialize the technology exclusively for this reaction in conjunction with Stevens, and possibly with the help of DOE-ITP. Towards this end, BMS and IFF safety personnel with extensive experience in hazard review in conjunction with Stevens conducted a thorough safety review of the production unit before testing began. The exercise which was conducted in stages was carried out at Stevens with the help and support of our industrial collaborators from BMS (Don Kientzler), IFF (Puvin Pichai and James Stevens), and a consultant on Control Systems, Dino Favetta, President of Controlamatics. A number of suggestions were made on the operational procedure that would ensure the safe running of the system, and these were compiled into a report for internal use.

II. Multi-channel Reactor Packing with Particulate Catalyst

We designed and fabricated a special manifold for packing the multi-channels of our custom-manufactured microreactor with particulate catalysts. This manifold when incorporated into a previously designed set-up also enables the removal of the particulate catalysts from the multi-channel reactor using high-pressure steam. The whole set-up was tested with a demo reactor but not with the actual reactor. Our plan was to implement this step after the complete evaluation of the automated skid-mounted micro-reactor system as described in the next section.

III. Evaluation of Skid-mounted Micro-reactor System

For the purpose of evaluating the micro-reactor system, we broke up the system into the following units based on the unit operations they perform: (1) Liquid reactant/inert feed (2) Reactor cooling (3) Reaction (4) Product separation (5) Recycle and purge (6) Hydrogen generation and compression, and (7) Gas reactant feed and compression.

After the identification of these separate sections, the chemical synthesis facility was next clearly documented through the preparation of P&ID for each section based on each independent unit operation, including the instrumentation and control loops. Physical instruments versus software "virtual devices" were described and documented, as a prelude to the development of a complete User's Manual and Operating and Troubleshooting Guide. Several of the individual unit operations were commissioned using de-ionized water to check for leaks and to calibrate and tune the control loops. The liquid reactant/inert feed unit was checked for automatic re-fill interlocks, pump flow rates and flow control using de-ionized water as model feed. Several devices in these loops required fine tuning and were set to acceptable limits of operation. The Micro-channel reactor cooling loop was tested in a partial simulation mode using external electric heating elements to heat the reactor since no true exothermic reaction was actually in progress. All the tests of the unit operations sections were successfully completed

For the first demonstration of multi-phase reaction in the pilot plant, we identified a suitable heat-transfer limited liquid-liquid reaction for our initial production run. The catalyst for this liquid-liquid reaction is also in the liquid phase hence its implementation in the microreactor system did not require the packing of the reactor with particulate catalyst (see section above). This reaction had already been tested in the single-channel microreactor system and the microreactor system demonstrated superior performance in comparison to the conventional semi-batch reactor system. In order to ensure not only a safe exercise but also a successful implementation of this reaction in the pilot plant, we undertook the following:

- The entire process system was checked for leaks with air and deionized (DI) water after all springs and relief valves were adjusted. The system was brought to high pressure (500 PSIG). Several small leaks were detected and corrected, and some fittings were replaced.

- The compressor high-pressure relief vents were connected to the safety vent in preparation for processing of any hazardous gases.

- The reactor was operated with DI water using dyes. One DI water stream was used for the process side, while another DI water stream was used for the cooling side. Into each of the stream was added a small amount of a dye of different color to test for cross-communication between the heat exchanger channels and the reactor channels. No cross-communication was found and the streams appeared to be isolated from each other.

- A considerable amount of time was spent on reducing measurement errors. Due to small flows and capillary effects, some gas entrainment in the small tubes created pocketing and liquid flow transient measurement errors. New mounting brackets were fabricated to adjust the orientation of the three coriolis mass flow meters to eliminate the problem.

- Some thermocouple sensors were replaced due to damage or relocated for better measurement.

- The reactor inlets were wrapped with heat trace to simulate heat generation when testing with water to check the reactor cooling capability and tune the control loop.

- Gas feed pressure regulators were added to the compressor inputs from the main clean air supply to test the triggers of the low pressure switches while operating, and to limit the flow into the skid at lower operating pressures from the higher pressure supply which was causing compressor blow-through.

The Stevens' team met with the team from International Flavors and Fragrances (IFF) to plan the kick-off of the chemical synthesis test using the process unit. The selected liquid/liquid reaction simplified the use of the process unit by eliminating any gas subsystems (compressors, regulators, gas flow controllers, and vents but it necessitated the modification of the pilot plant. The implementation of the modifications rendered the pilot plant versatile as both gas-liquid and liquid-liquid reactions can now be safely and successfully carried out in the system.

III.1. Experiment for heat transfer coefficient:

An experiment was conducted for determining the heat transfer rate in the microreactor. A heating tape was wrapped around the inlet of the liquid reactant line, and the heating was controlled using a variable voltage transformer. The overall heat transfer coefficient was determined. The reactant side water flow rate used was 30 ml/min while actual coolant water flow rate as read on the flowmeter was 278 ml/min. The heating tape was subjected to the maximum voltage possible. The measured inlet reactant line water temperature was 48.9^{o}C, reactant line outlet water temperature was 27.0^{o}C, coolant water inlet temperature was 23.8^{o}C and coolant water outlet temperature was 27.6^{o}C. The overall heat transfer coefficient for this water-water system in the microreactor was calculated based on reactor side area to be 22.5 W/ (m^2K). Conventional heat exchangers for water-water system have a maximum overall heat transfer coefficient of around 400 – 500 W/ (m^2.K). However, our microreactor has a surface area to volume ratio of 738 m^{-1} while conventional heat exchangers have surface area to volume ration of around 16 – 20 m^{-1}. Thus our microreactor is found to have a UA (product of overall heat transfer coefficient and area) which is 2 – 3 times larger than conventional heat exchangers.

III.2. Experiment for reaction run:

Experiments for a preliminary single phase reaction involving two liquid reactants were conducted in the pilot plant microreactor. For confidentiality reasons, we cannot report the results of this experimental run at this point.

III.3. Future Work

The preliminary reactor system performance data from the liquid-liquid reaction conducted in the multichannel micro-reactor system indicated the need to optimize the process. In addition to other modifications to the reactor system that have been planned as part of the optimization process, a re-design of the multichannel reactor was also initiated. This re-design was completed. Some of the changes to the reactor include (i) increase of the length of both the reaction and cooling channels (ii) increase of the number of both the reaction and cooling channels, (iii) a slight modification to the design of the manifold, and (iii) a different and more robust approach to ensuring a perfect seal between the reactor and the manifold. The fabrication of the

reaction/cooling plates was completed and the plates stacked and diffusion-bonded to form a single unit of reactor/heat exchanger, and further experimental runs will be performed in the system in the near future with all the changes incorporated.

6. Products Developed and Technology Transfer Activities

a. Publications & Presentations

S. Tadepalli, and A. Lawal, "Catalytic Hydrogenation of Aromatic Nitro-ketone in a Packed-bed Microreactor: Reactor Performance and Kinetic Studies," *International Journal for Chemical Reactor Engineering*, 6 (2008) A112.

S. Tadepalli, D. Qian, and A. Lawal, "Comparison of Performance of Micro-reactor and Semi-batch Reactor for Catalytic Hydrogenation of o-Nitroanisole *Catalysis Today*," 125 (2007) 64 – 73.

S. Tadepalli, R. Halder, and A. Lawal, "Catalytic Hydrogenation of o-Nitroanisole in a Micro-reactor: Reactor Performance and Kinetic Studies," *Chemical Engineering Science*, 62 (2007) 2663 – 2678.

S. Tadepalli, "Microchannel Reactor System for Catalytic Hydrogenation of Nitro-aromatics," *Ph. D. thesis*, 2008

D. Qian, and A. Lawal, "Numerical Study on Gas and Liquid Slugs for Taylor Flow in a T-junction Microchannel," *Chemical Engineering Science*, 61 (2006) 7609 – 7625.

H. Chen and W. Y. Lee, "Synthesis of Cellular Silica Structure under Microchannel Confinement," J. Am. Ceram. Soc., 90[1], 36-43 (2007).

H. Qiu and W. Y. Lee, "Infiltration and Immobilization of Catalyst Particles into the Confined Space of Microstructured Reactors via Layer-by-Layer Self-Assembly," Applied Catalysis A, 314, 200-207 (2006).

H. Qiu, S. Sukhishvili, and W.Y. Lee, "Layer-by-Layer Self-Assembly of Ceramic Particles as a Non-line-of-Sight Technique for Coating Complex Shape Substrates, J. Am. Ceram. Soc., 89[4], 1180-87 (2006).

H. Chen, L. Bednarova, R. S. Besser, and W. Y. Lee, "Surface-Selective Infiltration of Thin-film Catalyst into Microchannel Reactors," Applied Catalysis A, 286, 186-195 (2005).

J. Huang, J. Weinstein, and R.S. Besser, "Particle loading in a catalyst-trap microreactor: Experiment vs. simulation," *Chemical Engineering Journal*, 155, 388-395 (2009).

S. McGovern and R.S. Besser, "Investigation of Multiphase Hydrogenation in a Catalyst-Trap Microreactor," *Journal of Chemical Technology and Biotechnology*, 84:382-390 (2009).

S. McGovern, G. Harish, C.S. Pai, W. Mansfield, J.A. Taylor, S. Pau, R. Besser; Chem Eng Journal, "Multiphase flow regimes for hydrogenation in a catalyst-trap microreactor," *Chemical Engineering Journal*, (135) Supplement 1, S229-S236, (2008).

H. Surangalikar, S. McGovern, R.S. Besser, "Gas-Liquid-phase Reactions," *in Micro Process Engineering, A Comprehensive Handbook, Volume 2: Devices, Reactions, and Applications*," V. Hessel, A. Renken, J.C. Schouten, J. Yoshida, eds., Wiley-VCH: Weinheim, Germany, 167-186 (2009).

H. Gadre, S. McGovern, R.S. Besser, "Flow Regimes in a Catalyst Trap Microreactor," *Proceedings of the AIChE 2006 Fall Meeting*, San Francisco, CA, (2006).

S. McGovern, H. Gadre, R.S. Besser, "Catalyst-Trap Microreactor for Hydrogenation of a Pharmaceutical Intermediate," *Proceedings of the AIChE 2006 Spring Meeting*, Orlando, FL, (2006).

A. Lawal, S. Tadepalli, H. Qiu, W. Y. Lee, D. Kientzler, J. Muslehiddinoglu, and L. Chenie, "Microchannel Reactor System for Catalytic Hydrogenation," ***Invited Presentation***, *AIChE Spring National Meeting, Houston, TX, April 24-25, 2007.*

A. Lawal, S. Tadepalli, R. Halder, H. Qiu, W. Y. Lee, R. Besser, L. Achenie, and D. Kientzler, "Microchannel Reactor System for Catalytic Hydrogenation," ***Invited Presentation***, *Process Intensification Topical Conference, AIChE Spring National Meeting, Atlanta, GA*, April 13, 2005.

A. Lawal, S. Tadepalli, R. Halder, H. Qiu, W. Y. Lee, R. Besser, L. Achenie, and D. Kientzler, "Microchannel Reactor System for Catalytic Hydrogenation," ***Invited Presentation***, *Process Intensification Topical Conference, AIChE Spring National Meeting, New Orleans*, April 28, 2004.

S. Tadepalli, A. Lawal, D. Kientzler, and J. Muslehiddinoglu, "Kinetic Study of Catalytic Hydrogenation of Aromatic Nitro Compound in a Microchannel Reactor," *AIChE Spring National Meeting, Houston*, TX (April 23, 2007)

S. Tadepalli, A. Lawal, R. Halder, D. Kientzler, and J. Muslehiddinoglu, "Microchannel Reactor System for Catalytic Hydrogenation of nitro aromatics," *ACS National Meeting, Chicago, IL* (March 28, 2007)

S. Tadepalli, A. Lawal, R. Halder, D. Kientzler, and J. Muslehiddinoglu, "Microchannel Reactor System for Catalytic Hydrogenation," *AIChE Spring National Meeting, Orlando, FL* (April 26, 2006)

L. Bednarova, H. Qiu, and W.Y. Lee, "Layer-by-Layer Self-Assembly of Catalyst Particles as a Catalyst Integration Method for Microreactor Applications," 9th International Conference on Microreaction Technology, Postdam, Germany, September 2006.

Y.-F. Su, H. Kim, H. Qiu, R. Halder, S. Koven, and W.Y. Lee, "Synthesis of Functionalized Nanoparticles Using Microreactor," 9th International Conference on Microreaction Technology, Postdam, Germany, September 2006.

H. Qiu, Y.-F. Su, J. H. Lee, and W. Y. Lee, "Layer-by-Layer Self-Assembly of Nanoparticles for Thin-Film Synthesis in Complex Microscale Geometries," NSTI NanoTech Conference, Boston, MA, May 2006. (Invited)

W.Y. Lee, "A Nanotechnology Perspective on Chemical and Biological Microreactor Design and Use," 4th International Workshop on MicroChemical Plants, Kyoto, Japan January 2006 (Plenary Lecture)

H. Chen and W.Y. Lee, "Development of Tunable Cellular Structures as a Catalyst Integration Platform for Microreactors," MRS Fall Annual Meeting, Boston, MA, November 2005.

H. Qiu, H. Chen, and W.Y. Lee, "Synthesis of Cellular Catalytic Structures via Self-Assembly of Nano- and Micro-Particles for Microreactor Systems," Particles 2005, San Francisco, CA, August 2005.

H. Chen and W.Y. Lee, "Design and Fabrication of Infiltratable Multiscale Catalytic Cellular Structures into Microchannel," 8th International Conference on Microreaction Technology - AIChE National Spring Meeting, Atlanta, GA, April 2005.

H. Qiu and W.Y. Lee, "Layer-by-Layer Self-Assembly of Nano- and Micro-particles as a Catalyst Integration Method for Microreactor Applications," 8th International Conference on Microreaction Technology - AIChE National Spring Meeting, Atlanta, GA, April 2005.

R.S. Besser, "A Closer Look at Microchemical Systems as Platforms for Efficient Chemical Processing: a Discussion of Advantages and Limitations," Metro MEMS/NEMS, Hoboken, NJ, July 23, 2007.

R.S. Besser, "A Closer Look at Microchemical Systems as Platforms for Efficient Chemical Processing: a Discussion of Advantages and Limitations," University of Connecticut, Department of Mechanical Engineering, Storrs, CT, April 12, 2007.

R.S. Besser, "Microchemical Systems as a Tool for Pharmaceutical Manufacturing," International Society of Pharmaceutical Engineers, Student Chapter Meeting, Stevens Institute of Technology, Jan. 16, 2007.

R.S. Besser, "A Look at Microchemical Systems: What Are They? What Are Some Key Limitations?" Rutgers University, Department of Mechanical Engineering Seminar, Piscataway, NJ, Feb. 22, 2006.

R.S. Besser, W.Y. Lee, A. Lawal, S. Kiang, D. Kientzler, "Microreaction Technology in Pharmaceutical Manufacturing: The New Jersey Center for Microchemical Systems," Invited Keynote Address, 8th International Conference on Microreaction Technology (IMRET), Atlanta, Georgia, April 11, 2005.

R.S. Besser, "Micro and Nano Technology for Chemical Processing," Invited Keynote talk, NJNC Nanotechnology Conference, Lucent Bell Labs/New Jersey Nanotechnology Consortium, Feb. 3, 2005.

S. McGovern, H. Gadre, R.S. Besser, "Conversion Effects in a Catalyst-Trap Microreactor for Hydrogenation of a Pharmaceutical Intermediate," International Society for Pharmaceutical Engineers NJ Chapter Poster Contest, April 2005. Honorable mention winner.

H. Gadre, S. McGovern, R.S. Besser, "Catalyst-Trap Microreactor for Hydrogenation of a Pharmaceutical Intermediate," International Society for Pharmaceutical Engineers NJ Chapter Poster Contest, April 2005.

H. Gadre, S. McGovern, R.S. Besser, "Flow Regimes in a Catalyst Trap Microreactor," AIChE 2006 Fall Meeting, San Francisco, CA, Nov. 22-27, 2006.

S. McGovern, H. Gadre, R.S. Besser, "Catalyst-Trap Microreactor for Hydrogenation of a Pharmaceutical Intermediate," AIChE 2006 Spring Meeting, Orlando, FL, May 22-27, 2006.

b. Web site or other Internet sites that reflect the results of this project

Feature articles about the project in:
Chemical Engineering Progress,(October 2003, pg. 51)
Inside the Fuel-Cell Industry (10/12 – 10/19/03)
EurekAlert (10/14/03)
News and Articles on Materials Engineering (10/14/03)
Jersey Journal (10/14/03)
Small Times News (12/8/03), and
C&ENews (10/11/04)

c. Networks or collaborations fostered

Stevens Institute of Technology and Karlsruhe Research Center (KRC), a German organization with renowned expertise in the fabrication of metallic multichannel microreactors, signed a Memorandum of Understanding in June 2003 that allowed us to collaborate on microreactor fabrication. As part of the agreement, KRC made available to

us on loan, a micromixer (which was incorporated into our experimental set-up), and a multichannel microreactor/heat exchanger. KRC and Stevens Institute of Technology have continued to exchange useful technical information on microreactor systems for chemical synthesis.

Stevens Institute of Technology and Cornell Nanofabrication Facility (CNF) – an NSF Center at Cornell signed a Memorandum of Understanding in August 2005 that enabled Mr. John Adeosun, the PI's graduate student to use the state-of-the-art MEMS facilities at CNF to fabricate two micromixers, one a T-junction mixer and the other Multilaminated/Elongational Flow Micromixer (MEFM-4)**,** both from silicon.

Our work on microreactors has been widely disseminated, and we have received numerous requests for information on this project and others being carried out at our Center. International Flavors and Fragrances (IFF) approached us in August 2006 to develop a framework for a collaborative effort on the use of microreactors for immiscible liquid-liquid reactions. Subsequently, we identified a liquid-liquid reaction of industrial importance to IFF and a microreactor study of this reaction began in August 2006 with IFF providing partial financial support for a PhD student, Mr. Obi Okafor assigned to work on the project. IFF hired Ms. Sunitha Tadepalli after the completion of her PhD study on this DOE-sponsored project.

d. Technologies/Techniques

Microreactor System for Chemical Processing

e. Inventions/Patent Applications, licensing agreements

A. Lawal, and D. Qian, "Scalable Microreactors and Methods for Using Same," United States Patent 7,670,567 B2, March 2, 2010

f. Other products – *Not Applicable*